Biological mechanisms underlying ionising radiation-induced cataracts

ALICE UWINEZA

Biological mechanisms underlying ionising radiation-induced cataracts

Alice Uwineza

A Thesis presented for the degree of

Doctor of Philosophy

Department of Biosciences

University of Durham

United Kingdom

January 2020

Biological mechanisms underlying ionising radiation-induced cataracts

Alice Uwineza

Submitted for the degree of Doctor of Philosophy

January 2020

Abstract

Epidemiological data correlate exposure to ionising radiation (IR) with cataract formation. In 2012, the International Commission on Radiological Protection reduced its recommended threshold for IR effects on the eye lens to 0.5 Gy and acknowledged that the biological mechanisms underlying IR-induced cataracts are largely unknown. To determine these processes, the influence of IR on the lens epithelium, cholesterol and membrane proteins was investigated. CD1, C57BL/6J and B6C3F1 mice were exposed to 0.5 - 2 Gy at 0.3 or 0.063 Gy/ min. Lens epithelium cell density was examined at 4 and/ or 12 months post-IR. Differential response to IR in these mice was observed in a strain-, dose-, dose rate-, sex-, $Ptch1^{+/-}$ and $Ercc2^{+/-}$ -dependent manner and the data indicated that low dose IR-induced cataractogenesis requires a relatively long latency period, which is consistent with epidemiological data from longitudinal studies. The plasma membranes of lens fibre cells are among the cholesterol richest membranes in the human body and cholesterol has a vital role in biophysical properties of these membranes. Analysis of IR exposed bovine eye lens membrane extracts (5 and 50 Gy) and eye lenses taken from whole body irradiated mice (0.1 and 2 Gy) showed that IR induced a significant increase in cholesterol oxides i.e. oxysterols. Unlike the isolated lens membranes, the observed enhancement of oxysterol levels *in vivo* was transient. Furthermore, adding α-tocopherol to isolated lens cortex membranes before exposure to IR prevented the build-up of oxysterols. The increase of oxysterols in mice eye lenses was shown to also be age-related, and was observed in the hippocampus as well. In addition, a dose-dependent increase in protein glycation was noted after IR exposure of lens membrane extracts. Collectively, these data underline that IR contributes to the cataractogenic load through compromising lens membrane integrity and lens epithelium homeostasis.

Table of content

List of tables

List of figures

List of abbreviations

•NO: nitric oxide

•OH: hydroxyl radical

27-OHC: 27-hydroxycholesterol

4β-OHC: 4β-hydroxycholestrerol

5α, 6α-epoxy: 5α, 6α-epoxycholesterol

5β, 6β epoxy: 5β, 6β-epoxycholesterol

7-keto C: 7-ketocholesterol

7α-OH-3-oxo-4-CA: 7α-hydroxy-3-oxo-4-cholestenoic acid

7α-OHC: 7α-hydroxycholesterol

7β-OHC: 7β-hydroxycholesterol

A-bomb: atomic bomb

ACN: acetonitrile

ACSF: artificial cerebrospinal fluid

ACTA2: α-actin 2

AD: Alzheimer's disease

AGEs: advanced glycation end products

ANOVA: analysis of variance

AQP0, MIP: aquaporin 0

ARC: age-related cataract

Asc: ascorbic acid

Avg.: average

Aβ-peptides: amyloid β peptides

BCA: bicinchoninic acid

BFSP1/2: beaded filament structural protein 1 and 2

BoC: bovine cortex

BoN; bovine nucleus

BSA: bovine serum albumin

CAT: catalase

CDH2: cadherin-2

CEA: N^7-carboxyethyl arginine

CEL: N^6-carboxyethyl lysine

CLSM: confocal laser scanning microscope

CML: carboxymethyl lysine

CRYAA: α-crystallin A

CRYBA4: β-crystallin A4

CT: computed tomography

CTNNB1: β-catenin

Ctrl: control

CZ: central zone

D: days

DCM:MeOH: dicholoromethane:methanol

DHA: dehydroascorbate anion

DNA: deoxyribonucleic acid

DNPH: 2,4-dinitrofenylhydrazine

DSBs: double stranded DNA breaks

DTT: dithiothreitol

DU: Durham University

e.g.: exempli gratia

e.i.: id est

e^-: electrons

ENEA: Italian National Agency for New Technologies, Energy and Sustainable Economic Development

EPR: electron paramagnetic resonance

FA: formic acid

FHL124: fetal human lens-124

FLOT2: flotillin-2

GOLA: glyoxal lysine amide

GPx: glutathione peroxidase

GSH: glutathione

GSSG: glutathione disulphide

Gy: Gray

GZ: germinative zone

h: hour(s)

$H^{\bullet}$: hydrogen radical

H_2O: water

H_2O_2: hydrogen peroxide

H_3O^+: ionized water

HEPES: 4-(2-hydroxyethyl)-1-piperazineethanesulfonic acid

HFBA: heptafluorobutyric acid

HILIC: hydrophilic interaction liquid chromatography

HLEC1: human lens epithelial cells 1

HMGU: Helmholtz Zentrum München

IAA: iodoacetimide

ICRP: International Commission on Radiation Protection

IPA: isopropanol

IR: ionising radiation

LC-MS: liquid chromatography mass spectrometry

LECs: lens epithelial cells

LFCs: lens fibre cells

LSSU: life sciences support unit

MG-H1: methylglyoxal hydroimidazolone 1

MGMT: methylguanine methyltransferase

Min : minutes

MMPs: matrix metalloproteinases

MoC: mouse cortex

MoN: mouse nucleus

MR: meridional rows

MRM: multiple reaction monitoring

n: amount

Ndrg2: N-Myc downstream regulated gene2

O_2: oxygen

$O_2^{\bullet-}$: superoxide

OFZ: organelle free zone

$ONOO^-$: peroxynitrite anion

PBS: phosphate buffered saline

PFA: paraformaldehyde

PHE: Public Health England

PR: peripheral zone

PSCs: posterior subcapsular cataracts

PTMs: post-translational modifications

QTOF: quadrupole Time-Of-Flight

RNS: reactive nitrogen species

ROS: reactive oxygen species

RT: room temperature

s: second(s)

SDS-PAGE: sodium dodecyl sulphate polyacrylamide gel electrophoresis

Shh: sonic hedgehog

SLC2A1: glucose transporter member 1

SOD: superoxide dismutase

Stdev: standard deviation

Sv: Sievert

TBS-T: tris buffered saline-Tween 20

TFA: trifluoroacetic acid

TFIIH: transcription factor IIH

TZ: transition zone

UK: United Kingdom

UL: University of Leuven

US: United States

UV: ultraviolet

vs.: versus

wt: wild type

α – alpha

α-toco radical: α-tocopheryl radical

α-toco: α-tocopherol

β – beta

γ – gamma

Declaration

The work in this thesis is based on research performed at the Department of Biosciences, Durham University, England. No part of this thesis has been submitted elsewhere for any other degree or qualification and it is all my own work unless referenced to the contrary in the text.

Acknowledgements

I am deeply indebted to my supervisors Liz Ainsbury and Roy Quinlan. Thank you for giving me the opportunity to pursue a PhD, for the ongoing support, guidance and patience. Your input has been essential in my growth as an experimental scientist and strengthing my science communication skills. The past three years contained many incredible opportunities and a lot of challenges, and you were the epitome of supervisory team in providing the encouragement I needed. I am obliged to Public Health England, Durham University, EuroCellNet COST Action and Euratom research and training programme for providing the funds and research facilities to enable this project.

My sincere gratitude to Ian Cummins for teaching me the ins and outs of lipid mass spectrometry. Working with you has been extremely pleasant and the Biosciences department always felt brighter with you around. I hope this thesis venerates everything you taught me, *requiescat in pacem*.

Many thanks to Miguel Jarrin and Alexia Kalligeraki for familiarising me with the molecular biology techniques used in the RAQ laboratory and the intense scientific discussions. I am also thankful to the members of the Durham University Life Sciences Support Unit for their help with the animal work, and Joanne Robson and Tim Hawkins from the Durham Centre for Bioimaging Technology for their help with the imaging work. I would like to thank Robert Pal for training me to use the confocal laser scanning microscope and giving me access to his microscope for countless hours. In addition, thanks a million to Matthew Warren and Monika Jakimowicz for all their help with imaging the mice eye lenses and Boguslaw Obara for writing the Matlab code enabling cell density analysis of the images. I also appreciate Barry and Gary from Linden Burradon Food Supply for providing bovine eyes and Oliver Alainis for collecting the eyes countless times.

I am very thankful to all the members of the LDLensRad team and its partners for providing a pleasant and encouraging working atmosphere. Great thanks to Stephen Barnard and Jayne Moquet for their help with the irradiation of mice and bovine membrane extracts, and to Liz Ainsbury for her assistance with the statistics.

The age-related studies would not have been possible without Detlef Balschun and An Schreurs from the University of Leuven providing the mice, thank you for welcoming my ideas with so much excitement and to An Schreurs specifically for dissecting the hippocampus.

Warm thanks to Giancarlo Aldini and the members of School in Pharmaceutical Sciences at the University of Milan for welcoming me to their laboratory. Special thanks to Marco Mol for introducing me to the VC1 technology and showing me how to carry out OxyBlot, Genny Degani

for teaching me how to perform the VC1 pull down and Alessandra Altomare for lending a helping hand with the protein mass spectrometry and STRING analysis. Furthermore, I am very grateful for the assistance provided by Adrian Brown to facilitate all the protein work.

My sincere thanks to Irundika Dias for her warm reception to the Aston University and helping me to complete the lipid mass spectrometry work.

My deepest thanks to Letal Salzberg for reading a great deal of my written work and providing me with feedback on how to become a better writer without any obligation throughout the years.

I must express my heartfelt gratitude to my parents and siblings. The encouragement of my parents, Dina Nyirababirigi and Theophile Munyejabo, has been vital towards getting to this stage of my academic education, though most of all I greatly appreciate the six astonishing siblings you gave me. Aurore Mahoro, thank you for being the voice of reason when times are hard, Aline Nyirahumure for making me believe everything is still possible, Noela Umumararungu and Olivier Heerwegh for providing a second place to call home, Flavien Hirwa for keeping me grounded, Florent Mbabazi for your hidden wisdom and being my unofficial twin, and Brenda Uwinbabazi for being my cheerleader. Oma Denise en opa Wim Zeeuwe, een glimlach van jullie liet me altijd weten dat alles in orde komt.

Lastly, thank you to all the friends who supported me in all the ways they could: Marina Lamparter for always listening without judgement, An Schreurs for sharing and encouraging my passion for biochemistry, Weiju Wu for continuously checking up on me, Ileana Pirani for reminding me the finer things in life, Daniel Landes for your contagious tranquillity, Maureen Padden for showing me the value of integrity in the hardest times, Lily Bossin for your endless optimism during the last year and the Red Ramblers team for the many mind clearing walks and pub trips.

List of publications

Alice Uwineza, Alexia Kalligeraki, Nobuyuki Hamada, Miguel Jarrin and Roy Quinlan (2019). *Cataractogenic load – A concept to study the contribution of ionising radiation to the accelerated ageing in the eye lens.* Mutation Research - Reviews

Chapter 1: General Introduction

1.1. Ionising radiation in the human population

Awareness and understanding of radiation began in 1895 when Wilhelm Roentgen discovered X-rays. Since then, radiation has been heavily investigated and besides natural occurring radiation e.g. radioactive carbon-14 in living organisms and potassium-40 in bananas, man-made radiation sources have been developed for societal use such as nuclear energy and medical treatment. However, it also had its repercussions on human health including the crucial sense of sight. The transparent eye lens that refracts incoming light onto the retina in collaboration with the cornea is among the most radio-sensitive tissues in the human body (ICRP, 2007, Sievert and Failla, 1959).

1.1.1. What is ionising radiation?

Depending on the amount of energy carried by radiation, absorption of radiation by molecules can cause the movement of an electron to a higher energy orbital (excitation) or remove an electron from a molecule (ionisation) (Hall and Giaccia, 1973). The dividing line has been defined based on the amount of energy required to ionise water (H_2O), 1216 kJ/mol (Figure 1.1) (Brown et al., 2013). Radiation that carries more energy than 1216 kJ/mol is referred to as ionising radiation (IR) and radiation that is able to excite, but unable to ionise H_2O is called non-IR. Power lines, radios, cell phones, microwaves and visible light with long wavelengths are classified as non-IR (Figure 1.1). Although also non-ionising by definition, the higher spectrum of ultraviolet (UV) (around 150 nm wavelength) can induce IR-associated damage (Rendic and Guengerich, 2012). X-rays and γ-rays with short wavelengths are IR.

Given that IR can change the structure of atoms and therefore also the structure of the building blocks of the human body, it can be damaging to human health. Radioactive materials, which emit α, β, γ, X-rays and neutron radiation, are the sources of IR (Hall and Giaccia, 1973, Brown et al., 2013). Despite being unable to penetrate human skin, α-particles interact strongly with biomolecules and are a health hazard when ingested, e.g. Alexander Litvinenko was poisoned by polonium-210 (Scott, 2007).

β-particles, e.g. released by strontium-90 found in nuclear energy waste, can infiltrate a few layers into the skin (Jacobsen et al., 1958). However, similar to α-particles, most damage from β-particles occurs through internal contamination (Harrison and Stather, 1996). γ- and X-rays, both emitted by radon, can easily migrate through the human body and pose a serious external health hazard (Graupner et al., 2017). Emitted by nuclear fission or cosmic radiation, neutron radiation has the least ionising power. Although it cannot easily ionise biomolecules, neutron radiation renders other molecules radioactive (Hall and Giaccia, 1973).

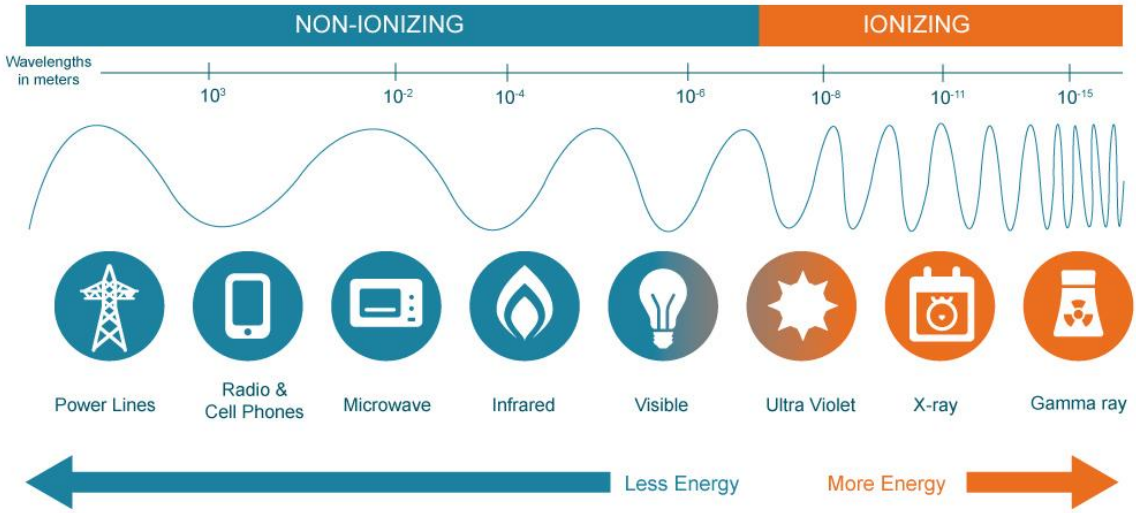

Figure 1.1: Diagram showing different sources of non-IR (power lines, radio and cell phones, microwaves, infrared and visible light) and IR (X- and γ- rays) used for the benefit of society. Non-IR sources have long wavelengths and thereby also less energy, while ionising radiation sources have short wavelengths and more energy. Although also non-IR by definition, the higher spectrum of ultraviolet (around 150 nm wavelength) can induce IR-associated damage. (Source Mirion Technologies website, 02/01/2020, used with permission of the company).

1.1.2. IR in everyday life and the societal benefits

IR is measured using two units, gray (Gy) and sievert (Sv). While Gy represents the absorbed dose by the human body, Sv is defined as the effective dose because it also accounts for the damaging level of the radiation type and the sensitivity of the exposed body part (Charles, 2001). Annually, each person on earth is exposed to natural background radiation of averagely 2.4 mSv per year (Charles, 2001) (Figure 1.2). The main sources of this natural background radiation are cosmic radiation, radioactive gases in the air, alimentation, radionuclides found in rocks and soil, and account for approximately 80% of the radiation each individual is exposed to (Mc Laughlin, 2015). The other 20% is from man-made sources used during medical treatment.

1.1.2.1. Medicine

In the medical field, non-IR and IR sources are used during diagnostics and therapeutics (Institute-of-Medicine, 1996). Non-IR are mainly used during diagnostics and applied external to the patient

i.e. magnetic resonance imaging and ultrasounds. Furthermore, in diagnostics, IR can be administered external or enteral. In radiology the core objective is to generate high resolution anatomical images and this is achieved by external administration of X-rays (Figure 1.2). On the other hand, radiopharmaceuticals that are injected into the human body and emit γ-rays are used in nuclear medicine, which aims to analyse physiologic functions.

Analogous to diagnostics, the use of IR in therapeutics is classified based on the whether the IR source is implemented inside or outside of the patient. In the radiation oncology medical field, cancer patients are treated with external X-rays and cobalt-60 γ-rays sources (Institute-of-Medicine, 1996). This is called teletherapy. Internal sources are used during brachytherapy and therapeutic nuclear medicine. Whilst in brachytherapy sealed sources of radionuclides, e.g. ceasium-137 and iridium-192, are placed specifically into the target tissue or body cavities, in the therapeutic nuclear medicine unsealed radionuclides, e.g. iodine-131 and strontium-89, are injected into the body and migrate to the desired tissue.

1.1.2.2. Security and safety

X-rays have been used to scan objects for a long time in airports. However, since 9/11 body scanners were gradually introduced to enhance airport security. These body scanner operate mainly based on backscatter X-rays, though also transmission X-ray system is applied to examine suspected smugglers (Vogel, 2010). Another way IR is used to assure security is the use of americium-241 in smoke detectors (Bramlet, 1978). This isotope emits α-particles which ionises the air between two electrodes inside a smoke detector, the presence of smoke interrupts this flow of current and therewith signals danger. Furthermore, X- and γ-rays are used to eliminate bacteria in food and extend its shelf life (Ravindran and Jaiswal, 2019), and to sterilise medical and laboratory equipment (Harrell et al., 2018).

1.1.2.3. Energy

With fossil fuels reserves decreasing, new sources of energy are in high demand (Armaroli and Balzani, 2007). Fission of uranium-235 in nuclear power plants producing low-carbon energy offers a solution to this request, while limiting the cost of energy production (Figure 1.2).

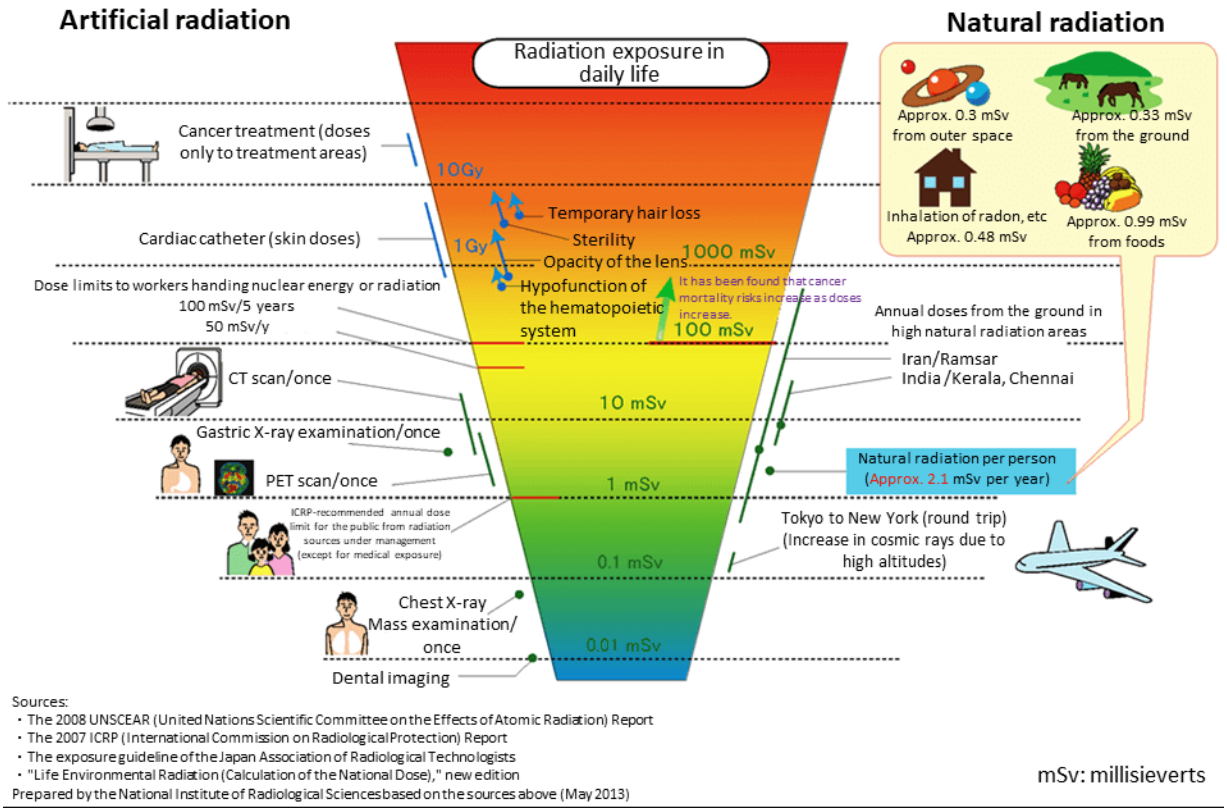

Figure 1.2: Sources of IR people are exposed to during their everyday life. Left side represents artificial radiation people are exposed to and the absorbed dose at each region is described in Gy, right side describes the natural background radiation and the effective dose a person is exposed to per year is illustrated in mSv. https://www.env.go.jp/en/chemi/rhm/basic-info/1st/02-05-12.html, 02/01/2020, used with permission of website owners.

1.1.3. Radioprotection principals

The negative effects of radiation exposure on health are wide-raging. The international commission on radiation protection (ICRP) classified these into deterministic and stochastic effects for the purpose of regulating exposure dose limits (Hamada and Fujimichi, 2014). Stochastic effects were defined as biological events arising as a function of dose without threshold (Beck, 1982). Effective dose limits were suggested to minimise the probability of these stochastic effects occurring and were based on the assumption that these manifest through a linear no-threshold dose-response model. Cancer development and hereditary diseases were included in this category (Walker et al., 1989). Deterministic effects, also called tissue reactions, were identified as detrimental biological

activities that vary with dose and are tissue-specific, but all appear only above a certain dose threshold (ICRP, 1991). The proposal of equivalent dose limits focused on preventing these tissue effects by establishing the dose threshold for individual organs and tissues including dose limits to avoid vision impairing cataracts in eye lenses (Stewart et al., 2012).

To minimise these negative radiation effects, the ICRP introduced three fundamental principles to ensure effective radiation protection (Do, 2016, ICRP, 2007). The principle of justification emphasises that every change applied in radiation exposure should have a beneficial impact, and the principle of optimisation highlights the levels of radiation should be kept as low as reasonably achievable, while also considering social and economic factors. For planned exposures, the principle of dose limit applies, meaning that no individual should be exposed to more than the ICRP recommended thresholds excluding during medical treatment.

1.1.4. Epidemiology of IR-induced cataracts

Cataract is the opacification of the eye lens which leads to a progressive decrease of the eyesight, and is the main cause of blindness in the world (Roodhooft, 2002) (Figure 1.3A). A small fraction of these cataracts is inherited and congenital, however most cataracts are a consequence of multiple factors and develop later in life (Graw, 2004, Shafie et al., 2006). The cataractogenic load is defined as the combination of the genetic factors, lifestyle choices and environmental processes such as IR that contribute to gradual cataract development (Uwineza et al., 2019). Based on the location in the lens where the opacities appear, cataracts are classified into nuclear, cortical and posterior subcapsular cataracts (PSCs) (Heyworth et al., 1993, Heruye et al., 2020) (Figure 1.3B, C and D). Progressive opaqueness appears at the centre of the eye lens in nuclear cataracts, while in cortical cataracts opacities are observed in the outer layers of the eye lens and clouding towards the back of the eye lens is noted in PSCs.

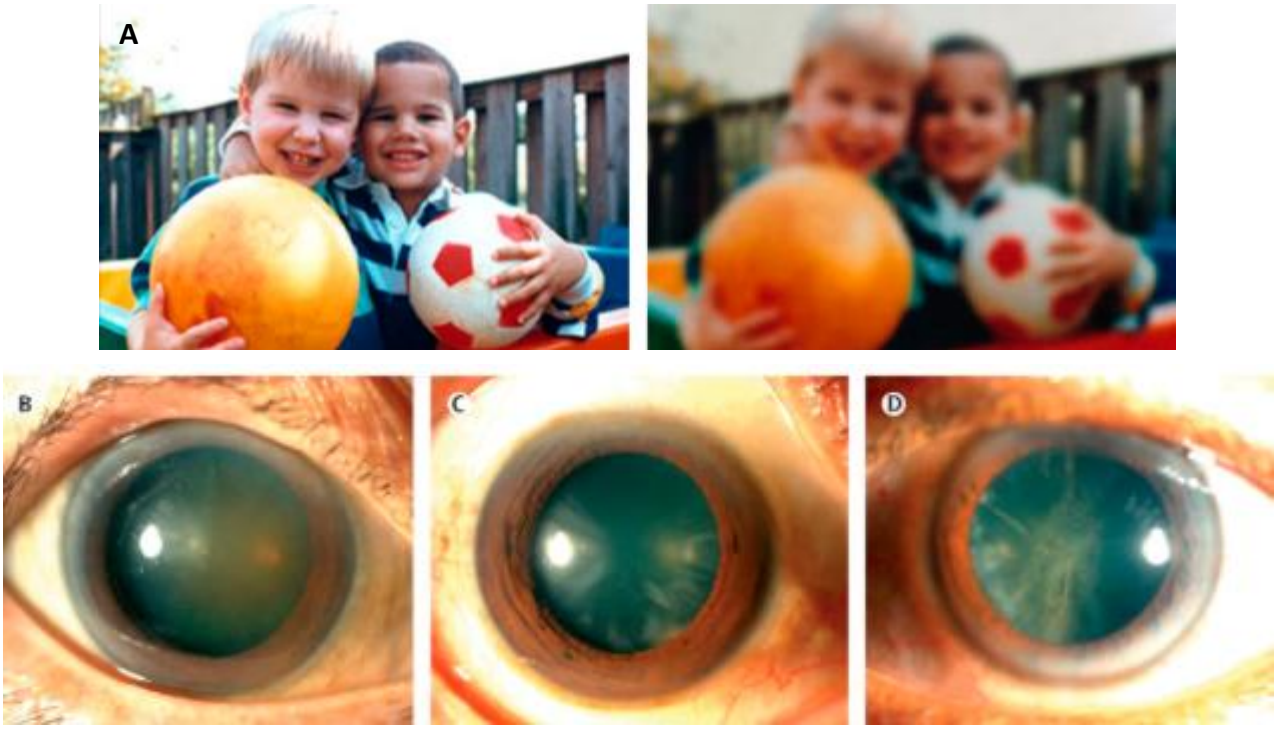

Figure 1.3: The clouding of the eye lens, also known as cataract, causes decreased vision. A) Left, image seen by a person with healthy eve lenses and right, the same image seen by a cataract patient. Cataracts are classified based on the location of where the clouding appears: B) in nuclear cataracts the clouding is observed at the centre of the eye lens, C) in cortical cataracts the loss of transparency appears in the outer layers of the eye lens and D) in poster subcapsular cataracts the clouding is identified at the back of the eye lens. Figure adapted from Heruye et al. *2020, Pharmaceuticals.*

Although IR caused enormous progress in the medical field (Figure 1.2), shortly after the discovery of radiation, the first IR-induced cataracts in humans were reported (Chalupecky, 1897). The first epidemiological data showing association between cataractogenesis and IR appeared in 1949 based on atomic bomb survivors and cyclotron workers (Cogan et al., 1949, Abelson and Kruger, 1949). Consequently, the ICRP recommended lens dose exposure limits (ICRP, 1955). Investigation of the prevalence of cataract in a cohort of radiation therapy patients showed that while patients exposed to radiation < 1.3 Gy did not develop cataracts, lens opacities were observed in patients acutely exposed to ≥ 1.3 Gy (Merriam and Focht, 1957). Therefore, cataracts were classified as tissue effects, i.e. cataracts only developed above a certain threshold and the severity increases in a dose-

dependent manner, with threshold for detectable lens clouding of 2 Gy for acute and 4 Gy for fractioned exposure (ICRP, 1991, ICRP, 2007, Edwards and Lloyd, 1998).

Reanalysis of the Merriam and Focht study showed that a limited cohort (20 patients) received a dose < 2 Gy, and that the monitoring time was 8 years post-IR on average, which only allowed the detection of early onset IR-induced cataracts (defined as < 10 years latency period, (Hamada et al., 2019)) (Shore, 2016). Further reinvestigation of other datasets, improved dosimetry systems and statistical analysis, animal experimental work and epidemiological studies focused on lower doses IR effects suggested a correlation between cataractogenesis and IR exposure at doses < 2 Gy (Ainsbury et al., 2009, Shore, 2016, Shore et al., 2010).

1.1.4.1. Atomic bomb survivors

Systematic ophthalmologic examination of 873 atomic bomb (A-bomb) survivors up to 55 years after exposure showed that IR-induced cataracts appeared as early and late onset effects (Miller et al., 1967, Choshi et al., 1983, Minamoto et al., 2004). This cohort included survivors who were < 15 years old at exposure and were exposed to doses < 2 Gy. Using a standardized opacity scoring system, they reported association between exposure to IR and cortical cataract and PSC at doses as low as 1 Sv in contrast to nuclear cataracts for which no link with IR exposure was observed. A long-term follow-up of non-cancer diseases in 10000 A-bomb survivors study showed higher prevalence of cataracts among these individuals over the period of 1958 - 1998 in comparison with the general Japanese population (Yamada et al., 2004). Using an updated data set, an upgraded dosimetry system and lens photographs analysed by a single ophthalmologist for better standardisation of cataract diagnosis, a threshold of 0.6 Sv was estimated for PSC and 0.7 Sv for cortical cataracts, both showing statistically significant association with IR in contrast to nuclear cataracts (Nakashima et al., 2006). Moreover, in the same study an inverse association between age at exposure and risk for PSC was observed. In 2007, a linear dose response with no threshold for IR-induced cataractogenesis was determined using a cohort of 3761 A-bomb survivors in which 479 surgical-cataract cases were documented (Neriishi et al., 2007).

1.1.4.2. Occupational workers

Chernobyl clean-up workers (n= 8600) examined 12 to 14 years after exposure revealed that 25% of the cohort developed cortical or subcapsular cataracts (Worgul et al., 2007). Dose reconstruction studies showed that 95% of these individuals were exposed to < 0.5 Gy γ-rays and β-particles (Chumak et al., 2007). Similar to Nakashima et al.'s study, this clean-up worker cohort showed that those exposed at a younger age were at a higher risk of developing catarats .

Astronauts, flight attendants and pilots are exposed to higher levels of cosmic radiation than the general public. Among 295 national aeronautics and space administration astronauts wearing a personal thermoluminescence dosimeter for total exposure dose estimation, higher prevalence of cataract was observed in astronauts exposed to doses > 8 mSv in comparison with those exposed to

lower doses (Cucinotta et al., 2001). During a follow-up study in which the IR dose was not mentioned, a computer software was used to compare lens images of 171 astronauts who went into space at least once to those that did not (n= 95) and 99 members of the military (Chylack et al., 2009). This showed an increased incidence of PSC among astronauts who went into space. A separate study analysing the occurrence of cataracts in aviation relative to space crew showed that although cataract incidence was higher among astronauts, the average age of onset was significantly lower in the United States (US) Air Force and Navy pilots (Jones et al., 2007). Interstingly, in a group of 445 commercial airline pilots nuclear cataracts were significantly elevated among pilots exposed to cosmic radiation compared to age-matched controls (non-pilots) (Rafnsson et al., 2005).

A long-term study in which of 35705 US radiation technologists were monitored by questionnaires over 19.2 years showed that their eye lenses were exposed to averagely 0.028 Gy (range 0.005 - 0.06 Gy). Although these doses were far short of the ICRP recommended threshold, an association between IR exposure and PSC and cortical cataracts was noted (Chodick et al., 2008).

1.1.4.3. Medical treatment

One of the initial reports showing association between medical treatment and low dose IR-induced cataract was in 1968 during which comparison of 234 children treated with X-rays for scalp ringworms to 232 children who did not receive X-rays treatment showed that minor opacities appeared earlier in the eye lenses of children exposed to 0.5 Gy (Albert et al., 1968). A group of 20 individuals treated with radium-226 for skin hemangioma in and around the eyelid at a mean age of 6 months were examined 30 - 45 years post-IR exposure for lens opacities (Wilde and Sjostrand, 1997). Dose-dependent PSC and cortical cataracts were observed with PSCs even appearing on sites that received estimated doses of 0.1 Gy. Later, a bigger cohort of 484 Swedish patients with skin hemangiomas treated with radium-226 and 89 controls showed that 37% of the cohort that received radiation therapy developed PSCs and cortical cataracts, while this was equal to 20% in controls at a mean age of 46 years (range 36 - 54 years) (Hall et al., 1999). Dose estimation suggest that the lenses of these skin hemangiomas were exposed to an average of 0.4 Gy γ-rays (range 0 - 8.4 Gy) (Lundell, 1994, Shore et al., 2010).

These epidemiological studies showing that doses of < 2 Gy are also linked to cataractogenesis encouraged the ICRP to report that the lens is among the most radiosensitive tissues in the human body. Moreover, they lowered the occupational equivalent dose limits for the lens from 150 to 20 mSv per year averaged over a 5 years period, with no single year exceeding 50 mSv (ICRP, 2007, Stewart et al., 2012). The ICRP currently recognises cataracts as tissue effects with a nominal threshold of 0.5 Gy independent of the dose rate (Figure 1.4). Following consultation, 20 mSv per year dose limit for the eye lens during occupational exposure was incorporated into European Union Basic Safety Standards (Mairs, 2016) and is still being considered elsewhere.

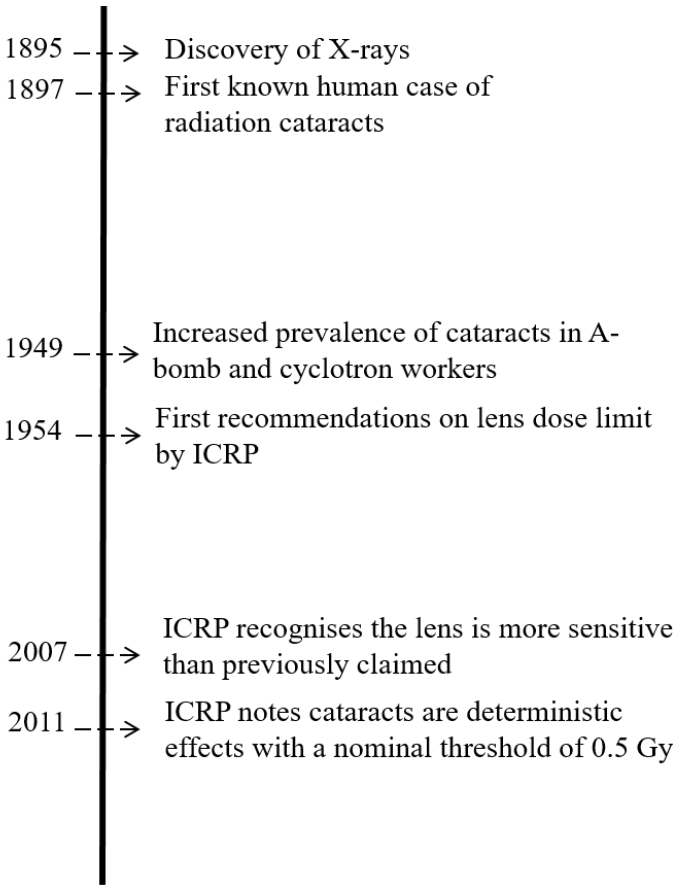

Figure 1.4: Timeline marking important moments in IR-induced cataract research.

1.1.4.4. Current development in radiation cataract epidemiology

Since the 2011 ICRP report, more studies with larger cohorts and longer follow-up time have been conducted in patients receiving medical treatment including radiotherapy and occupational workers.

The association between head and neck computed tomography (CT) scans and cataractogenesis was investigated in a cohort of 2776 Taiwanese patients with head, neck or brain tumours, aged between 10 and 50 years, who received one to four CT scans relative to a 27761 control group who did not undergo a CT scan (Yuan et al., 2013). Although the dose absorbed by the eye lens during a CT scan was unknown, estimated values for a head CT are 0.01 – 0.06 Gy depending on the protocol and equipment used (Michel et al., 2012). Analysis of 10-year follow-up data showed that cataract surgery and medication was more prevalent in the exposed group, and that the occurrence of

cataracts increased with number of CT scans. Childhood cancer survivors in the US with a mean age of 8.3 years at the time of treatment were followed-up during 21.4 years (Chodick et al., 2016). The eye lenses of these 13902 patients received on average 2.2 Gy (range 0 – 66 Gy) IR. Based on self-reports, a linear dose response was observed in the radiation exposed patients. Notably, this study reported that the latency period decreased with increasing dose. A total of 8221 thyroid cancer patients who were on average 43 years old when being treated, were followed up for 6 to 10 years (Lin et al., 2016). 69% were treated with iodine-131 and their eye lenses received an estimated dose of 0.06 Gy. No increased risk for cataract surgery was observed among the group treated with iodine-131. In comparison to other studies, this study has a limited incubation time and further follow-up would be interesting to verify if this lack of association continues.

Strikingly, during a nationwide study in France, 60% of the interventional cardiologist were found to exceed the occupational eye lens dose limit of 20 mSv per year. The eyes of these 106 interventional cardiologist and 99 age and sex-matched controls were examined to determine the cataract risk for interventional cardiologist (Jacob et al., 2013). The mean age of this cohort was 51 years and retrospective dose estimations indicated that their eye lenses were exposed to averagely 0.423 Gy (range 0.025 - 1.6 Gy). Results showed that the risk to develop PSCs was higher among interventional cardiologist compared to the control group. However, no association between IR and nuclear or cortical cataracts was noted. In China, 1401 radiographers exposed to a mean of 70 mSv (range 0 - 236 mSv) and 1878 unexposed workers were examined regularly by ophthalmologists as part of their employee medical program (Lian et al., 2015). The risk for PSC, cortical and mixed cataracts development was higher in the radiographers compared to the unexposed group, however, PSCs were the most widespread among the radiographers. A cohort of 67246 US technologists that absorbed an estimated cumulative dose of 0.0557 Gy (range 0.0236 - 0.069 Gy) over 5 years was examined for cataract risk with periodic questionnaires (Little et al., 2018), this study showed a clear association between IR exposure and cataract at doses < 0.1 Gy.

The first report showing an association between nuclear cataracts and IR in a large cohort was a study including 22377 occupational workers in the Mayak Production Association who received an annual eye examination for averagely 30 years (Azizova et al., 2016). Regrettably, the doses the eye lens were exposed to were unavailable (Khokhryakov et al., 2013). Hence, absorbed dose at a point of fixation of a radiation dosimeter on the body was used to estimate the dose. During a mean time of employment of 14 and 15 years, a cumulative dose of 0.46 and 0.54 Gy for female and male respectively was measured. The risk PSC, cortical and nuclear cataract showed a linear increase with dose (Azizova et al., 2018, Azizova et al., 2016). Furthermore, cataracts were more frequent among women than men.

Background radiation is generally perceived as low risk (ICRP, 2007). However, comparison of lens opacities in 479 high natural background radiation region residents with 462 people living in a low background radiation region in china showed that the prevalence of PSC and cortical cataracts was higher in the high natural background radiation region population (Wang et al., 2016a). At time of diagnosis, the average age of the examined group was 66 years. Lenses of people living in high natural background radiation region received a cumulative dose of 141 mSv, while this was 43 mSv in residents of low natural background radiation region population.

1.1.4.5. Sources of uncertainty in epidemiological data

Although epidemiological data offer a substantial amount of information, some aspects challenge the value of the data and render data comparison difficult. Some studies used cataract surgery as measure of vision impairment (Yuan et al., 2013, Lin et al., 2016, Neriishi et al., 2007), while others employed the lens opacity classification system to grade lens clouding (Merriam and Focht, 1957, Nirmalan et al., 2004). This grading was sometimes performed manually by a single or several ophthalmologists (Yamada et al., 2004, Nakashima et al., 2006), or automatically by Scheimpflug imaging (Birkeldh et al., 2015). Similarly, the dosimetry is not consistent between epidemiological investigations and in some reports this was self-reported. At low doses, the contribution of variations in dosimetry to uncertainty increases and the introduced errors could prevent the detection of a true event (Gilbert, 2009).

Collectively, all these epidemiological studies confirm that the eye lens is a radio-sensitive tissue and associate IR mainly with PSCs. Although in the past nuclear cataracts were not linked with IR-induced cataractogenesis, a recent study with a large cohort and long follow-up period suggests the contrary (Azizova et al., 2018). Moreover, the more current studies emphasise the need for further investigation concerning the classification of cataracts as tissue effects with no dose rate effect. Factors that affect radio-sensitivity of the eye lens such as sex and age at exposure warrant more attention (Hamada et al., 2019). However, only in combination with a profound understanding of the biological mechanisms underlying these IR-induced cataracts will epidemiological data facilitate the refinement of the current ICRP recommendations and possibly the development of novel therapies for IR-induced cataracts.

1.2. The eye lens

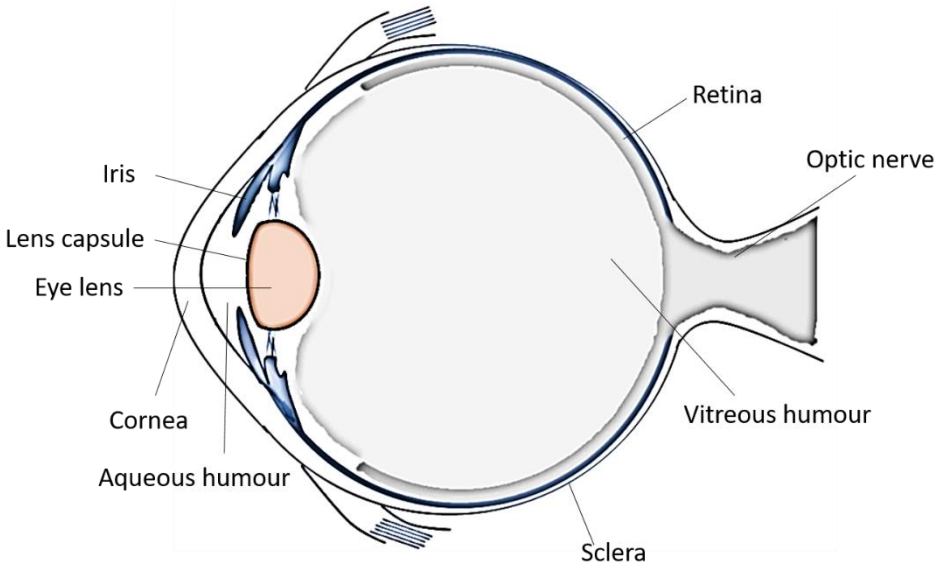

Figure 1.5: Diagram of the eye. Adapted from Uwineza et al. 2019, Mut. Res.

1.2.1. Anatomy and development

The eye lens is located between the cornea, sclera, aqueous humour on the anterior side and the vitreous humour and the retina on the posterior side (Figure 1.5). Cornea and sclera protect the eye from harmful components (Kolb, 1995), the aqueous humour maintains the intraocular pressure and contains nutrients for the surrounding tissue and the iris is a muscle that modifies the size of the pupil to regulate the amount of light entering the eye. The vitreous humour sustains the spherical structure of the eye. In collaboration with the cornea, the eye lens focuses incoming light onto the retina which translates this light into electrical signals. Through the optical nerve, these signals migrate to the brain and are translated into an image.

In humans, 4 to 5 weeks after fertilization (Carnegie stage 13 - 15) a lens vesicle is formed from the overlying ectoderm (Oguni et al., 1994, Hamilton, 1949, Pearson, 1980). Posterior lens epithelial cells (LECs) differentiate into primary lens fibre cells (LFCs) and fill the lens vesicle. Around 8 weeks post fertilization (Carnegie stage 21 - 22) lens vesicle formation is complete and lens polarity is established. During development, the cells in the LECs monolayer migrate from the

anterior surface towards the lens equator. Proliferation of these cells peaks in the germinative zone of the LECs layer, the daughter cells migrate and differentiate into LFCs (Rafferty and Rafferty, 1981, Srinivasan and Harding, 1965). This process is extremely active during prenatal development as a logarithmic increase in lens size is observed until soon after birth, thereafter the growth of the lens is linear (Augusteyn, 2007, McAvoy et al., 1991). The underlying mechanisms of this sudden decrease in proliferation are not fully understood.

To maintain transparency and elasticity, vital properties for the lens function, the LECs layer is covered by a capsule, a transparent basement membrane with collagens that contribute to the elasticity of the lens (Wormstone and Wride, 2011). Furthermore, after LECs have differentiated into LFCs, they internalise at the lens equator and elongate in the direction of the anterior and posterior poles, and pack uniformly as a result of their hexagonal structure (Pearson, 1980, Menko et al., 1984). Simultaneously, intracellular organelles are degraded leading to the formation of an organelle free zone (OFZ) in mature LFCs and highly organised crystallins fill the cytoplasm of these cells (Delaye and Tardieu, 1983). Throughout a lifetime, LFCs are not degraded, moreover the formation of new LFCs continues. The youngest LFCs are found in the cortex alongside the lens epithelium. The oldest cells are in the centre together with the primary LFCs in the core of the lens, which is known as the nucleus. Completely depleted of cell organelles, these cells have to be supplied with nutrients, ions and water. A circulation system established by gap junction, water channels and Na^+/K^+ pumps that removes waste at the lens equator and distributes ions and nutrients at the central anterior has been suggested (Donaldson et al., 2001, Mathias et al., 2010). Measurements with the ^{14}C bomb-pulse technique support the latter hypothesis given that younger water-soluble proteins were detected in the nucleus, together with older water-insoluble proteins (Stewart et al., 2013).

1.2.2. Physiology and metabolic activity

The lens is a closed, avascular system with limited protein and lipid turnover. To assure these proteins and lipids can last a lifetime, highly specialized systems are present in the lens:

Establishing the OFZ is necessary for transparency. However, this restricts transcription and translation to the lens epithelium and the outer layers of the cortex and minimizes the metabolic activity in the inner layers of the cortex and the nucleus (Zhu et al., 2010, Scharf et al., 1987, Dovrat et al., 1984). The LECs and outer LFCs are metabolically active and provide metabolic support to the rest of the lens (Donaldson et al., 2009). To enable this, cytoskeletal proteins optimise cell-to-cell organisation. Vimentin, beaded filament structural protein 1 and 2 (BFSP1/2) are the most highly expressed cytoskeletal proteins in the eye lens (reviewed by (Song et al., 2009)). BFSP1/2 help preserve the membrane organisation of LFCs and hereby also mediate the packing of LFCs (Sandilands et al., 2003). Defects in vimentin leads to aberrations in the shape and size of LFCs (Matsuyama et al., 2013), consequently disturbing the hexagonal structure required for transfer of

molecules between cells. Optimal cell-to-cell organisation permits cell-to-cell communication via connexins that form gap junctions for nutrient transport, AQP0 to establish water channels, and Na^+/K^+ pumps and K^+ channels to collectively generate a negative electromotive potential (Donaldson et al., 2017, Donaldson et al., 2001, Mathias et al., 2010). While cytoskeleton proteins maintain cellular organisation, crystallins safeguard intracellular organisation. Ninety percent of the proteins present in the lens are α-, β- and γ- crystallins (Sharma and Santhoshkumar, 2009, Hoehenwarter et al., 2006). The high concentration and tight order of these water-soluble, long-lived, proteins in LFCs is essential for the transparency and refractive index of the lens (Delaye and Tardieu, 1983). In addition to their structural activity, α-crystallins function as a molecular chaperone, preventing protein misfolding (Horwitz, 1992).

The functionality of these long-lived proteins can last a lifetime due to the various protective mechanisms that maintain a low oxidative stress environment in the lens. Firstly, the lens has low oxygen levels relative to other tissues (Brennan et al., 2012, McNulty et al., 2004). The levels of oxygen at the anterior side is 14 mm Hg and this gradually decreases across the lens (Helbig et al., 1993), oxygen levels < 8 mm Hg have been measured on the posterior side of human lenses (Holekamp et al., 2005). On the anterior side of the lens reside the cells that still have cell organelles; these consume 90% of the oxygen in the lens and hereby limit the oxygen levels in the other parts of the lens (McNulty et al., 2004). Secondly, the lens membrane provides protection through changes in the lipid composition over time (reviewed by (Borchman and Yappert, 2010)). Human lens membranes contain mainly the phospholipids phosphatidylethanolamine, sphingomyelin, dihydrosphingomyelin, and a high concentration of cholesterol (Talbott et al., 2000, Huang et al., 2005, Rujoi et al., 2003). The levels of dihydrosphingomyelin and cholesterol increase with age rendering the membrane more rigid and less permeable for oxygen (Plesnar et al., 2018, Huang et al., 2005, Mainali et al., 2017, Sargis and Subbaiah, 2006). Lastly, when oxidative stress penetrates through the lens, an extensive antioxidant system is present to combat this. This anti-oxidant system encompasses free-metal binding proteins; scavengers of free radicals including carotenoids, glutathione (GSH), vitamins C (ascorbic acid), vitamin E (tocopherol), thioredoxin, peroxiredoxins, GSH peroxidase, catalase, superoxide dismutase and GSH reductase; enzymes that mediate the synthesis of these anti-oxidants; and chaperone proteins and thioltransferases that limit aggregation of oxidized proteins (reviewed by (Brennan et al., 2012, Shang et al., 2001)). Tocopherol also provides a defense mechanism for the lipids.

1.3. Factors and mechanisms increasing the cataractogenic load

The efficiency of the protective mechanism declines with age and thus, oxidative damage builds up in cells. Most cell types break down the damaged biomolecules through upregulating the synthesis of nucleases, lipases, proteases and glycosidases, and processes such as autophagy and proteasome pathway (reviewed by (Dennis, 2015)). However, cells without a nucleus such as mature erythrocytes and LFCs in the OFZ can make only limited use of this (reviewed by (Uwineza et al., 2019, Kaestner and Minetti, 2017)). Erythrocytes are continuously replaced, in contrast to the LFCs that last for life (Mathieson et al., 2018). Therefore, over time, biomolecules in the lens accumulate damage (Figure 1.6). As a result, in the 5th decade of life, a large part of the human population develop presbyopia i.e. gradually lose the ability to focus on close objects (Weale, 1962, Glasser and Campbell, 1998).

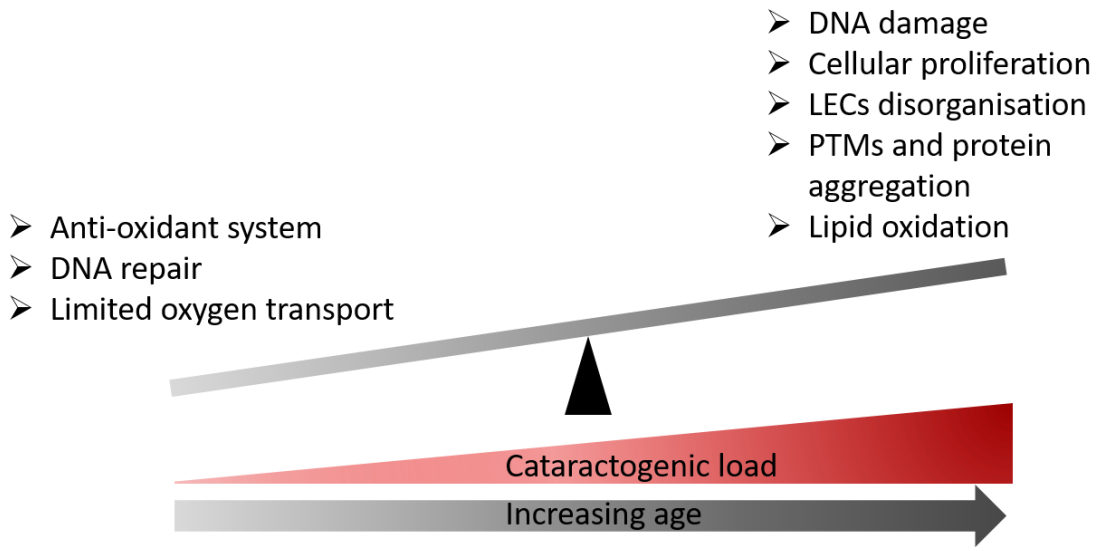

Figure 1.6: The cataractogenic load is defined as the combination of the genetic factors, lifestyle choices and environmental processes that contribute to gradual cataract development With age the protective mechanism in the eye lens (e.g. anti-oxidant system, DNA repair and limited oxygen transport) cannot tackle the damage occurring to the biomolecules (e.g. DNA damage, abberant cellular proliferation, disorganisation of LECs PTMs including protein aggregation and lipid oxidation), hence the cataractogenic load increases.

1.3.1. Damage to the lens epithelium

Deoxyribonucleic acid (DNA) damage can be repaired by non-homologous and homologous end joining, base and nucleotide excision repair, and mismatch repair (Hamada and Fujimichi, 2015, Kinsella, 2009). LECs express more than 92 genes involved in DNA repair (Wang et al., 2017b). With increasing age, their expression decreases and DNA damage accumulates (Figure 1.6). Accordingly, expression of the DNA repair gene methylguanine methyltransferase (*MGMT*), involved in the maintenance of genomic stability, was shown to be repressed through hypermethylation in the promotor region of the gene in lenses of people with age-related cataract (ARC) (Li et al., 2014a). Epigenetic studied also demonstrated that UVB light (1000 J/m^2), present in sun light, induced hypermethylation in the promotor region of the DNA repair gene *ERCC6* and therewith repressed its transcription (Wang et al., 2016b).

Correlatively, increased double stranded DNA breaks (DSBs) have also been measured in ARC lenses compared to transparent lenses (Schurman et al., 2012). On the cellular level, an age-related decrease in cell proliferation and cell density have been observed in the lens epithelium (Guggenmoos-Holzmann et al., 1989, Dawes et al., 2013). Furthermore, in older humans, the cellular organisation in the meridional rows is gradually lost (Wu et al., 2015).

1.3.2. Protein damage

Around the 5^{th} decade of life, an increasing amount of soluble proteins becomes membrane associated in the lens such as the age-dependent accumulation of α-crystallins on lens membranes (Borchman and Tang, 1996). Therewith, their chaperone activity is gradually lost and simultaneously a decrease in lens transparency is observed (Donaldson et al., 2017). Post-translational modifications (PTMs), including isomeration, racemisation and truncations, have been shown to be the cause of the observed insolubilisation and aggregation of crystallins (Michael and Bron, 2011, Yanshole et al., 2013). Some amino acids are intrinsically unstable and are subjected to spontaneous isomerisation, deamidation and racemisation (Zhu et al., 2018, Hooi and Truscott, 2011) (Figure 1.6). The site of these PTMs depends on the cellular environment, and secondary structure, tertiary structure and sequence of the amino acids (Fujii et al., 2018). The accumulation of all the aforementioned spontaneous PTMs in the long-lived lens proteins is associated to ARC (Lampi et al., 2014, Hooi and Truscott, 2011, Lyons et al., 2014). Although glycation of proteins and protein oxidation occurs at an order of magnitude lower than isomerisation, deamidation and racemisation (Truscott and Friedrich, 2016), they are also associated with ARC (Nagaraj et al., 2012, Truscott and Augusteyn, 1977, Smuda et al., 2015). The concentration of advanced glycation end products (AGEs) is very low in human non-cataractous and cataractous lenses (Smuda et al., 2015), and sample enrichment for these adducts is required to enable their investigation (Degani et al., 2017, Smuda et al., 2015) in contrast to isomerisation, deamidation, racemisation and protein oxidation which can be detected with standard enzymatic protein digestion and mass spectrometry

(Fujii et al., 2012). Furthermore, changes in metabolic activities such as age-related increase in calcium concentration can also contribute to increased PTMs in lens proteins (Tang et al., 2003a), e.g. culturing rabbit lenses in medium with high concentrations of calcium induced formation of high molecular weight proteins and lens clouding (Giblin et al., 1984). Besides crystallins, also PTMs in other proteins present in much lower concentration, such as calcium-induced aggregation of cytoskeleton (Clement et al., 1998), can also lead to cataractogenesis (Clark et al., 1999).

1.3.3. Lipid damage

The lipidome is a target for oxidative stress (Figure 1.6). Glycerophospholipids such as phosphatidylethanolamine are more prone to oxidation than sphingomyelin (Oborina and Yappert, 2003). Over time, glycerolphospholipids, lysophosphatidylethanolamines excluded, decrease simultaneously with the increase of sphingomyelin and dihydrosphingomyelin (Huang et al., 2005) and cholesterol (de Vries et al., 1991). In line with this, it has been hypothesised that over the years oxidized glycerophospolipids are broken down and replaced by sphingomyelins and cholesterol (Borchman et al., 2004). The presence of phospholipase A2 that is able to recognise oxidised lipid-induced modifications in membrane structure and eliminate these supports that hypothesis (Noordam et al., 1982). The impact of the increased levels of sphingomyelin and cholesterol has been debated. While some research groups have claimed that the augmentation of sphingomyelin and cholesterol in lens plasma membrane leads to light scattering because of the increased membrane stiffness (Huang et al., 2005, Tang et al., 2003b), others suggest a protective role due to decreased oxygen permeability of the membrane (Girao et al., 1999, Plesnar et al., 2018, Mainali et al., 2013). Supporting the latter claim is that increased levels of cholesterol oxidation products are associated with ARC (Girao et al., 1998).

Lipids and proteins do not function in an isolated system e.g. the age-related increase of sphingomyelins and cholesterol reduce the permeability of AQP0 (Tong et al., 2013). How the interactions between lens lipids and lens proteins are affected by the age-related changes is not fully understood.

1.3.4. Anti-oxidants

As mentioned before, the lens has an extensive anti-oxidant system (reviewed by (Pescosolido et al., 2016)). The efficiency of this anti-oxidant system declines with time due to the decreased expression of anti-oxidant enzymes and reduced levels of non-enzymatic anti-oxidants (Figure 1.6) (Giblin, 2000). Curiously, around the 4th decade of life the diffusion of the main anti-oxidant, GSH, from the cortex into the nucleus stops (Sweeney and Truscott, 1998). The formation of this glutathione barrier correlate(Eldred et al., 2011)s with increased protein oxidation in the lens nucleus observed in age-related nuclear cataracts (Sweeney and Truscott, 1998, Truscott and Friedrich, 2016).

1.3.5. Mechanisms underlying different types of cataracts

Cataract is a multifactorial disease (Uwineza et al., 2019). As mentioned above in section 1.1.4, based on the location the opaqueness appears, it is classified in PSC, nuclear and cortical cataracts (Heyworth et al., 1993). Nuclear cataracts are mainly caused by increased oxidative stress in the lens nucleus induced by the glutathione barrier that forms around the 4th decade of life (Sweeney and Truscott, 1998, Truscott, 2005). Increased protein oxidation leads to the accumulation of insoluble proteins and high molecular weight aggregates, this prevents the eye lens from focussing light on the retina by eliciting light scattering and loss of elasticity (Michael and Bron, 2011). The molecular basis of cortical cataracts is mostly associated with increased membrane permeability (Michael and Bron, 2011), which could be a consequence of lipid peroxidation (Girao et al., 1999, Mainali et al., 2015). With age, increased permeability to sodium and calcium dysregulates AQP0 water channels, Na^+/K^+ pumps and stimulates protein aggregation and proteolysis leading to light scattering (Németh-Cahalan et al., 2013, Michael and Bron, 2011, Borchman and Yappert, 2010). The molecular mechanism predominantly associated with PSCs is aberrant LFCs differentiation (Michael and Bron, 2011). Although each type of cataract has been chiefly associated with irregularities in specific biological processes, most aetiologies are interlinked with all cataracts e.g. abnormalities in the molecular and cellular organisation of the lens epithelium (Eldred et al., 2011). The type of cataract developed by individual depends on the cataractogenic risk factors individuals are exposed to during their lifetime.

1.3.6. Mechanism via which IR adds onto the cataractogenic load

A prime example of environmental factors contributing to cataractogenic load is IR (Uwineza et al., 2019). Epidemiological data have clearly shown an association between cataract and IR (Shore et al., 2010). Moreover, this data suggest that the lens cortex is more affected by IR than the lens nucleus, IR dose is inversely correlated with latency period, and sex- and age-dependent response to IR (Hamada et al., 2019). While in the past the main focus was on the aftermath of horrible events such as Chernobyl and the A-bomb, currently, research chiefly concentrates on the effects of occupational and medical exposures (Azizova et al., 2016, Little et al., 2018). Understanding the underlying biological mechanisms is a vital component of being able to assure good working conditions for occupational workers and safe medical treatment for patients. In this section an overall introduction to known mechanisms underlying IR-induced cataracts is provided. Further details of these mechanisms are presented in the associated results chapter.

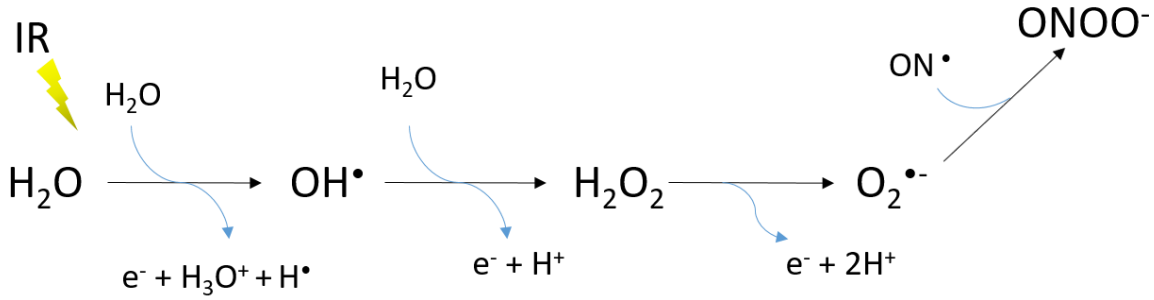

Figure 1.7: Water radiolysis occurs when water is exposed to IR, this leads to the formation of free radicals such as the reactive oxygen species hydrogen radical ($H^{\bullet}$), ionized water (H_3O^+), hydroxyl radical ($^{\bullet}OH$), hydrogen peroxide (H_2O_2) and superoxide ($O_2^{\bullet-}$) and reactive nitrogen species e.g. peroxynitrite anion ($ONOO^-$).

1.3.6.1. Direct and indirect damage induced by IR

IR can induce direct and indirect damage to macromolecules in cells. Direct damage entails immediate ionisation of macromolecules such as the breakage of chemical bonds, while indirect damage in the cell results primarily from water radiolysis inducing the formation of free radicals, therewith increasing oxidative stress (Reisz et al., 2014). X-rays and γ-rays mainly induce indirect damage (Hall and Giaccia, 1973). In cellular environment, they react with water to generate ionized water (H_3O^+), hydrogen radicals ($H^{\bullet}$), electrons (e^-) and highly reactive hydroxyl radicals ($^{\bullet}OH$) (Singh and Singh, 1982). Subsequently, other reactive oxygen species (ROS) products, hydrogen peroxide (H_2O_2) and superoxide ($O_2^{\bullet-}$) are formed (Figure 1.7). Besides ROS, also reactive nitrogen species (RNS) are formed in the cell. These species arise from reactions such as $O_2^{\bullet-}$ interacting with intracellular nitric oxide ($^{\bullet}NO$) to form peroxynitrite anion ($ONOO^-$) (Figure 1.7) (Darley-Usmar et al., 1992). The formation of ROS and RNS occurs within picoseconds, and the reaction of these radicals with proteins, DNA and lipids can create more reactive molecules (Reisz et al., 2014).

1.3.6.2. DNA damage

As mentioned before, although UV is classified as non-ionising, the higher spectrum of UV can act similar to IR and induce damage (Rendic and Guengerich, 2012). Using the alkaline elution technique (Koch and Giandomenico, 1994), DNA damage in rabbit LECs after exposure to UVA (180 kJ/ m^2) demonstrated that UVA exposure induced single stranded breaks (SSBs) in rabbit LECs in a linear dose-dependent manner (Sidjanin et al., 1993). Interestingly, after 4 h, 80% of the SSBs were repaired. γH2AX, RAD51 and 53BP1 are proteins involved in the repair of DSBs and are therefore used as markers of DSBs. Measurement of γH2AX and RAD51 levels in X-ray (0.140 - 2.28 Gy) exposed fetal human lens-124 (FHL124) cell line showed a linear dose response 1 h post-IR (Markiewicz et al., 2015). In contrast, exposure of human lens epithelial cells 1 (HLEC1) to 0.025 - 1.5 Gy X-rays showed an exponential increase in DSBs 30 min after IR-exposure (Hamada, 2017). However, this damage did not persist as 48 h post-IR the amount of 53P1 foci were back at baseline levels. Furthermore, IR-induced DNA damage was also observed in LECs *in vivo*. Whole body exposure of C57BL/6 mice to 0.5, 1 and 2 Gy γ-radiation showed a linear dose response at 4 and 24 h post-IR for 53BP1 foci per cell. However, the steepens of the linear dose response curve was lower at 24 h than at 4 h (Barnard et al., 2019). Markiewicz *et al.* also observed a linear increase of DNA damage with dose after exposing C57BL/6 mice to 0.02, 0.1 and 1 Gy X-rays and measuring γH2AX foci formation (Markiewicz et al., 2015). At 24 h post-IR, γH2AX foci levels were back to the same levels as in unexposed mice. Taken together, these studies suggest that although IR-induced SSBs are quickly repaired, DSBs persist longer in the lens epithelium (Figure 1.8).

1.3.6.3. Aberrant gene expression

The increase of oxidative stress in HLECs by adding H_2O_2 induced changes in gene expression including the upregulation of the N-Myc downstream regulated gene2 (Ndrg2) protein expression (Zhang et al., 2011). This protein mediates cellular processes such as proliferation and differentiation. Direct evidence of IR triggering modifications in gene expression has been produced by exposing HLECs and differentiating human LFCs to doses up to 4 Gy (55 mega-electrovolt/ atomic mass unit of protons) (Chang et al., 2007). Real time quantitative polymerase chain reaction showed the downregulation of matrix metalloproteinases (MMPs) within 1 h post-IR in HLECs while no changes were observed in the expression of MMPs in human LFCs, which shows that IR-induced changes in the eye lens are cell type specific.

1.3.6.4. Protein damage and misfolding

Increased levels of crystallin water-insoluble aggregates is a phenotype associated with cataractogenesis (Figure 1.8) (Truscott and Friedrich, 2016, Giblin et al., 1984, Lund et al., 1996). Exposure of purified bovine α-crystallin to 1-50 J/ cm^2 UVC induced its oxidation and racemisation, and reduced its chaperone activity (Fujii et al., 2004). The secondary structure of α-crystallin was also affected given that with increasing dose a gradual loss of β-sheets was observed. Liquid

chromatography mass spectrometry (LC-MS) of 5 Gy γ-irradiated rabbit lenses showed that IR caused an increase in oxidised γ-crystallin levels in the water soluble and water-insoluble fractions. The identified oxidised sites were similar to the ones detected in ARC (Kim et al., 2015). The influence of lower doses of IR on lens proteins still has to be investigated.

1.3.6.5. Lipid damage

Research on IR-induced lipid damage in the lens is quite sparse. Given that increased cholesterol oxides have been associated with ARC compared to their age-matched controls (Girao et al., 1998) and IR-induced oxidative stress can oxidise the lipids in lens plasma membranes (Pamplona, 2008, Halliwell and Gutteridge, 1986), it is reasonable to suggest that this is a possible biological mechanism leading to the development of radiation cataracts (Figure 1.8).

1.3.6.6. Downstream effectors

The above mentioned damage to macromolecules and gene expression are accompanied by unfavourable downstream effects stimulating the increase of the cataractogenic load (Uwineza et al., 2019).

At a cellular level, IR has been shown to induce changes in the proliferation, organisation, differentiation and migration of LECs (Ainsbury et al., 2016, Hayden et al., 1980). Irradiation of eye lenses caused disorganisation of the meridional rows (Hayden et al., 1980) and aberrant differentiation of the cells (Worgul et al., 1989) in the lens epithelium. However, the noted responses of LECs proliferation and differentiation to IR exposure were quite variable depending species, dose, age at exposure and region in the lens epithelium being studied (Hanna and O'Brien, 1963, Von Sallmann et al., 1955, Markiewicz et al., 2015).

Exposure of human LECs (HLECs) immortalized with simian virus40 T antigen (SRA01-04) to 50 μM H_2O_2 induced morphological changes three days post-exposure (Zhang et al., 2011). These alterations included the accumulation of granular cytoplasmic inclusion, cell enlargement and flattening. Time-lapse imaging after exposure of the same HLECs cell line to UV (up to 10 mJ/ cm^2) showed that at 12 h post-exposure the UV-irradiated cells exhibited morphological features of apoptotic cells including disruption of the plasma membrane and chromatin condensation, and also of necrotic cells such as swelling of the nucleus and cell body (Haines et al., 2013). IR also causes morphological changes in the lens epithelium layer by decreasing the amount of cells (Markiewicz et al., 2015) and eventually, in the entire eye lens by inducing lens clouding (Worgul et al., 1989).

Genomic instability, i.e. increased probability in genetic alterations during the lifetime of a cell (Shen, 2011), is another downstream effector of IR-induced damage to the biomolecules in the lens. IR-induced DNA damage of LECs in the germinative zone (Markiewicz et al., 2015) can be transferred to their progeny cells, thereby possibly affecting their proliferation and differentiation capacity. Moreover, oxidative stress triggered by IR has been shown to contribute to genomic

instability in other cell types such as bone marrow and ovary cells (Clutton et al., 1996, Limoli et al., 2001). Similarly, IR-induced oxidative stress could contribute to genomic instability in lens cells. In line with this, oxidative stress-induced DNA damage has been observed in LECs of cataractogenic lenses (Osnes-Ringen et al., 2016). Another possible mechanism through which IR could induced genomic instability is lipid peroxidation, reactive oxygen species produced via lipid peroxidation have been shown stimulate spontaneous DNA damage (Tappel, 1973).

Non-irradiated cells displaying traits of their neighbouring irradiated cells is defined as radiation-induced bystander effects. This phenomena was observed in cell types other than lens cells, and has been shown to occur through intercellular communication via gap junctions, extracellular vesicles and release of signalling molecules such as cytokines and free radicals (Kadhim et al., 2013, Hamada et al., 2011, Ainsbury et al., 2016). Although radiation-induced bystander effects have not been demonstrated yet in LECs or LFCs, the processes involved are present in the eye lens and could be contributing to radiation cataracts.

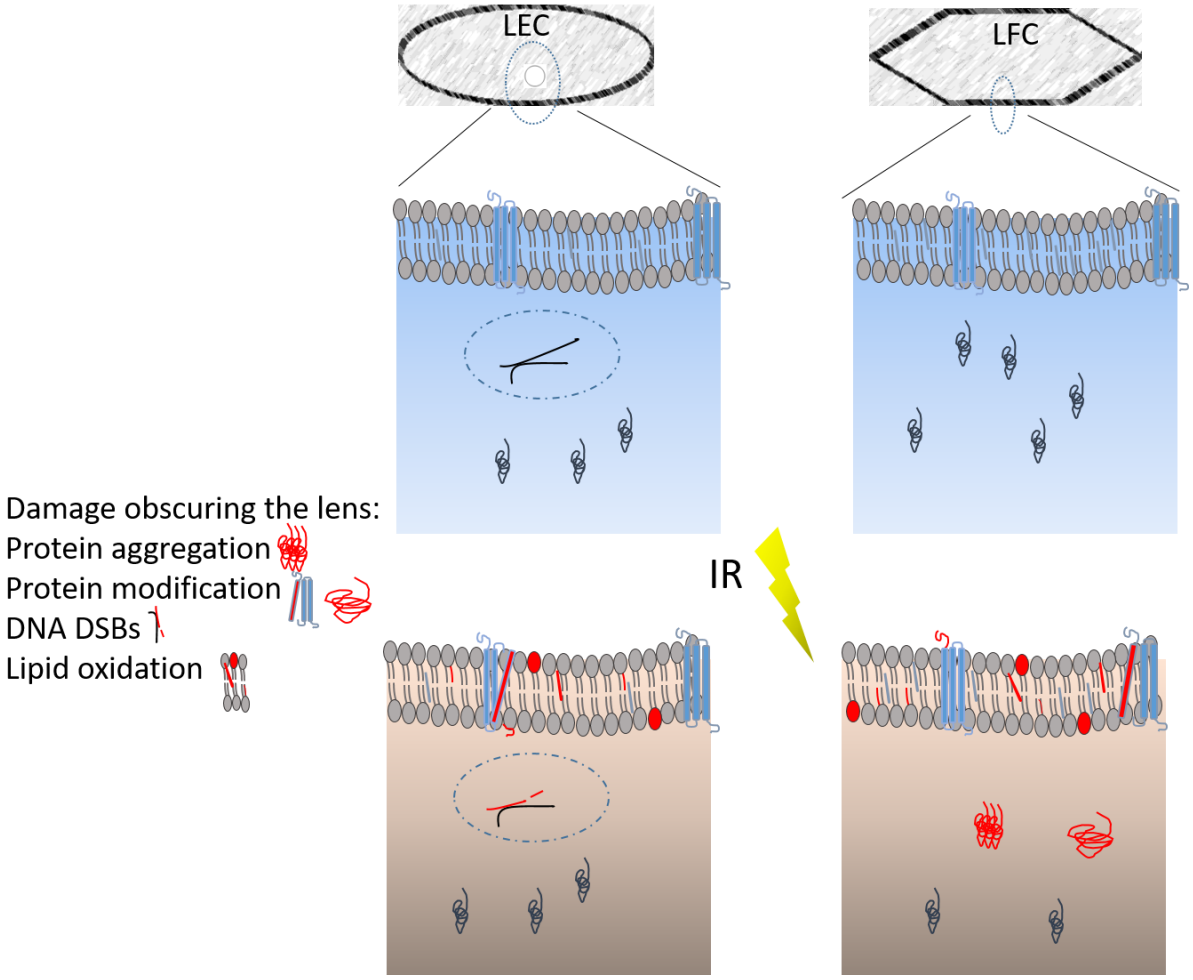

Figure 1.8: Mechanisms through which IR can induce damage to biomolecules in the lens. DNA DSBs, protein modification and aggregation have been detected in irradiated LECs cell lines and eye lens tissue post-IR exposure. Lipid oxidation has not been studied yet in this context. IR: ionising radiation, DSBs: double stranded breaks (Modified from Uwineza et al., 2019, Mut. Res.).

Ultimately, the occurrence of these modifications in the lens depends not only on IR, but also on the genetics, lifestyle and other environmental factors. The level of contribution of each factor to the cataractogenic load is different for each individual. Studies with mononzygotyic human twins raised under different environmental factors showed that these affect aging and lifespan (Fraga et al., 2005, Talens et al., 2012). Genetic factors mediate approximately 30% of our lifespan (Cournil and Kirkwood, 2001), the other 70% depends on lifestyle and environmental factors such as

smoking, exercise and place of habitation (Timmers et al., 2019, Wang et al., 2016a, Csiszar et al., 2009). These factors can induce epigenetic changes (Fraga et al., 2005), affect the levels of oxidative stress in the human body (Csiszar et al., 2009), and therefore accelerate or slow down ageing.

Chapter 2: Aims of the project

Cataracts are the main cause of blindness in the world (Roodhooft, 2002). The aetiology of cataracts is multifactorial and not fully understood. To encapsulate this, the term cataractogenic load has been redefined as the damage to proteins, lipids, nucleic acids and metabolic activity that occurs as a consequence of genetic, lifestyle and environmental factors (Uwineza et al., 2019). Ionising radiation (IR) is one of these factors and is predominantly associated with posterior subcapsular cataracts (Ainsbury et al., 2009, Shore, 2016, Shore et al., 2010, Uwineza et al., 2019). Mainly based on epidemiological data, the international commission for radiation protection reduced the occupational equivalent dose limits for the lens from 150 to 20 mSv per year averaged over a 5 years period, with no single year exceeding 50 mSv (Stewart et al., 2012). Moreover, IR-induced cataracts were defined as tissue effects with a nominal threshold of 0.5 Gy independent of the dose rate. Recent epidemiological data suggest that this threshold might be lower (Azizova et al., 2018, Hamada et al., 2019, Little et al., 2018). The biological mechanisms involved in IR-induced cataractogenesis are largely unclear. Therefore, the EU CONCERT LDLensRad project was initiated to work towards a better understanding of low dose IR-induced cataracts. For this, research groups from Durham University, Public Health England, Helmholtz Zentrum München, Italian National Agency for New Technologies, Energy and Sustainable Economic Development and Oxford Brooks University collaborated to unravel the underlying biological mechanisms and to determine whether the lens model could be used as a biomarker for early low dose IR effects. This thesis work was executed as part of LDLensRad and had the following objectives:

2.1. Aim 1: Study IR-induced cell density changes

Several research groups showed that females of the human species are more radiosensitive than their male counterpart (Azizova et al., 2016, Chodick et al., 2008). Moreover, lower doses have been associated with longer latency period (Chodick et al., 2016) and an inverse correlation between dose rate and double stranded breaks in the lens epithelium has been reported (Barnard et al., 2019). To gain more insight in how sex, dose, dose rate, genetic background and genetic mutations affect radiosensitivity, multiple strains of male and female mice were exposed to various doses and dose rates. Subsequently, their eye lenses were collected at different time points post-IR and changes in cellular organisation and cell density of the lens epithelium were examined. To ensure the full range of lens epithelium regions was analysed, from the central zone to the meridional rows, and to allow comparison between these different regions, relative cell densities (defined as normalised cell number/ segment) were determined and profiles of normalised cell numbers across the lens epithelium were plotted. This experiment was performed with multiple strains, wild type and mutants, to study the influence of genetic background on IR-sensitivity.

2.2. Aim 2: Test hypothesis of IR-induced cholesterol oxidation *in vitro* and *in vivo*

The lens plasma membrane is among the most cholesterol enriched membrane in the human body (Borchman and Yappert, 2010, Mainali et al., 2017). Furthermore, cholesterol oxides were shown to accumulate in eye lens of patients with age-related cataracts compared to their age-matched controls (Girao et al., 1998). Therefore, it was hypothesised that IR-induced oxidative stress leads to cholesterol oxidation and that the gradual accumulation of cholesterol oxidation adducts caused lens opacities. First, this was examined *in vitro* by exposing bovine lens membrane extracts to IR and studying cholesterol oxidation adducts via lipid chromatography followed by mass spectrometry (LC-MS). Secondly, to verify whether the findings *in vitro* also occur *in vivo,* mice were exposed to IR and their eye lenses were studied for changes in cholesterol and cholesterol oxides levels.

2.3. Aim 3: Comparison of age-related cholesterol oxidation changes in the eye lens and hippocampus

With approximately 25% of the total cholesterol in the human body, the brain is the tissue with the highest concentrations of cholesterol (Dietschy, 2009). To study whether the age-related changes in cholesterol and cholesterol oxides levels observed in the eye lens are correlated with those occurring in the brain, 6 and 30 month- old murine hippocampus and eye lenses were collected for cholesterol and oxysterols analysis via LC-MS.

2.4. Aim 4: Examine the protective role of anti-oxidants in IR-induced lens membrane damage

The lens has an extensive anti-oxidant system (Brennan et al., 2012), which could provide the lens with a protection mechanism against IR-induced oxidative stress. To study this, non-enzymatic anti-oxidants were added to bovine lens membrane extracts pre- and post-IR exposure and the levels of oxysterols were measured. Furthermore, to study the mechanism through which α-tocopherol performs its anti-oxidative function, a membrane binding experiment with bovine membrane extracts and α-tocopherol-d6 was conducted.

2.5. Aim 5: Investigate the influence of IR in lens membrane proteins

Lastly, the effect of IR on lens membrane proteins was examined using sodium dodecyl sulphate polyacrylamide gel electrophoresis (SDS-PAGE), OxyBlots and immunoblots. A focus was put on advanced glycation end products (AGEs) given that the accumulation of these has been reported in human age-related cataracts (Smuda et al., 2015) and non-IR has been shown to induce their formation in lens proteins (Prabhakaram and Ortwerth, 1992). IR-induced modifications in the levels of AGEs in bovine lens membrane extracts were studied using LC-MS and the novel VC1-pull down method (Degani et al., 2017).

Chapter 3: Materials and Methods

3.2. Objectives

The methodologies used for studying alterations in lens epithelium cell density, cellular organisation and proliferation as a consequence of IR, the influence of IR on cholesterol oxidation in bovine lens membrane extracts, modification in oxysterol levels *in vivo* after IR exposure, age-related changes in oxysterol levels in hippocampi and eye lenses, the effect of anti-oxidants on IR-induced oxysterol formation, and whether the concentration of advanced glycation end products in bovine lens membrane extracts is affected by IR are all presented in this chapter. The individual results chapters refer to specific section in this chapter in which the materials and methods used to address their research question are presented in detail.

3.3. Animal maintenance

3.3.1. Ethical approval

The experiments were performed according to the Council Directive 2012/707/EU (of 14/11/2012), regarding the protection of animals used for experimental and other scientific purposes. All work was carried out under specific authorizations for personnel, establishment and animal facility licenses. Every person handling animals holds a special permission/license from the independent local governmental administration:

- Durham University (DU): C57BL/6J mice were bred and housed in the life sciences support unit (LSSU). The experimental procedures involving these mice were performed according to the UK Animals (Scientific Procedures) Act 1986, and ethical approval was obtained from the United Kingdom Home Office and the local Animal Welfare and Ethical Review Body at DU.
- Public Health England (PHE): Female mice C57BL/6JOla/Hsd (C57BL/6J) were obtained from Envigo RMS (UK) Ltd. (Blackthorn, Bicester, Oxfordshire OX25 1TP) and received standard care at PHE. Similar to DU, the conducted experiments followed the UK Animals (Scientific Procedures) Act 1986, and ethical approval was acquired from the United Kingdom Home Office and the local Animal Welfare and Ethical Review Body at PHE.
- University of Leuven (UL): C57BL/6J mice were locally bred. The housing conditions and procedures performed with the hippocampus and eye lenses were approved by the KU Leuven Ethical Committee (P203/2012) and in accordance with European Directive 2010/63/EU.
- Helmholtz Zentrum München (HMGU): B6C3F1 mice were housed in the German Mouse Clinic according to the German Law of Animal Protection, the ARVO Statement for the Use of Animals in Ophthalmic and Vision Research, and the tenets of the Declaration of Helsinki (approved by the government of Upper Bavaria ROB-55.2-2532.Vet_02-16-80).
- Italian National Agency for New Technologies, Energy and Sustainable Economic Development (ENEA): housing and experimental procedures performed with CD1 and C57BL/6J mice followed the Directive 2010/63/EU of the European Parliament on the protection of animals used for scientific purposes and were approved by Institutional Animal Care and Use Committees of ENEA.

All animals were fed *ad libitum* and received standard care including social housing at constant temperature.

All animal work carried out at DU, UL, PHE, HMGU and ENEA followed the 3Rs principals:

- Replacement: The development of cataract cannot be studied in cell lines. Therefore, living mice were irradiated and examined post-mortem. The time points, doses and dose rates implemented during the cell density mouse experiments were chosen based on *in vitro* investigations.
- Reduction: The experimental aspects of this proposal have been carefully planned to maximise the amount of information that will be forthcoming while minimising the number of mice needed.
- Refinement: Where possible, power analysis for each experimental endpoint has been carried out by experienced statisticians to ensure that sufficient mice will be available for statistical significance. Skilled experimentation also allowed optimal use of the animals.

3.3.2. Cholesterol oxidation work

Bovine eyes were obtained from Linden Burradon Food Supply (FSA approved Scientific Research Material collection No. 2056). The cows lived on farms in the United Kingdom (UK) and were sacrificed to provide meat for human consumption.

Mice tissues were collected at various collaborating institutions. Brain and eye lens tissues were harvested at DU and UL. Collaborators at PHE provided snap frozen IR-exposed eye lenses.

3.3.3. Cell density work

Samples received for this work were from HMGU and ENEA in accordance with the EU CONCERT LDLensRad project scheme.

3.4. Hoechst staining and Ki-67 immuno-labelling of LECs

3.4.1. Dissection of the eye lens

The mice were sacrificed by cervical dislocation, eyes were surgically removed (Figure 3.1). To fix the tissue, a small incision around the optic nerve was made and the lenses were submerged in 4% paraformaldehyde (PFA) (Sigma/ Merck, UK) in phosphate buffered saline (PBS) (VWR, US) (for 1 h 30 min. Subsequently, they were washed three times with PBS for 10 min and stored at 4 °C. To isolate the eye lenses, a deep incision around the optic nerve was made and the vitreous fluid removed utilizing a dissection microscope (Leica, Germany).

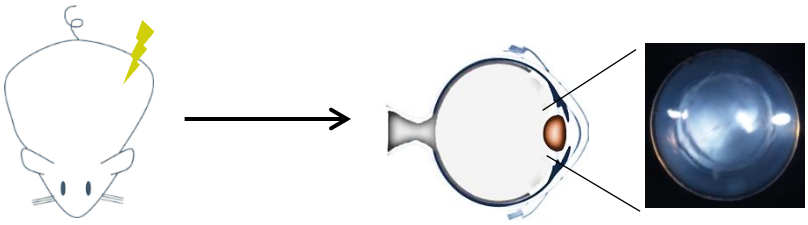

Figure 3.1: After the exposure of mice to IR, eyes were removed and fixed with PFA. Subsequently, the eye lenses were isolated for further experimentation.

3.4.2. Generating flat mounts

With the help of a dissection microscope (Leica, United Kingdom), the eye lens was orientated with the anterior region facing the surface of the microscope slides. With micro scissors (Sigma, UK), a cross cut was made in the capsule at the posterior region and using forceps (Sigma, UK) the capsule with the adherent LECs were peeled of the remaining of the lens. To create a water-repellent barrier around the tissue on a microscope slide (Agar Scientific, UK), a circle was drawn around the capsule using a hydrophobic barrier pen. The lens epithelium was submerged in PBS and stored in a wet chamber at 4 °C.

3.4.3. Whole mount Hoechst staining

The eye lenses were washed one time with PBS for 5 min and subsequently stained with 1 in 50 dilution in PBS of 10 mM Hoechst 33342 (Thermo Fisher Scientific, US) dissolved in 100% ethanol (Merck, United Kingdom) for 45 min under gentle agitation. After washing the eye lenses three times with PBS

for 10 min, these were visualized with the confocal laser scanning microscope (CLSM) (Leica, Germany) using a 10x dry objective.

3.4.4. Double staining: Hoechst and Ki-67

The staining of flat mounted LECs was performed on a microscope slide in a wet chamber while whole mount staining was performed in Eppendorf tubes (Starlab, UK). The LECs were permeabilised with 0.5% (v/v) Triton-X 100 (Sigma, UK) in PBS for 30 min at room temperature (RT) and incubated in 1% (w/v) bovine serum albumin (BSA) (VWR, US) and 0.05 % (v/v) Triton-X 100 diluted in PBS for 1 h. After this blocking step, conjugated Ki-67 antibody (SolA15, Thermo Fisher Scientific, United States (US)) at 1 in 500 dilution in PBS was added to the samples and incubated for 45 min at RT. The samples were washed three times with PBS for 10 min followed by staining them with a 1 in 50 dilution of 10 mM Hoechst 33342 (Thermo Fisher Scientific, US) for 45 min. As a last step, the samples were washed with PBS for 10 min three times. These samples were imaged using the 63x oil objective on the CLSM for flat mounts and the 10x dry objective for whole mounts.

3.4.5. Analysis of cell density with MATLAB

Images acquired with the CLSM were exported from the LAS X software as TIFF file. Using Image J, the individual images were assembled into a z-stacked image. Subsequently, an in-house developed Matlab program was used to calculate the relative cell density changes between the central zone and the meridional rows (Figure 3.2; code see appendix 1):

3.4.5.1. Nuclei detection

Using a Gaussian kernel defined by the radius, the z-stacked image was converted into a likelihood 3D map of Hoechst 33342 signal maxima (nuclei). Subsequently, the position of each nucleus was estimated using grayscale morphological dilation of the image. The dilation process entailed gradually enlarging the boundaries of regions of foreground pixels while holes within those regions became smaller. This allowed to assign the maximal pixel value detected over the neighbourhood of a Hoechst 33342 signal defined by the spherical shape and the radius to a nucleus. The spherical shape and Hoechst 33342 signal threshold was defined by the user and required to be redefined for each image to ensure maximal detection of all Hoechst 33342 stained nuclei.

3.4.5.2. Region of interest analysis

To calculate the relative cell density, the user defined the starting point (in the central zone) and end point (top of the meridional rows) of the region of interest. The length of this central line for the lenses analysed in this thesis was kept constant. This allowed the relative cell density profile to be assessed for each lens epithelium allowing lenses to be compared and differences tested for significance. The program counted the nuclei in contact with the user-defined central line as a sampling approach and then used a nearest neighbour approach to count all the nuclei that either touched or were directly adjacent to the central line (Appendix Figure 1).

3.4.5.3. Calculation of relative cell density

The region of interest and its central line was divided into 100 equal rectangular grids (= segments). Within each segment, the number of nuclei was normalised to 'number of nuclei per µm' (Appendix Figure 1). Given that each LEC has one nucleus, normalised nuclear number is equivalent to a normalised cell number. The output values representing normalised cell number (= number of nuclei per µm) in each segment were referred to as relative cell densities and when plotted against segment number, produced a profile of the cell number and how it changed across the lens epithelium.

3.4.5.4. Histograms

Profile plots of normalised cell number/ segment (= relative cell density) for the epithelium of each lens were considered the most appropriate to answer the research questions posed in this thesis. Numerical values of relative cell density have been uploaded on STORE and can be accessed through the following link (CD1 [DOI:10.20348/STOREDB/1116/1232], B6C3F1 [DOI:10.20348/STOREDB/1116/1234] and C57BL/6J [DOI:10.20348/STOREDB/1116/1233]). Additional data collection and analysis is still ongoing in collaboration with the LDLensRad group.

3.4.5.5. Statistical analysis

Statistical analysis was performed with R and R studio together with collaborators. The Kruskal-Wallis test using mutation, sex, dose rate and dose as independent factors, and relative cell density as dependent factor was applied for the CD1 and C57BL/6J strain because their distribution was not normal. Kruskal-Wallis is a ranked test and allows the detection of significant differences in the course/ gradient of the graphs. Power calculations were carried out and maximum relative cell density was selected as the most appropriate value to compare the responses in the B6C3F1 data. General Linear Model Analysis of Variance using time, mutation, sex and dose as independent factors and maximal relative cell density as dependent factor was applied during statistical analysis on the collective B6C3F1 cell density data which showed a normal distribution.

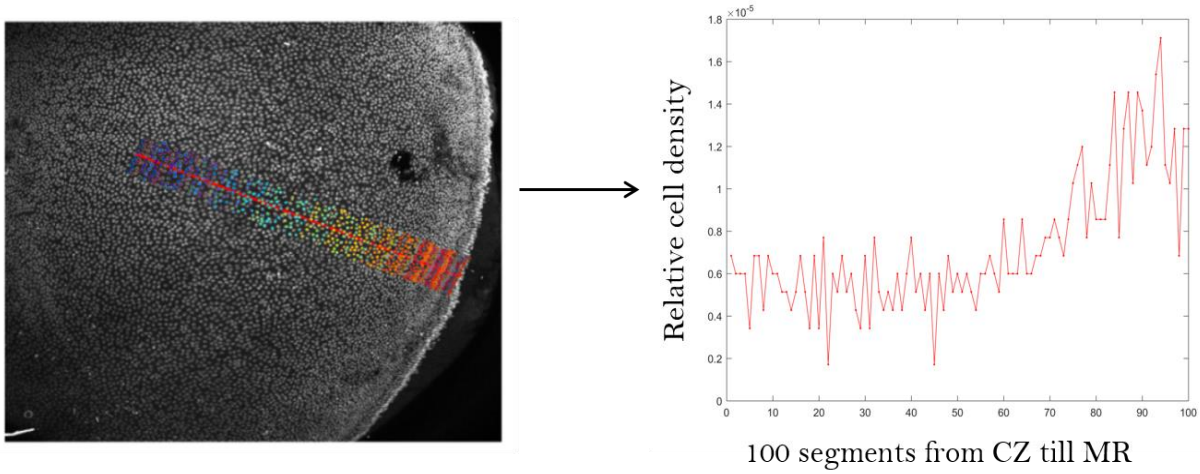

Figure 3.2: Eye lenses isolated from IR-exposed mice were stained with Hoechst 33342 and imaged with a CLSM. The generated images were stacked using Image J and analysed with an in-house developed Matlab program. A line was manually drawn from the central zone to the end of the meridional rows. The program divides this central line in 100 segments and uses the length of the line included in each segment to calculate the cell number/µm, thereby a relative cell density (normalised cell number/ segment) profile is generated when each value is plotted against the corresponding segment number. CZ: central zone, MR: meridional rows.

3.5. X-rays exposure and extraction of lipid membranes

3.5.1. Bovine lenses membrane extraction

Bovine eyes were obtained from Linden Burradon Food Supply (FSA approved Scientific Research Material collection No. 2056). To collect the cholesterol enriched lens membranes, a protocol used to purify lens membrane fractions was adapted from Taopodi *et al.* (Tapodi et al., 2019): decapsulated eye lenses were aqua-dissected by stirring them in a low salt phosphate buffer (10 mM Na_2HPO_4 [pH 7.4] (VWR, US), 100 mM NaCl (Sigma/ Merck, UK) and 5 mM EDTA [pH 8.0] (VWR, US)) to first collect the cortical fraction of the LFCs followed by the nuclear fraction. Subsequently, a series of buffer extractions designed to enrich for integral membrane proteins and lipid membranes were performed (Gold et al., 2012). The LFCs were centrifuged, resuspended and consecutively homogenised using a Dounce homogeniser (Sigma/ Merck, UK) in a high salt buffer (10 mM Na_2HPO_4 [pH 7.4], 1.5 M KCl, 5 mM EDTA [pH 8.0]), an ammonium bicarbonate buffer (100 mM NH_4HCO_3 (Sigma/ Merck, UK), 1 mM EDTA [pH 8.0]), an urea buffer (10 mM Na_2HPO_4 [pH 7.4], 8 M Urea (Sigma/ Merck, UK), 5 mM EDTA [pH 8.0]) and a sodium hydroxide buffer (100 mM NaOH) (Sigma/ Merck, UK), with a low salt phosphate buffer wash between each buffer. The final cortical (BoC) and nuclear (BoN) membrane fractions were dissolved in the low salt phosphate buffer and stored at 4 °C until analysis.

3.5.2. *In vitro* X-rays exposure

The BoC and BoN fractions (10 mg wet weight) were resuspended in 1 mL of the low salt phosphate buffer and exposed to 5 and 50 Gy in a single X-ray dose using a X-ray chamber irradiator calibrated to national standard (IRR320, aluminium filtered 320 kV, dose rate 5 Gy/min) (AGO Ltd., UK, model no.: CD160/1 Serial no.: 1032–1109). Dose delivery was verified at the exact site where the samples were placed with aluminium oxide chips (Vertec Scientific Ltd., UK) to confirm accurate dose delivery.

3.5.3. Whole body X-rays exposure

At 3 months of age, female mice were exposed in groups of four to 0.1 or 2 Gy in a single X-ray dose (CD160/1, AGO X-ray Ltd., UK, aluminium and copper filtered (~1 mm) containing a Varian NDI-320 source; 250 kVp; dose rate 0.5 Gy/min). Dosimetry was performed with a calibrated reference ionisation chamber for the applied exposure setup. The monitoring of the exposures was accomplished with a calibrated UNIDOS E electrometer and 'in-beam' monitor ionisation chamber (PTW). To verify whether the dose was delivered to the entire area of the box, spatial dose uniformity was measured with Gafchromic EBT2 films (Vertec Scientific Ltd., UK). Subsequently, the mice were returned to their cages and received standard care until the time of sacrifice.

3.5.4. Murine lenses membrane extraction

The mice were sacrificed by cervical dislocation and eyes were surgically removed. To isolate the eye lenses, a deep incision around the optic nerve was made, and the vitreous fluid and eye lens capsule were removed utilizing a dissection microscope (Leica, Germany). The eye lenses were snap frozen and stored in the -80 °C.

Eight lenses were removed and processed together as described above for bovine eyes using the following buffer sequence: low phosphate, urea, low phosphate and sodium hydroxide buffer. The final cortical (MoC) and nuclear (MoN) membrane fractions were resuspended in the low salt phosphate buffer and kept at 4 °C until further analysis.

3.5.5. Dissection of the hippocampus

After cervical dislocation, the brain was removed and submerged in ice-cold artificial cerebrospinal fluid (ACSF), saturated with carbogen gas (95% O2, 5% CO2). ACSF consisted of 124 mM NaCl, 4.9 mM KCl, 1.3 mM MgSO4 (Sigma/ Merck, UK), 2.5 mM CaCl2, 1.2 mM KH_2PO4 (Sigma/ Merck, UK), 25.6 mM $NaHCO_3$ (Sigma/ Merck, UK) and 10 mM glucose (pH 7.4) (Sigma/ Merck, UK) (Schreurs et al., 2017). The hippocampi were snap frozen and stored at -80 °C.

3.6. Protective mechanism of anti-oxidants

3.6.1. Anti-oxidants protection from IR-induced oxidative stress

Ascorbic acid (3 mM) (Sigma/ Merck, UK), α-Tocopherol (1 mM) (Sigma/ Merck, UK) and glutathione (4 mM) (Sigma/ Merck, UK) were added to the cortical and the nuclear fractions of bovine lens membrane extracts (10 mg wet weight) dissolved in 1 mL of low salt phosphate buffer pre- and post-IR exposure. After the addition of 0.02 % sodium azide (Sigma/ Merck, UK), the samples were incubated for 18 days at 37 °C in the dark.

3.6.2. Deteurated lipids membrane binding assay

The BoC and BoN fractions (10 mg wet weight) were dissolved in 1 mL of the low salt phosphate buffer and 2 µM of tocopherol–d6 (Avanti Polar Lipids, US), cholesterol-d6 (Avanti Polar Lipids, US) and dicholoromethane:methanol (DCM:MeOH) (Thermo Fisher Scientific, US) and low salt phosphate buffer as control were added. After the addition of 0.02 % sodium azide (Sigma/ Merck, UK) and vortexing, the samples were incubated at 37 °C and harvested at the following time points: 0 h, 1 h, 8 h, 1 day, 3 days and 7 days. The lipid bound membranes were collected via centrifugation at 14 000 g for 10 min (RT) followed by a wash with low salt phosphate buffer. These samples were stored at 4 °C.

3.7. Sodium dodecyl sulphate polyacrylamide gel electrophoresis (SDS-PAGE)

Polyacrylamide gels (10 and 15 % (w/v)) were prepared and the samples were resuspended in an SDS buffer (1 mM EDTA pH7.8, 50 mM Tris pH 6.8 (VWR, US) and 1% (w/v) SDS (Sigma/ Merck, UK) ((Laemmli, 1970) as modified in (Tapodi et al., 2019)). After diluting the samples in 4× sample buffer (250 mM Tris-HCl pH 6.8, 10% (w/v) SDS, 0.008% (w/v) Bromophenol Blue (Sigma/ Merck, UK), 2.854 M β-mercaptoethanol (Sigma/ Merck, UK), 40 % glycerol (Sigma/ Merck, UK)) and loading them on the gels along with a Precision Plus Protein Standards ladder (Thermo Fisher Scientific, UK), they were run in 1× running buffer (3 g/ L Trizma (VWR, US), 2% (w/v) SDS, 14.4 g/ L glycine (Sigma/ Merck, UK)) at a voltage of 100 V. To visualise the proteins, the gels were transferred into fixing solution (50% (v/v) methanol, 10% (v/v) acetic acid) for 30 min, stained with Coomassie blue (50% (v/v) methanol (Thermo Fisher Scientific, US), 10% (v/v) acetic acid (Thermo Fisher Scientific, US), 0.25% (w/v) Coomassie brilliant blue (Sigma/ Merck, UK)) during 30 min and destained by performing 5 min washes with destaining buffer (10% (v/v) methanol, 5% (v/v) acetic acid).

3.8. Blotting

3.8.1. Western blotting

Equal amounts of proteins were separated via SDS-PAGE. Subsequently, the gels were immersed in buffer B (0.025 M Tris, 20% methanol). Per gel, 18 pieces of Whatman™ chromatography paper (3mm) (Thermo Fisher Scientific, US) and one nitrocellulose or PDVF membrane (0.2 µm pore size, Millipore, UK) were cut to the same sizes as the gel (8 cm x 6 cm). 6 pieces of the Whatman™ paper were soaked in buffer A (0.3 M Tris, 20% methanol (MeOH)), 3 pieces in buffer B (0.025 M Tris, 20% MeOH) and the other 9 pieces were submerged in buffer C (0.025 M Tris, 20% MeOH, 0.04 M glycine). The pieces of paper soaked in buffer A, 3 pieces in buffer B, the membrane which first submersed in buffer B, the gel and the 9 pieces in buffer C were respectively stacked in the semi-dry western blotting machine (Thermo Fisher Scientific, US). The transfer was run at 38 mA for 90 min. After the transfer, the membrane was rinsed extensively with ultrapure H_2O, stained with Ponceau red dye for 5 min (0.5% (w/v) Ponceau (Sigma/ Merck, UK), 1% (v/v) acetic acid (Thermo Fisher Scientific, UK)) followed by three times 5 min with ultrapure H_2O to verify whether the transfer was successful. Subsequently, the membrane was blocked with 1.5% (w/v) BSA, 5% (w/v) milk powder (Sigma/ Merck, UK) dissolved in TBS-T (25 mM Tris-HCl (pH= 7.4), 100 mM NaCl, 0.1% (v/v) Tween-20 (Sigma/ Merck, UK)). After a 2 h incubation at RT under gentle agitation, the membrane was washed three times in TBS-T (Sigma/ Merck, UK) and transferred into a plastic bag. The primary antibody (rabbit anti-AQP0, 1/2000, in-house developed) diluted in 5% (w/v) BSA in TBS-T was added and the bag was sealed for an overnight incubation at 4°C, under gentle agitation. Following morning the membrane was removed from the bag and washed three times with 5% (w/v) milk powder in TBS-T. The nitrocellulose membrane was transferred to a new bag, secondary antibody (goat anti-rabbit 1/10000, Sigma/ Merck, UK) diluted in 5% (w/v) BSA added and incubated for 1 h under gentle agitation at 4 °C. After washing the membrane five times with 5% (w/v) milk powder in TBS-T, the blots were developed using ECL western blotting substrate (Thermo Fisher Scientific, US). This mixture was left for 5 min on the membrane in a dark room and subsequently, the blot was imaged using chemiluminescence imaging (FUJIFILM IR LAS-1000 Pro v. 3.02, UK).

3.8.2. OxyBlot

Detection of carbonylated proteins was performed with the OxyBlot protein oxidation detection kit (Millipore, UK). Analogous to Western blotting, equal amounts of proteins were separated via SDS-PAGE and electroblotted to a PDVF membrane via a semi-dry system. The blotted PDVF membrane was washed with ultrapure H_2O for 5 min, submerged in 100% MeOH for 15 s and allowed to air dry. Subsequently, the membrane was incubated for 5 min in the following solutions: respectively, 20% MeOH in PBS, 2,4-dinitrophenylhydrazine (DNPH) (Sigma/ Merck, UK) in 2 N HCl (Sigma/ Merck, UK), three times in 2 N HCl and five times in 100% MeOH. Blocking was performed with 5% (w/v) milk powder in TBS-T for 1 h under gentle agitation. The membrane was left overnight at 4 °C

submerged in rabbit anti-2,4-dinitrophenol (DNP) (1:1000 dilution in 5% (w/v) milk powder in TBS-T) (Sigma/ Merck, UK) under gentle agitation. After washing the membrane three times with TBS-T for 5 min each time, it was incubated with anti-rabbit HRP (1/10000 dilution in 5% (w/v) milk powder in TBS-T) for 1 h under gentle agitation. The blot was washed five times with TBS-T and developed using the ECL system described above (3.8.1).

3.9. Preparation of samples for Mass Spectrometry

3.9.1. Lipid purification

Lipids were purified using a modified Bligh-Dyer method (Bligh and Dyer, 1959). All glassware was rinsed with methanol and hexane. The bovine lens membranes (10 mg of wet weight) or mouse lens membrane extracts of eight eye lenses were transferred into clean glass culture tubes and 2 mL of 2:1 methanol:dichloromethane (MeOH:DCM) was added. Full left hippocampi were first transferred into a Dounce homogenizer (Sigma/ Merck, UK) and gently homogenised in 1 mL of 2:1 MeOH:DCM. The homogenate was transferred into glass culture tubes containing 1 mL of 2:1 MeOH:DCM. These samples were vortexed for 30 seconds and left to incubate for 30 min at RT. Subsequently 0.67 mL of DCM and 1.2 mL of 0.9% (w/v) KCl were added consecutively, with a 30 s vortex step after adding each solution. The samples were centrifuged at 1000 g for 5 min at RT and the lower lipid phase layer was transferred into a fresh glass tube with a Pasteur pipette (VWR, US). The lipids were dried under N_2 gas (nitrogen evaporator, VLM, US).

3.9.2. Acid protein hydrolysis

To study IR-induced advanced glycation end products (AGEs) formation, the acid protein hydrolysis protocol provided by Smuda *et al.* was modified (Smuda et al., 2015). Bovine lipid membranes (10 mg wet weight) were dissolved in 400 µL of 6 N HCl and heated overnight at 110 °C. Subsequently, the samples were freeze-dried (liquid nitrogen) resuspended in 1 mL of 0.1 N HCl, sonicated for 10 minutes in a water bath (VWR, US), followed by a 5 min centrifugation at maximal speed. Aliquots of the supernatant were diluted with 9 volumes of 85% acetonitrile (ACN) (Thermo Fisher Scientific, US).

3.9.3. Optimisation of solubilisation of lipid membranes

BoC and BoN lipid membrane fractions were centrifuged at 12000 g, 15 min, 4 °C and after removal of the supernatant, the pellet was dissolved in 0%, 0.1%, 0.5%, 1%, 2% or 4% SDS, 1 mM EDTA pH 7.8, 50 mM Tris pH 6.8. Following an incubation at RT under gentle agitation for 30 min, the samples were centrifuged at 12000 g, 15 min, 4 °C. The supernatant was transferred to new tubes, the pellet was resuspended in an SDS buffer (see section 3.7) and the proteins in these samples were separated via SDS-PAGE system along with SDS untreated lipid membranes.

3.9.4. Determination of protein concentration

The protein concentration in solubilised lipid membranes was measured via the bicinchoninic acid (BCA) assay according to manufacturer's instructions (Thermo Fisher Scientific, US) (Smith et al., 1985, Olson and Markwell, 2007).

3.9.5. VC1 pull down

The VC1 pulldown assay was performed using an adapted version of the Degani *et al.*, 2017 (Degani et al., 2017). Streptavidin magnetic beads (Sigma/ Merck, US) were washed with buffer 1 (20 mM 4-(2-hydroxyethyl)-1-piperazineethanesulfonic acid (HEPES) (Sigma/ Merck, US) pH 7.1, 100 mM

NaCl), followed by a 1 h incubation at 4 °C with recombinant VC1 protein (in house made) and buffer 1 for the control beads. To remove the excess of VC1, beads were washed with buffer 1. Subsequently, samples diluted to 0.21 mg/ mL in buffer 2 (20 mM HEPES pH 7.1, 100 mM NaCl, 0.5% Triton-X100 (Sigma/ Merck, UK)) were added to the beads and incubated 3 h under gentle agitation at 4 °C. The unbound fractions were collected in new Eppendorf tubes and the beads were washed with buffer 2. To elute, 4x Laemmli sample buffer (8% (w/v) SDS, 0.4% (w/v) Bromophenol blue, 40% (v/v) glycerol, 200 mM Tris-Cl, pH 6.8) (Laemmli, 1970) was added to the beads and incubated 1 h at RT and overnight at 4 °C. The eluate was collected and 15 uL of buffer 1 was added to the beads. After collecting the supernatant in corresponding elution tubes, SDS-PAGE and an in-gel trypsin digest was performed with these samples.

3.9.6. In-gel trypsin digestion

Following SDS-PAGE and Coomassie Blue staining, the proteins-of-interest were cut out of the gel. The collected bands were chopped into small pieces and transferred to an Eppendorf tube. First the gel pieces were destained by adding 50% ACN, 50 mM NH_4HCO_3 (Thermo Fisher Scientific, UK) and incubating the samples at 37 °C under maximum rotation per minute (rpm). This step was repeated until no staining solution was visible on the gel pieces. Subsequent to removing the solvent, 100% ACN was transferred into the tubes and incubated for 5 min, max rpm, 37 °C. After removal of ACN with the pipette, 100 mM dithiothreitol (DTT) (Sigma/ Merck, UK) was added and incubated for 1 h, 500 rpm, 56 °C. DTT was discarded and the gel pieces were washed with 50 mM NH_4HCO_3 and incubated with 55 mM iodoacetimide (IAA) (Sigma/ Merck, UK) for 45 min at RT in the dark, shaking at 500 rpm. Lastly, IAA was removed, gel pieces were washed with 50 mM NH_4HCO_3 and dried with 100% ACN before 0.2 µg of trypsin (Sigma/ Merck, UK) diluted in 50 mM NH_4HCO_3 was added to each sample and incubated overnight at 37 °C, 500 rpm. The next day, a quick spin was given to the samples and the solution was transferred to new tubes i.e. recovery tubes. In the tubes containing the gel pieces, the following solutions were added respectively, incubated at 37 °C for 10 min at max rpm followed by transferring the recovered solution in the corresponding recovery tubes: 150 µL of extraction solution (30% (v/v) ACN, 3% (v/v) trifluoroacetic acid (TFA)), 75 µL of extraction solution, 75 µL of 100% ACN and 50 µL of 100% ACN. Lastly, the tubes were dried in a SpeedVac (VWR, US) and stored at -20 °C.

3.10. Liquid Chromatography – Mass Spectrometer (LC-MS)

3.10.1. Lipidomics - sterols

Samples were analysed based on the methodology developed by McDonald and colleagues (McDonald et al., 2012). Quantitative analysis was performed with a Shimadzu UHPLC system linked to a hybrid triple-quadrupole mass spectrometer using electrospray ionization in positive (ESI+) mode (QTRAP 6500, AB Sciex) (Figure 3.3). For oxysterol analysis, the samples were dissolved in 50 µL of 1:1 acetonitrile:isopropanol (ACN:IPA) (Thermo Fisher Scientific, US) and separated on a Kinetex C_{18} HPLC column (150 × 2.1 mm, 2.6 µm particle size; Phenomenex,UK) with mobile phases A (60:40 ACN: H_2O, 10 mM NH_4HCO_2, 0.1% formic acid (FA) (Sigma/ Merck, UK)) and B (50:50 ACN:IPA, 10 mM NH_4HCO_2, 0.1% FA). For cholesterol analysis, the samples were dissolved in 500 µL 1:1 ACN:IPA and run under the same conditions on a Cortecs C_{18} UPLC column (100 × 2.1 mm, 1.6 µm particle size; Waters, UK). The flow rate was 140 µL/ min, and the column was maintained at 60 °C.

The mice IR-exposure time course experiment samples were dissolved in 84 µL of 70:30 MeOH:H_2O and analysed with a liquid chromatography UltiMate 3000 HPLC system (Dionex, Thermo Scientific Ltd., US) coupled on-line with a electrospray tandem triple quadrupole-linear ion trap mass spectrometer (QTRAP 5500, AB Sciex, US). The samples were separated using a reverse phase C_{18} column (100 × 3.2 mm, 5.0 µm particle size; Macherey-Nagel, Germany) with mobile phases A (70:30 MeOH:H_2O 0.1% FA) and B (90:10 IPA:MeOH, 0.1% FA). The flow rate used to run these samples is 200 µL/ min, and the column was maintained at 45 °C.

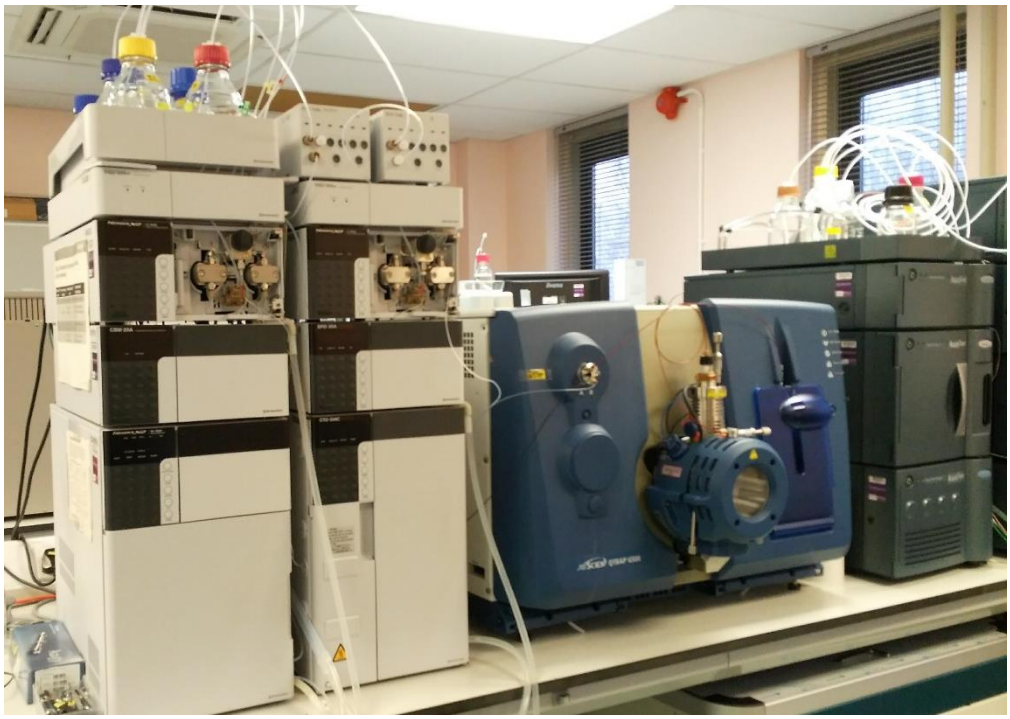

Figure 3.3: Shimadzu Ultra-High Performance Liquid Chromatography system linked to a hybrid triple-quadrupole mass spectrometer using electrospray ionization used to analyse oxysterols and advanced glycation end products.

3.10.2. Quantitation and statistical analysis of sterols

The areas under the elution curves on the generated chromatograms were integrated to generate quantitative values (analyte peak area) using quantification mode of the Analyst® 1.6.2 software. The bovine sample experiments were repeated three times, while two biological repeats were produced for the mice experiments. Minitab 18 was used to perform statistical analysis (State College, 2017). General Linear Model Analysis of Variance (ANOVA) followed by Tukey's post hoc test for pairwise comparison using dose, time and location as independent factors and (relative) analyte peak area as dependent factor was applied for statistical analysis. Retrospective power analysis was also performed using Minitab 18 (2 sample t-test, for a power of 80% (beta, acceptable chance of a type 2 error, of 0.20) and with an alpha, acceptable chance of a type 1 error, of 0.05). Qualitative consideration of the sources of uncertainty was carried out for each quantitative experiment, in order to narrow these down to quantitatively calculate the most appropriate estimate of standard error associated with the each

endpoint. Furthermore, qualitative power analysis was performed to estimate the advised sample size and actual power of each comparison using Minitab and qualitative uncertainty budget were determined to identify all the factors that contribute to uncertainties in measurement results during an experiment.

3.10.3. Advanced glycation end products

The samples were analysed by hydrophilic interaction liquid chromatography (HILIC) using a Waters amide column (1 mm x 100 mm) (Waters, UK) combined with mass spectrometric detection with QTRAP 6500 (AB Sciex, US) in ESI+ mode. Chromatographic separations were performed with mobile phase A (H_2O, 1.2 mL/ L heptafluorobutyric acid (HFBA)) and B (7:3 MeOH: H_2O, 1.2 mL/ L HFBA). Compounds-of-interest were monitored by multiple reaction monitoring (MRM) using conditions optimized for a QTRAP instrument as described by Smuda *et al.*, 2015 (Smuda et al., 2015).

3.10.4. Proteomics

Samples were analysed analogous to the methodology described by Carne *et al.* (Carne et al., 2019) using an Ekspert™ LC 425 system (Eksigent, US) coupled to a quadrupole Time-Of-Flight (QTOF) mass spectrometer (TripleTOF 6600, SCIEX, US) equipped with ESI. After dissolving the samples in 2% (v/v) ACN and 0.1% (v/v) FA to a concentration of 1 µg/ µL, 5 µL was injected for LC-MS. Peptides were separated via microflow liquid chromatography by trap-and-elute methods using reverse phase C_{18} Trap column (5 x 0.5 mm, 5 µm particle size, Phenomenex,UK) and C_{18} analytic column (150 x 0.3 mm, 3 µm particle size, Phenomenex,UK) with mobile phase A (0.1% (v/v) FA in H_2O) and B (0.1% (v/v) FA in ACN). The MS platform was used in positive high-sensitivity mode and data-dependent acquisition of the top 30 ions (based on intensity) selected from precursor ion scans performed. Using the MSConvert tool of the ProteoWizard software, precursor and fragment-ion lists were generated. Subsequently, the proteins were identified through ProteinPilot™ 2.5.1. Software and Bovine data subtracted from Uniprot.

Chapter 4: IR-induced changes in cell density, organisation and proliferation

4.1. Introduction

A single layer of lens epithelial cells (LECs) under the lens capsule covers the anterior hemisphere of the eye lens. Based on the proliferation capacity, the epithelium can be divided into the central zone, germinative zone, transition zone and meridional rows (Figure 4.1). While cell proliferation in the central zone occurs at a very low rate, it peaks in the germinative zone (Rafferty and Rafferty, 1981, Lovicu and McAvoy, 1999). The progeny cells from the germinative zone migrate to the transition zone where they exit cell cycle and differentiate into lens fibre cells (LFCs) (Srinivasan and Harding, 1965). These cells withdraw from the lens epithelium through lining up in the meridional rows and internalising at the equator and start breaking down their cell organelles to become mature LFCs. Collectively, germinative and transition zone are called the peripheral zone.

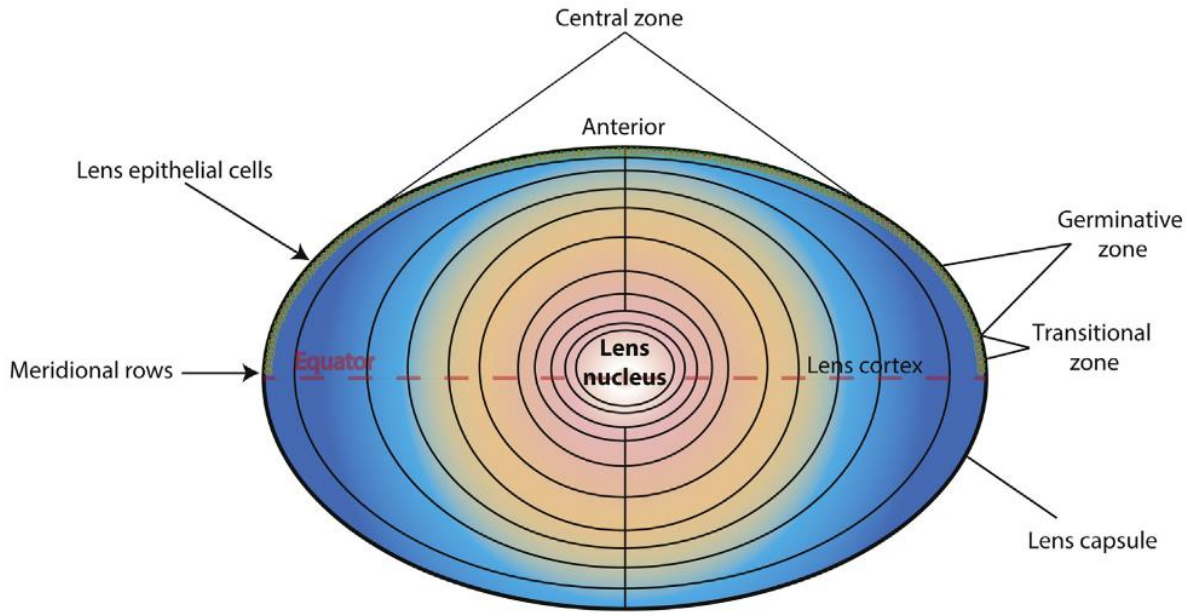

Figure 4.1: Schematic representation of the individual regions of the eye lens. The lens capsule covers the entire eye lens, while the lens epithelium extends from the anterior pole till the equator. The lens epithelium is divided into the central zone, germinative zone, transition zone and meridional rows. LECs differentiate into LFCs and internalise at the equator. The outer layers of the LFCs are part of the lens cortex and the inner layer is part of the lens nucleus (Ainsbury et al., 2016, Mut. Res. Rev, used with permission of the journal).

4.1.1. Ionising radiation-induced changes in the lens epithelium

A wide variety of studies showed that changes occur in the lens epithelium after exposure to ionising radiation (IR) (reviewed by (Ainsbury et al., 2016)). Exposure of solely the peripheral zone to radiation induced opacification of rabbit lenses (Goldmann and Liechti, 1938) while shielding the same area from IR exposure prevented cataract development (Alter and Leinfelder, 1953, Leinfelder and Riley, 1956, Rothstein et al., 1982). Measurements of cell proliferation after acute IR exposure of 15 Gy demonstrated an increase in proliferation in the germinative zone of rabbit lenses *in vivo* (Von Sallmann, 1952, Von Sallmann et al., 1953, Von Sallmann et al., 1955, Pirie and Drance, 1959). Interestingly, this effect was transient and after several weeks cell proliferation was similar to pre-exposure capacity. The latter research output strongly suggests that the peripheral zone is the most radiosensitive zone of the lens epithelium. This can be attributed to active dividing cells in the peripheral zone harbouring chromatin in a more relaxed state than their non-dividing counterpart cells in the central zone. Although the organisation of the cells in lens epithelium, LECs differentiation and cell density have received less attention, these traits are also affected by IR exposure. Similar to ageing (Wu et al., 2015), IR exposure was found to lead to the disorganisation of meridional rows and changes in cell density of frog LECs (Hayden et al., 1980). Aberrations in the differentiation of LECs (Hanna and O'Brien, 1963) and temporal decrease in cell density (Von Sallmann, 1952) have been observed after exposure to IR.

Notably, all the aforementioned research was performed with doses ≥2 Gy of IR and studies including lower exposure doses started to emerge only recently. Similar to the data of these high dose studies, increased proliferation and cell density was measured in mice for doses <0.5 Gy 1 h post-IR exposure (Markiewicz et al., 2015), and the proliferative capacity returned to pre-exposure baseline levels 24 h post-exposure. However, in contrast to the observations in mice exposed to doses >0.5 Gy, the increase in cell density was still detected 24 h after exposure to doses <0.5 Gy (Markiewicz et al., 2015). In addition to dose, dose rate is another factor that should be taken into account when investigating IR-induced cataracts. Exposing mice to X-rays <2.2 Gy at low dose rates, commonly defined as <0.005 Gy/ min (ICRP, 2007), leads to less double stranded breaks (DSBs) in lymphocytes in comparison to when the same dose was delivered at a higher dose rate (Turner et al., 2015). This implies that delivering IR during medical treatment at a low dose rate would induce less DNA damage. However, the same amount of damage was observed at a low dose rate as at a high dose rate in murine lymphocytes when mice were exposed to 4.45 Gy. In mice eye lenses, a study using only high dose rates showed that reducing the dose rate from 0.3 Gy/ min to 0.063 Gy/ min while delivering 2 Gy γ-rays correlated with an increased number of DSBs (Barnard et al., 2019). Strikingly, the effect of dose rate on the proliferative capacity, cell density and epithelial organisation is quite limited in the eye lens.

4.1.2. Mouse strains in IR-induced cataractogenesis research

Comparison of the eye lenses of mice, rats, guinea pig and rabbits exposed to various sources of IR (doses between 1 and 3 mega-electrovolt) revealed that mice were the most radio-sensitive among these vertebrates with lens opacities appearing at 8 months of age, which was 5 months earlier than in the control mice (Upton et al., 1956), making them the most suitable model organism to study IR-induced cataracts. IR-induced cataracts studies using CD1 mice heterozygous for *Ptch1* mutation showed that *Ptch1*$^{+/-}$ mice developed cataracts averagely 3 weeks sooner than their wild type (wt) counterparts when exposed to 3 Gy at 2 days of age (De Stefano et al., 2015). Remarkably, the trend of *Ptch1*$^{+/-}$ mutants to develop cataracts sooner than wt was also observed in unexposed mice, but lens opacities were detected much later in these mice compared to the irradiated ones (around 27 weeks later in *Ptch1*$^{+/-}$ mice). Analogous, introduction of the heterozygous Ser737Pro mutation into the *Ercc2* gene of the C3HeB/FeJ made mice more susceptible to cataractogenesis (Kunze et al., 2015). Furthermore, the *Ercc2*$^{+/-}$ mutants were shown to be less efficient in repairing IR-induced DSBs in comparison to wt C3HeB/FeJ after exposure to 1 Gy. Interestingly, a lifespan study with B6C3F1, F1 hybrid of C3HeB/FeJ and the radio-resistant C57BL/6J (Nowosielska et al., 2012, Kataoka et al., 2006), exposed to 0.5 Gy at a dose rate of 0.063 Gy/ min at 10 weeks of age showed that IR increased lens opacities only by 1% over a time course of two years (Dalke et al., 2018). Comparable to the human species, a lot of genetic variation is present between mice strains. However, the contribution of genetic variation to IR-induced cataractogenesis has typically been studied by introducing mutations in a specific mouse strain, while genetic differences between strains have been largely overlooked.

4.2. Objectives and experimental design

Cell density and proliferation analysis has classically been done through flat mounting the lens epithelium. An in-house developed cell density imaging technique of whole mount nuclei stained eye lenses was compared to the use of flat mounts (Figure 4.2; as described in chapter 3). Previous IR lens research using the CD1 and B6C3F1 strain focused mainly on DNA damage and the cataract phenotype (see section 4.1.2). Furthermore, CD1 and C3HeB/FeJ (the parental strain of B6C3F1) mice were shown to become more radio-sensitive when respectively *Ptch1*$^{+/-}$ and *Ercc2*$^{+/-}$ mutations were introduced. In the past no attempt has been done to compare the radio-sensitivity of the CD1 and B6C3F1 strain with radio-resistant C57BL/6J mice. To gain more insight into the biological mechanism through which dose, dose rate, genetic background and sex contribute to IR-induced modifications in lens epithelium, at 10 weeks of age male and female CD1 and C57BL/6J strains (wt and *Ptch1*$^{+/-}$) were exposed to 0.5, 1 and 2 Gy using Co^{60} γ-rays at 0.3 and 0.063 Gy/ min dose rates. 4 months post-IR exposure, the eye lenses were collected and the cell density across the lens epithelium was measured (Figure 4.2). Furthermore, 10 week- old male and female B6C3F1(wt and *Ercc2*$^{+/-}$) mice were exposed to 0.5, 1 and 2 Gy using Co^{60} γ-rays at a dose rate of 0.3 Gy/ min and harvested at 4 and 12 months post-IR exposure to study IR-induced alterations in cell density over time. Following nuclear staining, lenses were 3D-imaged with a confocal laser scanning microscope (CLSM) and subsequently analysed with Image J and an in-house relative cell density calculation MatLab script (code see appendix). The generated plots portrayed normalised cell number/ segment across the lens epithelium.

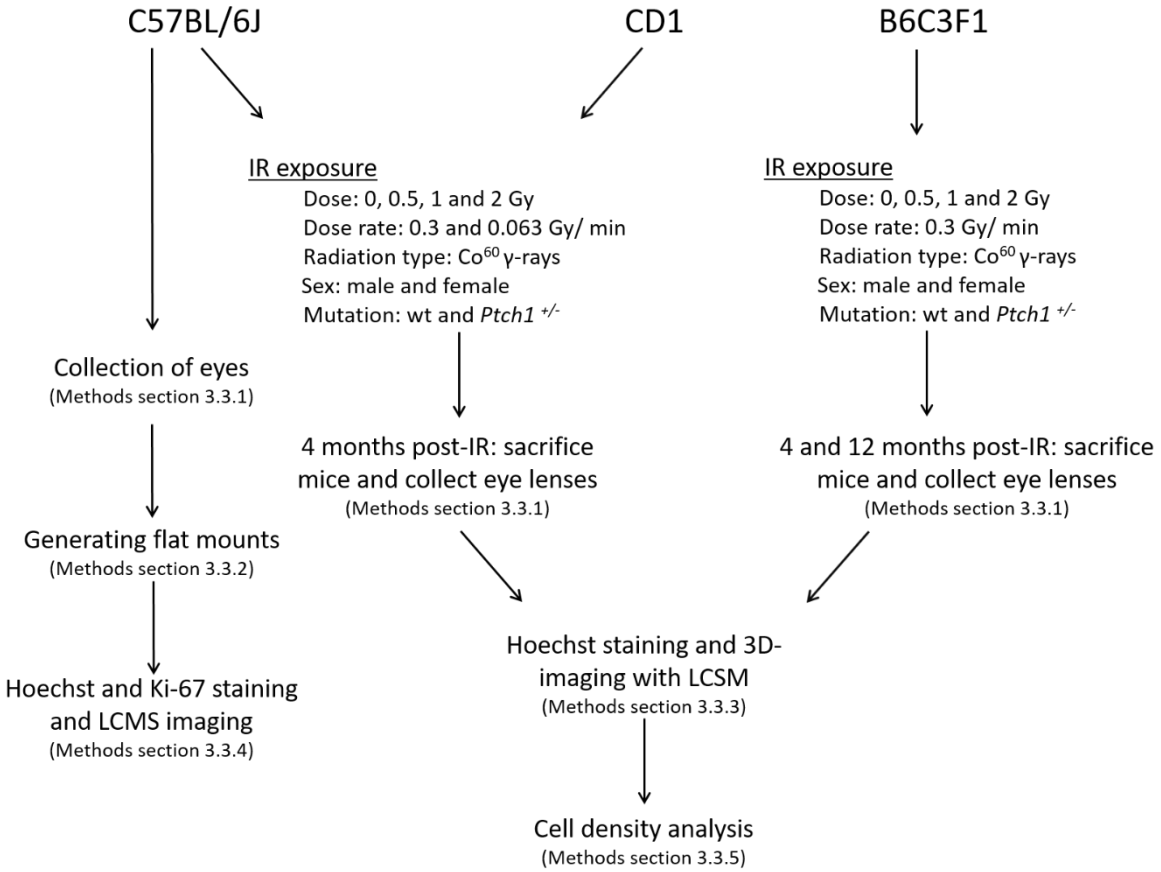

Figure 4.2: Diagram of the experimental design for analysis of IR-induced changes in cell density, lens epithelium organisation and cell proliferation in C57BL/6J. CD1 and B6C3F1 mice. Section numbers refer to the material and methods chapter section in which the protocol is described. CLMS: confocal laser scanning microscope.

4.3. Results

4.3.1. Whole mounts allowed rapid measurement of cell density

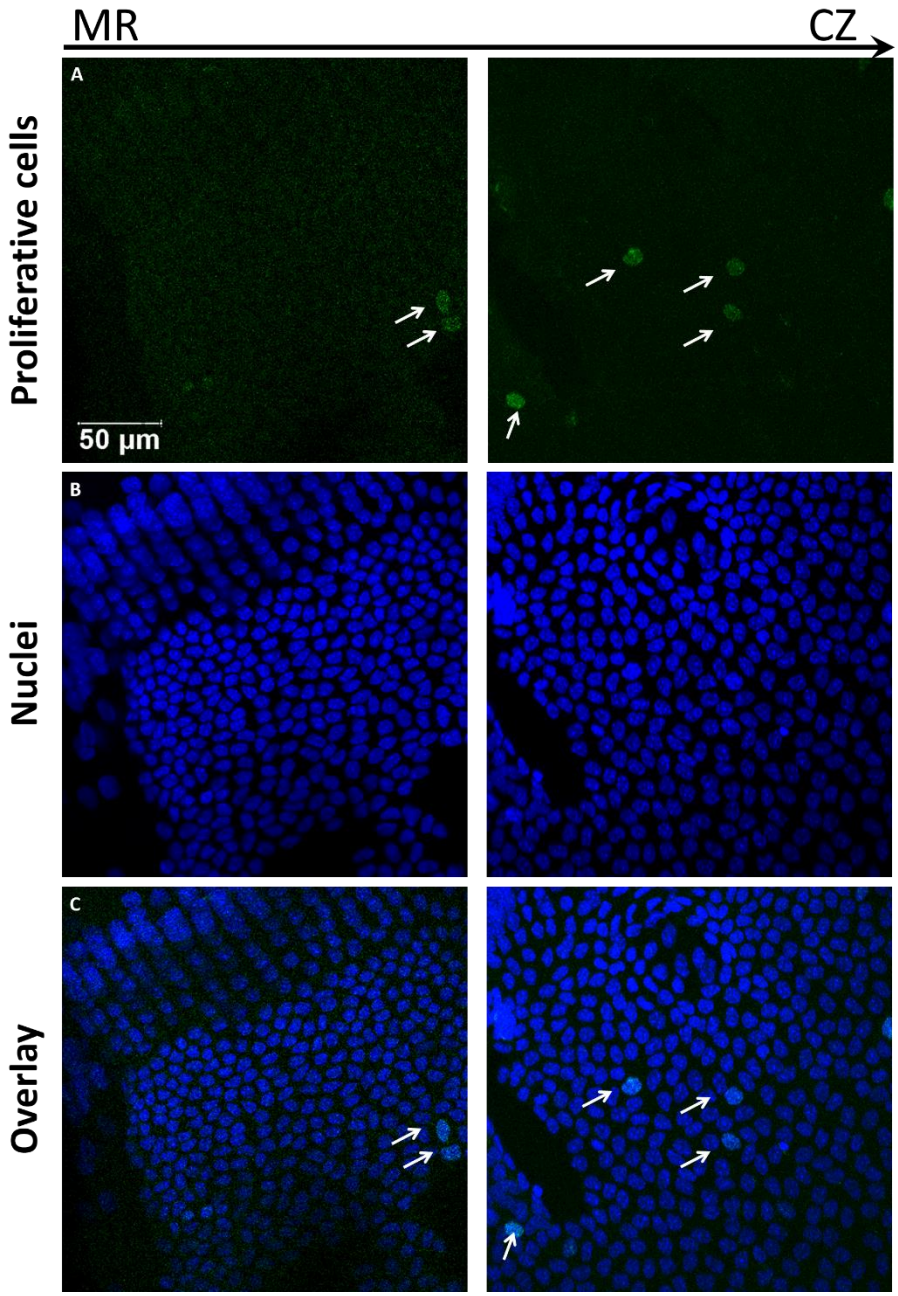

Figure 4.3: Wild type C57BL/6J, aged 6.5 months, flat mounted eye lens epithelium stained with A) Ki67, B) Hoechst 33342, and C) an overlay of these images. Images were acquired using a 63x oil objective, CLMS. White arrows point to the proliferating cells. MR: meridional rows, CZ: central zone.

The use of flat mounts and whole mounts to study epithelial organisation, cell density and proliferation was compared. Nuclear staining of flat and whole mounts allowed visualisation of the cellular organisation of the lens epithelium (Figure 4.3B and Figure 4.4B, respectively).

However, only whole mount staining maintained the full 3D structure of the lens epithelium, allowing easier and more detailed reconstruction of distinct areas, i.e. central zone, germinative zone, transition zone and meridional rows (Figure 4.4B).

Proliferative cells were visualised by Ki-67 staining. Although the staining worked flat and whole mounts, the proliferating cells were more easily distinguished from the background in flat mounts in comparison with whole mounts in which the staining was weak (Figure 4.3A and Figure 4.4A, respectively). Overlay of the nuclear and proliferation staining showed that proliferative mainly reside in the peripheral zone (Figure 4.3C and Figure 4.4C).

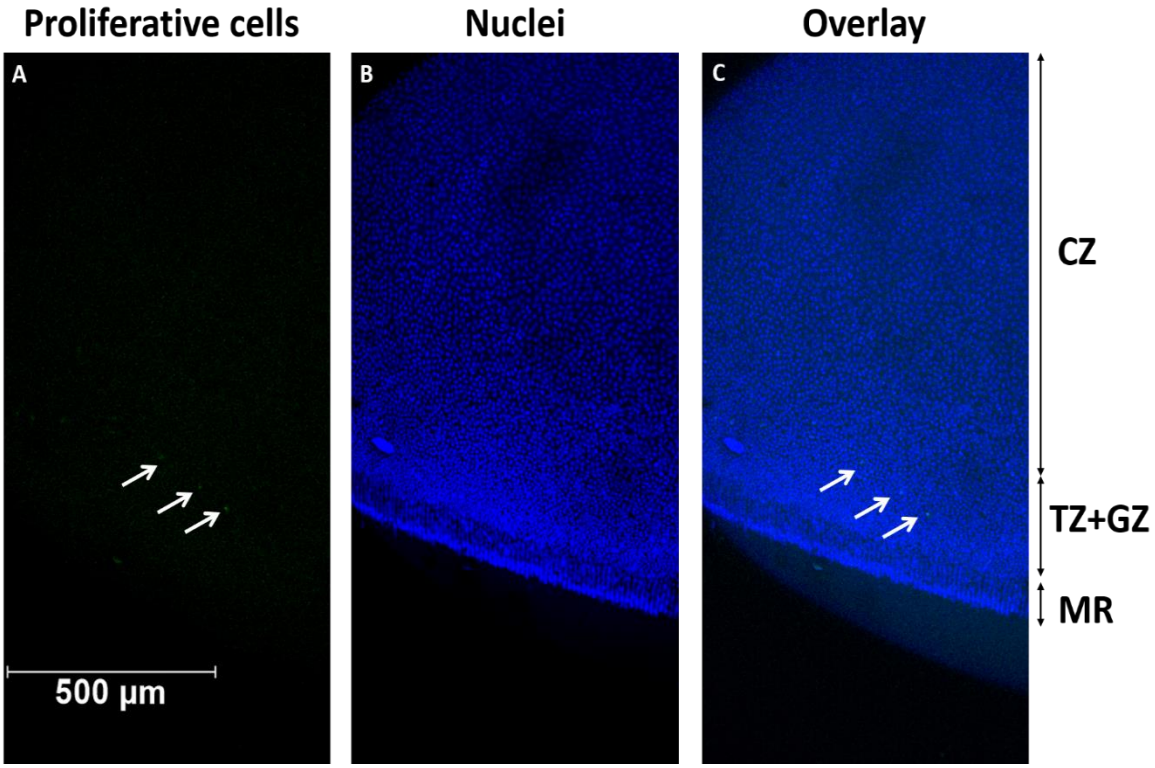

Figure 4.4: C57BL/6J wild type, aged 6.5 months, whole mount eye lens stained with A) Ki67 and B) Hoechst 33342, overlay of these images was generated in C). Images were acquired using a 10x dry objective. White arrows point to the proliferating cells. MR: meridional rows, GZ: germinative zone, TZ: transition zone, CZ: central zone.

4.3.2. Strain specific lens epithelium organisation

To compare the organisation of cells in the lens epithelium of various mice strains, whole mount nuclear staining of eye lenses of wt CD1, C57BL/6J and B6C3F1 was performed (Figure 4.2). All mice strains showed big nuclei in the central zone, whilst in the germinative and transition zone nuclei were smaller and the cell density was higher than in the central zone (Figure 4.5). The cells lined up in the meridional rows where the cell density was lower than in the germinative and transition zone, but still higher than in the central zone. The images illustrated that in contrast to the C57BL/6J and B6C3F1, in which the lining up of cells in the meridional rows is clearly observed, the cells in the meridional rows of the CD1 strain were less organised.

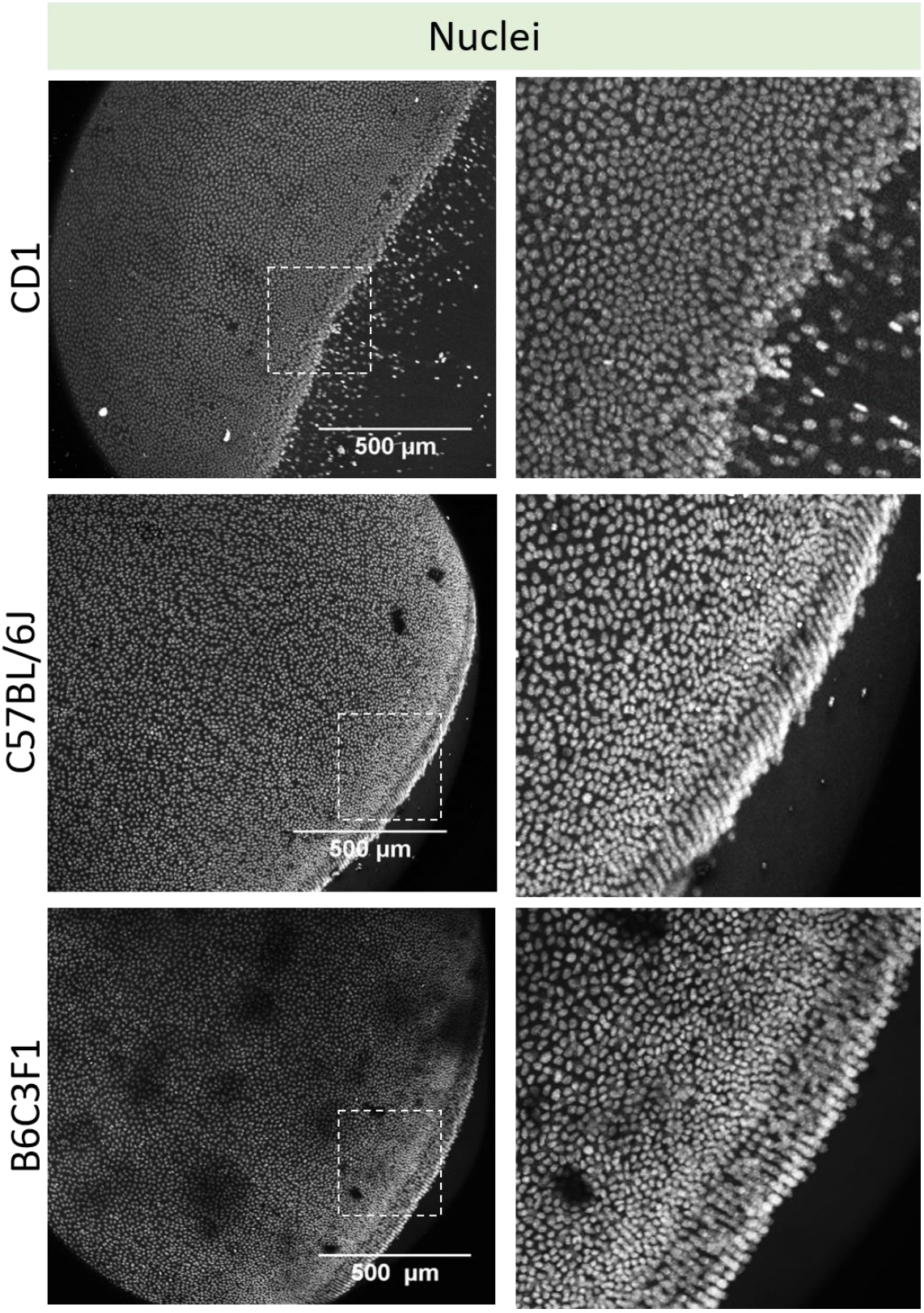

Figure 4.5: Hoechst 33342 staining of whole mount eye lenses of the CD1, C57BL/6J and B6C3F1 strain at an age of 6.5 months.

4.3.3. IR reduced cell density in the PZ and MR of the CD1 strain

Calculation of relative cell density illustrated that the cell density in the CD1 strain was relative constant in the central zone, but a lot of variation between individual CD1 mice was observed towards in the PZ and MR (Figure 4.6).

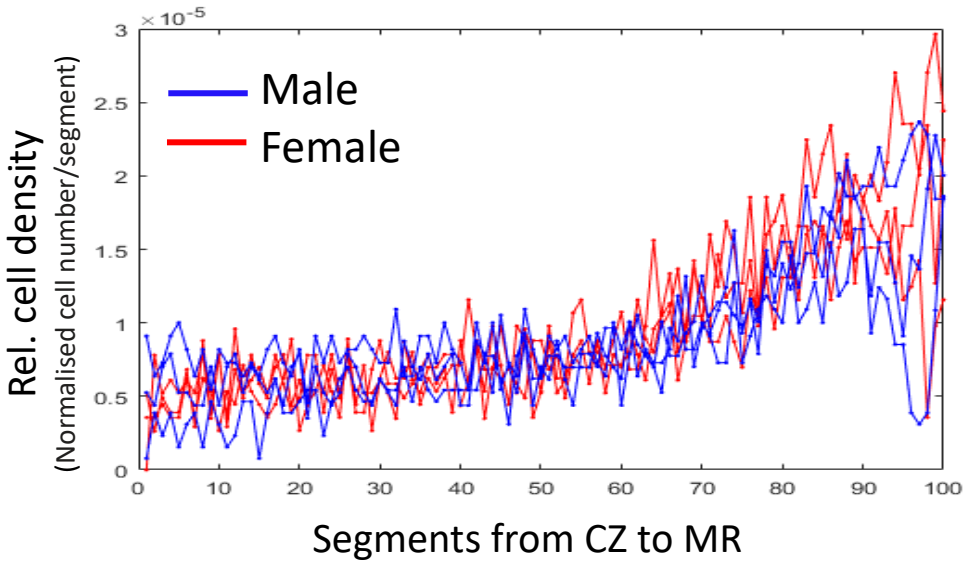

Figure 4.6: Plot of relative cell density versus segment number for the lens epithelium spanning the central zone to the furthest edge of the meridional rows for 6.5 month- old CD1 mice. This data was combined with the other CD1 data to assess statistical significance with the Kruskal-Wallis test using mutation, sex, dose rate and dose as independent factors and cell density as dependent factor. n= 4 for female and n= 3 for male mice Rel.: relative, CZ: central zone, MR: meridional rows.

Exposure to IR caused a decrease in the relative cell density variation in the PZ and MR (Figure 4.7). In the CZ, the relative cell density remained constant 4 months post-IR (Figure 4.7). Comparison of the 0.5, 1 and 2 Gy exposed CD1 mice with their unexposed counterparts demonstrated an IR dose-dependent decrease in relative cell density in the PZ and MR, with exception of two 2 Gy irradiated female mice that exhibited higher relative cell density than all the other IR-exposed mice (p= 0.072; Figure 4.7A, B, D, E, F vs. C). In contrast to the 0.5 Gy exposed CD1 mice, which showed higher relative cell density in the PZ and MR of mice exposed at a dose rate of 0.063 Gy/ min than those exposed at 0.3 Gy/ min (Figure 4.7A vs. D), the relative cell density in the PZ and MR of CD1 mice irradiated with 1 and 2 Gy at a dose rate of 0.063 Gy/ min was consistently lower compared to mice

exposed at a dose rate of 0.3 Gy/ min ($p= 0.059$; Figure 4.7B and C vs. E and F). The overall differences observed between male and female were not significant ($p= 0.153$; Figure 4.7).

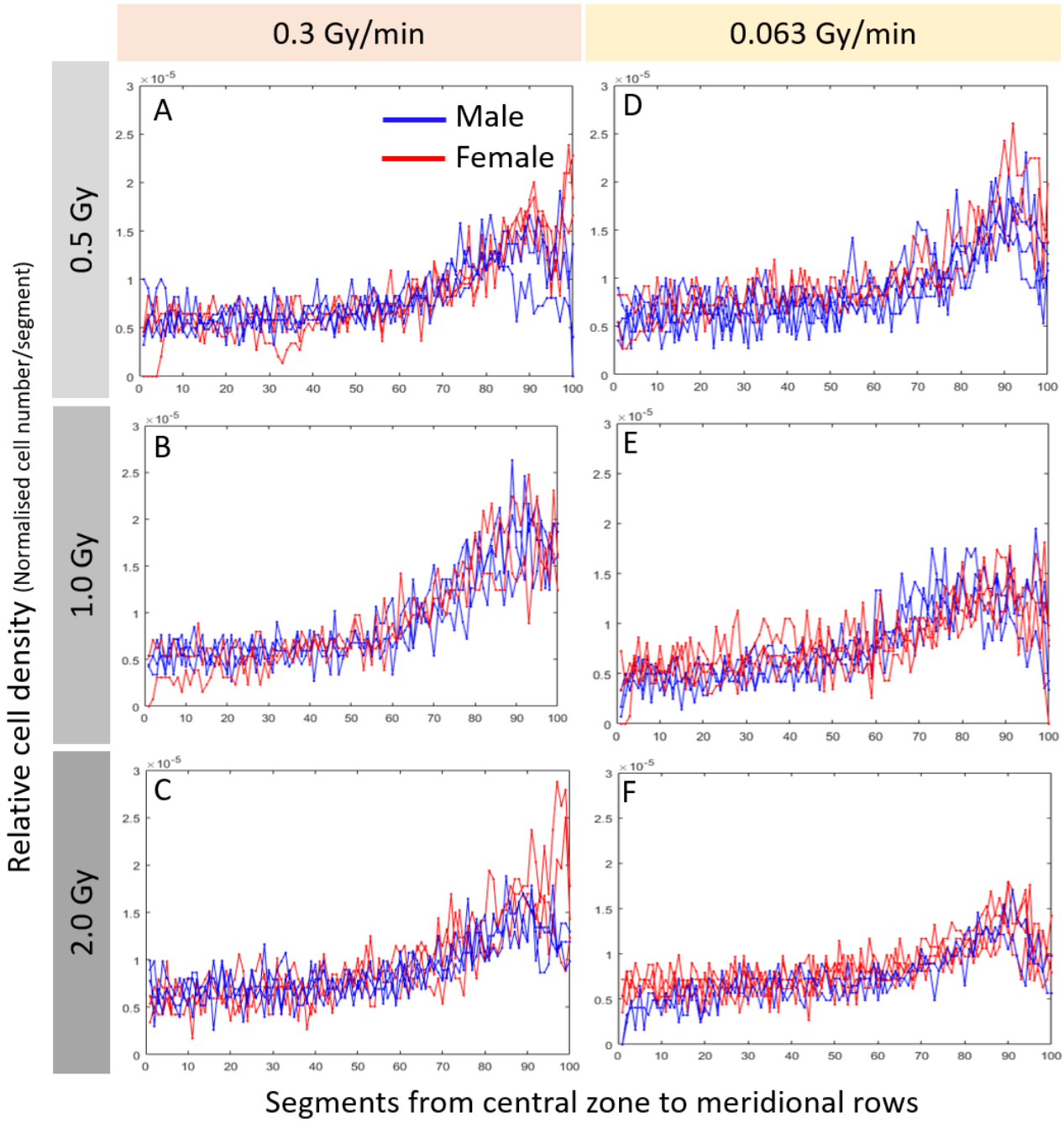

Figure 4.7: Plot of relative cell density versus segment number for the lens epithelium spanning the central zone to the furthest edge of the meridional rows of IR exposed CD1 mice at 10 weeks of age. Comparison of male and female mice 4 months post-IR that were exposed to A) 0.5 Gy, B) 1 Gy and C) 2 Gy at a dose rate of 0.3 Gy/ min, and D) 0.5 Gy, E) 1 Gy and F) 2 Gy at a dose rate of 0.063 Gy/ min. This data was combined with the other CD1 data to assess statistical significance with the Kruskal-Wallis test using mutation, sex, dose rate and dose as independent factors and cell density as dependent factor. n= 3 for female mice and n= 3 for male mice.

4.3.4. Ptch1$^{+/-}$ mutation in CD1 did not affect cell density or response to IR exposure

Plots comparing unexposed wt and *Ptch1*$^{+/-}$ CD1 mice showed no *Ptch1*$^{+/-}$ associated relative cell density alterations in the CZ, PZ and MR (Figure 4.8). The variation of relative cell density in the PZ and MR was lower in *Ptch1*$^{+/-}$ mutants compared to wt CD1 (Figure 4.8).

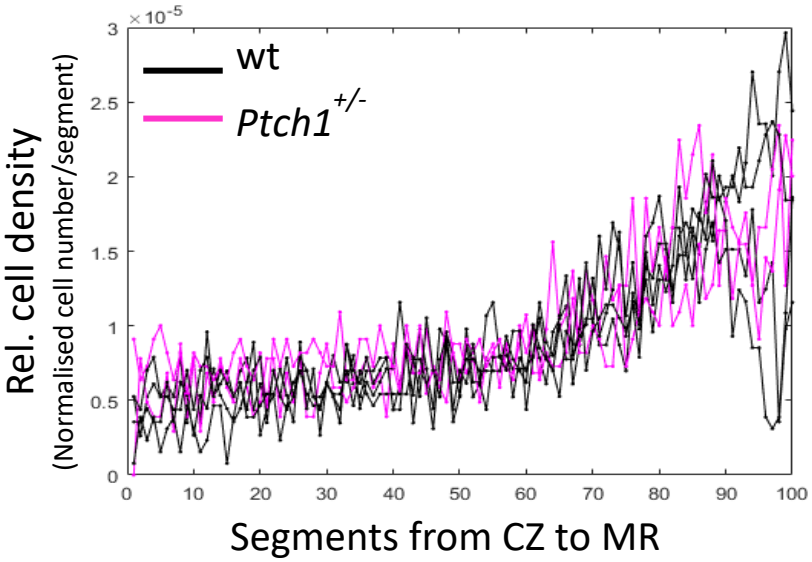

Figure 4.8: Plot of relative cell density versus segment number for the lens epithelium spanning the central zone to the furthest edge of the meridional rows of 6.5 month- old wt with Ptch1$^{+/-}$ *CD1 mice. This data was combined with the other CD1 data to assess statistical significance with the Kruskal-Wallis test using mutation, sex, dose rate and dose as independent factors and cell density as dependent factor. n= 4 for wt and n= 3 for* Ptch1$^{+/-}$ *mice Rel.: relative, CZ: central zone, MR: meridional rows, wt= wild type.*

Comparison of the relative cell density across the lens epithelium of 0.5, 1 and 2 Gy exposed wt and *Ptch1*$^{+/-}$ CD1 mice 4 months post-IR with their unexposed counterparts indicated that the *Ptch1*$^{+/-}$ mutation did not affect the response of CD1 mice to IR at both dose rates (p= 0.521; Figure 4.9A and D vs. B and E vs. C and F).

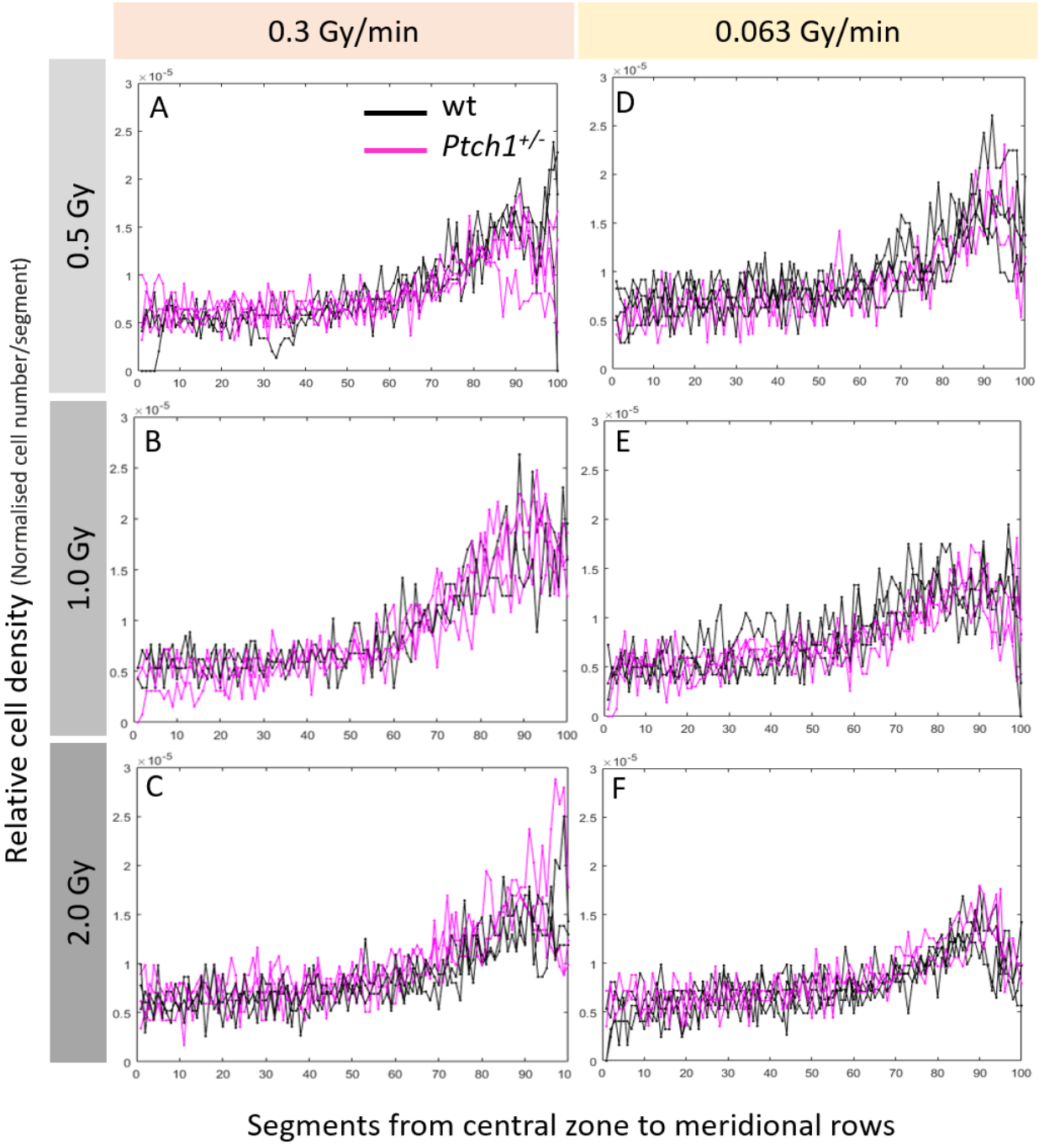

Figure 4.9: Plot of relative cell density versus segment number for the lens epithelium spanning the central zone to the furthest edge of the meridional rows of IR exposed CD1 mice at 10 weeks of age. Comparison of wt with Ptch1$^{+/-}$ *CD1 mice exposed to A) 0.5 Gy, B) 1 Gy and C) 2 Gy at a dose rate of 0.3 Gy/ min, and D) 0.5 Gy, E) 1 Gy and F) 2 Gy at a dose rate of 0.063 Gy/ min 4 months post-IR. This data was combined with the other CD1 data to assess statistical significance with the Kruskal-Wallis test using mutation, sex, dose rate and dose as independent factors and cell density as dependent factor. n= 3 for wt and n= 3 for* Ptch1$^{+/-}$ *mice per graph wt: wild type.*

4.3.5. Dose significantly influenced IR response of C57BL/6J

The gradient of the relative cell density graph of male and female C57BL/6J mice illustrated low relative cell density in the CZ that gradually increased and peaked in the PZ (Figure 4.10). Relative to the PZ, the relative cell density decreased in the MR, though it remained higher than in the CZ. No differences between male and female were observed.

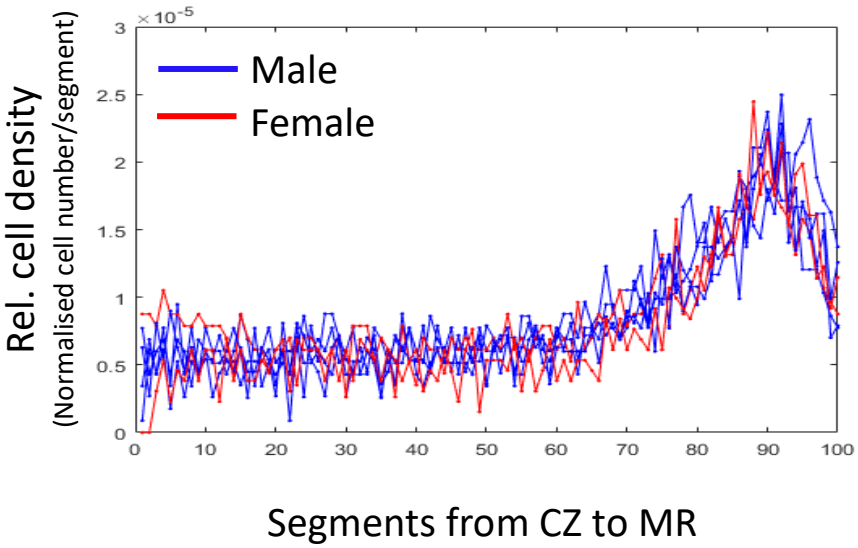

Figure 4.10: Plot of relative cell density versus segment number for the lens epithelium spanning the central zone to the furthest edge of the meridional rows of 6.5 month- old C57BL/6J mice. This data was combined with the other C57BL/6J data in this chapter to assess statistical significance with the Kruskal-Wallis test using mutation, sex, dose rate and dose as independent factors and maximum cell density as dependent factor. n= 4 for female and n=4 for male mice Rel.: relative, CZ: central zone, MR: meridional rows.

C57BL/6J mice showed variable responses to the IR depending on dose ($p< 0.001$; Figure 4.11). 4 months after exposure, a gradual decrease in relative cell density of the PZ compared to the control mice was observed in the C57BL/6J mice irradiated with 0.5 and 1 Gy (Figure 4.11A, B, D, and E vs. Figure 4.10). Mice irradiated at 0.3 Gy/ min presented no significant dissimilarities in response to IR from the ones exposed at a dose rate of 0.063 Gy/ min ($p= 0.151$; Figure 4.11A and B vs. D and E). Interestingly, the female mice exposed to 2 Gy at a dose rate of 0.3 Gy/ min showed similar relative cell density levels as the controls, contrary to the male mice which presented decreased relative cell

density in the PZ compared to their unexposed counterparts (Figure 4.11C vs. Figure 4.10). At the lower dose rate of 0.063 Gy/ min, the dissimilarity in response to 2 Gy IR exposure between male and female mice was more pronounced than at 0.3 Gy/ min, with female C57BL/6J mice demonstrating increased relative cell density in the PZ and their male counterpart showing decreased relative cell density in the same zone in comparison to the unexposed mice (Figure 4.11F vs. Figure 4.10). However, Kruskal-Wallis statistical test indicated that these observed differences between male and female were not significant ($p= 0.110$).

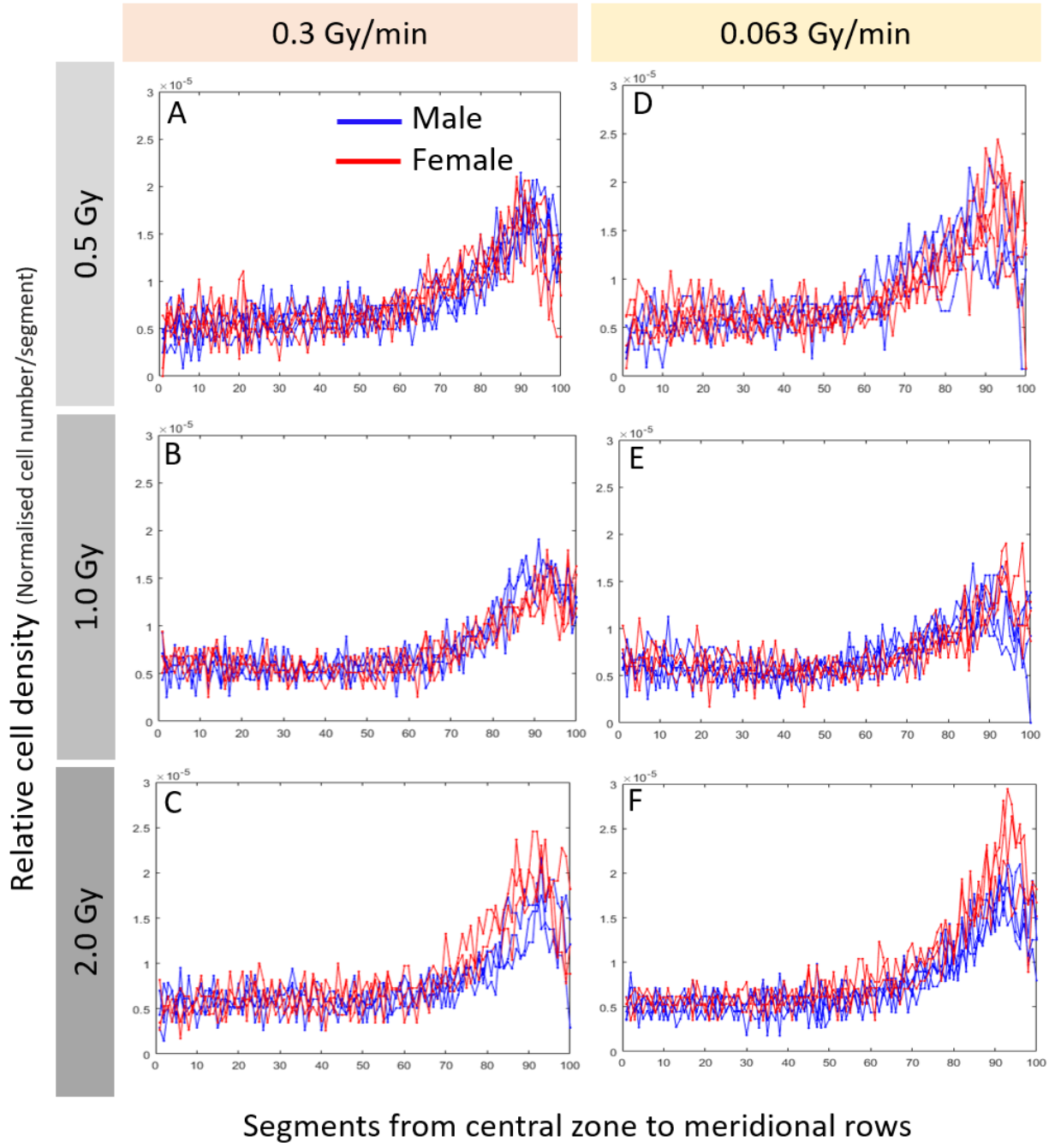

Figure 4.11: Plot of relative cell density versus segment number for the lens epithelium spanning the central zone to the furthest edge of the meridional rows of IR exposed C57BL/6J mice at 10 weeks of age. Comparison of male and female mice 4 months post-IR that were exposed to A) 0.5 Gy, B) 1 Gy and C) 2 Gy at a dose rate of 0.3 Gy/ min, and D) 0.5 Gy, E) 1 Gy and F) 2 Gy/ min at a dose rate of 0.063 Gy/ min. This data was combined with the other C57BL/6J data in this chaper to assess statistical significance with the Kruskal-Wallis test using mutation, sex, dose rate and dose as independent factors and maximum cell density as dependent factor. n= 3 for female mice and n= 3 for male mice per graph.

4.3.6. *Ptch1*$^{+/-}$ mutants react more severely to 2 Gy IR than wt C57BL/6J

To investigate the effect of *Ptch1*$^{+/-}$ on the lens epithelium cell density of C57BL/6J mice, plots comparing wt and *Ptch1*$^{+/-}$ C57BL/6J mice were generated. *Ptch1*$^{+/-}$ mutants illustrated the same relative cell density in the CZ, PZ and MR as wt C57BL/6J mice (Figure 4.12).

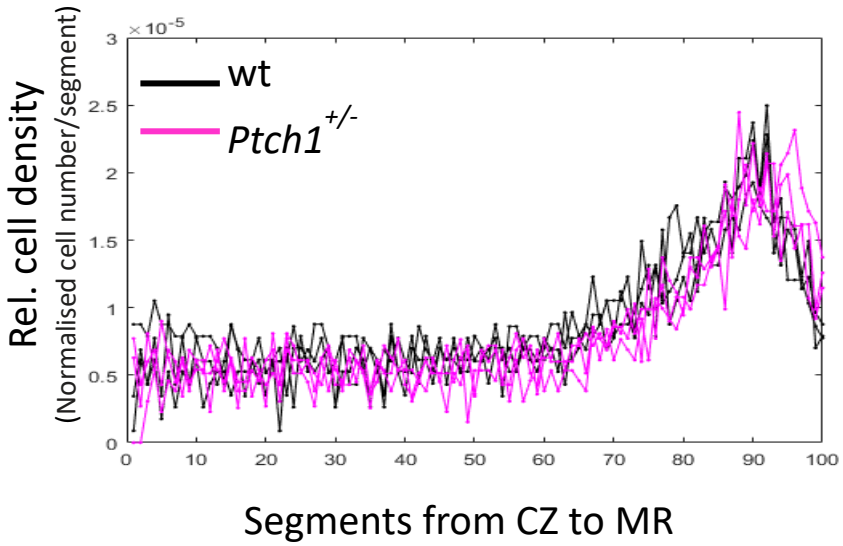

Figure 4.12: Plot of relative cell density versus segment number for the lens epithelium spanning the central zone to the furthest edge of the meridional rows of 6.5 month- old C57BL/6J mice. This data was combined with the other C57BL/6J data in this chapter to assess statistical significance with the Kruskal-Wallis test using mutation, sex, dose rate and dose as independent factors and maximum cell density as dependent factor. n= 4 for wt and n= 4 for Ptch1$^{+/-}$ *mice Rel.: relative, CZ: central zone, MR: meridional rows; wt= wild type.*

Comparison of the response to IR of *Ptch1*$^{+/-}$ mutants with the response of wt C57BL/6J mice showed no apparent differences at 0.5 and 1 Gy at the dose rates 0.3 and 0.063 Gy/ min 4 months post-IR (p= 0.130; Figure 4.13). Similar to the comparison of female with male mice (Figure 4.11C and F), at 2 Gy irradiated *Ptch1*$^{+/-}$ mutants demonstrated higher relative cell density in the peripheral zone than the wt C57BL/6J mice (Figure 4.13C). This divergence was more distinct at the 0.063 Gy/ min dose rate (Figure 4.13F).

Lastly, quantitative comparison of lens epithelium relative cell density in the CD1 and C57BL/6J strains revealed that the observed differences were significant ($p= 0.037$; Figure 4.6, Figure 4.7, Figure 4.8, Figure 4.9, Figure 4.10,Figure 4.11, Figure 4.12 and Figure 4.13).

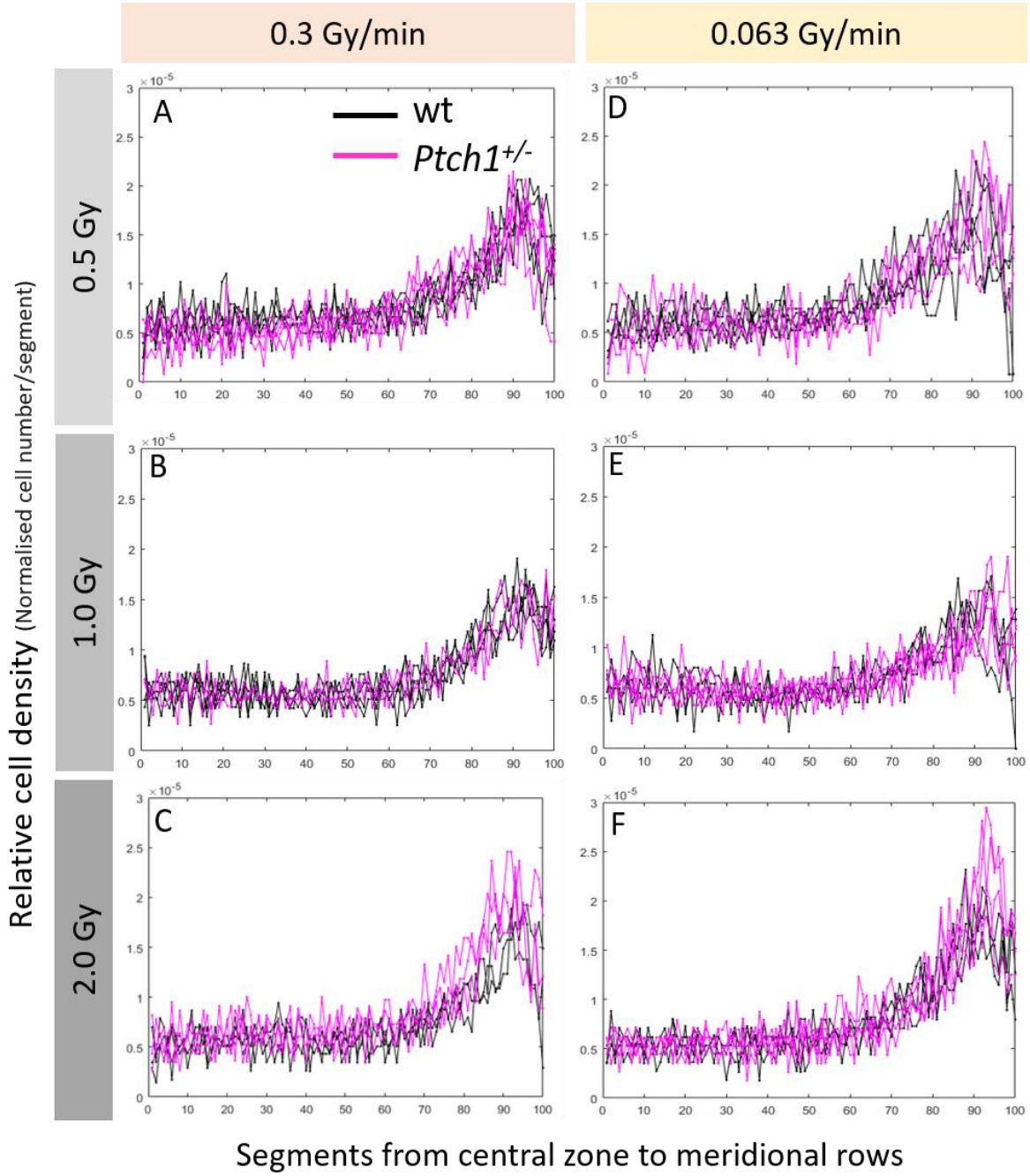

Figure 4.13: Plot of relative cell density versus segment number for the lens epithelium spanning the central zone to the furthest edge of the meridional rows of IR exposed C57BL/6J mice at 10 weeks of age. Comparison of wt with Ptch1$^{+/-}$ *C57BL/6J mice exposed to A) 0.5 Gy, B) 1 Gy and C) 2 Gy/ min at a dose rate of 0.3 Gy/ min, and D) 0.5 Gy, E) 1 Gy and F) 2 Gy/ min at a dose rate of 0.063 Gy/ min 4 months post-IR. This data was combined with the other C57BL/6J data in this chapter to assess statistical significance with the Kruskal-Wallis test using mutation, sex, dose rate and dose as independent factors and maximum cell density as dependent factor. n= 3 for wt and n= 3* Ptch1$^{+/-}$ *per graph wt: wild type.*

4.3.7. Eye lenses of mice collected 4 and 12 months post-IR showed minimal differences in cell density

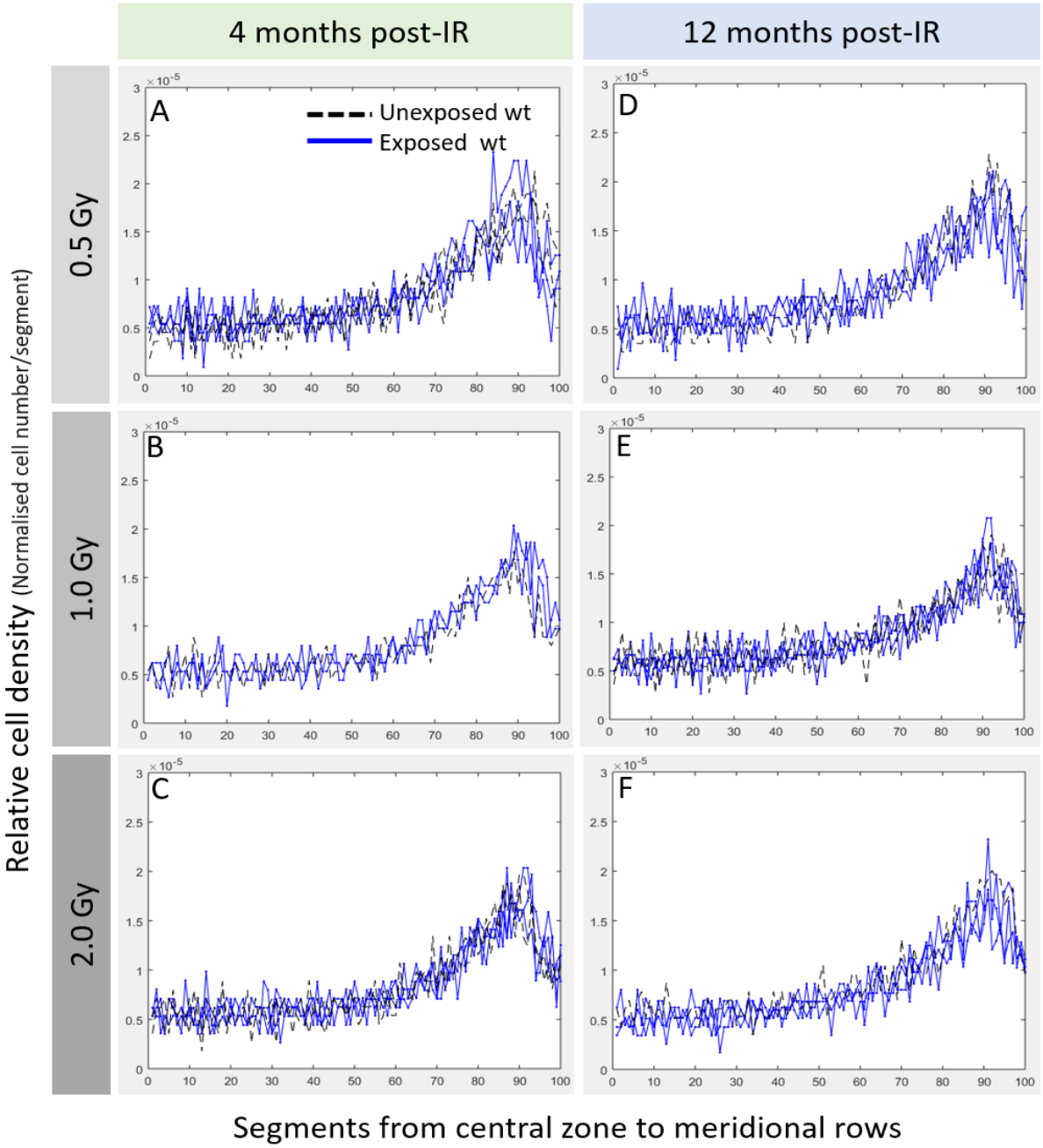

Figure 4.14: Plot of relative cell density versus segment number for the lens epithelium spanning the central zone to the furthest edge of the meridional rows of IR exposed B6C3F1 male mice at 10 weeks of age. Comparison of unexposed with IR exposed wt B6C3F1 mice (at a dose rate of 0.3 Gy/ min) to A) 0.5 Gy, B) 1 Gy, C) 2 Gy at 4 months post-IR exposure, and D) 0.5 Gy, E) 1 Gy, and F) 2 Gy at 12 months post-IR. General Linear Model Analysis of Variance using time, mutation, sex and dose as independent factors and maximum cell density as dependent factor was applied for statistical analysis on the collective B6C3F1 cell density data. n= 2 for unexposed and n= 4 for exposed per graph, wt: wild type, IR: ionising radiation.

To study the changes in cell density of the lens epithelium over time in irradiated B6C3F1, 10 week-old mice were exposed to 0.5, 1 and 2 Gy at a dose rate of 0.3 Gy/ min and the eye lenses were collected at 4 or 12 months post- IR exposure (Figure 4.2). The individual graphs showed minimal differences between the relative cell density in the CZ, PZ and MR of exposed wt B6C3F1 male mice in comparison with the relative cell density across the lens epithelium of the unexposed matched controls (Figure 4.14). No significant differences between 4 and 12 months post-IR were observed in the 0.5, 1 and 2 Gy IR-exposed wt B6C3F1 male mice ($p > 0.05$; Figure 4.14). Interestingly, comparison of the peak of the relative cell density in the PZ of the 0.5, 1 and 2 Gy irradiated mice indicated decreased relative cell density in 1 and 2 Gy relative to 0.5 Gy irradiated mice ($p < 0.005$; Figure 4.14C and F vs. A, B, D and E).

The involvement of the Ercc2 gene in the response of B6C3F1 lens epithelium cell density to IR was investigated by exposing heterozygous mutated mice to 0.5, 1 and 2 Gy at a dose rate of 0.3 Gy/ min (Figure 4.2). Similar to the trend noted in wt male B6C3F1 (Figure 4.14), the graphs showed minimal differences between the lens epithelium relative cell density of exposed male mice and their paired unexposed male mice (Figure 4.15). A dose-dependent decrease in the PZ was observed at 4 (Figure 4.15A, B vs. C) and 12 (Figure 4.15D, E vs. F) months post-IR exposure in *Ercc2*$^{+/-}$ mutants. Comparison of the peak of relative cell density noted at 4 and 12 months showed that the relative cell density in PZ was lower at 12 months in the 0.5, 1 and 2 Gy irradiated B6C3F1 male mice than at 4 months post-IR, though these differences were not statistically significant ($p > 0.05$; Figure 4.15A, B and C vs. D, E and F). The *Ercc2*$^{+/-}$ mutants demonstrated a similar, but more pronounced response to IR as wt B6C3F1 mice. Collective statistical analysis of the B6C3F1 mice data revealed that the *Ercc2*$^{+/-}$ mutants were significantly more sensitive to IR ($p = 0.009$; Figure 4.15 vs. Figure 4.16).

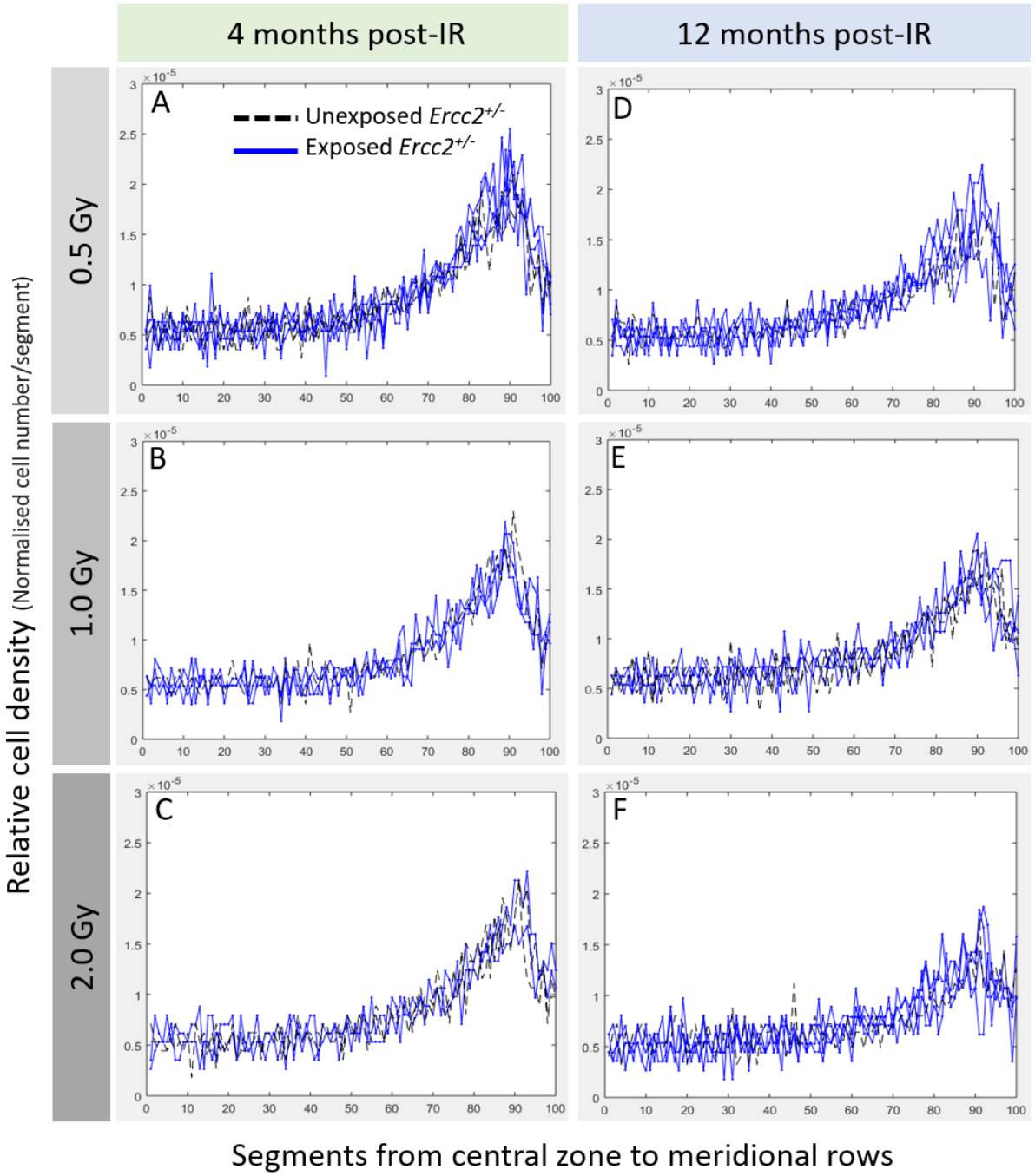

Figure 4.15: Plot of relative cell density versus segment number for the lens epithelium spanning the central zone to the furthest edge of the meridional rows of IR exposed B6C3F1 male mice at 10 weeks of age. Comparison of unexposed with IR exposed wt B6C3F1 mice (at a dose rate of 0.3 Gy/ min) to A) 0.5 Gy, B) 1 Gy, C) 2 Gy at 4 months post-IR exposure, and D) 0.5 Gy, E) 1 Gy, and F) 2 Gy at 12 months post-IR. General Linear Model Analysis of Variance using time, mutation, sex and dose as independent factors and maximum cell density as dependent factor was applied for statistical analysis on the collective B6C3F1 cell density data. n= 2 for unexposed and n= 4 for exposed per graph, IR: ionising radiation.

4.3.8. B6C3F1 female mice are more sensitive to IR than their male counterpart

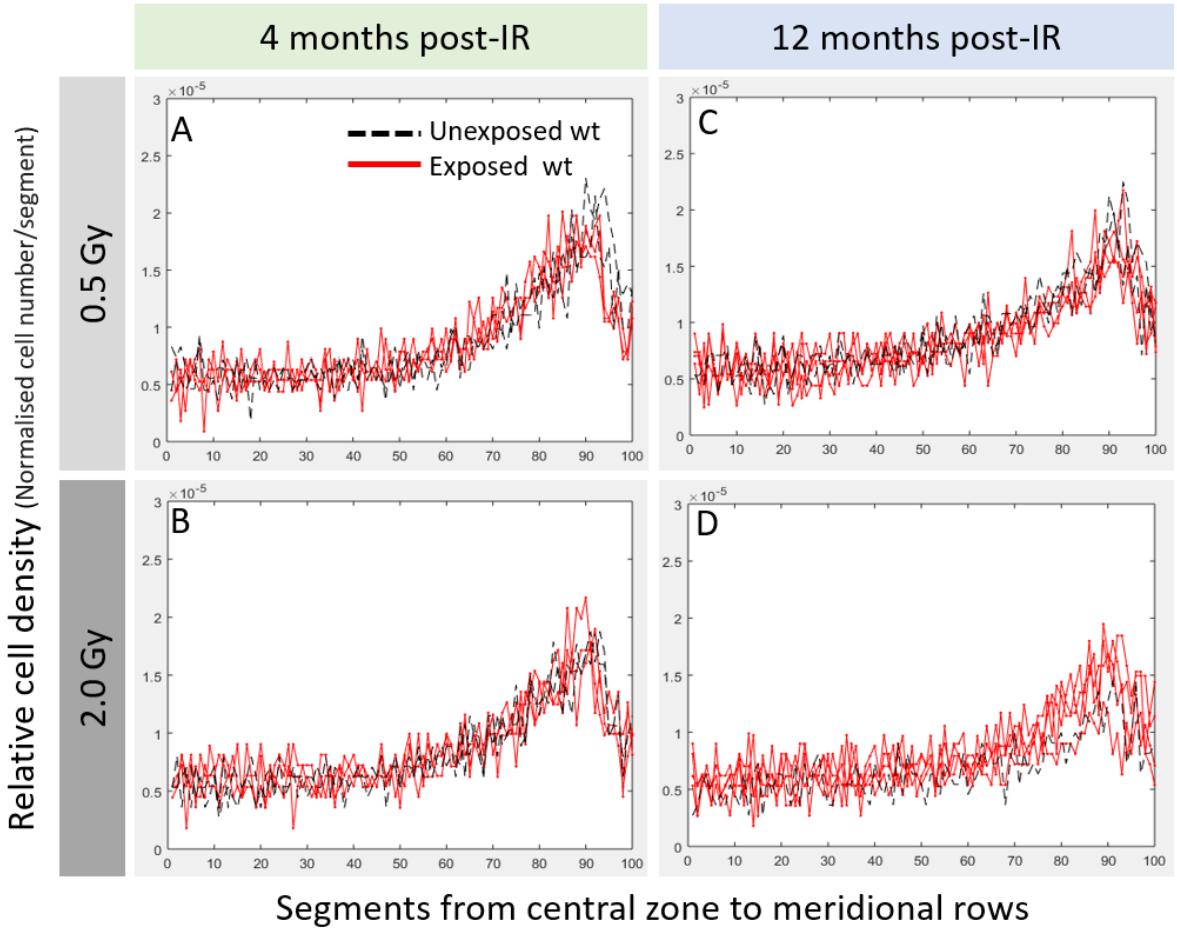

Figure 4.16: Plot of relative cell density versus segment number for the lens epithelium spanning the central zone to the furthest edge of the meridional rows of IR exposed B6C3F1 female mice at 10 weeks of age. Comparison of unexposed with IR exposed Ercc2$^{+/-}$ *B6C3F1 mice to A) 0.5 Gy and B) 2 Gy at 4 months post-IR exposure, and C) 0.5 Gy and D) 2 Gy at 12 months post-IR. Exposure was performed at a dose rate of 0.3 Gy/ min. General Linear Model Analysis of Variance using time, mutation, sex and dose as independent factors and maximum cell density as dependent factor was applied for statistical analysis on the collective B6C3F1 cell density data. n= 2 for unexposed and n= 4 for exposed per graph, IR: ionising radiation.*

To investigate whether the perceived trends in the IR-response of male B6C3F1 mice were sex specific, wt female B6C3F1 were exposed to 0.5 and 2 Gy (Figure 4.16). Comparison of relative cell density at 4 and 12 months post-IR showed minimal differences between both time points at 0.5 and 2 Gy (Figure 4.16A and B vs. C and D). Similar to their male counterparts (Figure 4.14), B6C3F1 female mice showed decreased relative cell density in the PZ of the 2 Gy in comparison with 0.5 Gy irradiated mice (Figure 4.16A and C vs. B and D).

Ercc2$^{+/-}$ B6C3F1 female mice were exposed to 0.5, 1 and 2 Gy to examine whether the mutation affected lens epithelium cell density response to IR exposure in female mice (Figure 4.2). Although minimal differences were detected between the exposed and their paired controls (Figure 4.17A, B, C, D, E and F), a dose-dependent decrease in the relative cell density in the PZ was observed (Figure 4.17A and D vs. B and E vs. C and F). This decline was more notable 12 months post-IR (Figure 4.17A, B and C vs. D, E and F). At 12 months post-IR exposure, the 2 Gy irradiated *Ercc2*$^{+/-}$ female mutants showed decreased relative cell density compared to their paired controls.

Comparison of the male *Ercc2*$^{+/-}$ mutants and wt B6C3F1 with their female counterparts revealed that although both sexes showed analogous responses to IR, female mice were significantly more sensitive to IR ($p= 0.029$; Figure 4.14,Figure 4.15, Figure 4.16 and Figure 4.17).

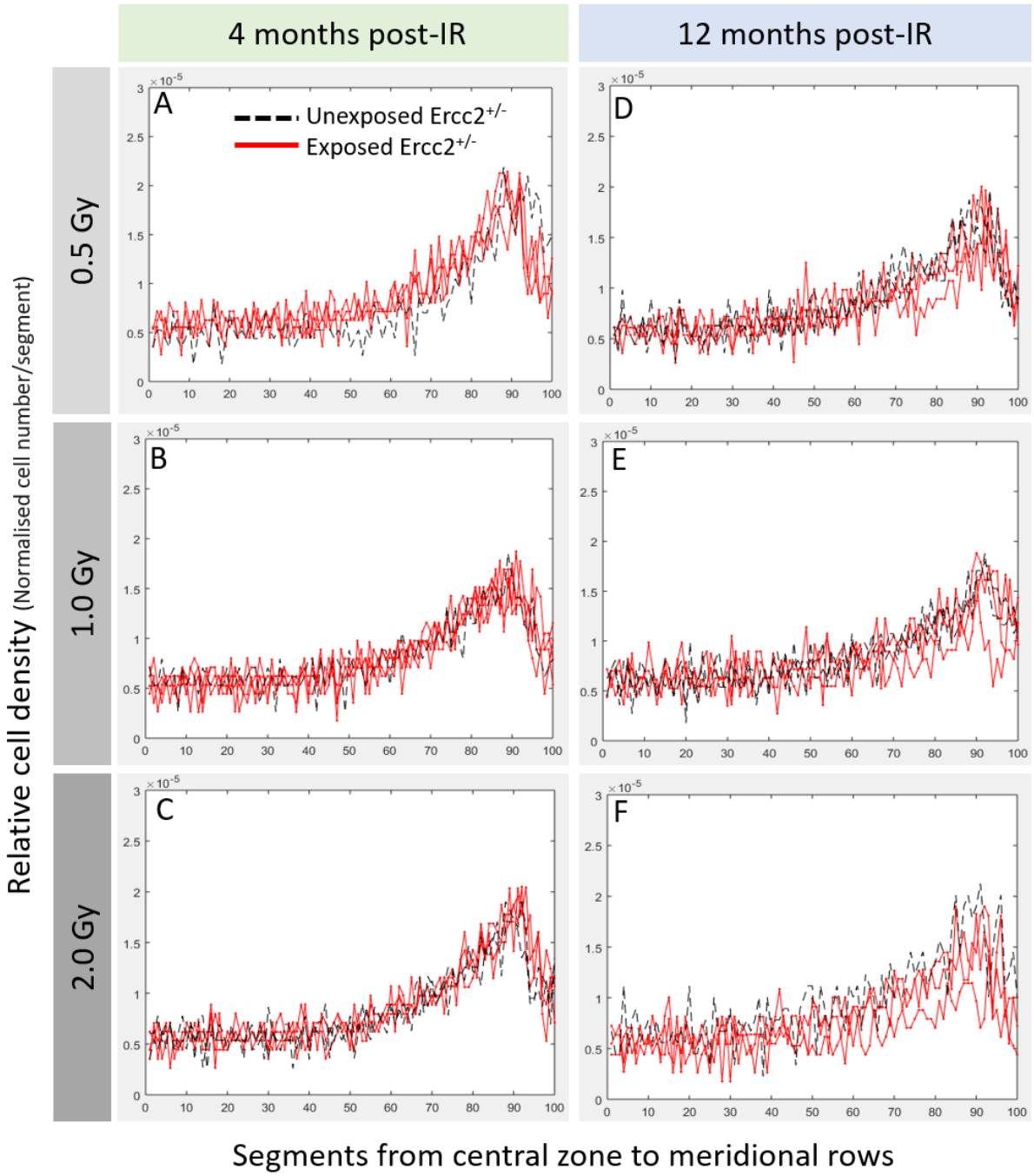

Figure 4.17: Plot of relative cell density versus segment number for the lens epithelium spanning the central zone to the furthest edge of the meridional rows of IR exposed Ercc2$^{+/-}$ *B6C3F1 female mice at 10 weeks of age. Comparison of unexposed with exposed* Ercc2$^{+/-}$ *B6C3F1 mice to A) 0.5 Gy, B) 1 Gy and C) 2 Gy at 4 months post-IR exposure, and D) 0.5 Gy, E) 1 Gy and F) 2 Gy at 12 months post-IR. Exposure was performed at a dose rate of 0.3 Gy/ min. General Linear Model Analysis of Variance using time, mutation, sex and dose as independent factors and maximum cell density as dependent factor was applied for statistical analysis on the collective B6C3F1 cell density data. n= 4 for exposed and n= 2 for the unexposed paired control.*

4.3.9. Uncertainty budget

An uncertainty budget summarises all the factors that contribute to uncertainties in measurement results during an experiment. This can be completed quantitatively by calculating the combined uncertainty value or qualitatively by determining all the factors that contribute to uncertainty, estimating their contribution and addressing the critical uncertainties. All factors which can be estimated via statistical analysis of repeated measurements are accounted for as type A (random) errors and are associated with a normal (Gaussian) distribution. The uncertainty contributors that cannot be estimated using statistics are grouped in type B (systematic) errors, these factors are coupled with a continuous uniform (rectangular) distribution because of their constant probability in variation. Twelve uncertainty contributors were identified during the quantification of IR-induced changes in cell density (Table 4.1). All factors were Gaussian distributed besides sex, which showed a rectangular distribution. "Age variability within a group of mice", phenotypic variability, animal house conditions, time of sacrifice, dose exposure, "efficiency of evenly staining across the lens epithelium", "distance from MR to CZ", time of sacrifice and "accurate detection of nuclei by the Matlab program" had a minor contribution in contrast to sex, dose rate, genetic variability and repeatability of cell density measurements which had a significant contribution to uncertainty.

Table 4.1: Uncertainty budget for the quantification of IR-induced alterations in cell density measurements.

Uncertainty contributor	Qualitative uncertainty	Parameter Unit	Type of Evaluation	Distribution
Age variability within a group of mice	minor	months	A	Gaussian
Phenotypic variability	minor	density	A	Gaussian
Genetic variability	significant	density	A	Gaussian
Animal house conditions	minor	density	A	Gaussian
Time of sacrifice	minor	density	A	Gaussian
Dose exposure	minor	density	A	Gaussian
Sex	significant	density	B	Rectangular
Dose rate	significant	density	A	Gaussian
Efficiency of evenly staining across the lens epithelium	minor	intensity	A	Gaussian
Distance from MR to CZ zone	minor	cm	A	Gaussian
Accurate detection of nuclei by the Matlab program	minor	intensity	A	Gaussian
Repeatability of cell density measurements	significant	density	A	Gaussian

4.4. Discussion

4.4.1. Strain with shorter lifespan has poorly organised cells in the MR

Transitioning from flat mounts to whole mounts provided an easier method to study cellular organisation in the lens epithelium (Figure 4.3 andFigure 4.4). However, the results showed further work is required to enable the use of this technique to directly study cell proliferation. The main challenge encountered during whole mount staining of proliferative cells was the migration of the conjugated Ki-67 antibody through the lens capsule which has very limited permeability, this could be surpassed by using EdU staining.

Whole mount imaging revealed that the lens epithelium of the CD1 strain was differently organised than the C57BL/6J and B6C3F1 strains at an age of 6.5 months (Figure 4.5). This was also reflected in the quantification of lens epithelium cell density that illustrated comparable curves of relative cell density from the CZ to the MR for C57BL/6J and B6C3F1 in contrast to the curve observed in CD1 mice (Figure 4.6 vs. Figure 4.10 andFigure 4.14). Comparison of lens epithelium cellular organisation across various species and strains noted in previous studies showed similar cell densities in CZ, PZ and MR as the ones observed the C57BL/6J and B6C3F1 mice during this investigation (Hayden et al., 1980, Wu et al., 2015) (Figure 4.10 and Figure 4.14). The poorly organised cells in the MR detected in CD1 mice correspond to the lens epithelium cellular organisation observed in aged mammals (Wu et al., 2015). Possibly, the ill organised MR are associated to the shorter lifespan of CD1 mice in comparison to C57BL/6J and B6C3F1 strains. The CD1 strain has an average lifespan of 15 months, while C57BL/6J and B6C3F1 live respectively around 31 and 27 months (Dalke et al., 2018, Pérez et al., 2009, Masoro and Austad, 2011). Interestingly, at 8 weeks of age CD1 mice already show a weaker visual performance than C57BL/6J mice (Abdeljalil et al., 2005, Redfern et al., 2011). Lifespan studies examining change in the cellular organisation of lens epithelium in CD1 versus C57BL/6J mice are needed to confirm the hypothesis of lens epithelium cellular organisation reflecting life expectancy.

4.4.2. Effect of dose on lens epithelium cell density is significant in all tested strains

The in-house developed cell density measuring Matlab program offered an approach of quantifying IR-induced changes in relative cell density across the different zones of the lens epithelium. Improvement to this tool is ongoing with the focus on removing the uncertainty contributor “distance from MR to CZ” that is manually determined in the current program. For this, the aim is to combine the reconstruction of the position of each nuclei in 3D space and automatically establishing the distance from the MR to the CZ (Table 4.1).

Comparison of the relative cell density in the CZ of CD1, C57BL/6J and B6C3F1 at 4 months post-IR showed that it remained constant between strains and was not affected by IR (Figure 4.6,Figure 4.7, Figure 4.8, Figure 4.9, Figure 4.10, Figure 4.11, Figure 4.12, Figure 4.13, Figure 4.14, Figure 4.15, Figure 4.16 and Figure 4.17). Measurements of IR-induced DNA damage and cell proliferation

modifications up to 24 hours post-IR in C57BL/6J showed that the CZ, though less than the PZ, is sensitive to IR (Barnard et al., 2019, Markiewicz et al., 2015, Barnard et al., 2018). These studies suggest that DNA repair in the CZ occurs significantly faster than in the PZ, and therefore, it is conceivable that by 4 months any IR-induced changes in cell density in the CZ have been restored while the modifications in the PZ still persist.

In contrast to the CZ, the cell density in the PZ was more affected by IR exposure in all strains (Figure 4.7,Figure 4.11 and Figure 4.14). Compared to unexposed mice, 0.5 and 1 Gy exposed mice showed decreased relative cell density in the PZ of the lens epithelium at 4 months post-IR (Figure 4.7A, B, D and E;Figure 4.11 A, B, D and E; Figure 4.14 A, B, D and E, and Figure 4.16A and C). However, the response to 2 Gy was variable between the strains (Figure 4.7C and F, Figure 4.11C and F, Figure 4.14C and F, and Figure 4.16B and D). The relative cell density in the PZ increased in 2 Gy C57BL/6J mice relative to the unexposed mice (Figure 4.11C and F vs. Figure 4.10), while in B6C3F1 and CD1 mice the dose-dependent decreasing trend compared with their unexposed counterparts was maintained (Figure 4.7C and F vs. Figure 4.6, Figure 4.14C and F, and Figure 4.16B and D). Non-linear response to IR in the lens epithelium has been reported before for DNA repair in the PZ of C57BL/6J (Markiewicz et al., 2015). The presented data suggest that C57BL/6J mice react differently to high (≥ 2 Gy) and low (< 2 Gy) doses. However, also that the threshold for defining high and low dose might be different between strains and still needs to be determined for the B6C3F1 and CD1 strain.

4.4.3. Dose rate effects are stronger at higher doses

IR-induced DNA damage in LECs was shown to increase with decreasing dose rate (Barnard et al., 2019). In line with this, exposing CD1 and C57BL/6J mice to IR at 0.3 and 0.063 Gy/ min showed that although the same dose response trends are observed at both dose rates, the lower dose rate caused a more pronounced response to IR which was nearly significant in CD1 ($p= 0.059$; Figure 4.7A, B and C vs. D, E and F), but not in the C57BL/6J strain ($p=0.151$; Figure 4.11A, B and C vs. D, E and F). These differences in dose rate dependent responses were more noticeable at 2 Gy (Figure 4.7C vs. F and Figure 4.11C vs. F). During the IR-induced DNA damage in LECs study, eye lenses were collected 4 and 24 h post-IR (Barnard et al., 2019), the presented data in this thesis showed that the dose rate effect can remain up to 4 months post-IR exposure.

4.4.4. Cell proliferation modifying mutations make the mice more sensitive to IR

The PTCH1 protein is a repressor of the sonic hedgehog (Shh) signalling pathway that regulates cell proliferation and differentiation through transcriptional activation of the transcription factor Gli1 (Jiang and Hui, 2008). Mutations in the Ptch1 gene were found to induce hypersensitivity to radiation in humans with the affected patients being more prone to develop skin cancers and interestingly, also showing higher prevalence of cataracts compared to the general population (Evans et al., 1993, Saran, 2010, O'Malley et al., 1997). Follow-up studies using CD1 mice showed increased cell proliferation in LECs of *Ptch1*$^{+/-}$ mutants in comparison to wt, and that this difference in proliferative activity decreased

with age (De Stefano et al., 2015). Reasoning that increased proliferative activity results in elevated relative cell density, Figure 4.8 and Figure 4.12 suggested that by the age of 6.5 months these dissimilarities in proliferative activity and thus also in relative cell density no longer exist in CD1 mice. Alternatively, small differences in cell proliferation were present, but due to the large variation in the peripheral zone cell density, these mutation-induced modifications were not detected. Increasing the amount of mice per cohort would be a possible way to overcome this. Retrospective power analysis needs to be performed to determine the amount of mice required to detect significant differences. Although C57BL/6J strain also showed no differences in relative cell density between *Ptch1*$^{+/-}$ mutants and wt at 6.5 months (Figure 4.12), further investigations are required to verify whether at an earlier age the proliferative capacity of *Ptch1*$^{+/-}$ mutants is different from wt C57BL/6J.

Furthermore, De Stefano and colleagues also demonstrated that *Ptch1*$^{+/-}$ mutants are more sensitive to IR-induced changes in cell proliferation than wt CD1 (De Stefano et al., 2015). No significant mutation specific IR-induced modifications in relative cell density were detected in the *Ptch1*$^{+/-}$ CD1 mutants relative to the wt when exposed to 0.5, 1 and 2 Gy (Figure 4.9A, B, C, D, E and F). Besides a dose-dependent decrease in relative cell density in the PZ, a dose-dependent decline in relative cell density variation is observed (Figure 4.9A, B, C, D, E and F). Transient increase in proliferation has been observed in irradiated rabbits that developed lens opacities (Alter and Leinfelder, 1953, Von Sallmann, 1952, Von Sallmann et al., 1953) which implied that the temporary upregulation of Shh pathway stimulated cataractogenesis later in life. Possibly, at 4 months post-IR other or additional pathways to the Shh pathway mediate the response of lens epithelium proliferative capacity and cell density to IR in CD1 mice. A good candidate is the mitogenic growth factor, FGF-2, which was shown to regulate age-related cell density decline in the lens epithelium (Dawes et al., 2013, Guggenmoos-Holzmann et al., 1989) and its expression in LECs to be affected by IR exposure (Hamada, 2017). In C57BL/6J mice, *Ptch1*$^{+/-}$ mutants showed a trend towards higher relative cell density in the PZ than wt mice after exposure to 2 Gy (Figure 4.13C and F). At doses <2 Gy, the heterozygous mutation did not affect the response to IR (Figure 4.13A, B, D and E). This suggested that the effect of *Ptch1*$^{+/-}$ mutation in C57BL/6J mice on IR exposure response is dose dependent.

The Ercc2 gene encodes the XPD protein, a subunit of the transcription factor IIH (TFIIH) complex, which is involved in DNA repair and regulation of gene transcription (Fuss and Tainer, 2011). Similar to the Ptch1 gene, mutation in Ercc2 has been associated with increased sensitivity to UV radiation leading to higher incidence of skin cancers (van de Ven et al., 2012). Introduction of *Ercc2*$^{+/-}$ in the parental strain of B6C3F1, C3HeB/FeJ, has been shown to increase sensitivity to IR (Kunze et al., 2015). Similarly, given that the impact of the *Ercc2*$^{+/-}$ mutation on IR response of B6C3F1 was significant ($p= 0.009$; Figure 4.15A, B, C, D, E and F, and Figure 4.17A, B, C, D, E and F), the presented data demonstrated that *Ercc2*$^{+/-}$ mutants are more sensitive to IR than wt B6C3F1. The mechanism through which this occurs is currently under investigation. Lower DSBs repair relative to wt C3HeB/FeJ, has

been detected in *Ercc2*$^{+/-}$ mutants (Kunze et al., 2015), though the induced epigenetic modification and their contribution to increased sensitivity to IR still has to be determined. Epigenetic research in the eye lens is already occurring (Alkozi et al., 2017), however this is not focused on IR effects yet.

4.4.5. Sex-specific effects more pronounced in the B6C3F1

Epidemiological data indicates that females are more sensitive to IR induced cataracts than males (Narendran et al., 2019, Fukutsu et al., 2018, Hamada et al., 2019, Azizova et al., 2018). Comparison of CD1, B6C3F1 and C57BL/6J suggest that sex-associated sensitivity to IR is strain specific (Figure 4.7 andFigure 4.11 vs. Figure 4.16). CD1 mice did not show sex-related cell density changes in response to IR (Figure 4.7). Relative cell density measurements in C57BL/6J mice suggested that females are more sensitive to IR at doses ≥ 2 Gy, though this effect was not significant (Figure 4.11A, B, D and E vs. C and F). In contrast to CD1 and C57BL/6J, female B6C3F1 mice were significantly more sensitive to IR compared with their male counterparts (Figure 4.14 vs. Figure 4.16). The mechanism underlying sex-dependent sensitivity to IR has not been elucidated yet. Remarkably, oestrogen has no role in the latter (Henderson et al., 2009).

4.4.6. Uncertainty budget: B6C3F1 data address the contribution of time of sacrifice

This study addressed a lot of factors contributing to uncertainty (Figure 4.2 and Table 4.1). Sex, dose rate, genetic variability were addressed and found to be significant contributors to IR response (Figure 4.6, Figure 4.7, Figure 4.8, Figure 4.9, Figure 4.10, Figure 4.11, Figure 4.12, Figure 4.13, Figure 4.14, Figure 4.15, Figure 4.16 and Figure 4.17). IR-response is known to be dependent of age at exposure (Thome et al., 2018, De Stefano et al., 2015). Therefore during this study, all mice were irradiated at the same age (10 weeks; Figure 4.2). Although the contribution of genetic variability was determined, assessing phenotypic variability was not in the scope of this research project. The contribution of this factor was minimised by housing CD1 and C57BL/6J in the same facility and offering both strains the same standard care. B6C3F1 was housed in another facility and the contribution of phenotypic variability in comparison with the other two strains will most probably be a little bit higher. Detailed data on the environment of all mice strains used during this research project have been collected and their contribution to the observed IR-response will be determined. Hoechst staining is an easy experimental procedure, however, to optimise accurate detection of nuclei by the Matlab program all cells have to exhibit the same intensity. Care was taken to ensure homogenous staining, hereby maximising the probability of each nuclei to display the same intensity under the microscope.

One uncertainty contributor addressed in the B6C3F1 data is the “time of sacrifice”. Mice, like humans and rats, are diurnal species (Refinetti, 2004). Melatonin, regulated by the circadian rhythm has been shown to mediate mitosis in rat lens epithelium (von Sallmann and Grimes, 1966). During this study, 2 control mice were paired with each group of exposed mice (Figure 4.14, Figure 4.15, Figure 4.16 and Figure 4.17). Interestingly, the cell density has the tendency to variate depending on the time of sacrifice which suggest that cell density is dependent of the circadian rhythm. Importantly, the contribution of

“time of sacrifice” to uncertainty in IR-induced changes in lens epithelium cell density studies can now be advised as minimal given that although the mice were sacrificed at different times during the day, it did not prevent the detection of significant dose-, dose rate-, sex- and mutation-dependent changes. Measuring the cell density at different times during the day together with determining the concentration of melatonin would provide a more precise answer to the level of contribution of this uncertainty contributor.

In conclusion, the cell density of the lens epithelium in mice is sensitive to IR. The severity of the contribution of factors such as dose rate, sex, cell proliferation mediating genes is specific to strain and IR-exposure dose. This highlights the influence of genetic background on IR-response and the importance of low versus high dose IR studies. Remarkably, the lens epithelium relative cell density measurements at 12 months post-IR in B6C3F1 mice showed that cell density remained constant over time (Figure 4.14,Figure 4.15, Figure 4.16 andFigure 4.17). None of the mice strains showed lens opacities, which emphasises the importance of longitudinal studies to understand IR-induced cataract. Although the gathered data provides insight into possible mechanisms involved in IR-induced cataracts, further work is required to fully understand underlying the mechanisms.

Chapter 5: In vitro studies show dose-dependent IR-exposure induced oxysterol formation

5.1. Introduction

5.1.1. Cholesterol in eye lens membrane

LFCs have one of the most cholesterol rich plasma membrane compared to other cell types and contain dihydrosphingomyelin as the most abundant phospholipid (Borchman and Yappert, 2010, Ferguson et al., 1996) (Figure 5.1). With age, the level of dihydrosphingomyelin and cholesterol continue to rise, crossing cholesterol the saturation limit, leading to lipid rafts formation. In contrast, the levels of glycerolipids decline (Rujoi et al., 2003, Mainali et al., 2017, Li et al., 1985, Huang et al., 2005). Electron paramagnetic resonance (EPR) spin-labeling showed that the molar ratio of cholesterol: phospholipid could increase up to 4:1 in the human nucleus (Mainali et al., 2015).

The role of cholesterol in the lens membrane remains ambiguous. Even though a couple of studies in the 19th and 20th century reported correlation between cataract and increased levels of cholesterol (Cahn, 1881, Feldman and Feldman, 1965), most recent research using upgraded techniques and equipment point towards a protective function of cholesterol. Cholesterol was shown to decrease oxygen permeability of plasma membranes and promote the reduction of the oxidative stress in bovine and human eye lenses (Widomska et al., 2007, Mainali et al., 2017, Subczynski et al., 2017, Plesnar et al., 2018, Subczynski et al., 2012). Measurements of cholesterol:phospholipid molar ratio demonstrated decreased cholesterol levels in cataractous lenses (Mainali et al., 2015, Jacob et al., 2001). Moreover patients with defects in genes coding for enzymes vital in the cholesterol synthesis pathway such as 7-dehydrocholesterol reductase in Smith–Lemli–Opitz syndrome (Cotlier and Rice, 1971) and mevalonate kinase in mevalonic aciduria (Wilker et al., 2010) show a higher incidence of cataracts compared to the general population, emphasizing the importance of cholesterol homeostasis to lens transparency.

5.1.2. Cholesterol oxidation products

Similar to ageing, IR leads to increased oxidative stress (Uwineza et al., 2019, Buonanno et al., 2011). Downstream effects of the elevated oxidative stress have been studied through ageing: the build-up of 7-ketocholesterol, a cholesterol oxidation adduct, with age was observed in the lens (Rodriguez et al., 2014). Also other cholesterol oxidation products, i.e. 20α-hydroxycholesterol, 25-hydroxycholesterol, 7β-hydroxycholesterol, 7-ketocholesterol and 5,6-epoxycholesterol, have been found to accumulate in cataractogenic lenses in comparison to clear lenses (Girao et al., 1998). The mechanism through which these oxysterol lead to lens clouding is an ongoing field of study. Oxysterols affect the structure of membranes by changing the permeability and through translocation into vesicles (Kulig et al., 2016, Theunissen et al., 1986). Adding 7-ketocholesterol, 7β-hydroxycholesterol and 25-hydroxycholesterol to artificial membranes demonstrated that these oxysterols induce membrane instability by rendering it more sensitive to heat (Vestergaard et al., 2011). Radiolabeling of sterols demonstrated that 7-

ketocholesterol, 7α/β-hydroxycholesterol and 25-hydroxycholesterol were transferred from membranes to lipoproteins and vesicles at a much higher rate than cholesterol (Theunissen et al., 1986).

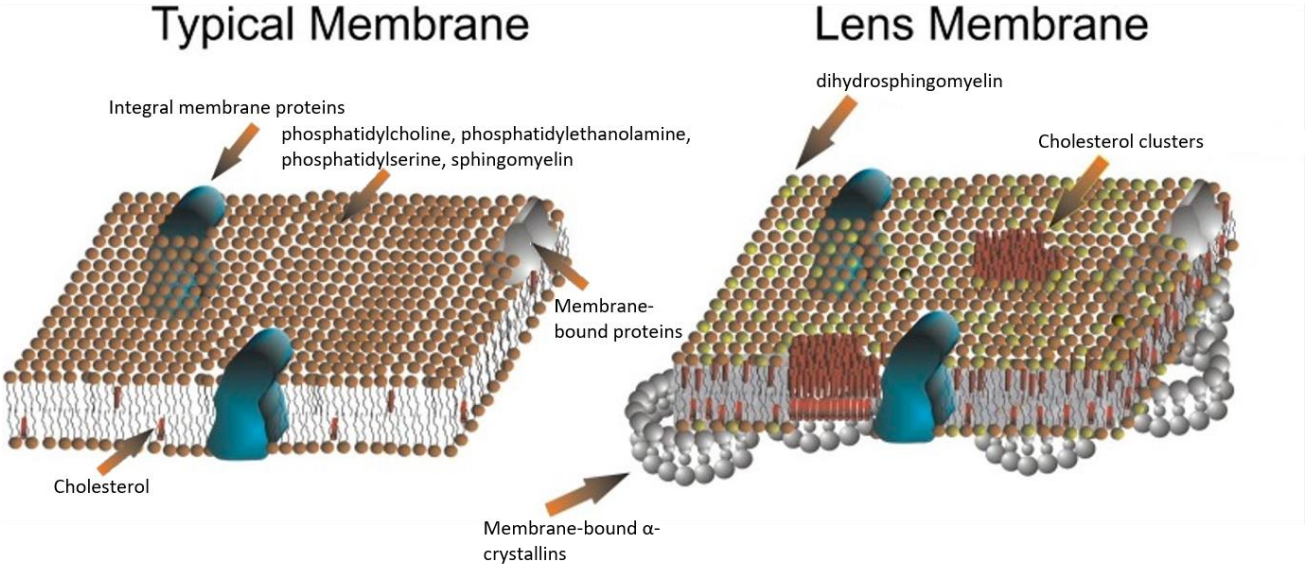

Figure 5.1: Comparison of the membrane of typical cells and lens membrane. Typical membranes contain phosphatidylcholine, phosphatidylethanolamine, phosphatidylserine and sphingomyelin as the predominant phospholipids. Besides integral membrane proteins and membrane-bound proteins, they also contain low levels of cholesterol. Lens membranes contain more cholesterol which can lead to the formation of cholesterol clusters and have dihydrosphingomyelin as the most abundant phospholipid. Lens membranes typically show more membrane-bound crystallins as they age. Schematic figure adapted from Borchman and Yappert, J Lipid Res, 2010.

5.2. Objectives and experimental design

IR and ageing are both factors that lead to an increase in oxidative stress (Reisz et al., 2014, Pescosolido et al., 2016) and therefore enhance the probability of cholesterol oxidation occurring. Given that the build-up of oxysterols in the eye lens has been shown to be associated with age-related cataractogenesis (Girao et al., 1998), the possibility of oxysterols being involved in IR-induced cataractogenesis was examined. As a first step, the effects of IR on the lipid in the membrane of LFCs were investigated by exposing bovine lipid membrane extracts to high levels of X-rays followed by liquid chromatography mass spectrometry (LC-MS) analysis, and the identifying and quantifying oxysterols (Figure 5.2). As this was a validation exercise and to maximize the probability of detecting an intense and clear signal of oxysterols which are present in very low levels compared to cholesterol levels, doses up to 50 Gy were applied.

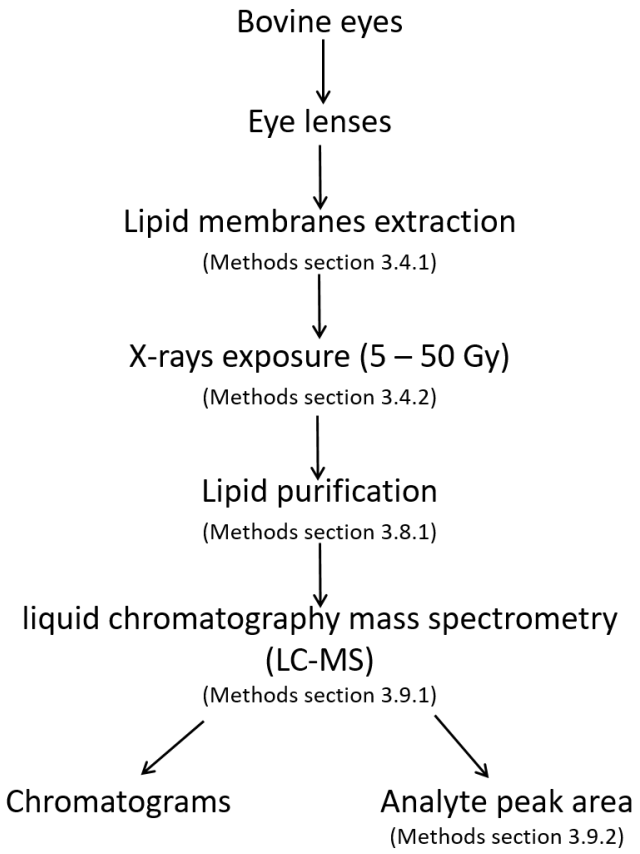

Figure 5.2: Schematic representation of experimental design of in vitro IR-induced oxysterol formation analysis.

5.3. Results

5.3.1. Cholesterol levels did not change significantly following IR exposure

To investigate the effect of IR exposure on highly cholesterol concentrated membranes, cholesterol levels in IR-exposed bovine eye lens membrane extracts were measured via LC-MS. The chromatogram of bovine lipid membrane extracts exposed to 5 and 50 Gy X-ray showed that radiation exposure did not lead to any noticeable changes in cholesterol levels (Figure 5.3A). Quantification via analyte peak area measurements confirmed that there are no statistical significant IR-dose dependent changes in cholesterol levels ($p= 0.794$; Figure 5.3B). Moreover, the nucleus contained significantly more cholesterol than the cortex ($p= 0.006$; Figure 5.3B).

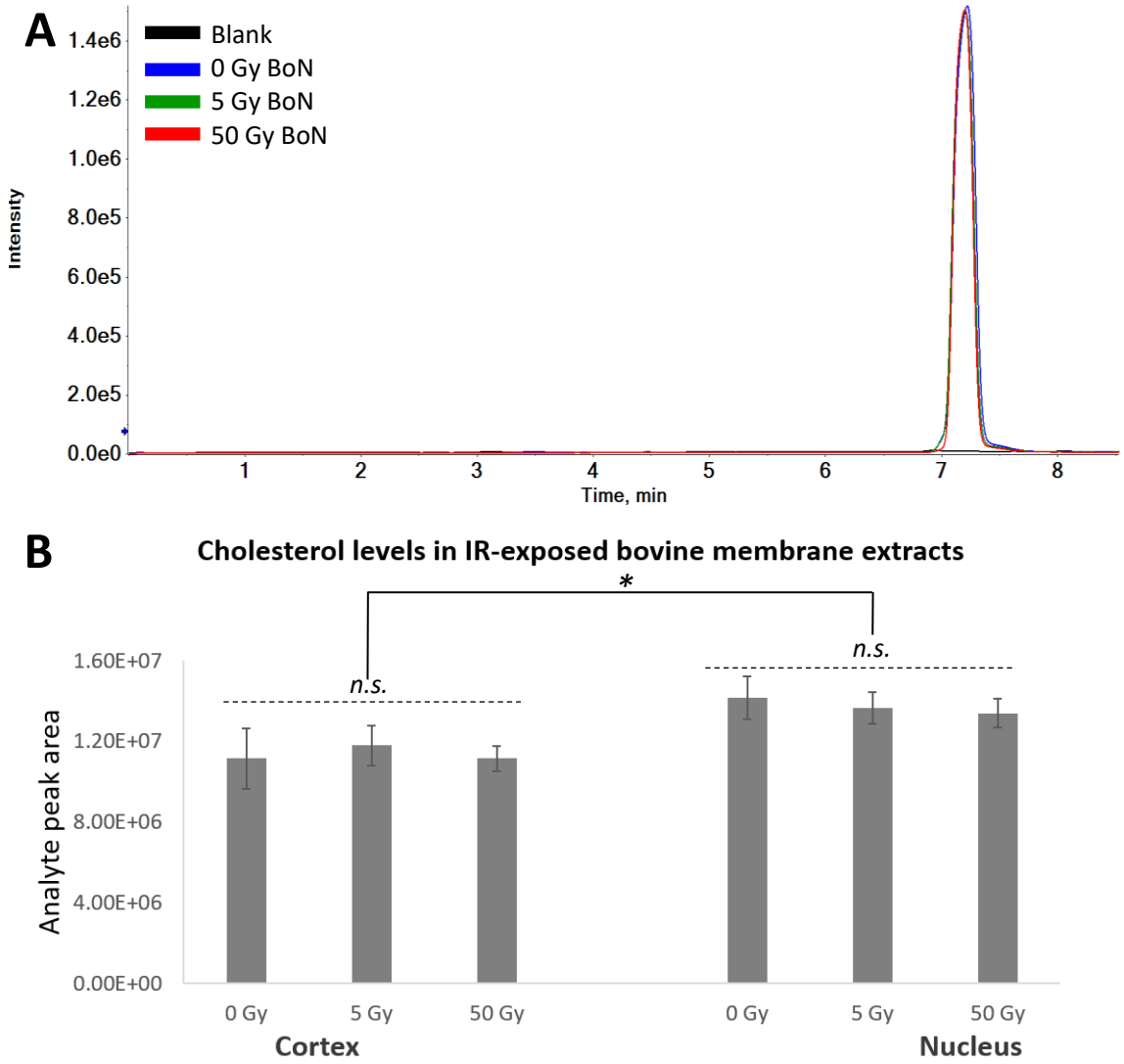

*Figure 5.3: Lipid membranes isolated from the cortex and the nucleus of bovine eye lenses were exposed to 0, 5 and 50 Gy of X-rays and analysed by LC-MS (separated by cortex column). A) Superposition of the chromatograms of the 0, 5 and 50 Gy BoN samples and B) quantification of cholesterol levels in the membrane samples, error bars represent standard deviation, *p<0.05 n= 3, n.s.: not significant, BoN: bovine nucleus.*

5.3.2. Identification of oxysterols in LFC lipid membranes

Overlay of chromatograms for 0 and 50 Gy irradiated bovine nuclear fraction samples showed that oxysterol levels in the lens lipid membranes increased after IR-exposure (Figure 5.4). The retention time for each peak was determined and the most abundant multiple reaction monitoring (MRM) detected in each peak was used in combination with the Lipidomics Gateway database and the data provided in the McDonald *et al.* 2012 publication to determine the identity of the peak (Table 5.1) (McDonald et al., 2012). Seven of the eleven examined peaks show an IR dose-dependent increase (Table 5.1). The presence of 7-ketocholesterol, 7β-hydroxycholesterol and 5,6-epoxycholesterol were confirmed by running undeuterated and/ or deuterated standards along with the samples (Figure 5.5).

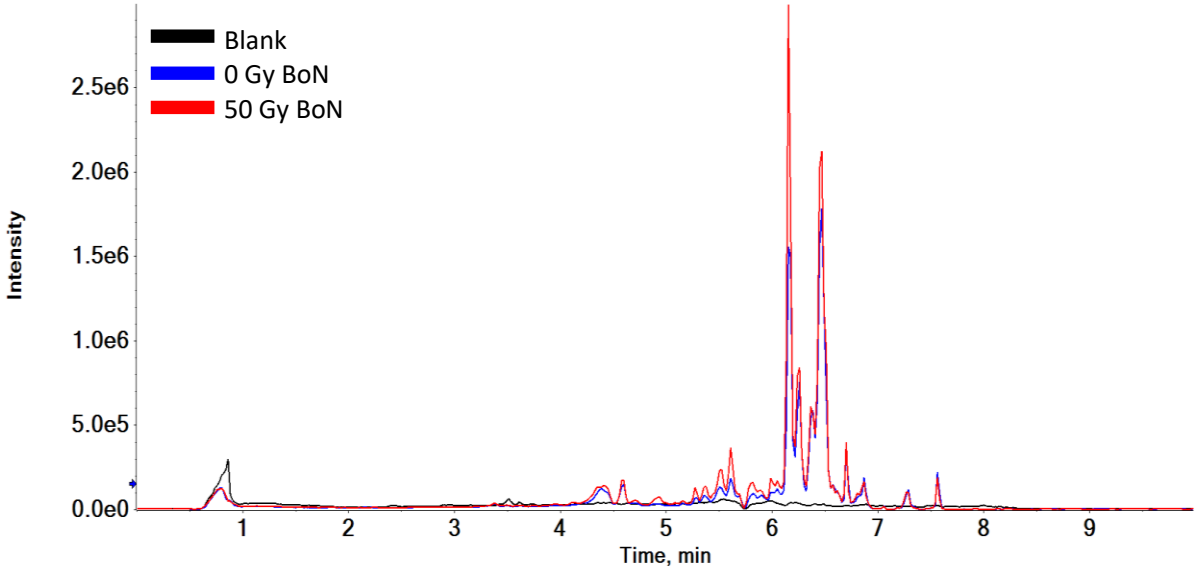

Figure 5.4: Superposition of oxysterol LC-MS chromatograms of bovine lens nucleus membrane extracts exposed to 0 and 50 Gy of X-rays. BoN: bovine nucleus.

Table 5.1: Retention times of peaks illustrated in Figure 5.4 and the corresponding dominating MRMs. The change with dose was determined by comparing the 0 and 50 Gy IR exposed bovine lens membrane extracts. Putative identification was achieved using the Lipidomics Gateway database and information provided by McDonald et al. (McDonald et al., 2012). Yellow marked oxysterols were confirmed using standards (Figure 5.5). Abbreviations of the putative IDs analogous to (McDonald et al., 2012).

Retention time on Kinetex	MRM	Change with dose	Putative ID
4.2	438 - 403	Yes	3b,5a,6b
4.37	420 - 385	Minimal	22r/s OHC, 27 OHC, 5/6b, 5/6a, 4b
4.58	418-383	No	24 OXO, 24/25 EPC
4.9	434 – 399 436 - 401	Yes	1,25 D3 3b16a27, 3b17a20a
5.2 – 5.8	385 - 367	Yes	8(14)3,15aOHC, 20 cholestenone, zymosterol 7-dehydrocholesterol
5.5	434 – 399	Yes	7β hydroxycholesterol
5.6	401 - 383	Yes	7-ketocholesterol
5.77 – 5.97	418 - 401	Yes	3o7o, 1aD3; 24,25 epoxy cholesterol
6.15	420 - 385	Yes	5, 6-epoxycholesterol
6.25 - 6.35	420 - 385	Yes	5/6a/b
6.5	434 - 399	No	unknown

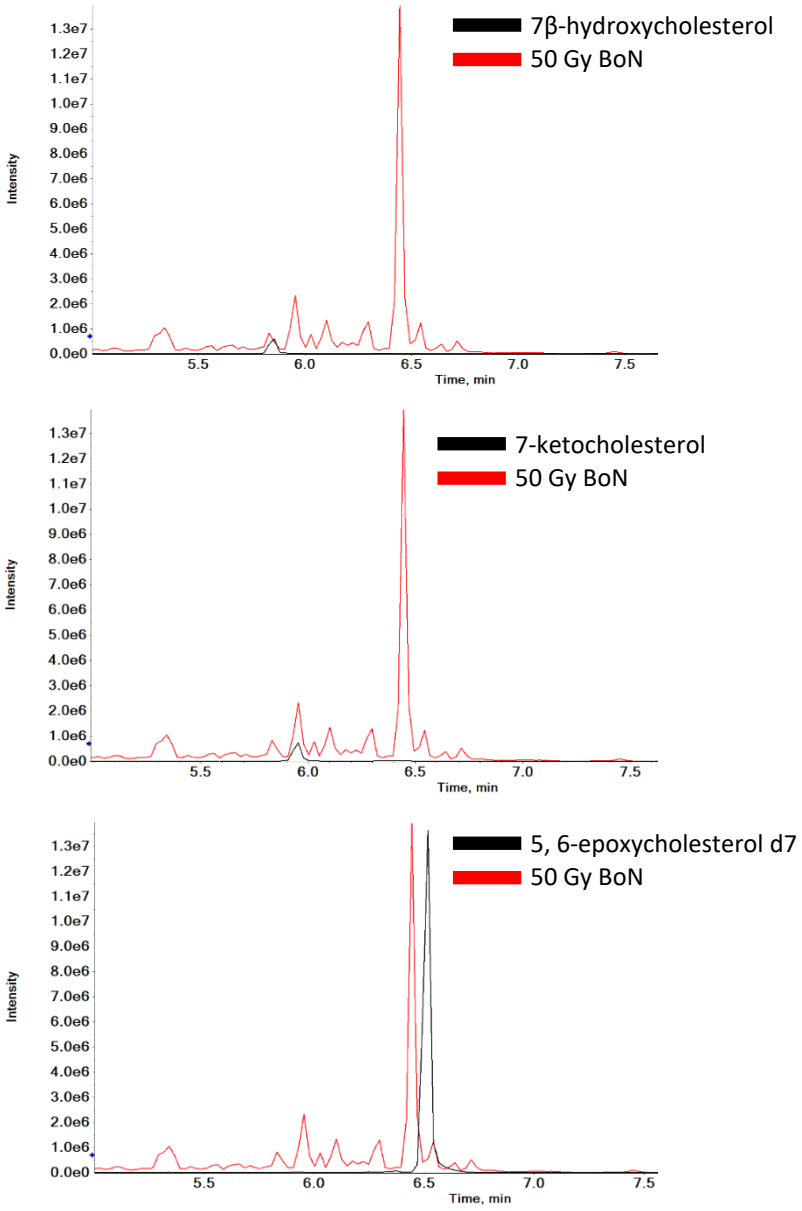

Figure 5.5: Superposition of LC-MS chromatograms of the 7β-hydroxycholesterol, 7–ketocholesterol and 5, 6-epoxycholesterol -d7 with the 50 Gy BoN sample. BoN: bovine nucleus.

5.3.3. Dose-dependent increase of specific oxysterols

Following the identification of 7-ketocholesterol, 7β-hydroxycholesterol and 5, 6-epoxycholesterol in the bovine lens nucleus plasma membrane extracts after IR exposure, lens cortex membrane extracts were also analysed.

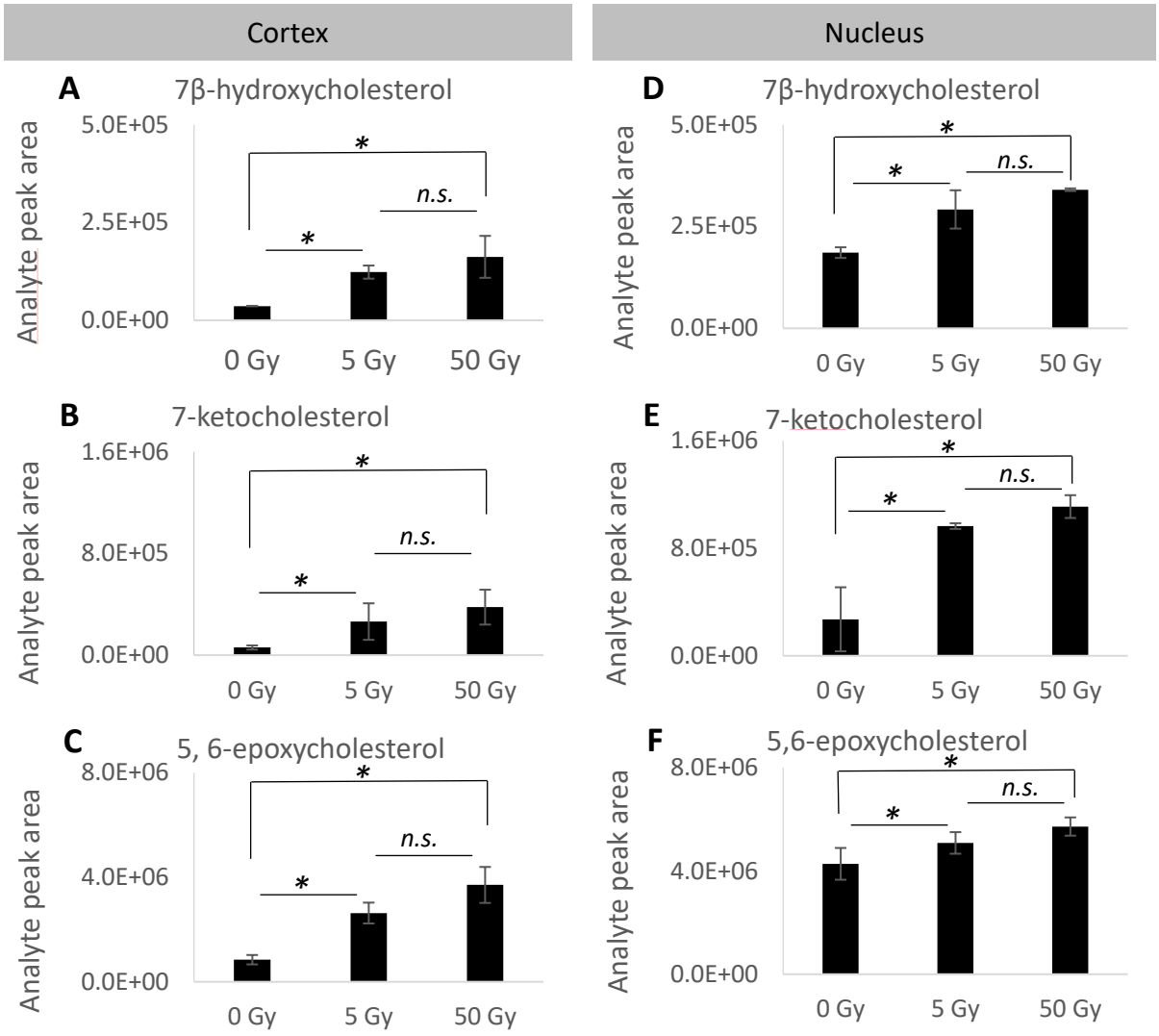

*Figure 5.6: LC-MS peak quantification of oxysterols in 0, 5 and 50 Gy IR-exposed bovine lipid membranes. A) 7β-hydroxycholesterol, B) 7-ketocholesterol and C) 5, 6-epoxycholesterol in bovine lens cortex membrane extracts, and D) 7β-hydroxycholesterol, E) 7-ketocholesterol and F) 5, 6-epoxycholesterol in bovine lens nucleus membrane extracts, error bars represent standard deviation, General Linear Model Analysis of Variance using dose, location and oxysterol as independent factors and analyte peak area as dependent factor was applied for statistical analysis, *p< 0.05 n=3, n.s.: not significant.*

As shown in Figure 5.6, oxysterol formation was induced by exposure to IR in a dose-dependent manner in the cortical and nuclear fractions of bovine membrane extracts (Figure 5.6). Comparison of the amount of oxysterol in the unexposed cortex and the nucleus revealed that the lens nucleus contains more oxysterols than the cortex and this trend was maintained after IR exposure ($p < 0.001$; Figure 5.6A, B and C versus Figure 5.6D, E and F). Although a gradual increase in the three analysed oxysterols was observed, only the changes between 0 and 5 Gy ($p = 0.002$), and 0 and 50 Gy ($p = 0.002$) were statistically significant (in contrast to the changes between 5 and 50 Gy). Furthermore, comparison of the two plasma membrane fractions showed that IR-induced oxysterol increase is more prominent in the cortex (Table 5.2). The increase in oxysterol levels after IR exposure was found to persist for 7β-hydroxycholesterol ($p = 0.869$; Figure 5.7A) and 7-ketocholesterol ($p = 0.180$; Figure 5.7B), even after 18 days at 37 °C. 5, 6-epoxycholesterol increased significantly ($p = 0.019$; Figure 5.7C). Moreover, an increase in oxysterol levels in the non-irradiated samples with time is also observed (Figure 5.7).

Table 5.2: Comparison of the IR-induced changes in the cortex versus the nucleus. The mean values of the analyte peak area in Figure 5.6 were used to calculate the ratios.

Ratio analyte peak area 5 Gy: 0 Gy			
	7β-hydroxycholesterol	7-ketocholesterol	5, 6-epoxycholesterol
Cortex	3.376	4.393	3.111
Nucleus	1.570	3.552	1.189
Ratio analyte peak area 50 Gy: 0 Gy			
	7β-hydroxycholesterol	7-ketocholesterol	5, 6-epoxycholesterol
Cortex	4.444	6.282	4.381
Nucleus	1.831	4.085	1.338

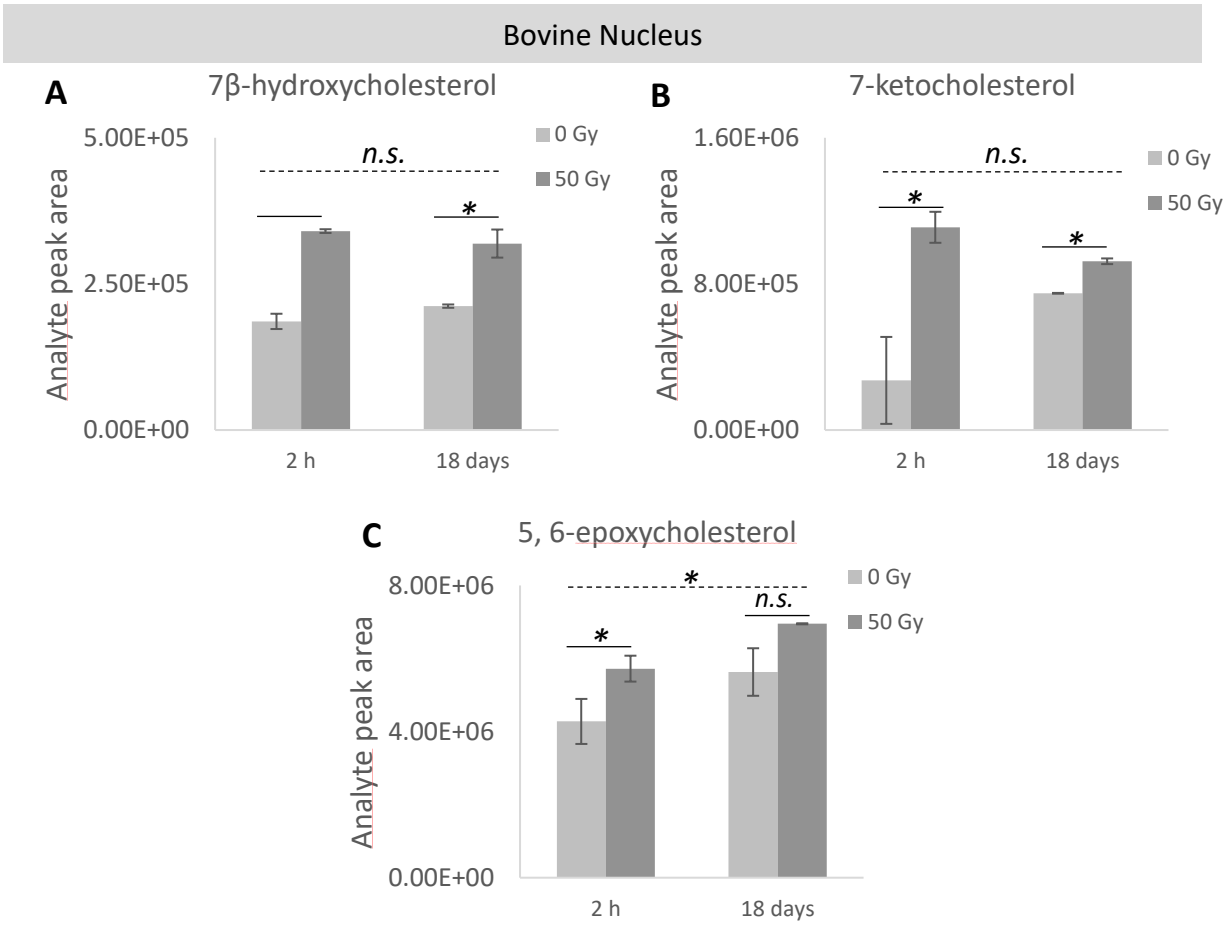

*Figure 5.7: Comparison of oxysterol levels 2 h and 18 days post-irradiation of bovine nucleus lipid membranes with 50 Gy, General Linear Model Analysis of Variance using dose, time and oxysterol as independent factors and analyte peak area as dependent factor was applied for statistical analysis, *p< 0.05 n= 3, n.s.: not significant.*

5.3.4. Retrospective power analysis

Although heuristics in biosciences research instructs three biological repeats to distinguish a true effect from a random variation, progressive practice advises the performance of a power analysis. Generally, the power analysis aids to determine the sample size that enables detection of a statistical significant effect when there is a true effect to be found. This statistical test is normally conducted before an experiment and calculated based on previously collected data found in literature. Besides (Girao et al., 1998), no attempt has been done to quantify oxysterol levels in the eye lens. Therefore, the advised

sample size for the target power of 0.8 based on the data that was collected above and the actual power were calculated, and compared to the actual sample size using Minitab.

Table 5.3: Power analysis to determine the advised sample size and the actual power of our experiment using Minitab.

	Sample size	Difference in mean value	Mean stdv	Actual power	Advised sample size for target power 0.8
Cortex 0 Gy vs. 5 Gy					
7β-hydroxycholesterol	3	86745	8671	1.000	2
7-ketocholesterol	3	203955	79942	0.653	4
5, 6-epoxycholesterol	3	1785500	289560	1.000	2
Cortex 0 Gy vs. 50 Gy					
7β-hydroxycholesterol	3	125745	27055	0.985	3
7-ketocholesterol	3	317455	76760	0.959	3
5, 6-epoxycholesterol	3	2860500	434517	1.000	2
Cortex 5 Gy vs. 50 Gy					
7β-hydroxycholesterol	3	39000	35155	0.184	14
7-ketocholesterol	3	113500	140435	0.121	26
5, 6-epoxycholesterol	3	1075000	543694	0.455	6
Nucleus 0 Gy vs. 5 Gy					
7β-hydroxycholesterol	3	106000	30045	0.891	3
7-ketocholesterol	3	693300	129613	0.997	3
5, 6-epoxycholesterol	3	810000	517107	0.31	8
Nucleus 0 Gy vs. 50 Gy					
7β-hydroxycholesterol	3	154500	8132	1.000	2
7-ketocholesterol	3	838300	161432	0.995	3
5, 6-epoxycholesterol	3	1445000	485287	0.777	4
Nucleus 5 Gy vs. 50 Gy					
7β-hydroxycholesterol	3	48500	25102	0.439	6
7-ketocholesterol	3	145000	53033	0.709	4
5, 6-epoxycholesterol	3	635000	386292	0.340	7
Nucleus 0 Gy vs. Cortex 0 Gy					
7β-hydroxycholesterol	3	149342	6823	1.000	2
7-ketocholesterol	3	211598	127140	0.346	7
5, 6-epoxycholesterol	3	3431800	398243	1.000	2

Stdev: standard deviation

The actual power for the comparisons made between 0 and 5 Gy, and 0 and 50 Gy in the cortical and nuclear fraction of the bovine lens membrane extracts was above 0.8 except for 7-ketocholesterol 0 vs. 5 Gy in the cortex, 5, 6-epoxycholesterol 0 vs. 5 Gy and 0 vs. 50 Gy in the nucleus (Table 5.3). The actual power for these was <0.8 and therefore, a bigger sample size was suggested. Similarly, for the comparison between the oxysterol levels in the cortex and nucleus 2 of the 3 measured oxysterols showed actual powers >0.8. Hence, only for 7-ketocholesterol was the advised sample size to detect significant differences in IR-induced changes in oxysterol levels above the applied sample size. In contrast, the advised sample sizes for cortex and nucleus 5 Gy vs. 50 Gy was overall higher than the sample size used during the experiments and the actual power of that comparison was <0.8 in the cortical and nuclear fraction of the bovine lens membrane extracts.

5.3.5. Uncertainty budget

Table 5.4: Uncertainty budget of the in vitro IR-induced oxysterol formation experiment.

Uncertainty contributor	Qualitative uncertainty	Parameter Unit	Type of Evaluation	Distribution
Variability in age within a group of cows in the context of plasma membrane lipid composition	minor	months	A	Gaussian
Membrane extraction efficiency	minor	mg	B	Rectangular
Purity of samples	minor	counts	A	Gaussian
Fluctuations in temperature of incubation room	minor	°C	A	Gaussian
Weighing errors	minor	mg	A	Gaussian
Dose exposure within runs	minor	Gy	B	Rectangular
Dose exposure between runs	minor	Gy	A	Gaussian
Pipetting	minor	mL	A	Gaussian
Lipid purification efficiency	minor	counts	B	Rectangular
Evaporation of solvent	minor	counts	B	Rectangular
Analyte peak area	minor	counts	A	Gaussian
Repeatability	significant	counts	A	Gaussian

As Table 5.4 showed, twelve uncertainty contributors in the quantification of *in vitro* IR-induced oxysterol formation experiment were identified (Figure 5.6). The "variability in age within a group of cows in the context of plasma membrane lipid composition", "fluctuations in temperature of incubation room", purity of the samples, weighing errors, pipetting, dose exposure between runs analyte peak area

and repeatability are all factors which can be estimated via statistical analysis of repeated measurements and are therefore accounted for as type A (random) errors which are commonly, and therefore also within the current experimental set up, associated with a normal (Gaussian) distribution. The membrane extraction efficiency, dose exposure within runs, lipid purification efficiency and evaporation of the solvent cannot be estimated using statistics and are therefore grouped in type B (systematic) errors. These factors are coupled with a continuous uniform (rectangular) distribution because of their constant probability in variation. Consideration of the relative magnitude of each of the factors leads to the conclusion that eleven contributors have a minor contribution and one, repeatability, a significant contribution to uncertainty. Thus only the repeatability was used to assess the uncertainty (in terms of standard deviation) in the measurements outputs, i.e. to produce the error bars on Figure 5.6 andFigure 5.7.

5.4. Discussion

5.4.1. LFCs membrane cholesterol is a sensor for IR-induced oxidative damage

The data presented here confirm that cholesterol in eye lens membranes is subjected to oxidative damage after exposure to IR (Figure 5.3, Figure 5.4, Figure 5.5 and Figure 5.6). Importantly, the cholesterol oxidation products (7β-hydroxycholesterol, 7-ketocholesterol and 5, 6-epoxycholesterol) detected after IR exposure are the same as those that have been correlated with age-related cataract (Girao et al., 1998). These oxysterols are generated via cholesterol autoxidation (Smith, 1987, Girotti and Korytowski, 2000, Zerbinati and Iuliano, 2017, Jin et al., 2010). One of the consequences of IR exposure is free radical generation from water radiolysis, which in turn generate hydrogen peroxide. The free radicals can be generated from hydrogen peroxide by transition metals such as iron via the Fenton reaction, which also damage lens biomolecules (reviewed in (Loh et al., 2009, Goralska et al., 2009)). Transition metal chelators help to limit oxygen radicals, thus mediate damage in the lens (Kleiman et al., 1990, Zigler et al., 1985, Goralska et al., 2009). The plasma membranes of LFCs contain high levels of cholesterol and dihydrosphingomyelin (Borchman and Yappert, 2010), but cholesterol is more prone to oxidative damage than dihydrosphingomyelin (Ahuja et al., 1999, Vejux et al., 2011). Cholesterol is also highly abundant in LFC membranes and its turnover appears minimal over the lifetime of the lens (Hughes et al., 2015, Hughes et al., 2012). Indeed cholesterol oxidation is a mark of age-related cataract (Borchman and Yappert, 1998, Bhuyan and Bhuyan, 1984, Bhuyan et al., 1986a, Bhuyan et al., 1986b, Micelli-Ferrari et al., 1996, Simonelli et al., 1989, Varma et al., 1984, Babizhayev et al., 1988). For these reasons, cholesterol can be considered a *de facto* biosensor of oxygen radical damage in the lens.

5.4.2. Cholesterol content of LFC plasma membranes helps protect against IR-induced production of oxysterols

Oxysterol products accumulate in age-related cataractogenic lenses (Girao et al., 1998) although that this study found no detectable levels of oxysterols in age matched control human lenses. Oxysterols were detected in non-irradiated bovine lens membranes using LC-MS (Figure 5.4 andFigure 5.6) and exposure of lipid membranes *in vitro* showed that IR caused an increase in cholesterol oxidation products (Figure 5.4 and Table 5.1). Amongst these oxysterols, the presence of 7β-hydroxycholesterol, 7-ketocholesterol and 5, 6-epoxycholesterol, which have been correlated with age-related cataract (Girao et al., 1998) was confirmed. Calculations of the actual power showed that enough repeats were generated to detect significant changes between 0 and 5 Gy, and 0 and 50 Gy for 7β-hydroxycholesterol and 7-ketocholesterol in the cortical and nuclear fractions of bovine lens membrane extracts. However, the actual power for differences between 0 and 5 Gy, and 0 and 50 Gy for 5, 6-epoxycholesterol in the lens nucleus is <0.8, and more experimental repeats are recommended to confirm the observed differences.

IR-dependent increase in oxysterols (Figure 5.6) was significant after exposure to both 5 and 50 Gy, but 50 Gy did not produce a 10 fold increase over the 5 Gy sample in the three oxysterols that were measured (Figure 5.6). DNA damage in the form of DSBs is linear over the range 1 mGy to 100 Gy 3 min after exposure (Rothkamm et al., 2003, Rothkamm et al., 2015), but the numbers of foci and the influence of repair mechanisms then affect DNA damage readout in the form of, for instance γ-H2AX foci e.g. (Barbieri et al., 2019). In the experiments performed during this study it is possible that free radical autoxidation mechanisms from water radiolysis induce oxysterol formation (Zerbinati and Iuliano, 2017), but cholesterol is also protective (Girao et al., 1999), offering an explanation for the observed attenuation. Interestingly, γ-irradiation of synthetically generated liposomes with a 4:1 phospholipid:cholesterol ratio generated more cholesterol oxidation adducts than liposomes with a 2:1 phospholipid:cholesterol ratio (Sevanian and McLeod, 1987), suggesting that oxysterol formation is cholesterol-ratio dependent. In the context of the eye lens, the cholesterol ratio is highest in the oldest fiber cells, i.e. those in the lens nucleus. These findings, combined with studies showing that high membrane cholesterol provides a hydrophobic barrier to limit oxygen permeability (Widomska et al., 2007), suggest that the lens membranes should also be protected against IR-induced oxidation of cholesterol. Perhaps the higher cholesterol content of the lens nucleus helps provide the cell biological environment to effect such protection against oxidative damage.

It is possible that the higher cholesterol content of the lens nucleus helps provide the cell biological environment to effect protection against IR-mediated oxidative damage in line with previous studies using reconstituted membranes and vesicles (Smith, 1991, Parasassi et al., 1995). The data presented for the bovine lens membranes isolated from the cortex and nucleus could seem to contradict the suggested protective environment of the lens nucleus afforded by higher cholesterol levels given that higher levels of oxysterols are present in the unexposed lens nucleus membrane extracts compared to those in the cortical membrane fraction (Figure 5.6). Power analysis confirmed that the experiment has enough actual power to detect differences in oxysterol levels between unexposed plasma membrane extracts in the cortex and in the nucleus (Table 5.3). In terms of the fold-increase over the baseline, the increase in oxysterols was greatest in the cortex and not the nucleus (Table 5.2). This observation is in line with epidemiological data revealing that IR-induced cataractogenesis mainly presents itself as posterior subcapsular cataracts (Miller et al., 1967, Wilde and Sjostrand, 1997).

5.4.3. Uncertainty budget

With age, the cholesterol content in the plasma membranes of LFCs changes (Mainali et al., 2013). Therefore, “Variability in age within a group of cows in the context of plasma membrane lipid composition” was taken into consideration. The abattoir mainly works with cows aged 6 months and during the lipid membrane extraction process 24 eye lenses are combined, presumably this sample size

is large enough to limit the contribution of age-related differences in cholesterol to the uncertainty budget. The membrane extraction efficiency, purity of the samples, pipetting, weighing errors, fluctuations in temperature of the incubation room, dose exposure within and between runs, and lipid purification efficiency are uncertainty contribution factors that mainly depend on the individual performing the experiment and the material used. All experiments were performed by one individual and material bought from the same supplier was used throughout the experiment. The purity of the samples was optimised by using ultrapure, high performance liquid chromatography grade solvents. The samples prepared for mass spectrometry were dissolved in a limited amount of solvent, hence evaporation could influence the quantitative comparison of various samples. To minimise evaporation, the tubes were immediately closed with screw-top lids after addition of the solvent and stored at -20 °C till further analysis. The analyte peak area was calculated automatically using Analyst 1.6.2, however the program occasionally failed to detect the right peak which required the user to select the right peak manually.

Importantly, processes occurring *in vitro* are isolated systems. Therefore, this experiment should be repeated in an *in vivo* setting to confirm that IR-induced oxysterol formation can contribute to IR-induced radiation cataracts.

Chapter 6: In vivo formation of oxysterols is time- and dose-dependent

6.1. Introduction

Oxysterols can be formed via enzymatic or non-enzymatic (autoxidation) processes (Figure 6.1); the exerted pathway and oxysterols formed depend chiefly on the available enzymes and the type of free radicals causing oxidative stress (Iuliano, 2011, Kulig et al., 2016, Griffiths et al., 2016). Ionising radiation (IR) can give rise to a large variety of free radicals (Spitz and Hauer-Jensen, 2014); however, not all of them can directly oxidise cholesterol (Sevanian and McLeod, 1987). The reactive oxygen species (ROS) hydroxyl radical and hydrogen peroxide, and the reactive nitrogen species peroxynitrites trigger cholesterol autoxidation primarily by removing a hydrogen atom at the C-7 position of cholesterol (Yin et al., 2011, Iuliano, 2011, Mutemberezi et al., 2016), while superoxide anions have been shown to be unable to react with cholesterol (Smith et al., 1977). The main enzymes involved in oxysterol metabolism are oxidoreductases, hydrolases and transferases. Although some of these enzymes have been reported in the cytoplasm and membrane (Zhang et al., 2012, Chen et al., 2007), they are predominantly found in the endoplasmic reticulum and mitochondria (Mutemberezi et al., 2016).

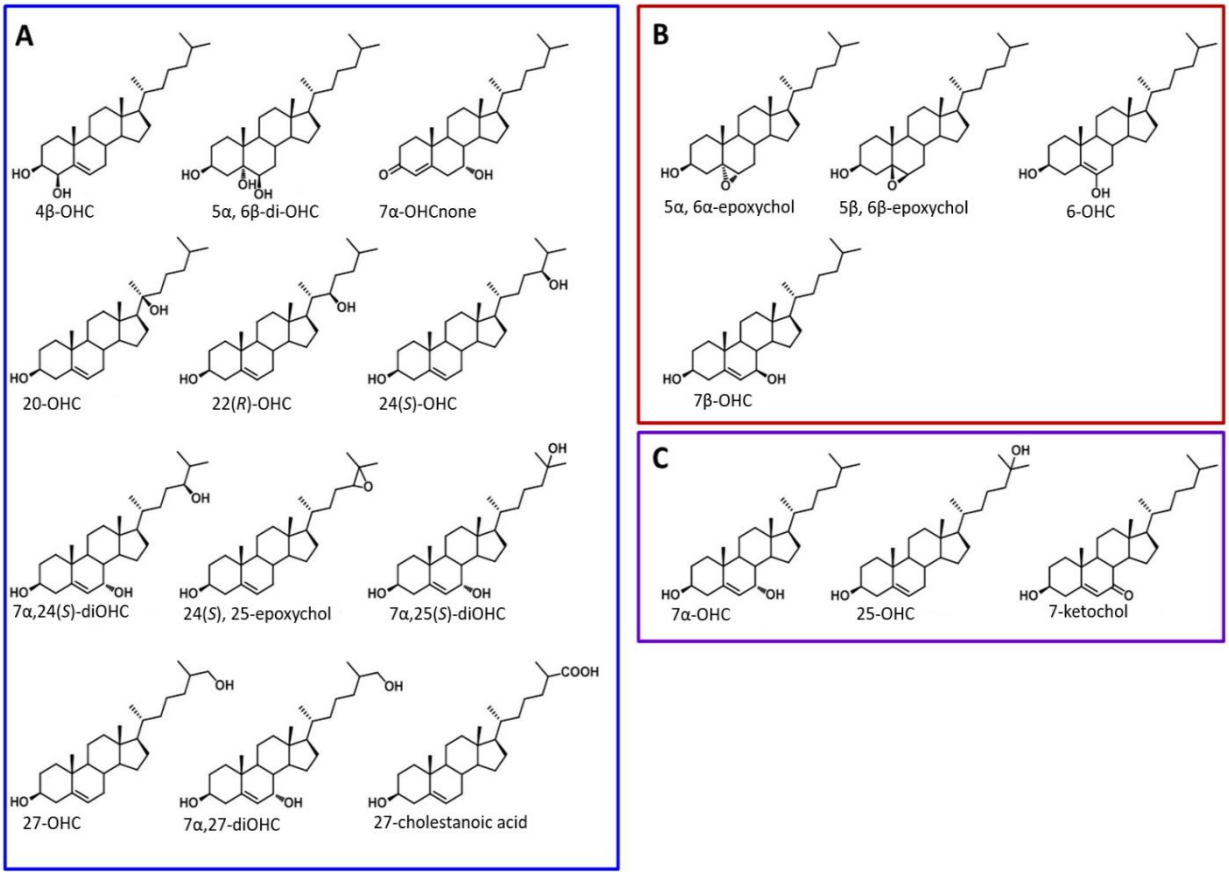

Figure 6.1: The predominant oxysterols in the human body. A) Enzymatically formed oxysterols, B) non-enzymatically formed oxysterols and C) oxysterols that can be formed via autoxidation and enzymatic reactions. Figure adapted from Mutemberezi et al, Prog Lipid Res, 2016 OHC: hydroxycholesterol; chol: cholesterol.

The function of oxysterols in humans is quite diverse: they serve as transport molecules for sterols, for example the conversion of cholesterol into 24(S)-hydroxycholesterol, which in contrast to cholesterol is able to pass the blood brain barrier and remove excessive cholesterol from the brain (Bjorkhem et al., 1998, Bjorkhem, 2006); they act as regulators of the cholesterol biosynthesis pathway, for example 27-hydroxycholesterol inhibits cholesterol biosynthesis while 7α-hydroxycholesterol stimulates the latter (Martin et al., 1997, Taylor et al., 1984); and they also function as signalling molecules e.g. 22(R)-hydroxycholesterol binds and activates liver X receptors α/β which are key transcription factors in lipid

metabolism with an anti-atherogenic role (Janowski et al., 1996, Joseph et al., 2002, Lala, 2004). However, oxysterols can also be pathogenic. Increased levels of 7β-hydroxycholesterol in blood plasma have been correlated with a higher risk of coronary heart disease (Zieden et al., 1999), 7-ketocholesterol downregulates the cytotoxicity of doxorubicin possibly leading to poor cancer treatment outcomes (Wang et al., 2017a), and some researchers have suggested that the binding of 5, 6-epoxycholesterol to liver X receptor might lead to atherosclerosis (Berrodin et al., 2010).

The cholesterol:phospholipid ratio in human eye lenses has been shown to be upto 54% higher in clear eye lenses than in cataractogenic eye lenses (Jacob et al., 2001). Furthermore, a study in which *in vivo* oxysterol levels were measured showed that compared with clear lenses, cataractogenic lenses contained elevated levels of 7β-hydroxycholesterol, 7-ketocholesterol, 5, 6-epoxycholesterol, 20α-hydroxycholesterol and 25- hydroxycholesterol (Girao et al., 1998). Although no studies have directly investigated the presence of enzymes involved in oxysterol metabolism in the eye lens, the detection of 20α- hydroxycholesterol by Girao *et al.* suggests the presence of these enzymes given that 20α-hydroxycholesterol is an oxysterol that can only be formed via enzymatic reactions (Figure 6.1) (Mutemberezi et al., 2016). In primary LEC cultures, the addition of 7-ketocholesterol represses proliferation and leads to the malfunctioning of the differentiation program of LECs into LFCs (Girao et al., 2003). Further, little is known regarding the function of oxysterols in the eye lens.

Epidemiological data show that exposure to high doses of IR and repeated exposure to low dose IR, such as 0.1 Gy, are associated with cataractogenesis (Miller et al., 1967, Cogan et al., 1952, Little et al., 2018). Exposure to IR leads to elevated levels of oxidative stress in cells (Buonanno et al., 2011), and one of the downstream targets of the generated free radicals are lipids (Azzam et al., 2012). Research showing *in vivo* IR-induced lipid peroxidation in the eye lens following cobalt 60 γ-irradiation of rats by assessing malondialdehyde levels was limited to measuring fatty acids as a substrate for oxidation (Karimi et al., 2017). However, the effect of IR on cholesterol in the eye lens *in vivo* has yet to be examined.

6.2. Objectives and experimental design

Experimental data in the previous chapter revealed that exposure of bovine lipid membrane extracts to IR leads to increase of oxysterol levels. However, given that protein denaturating agents are used before exposure to IR (Tapodi et al., 2019), the contribution of enzymes to IR response were examined in an *in vivo* system. Given that C57BL/6J is the most commonly used strain in radiation research, 3 month old C57BL/6J mice were exposed to 0.1 and 2 Gy to X-rays and the cholesterol and oxysterol levels in eight pooled eye lenses were examined (Figure 6.2). Furthermore, a time course experiment over a period of 7 days was performed to study the time-dependence of cholesterol oxidation.

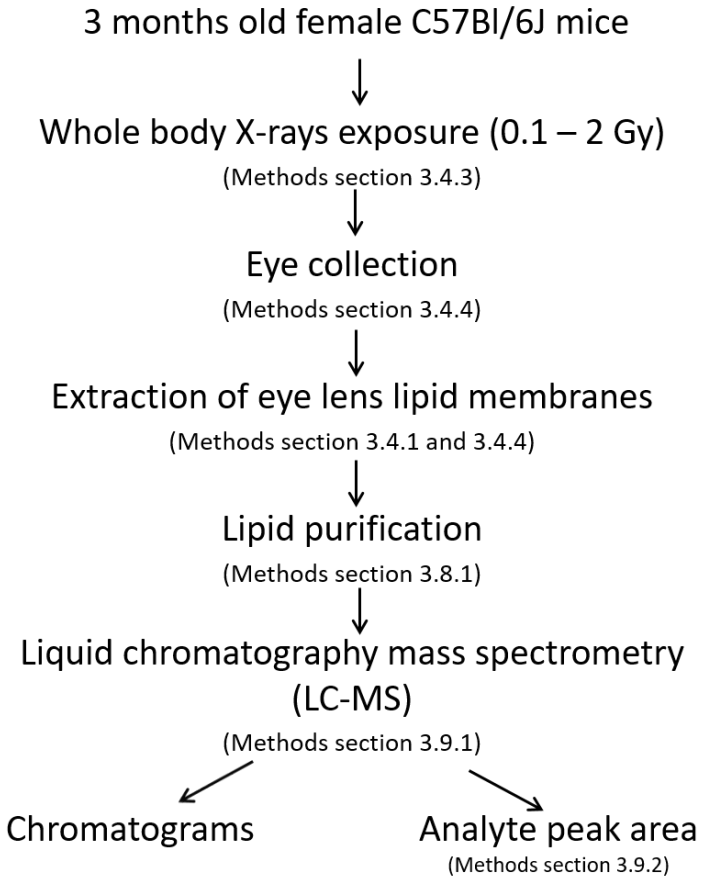

Figure 6.2: Schematic representation of the experimental design of the in vivo IR-induced oxysterol formation analysis. Section numbers refer to the material and methods chapter section in which the protocol was described.

6.3. Results

6.3.1. Doses as low as 0.1 Gy induced oxysterol formation in mice eye lenses

The effect of whole body X-ray exposure to a low dose (0.1 Gy) and a higher dose (2 Gy) on oxysterol levels in the eye lens was examined and compared to the *in vitro* IR-dose-dependent increase in oxysterols noted in the previous chapter. To optimise signal detection, eight eye lenses were pooled prior to lipid membrane extraction. In agreement with the bovine data, a dose-dependent increase was observed in 7β-hydroxycholesterol and 7-ketocholesterol in the eye lenses of 0.1 and 2 Gy irradiated mice (Figure 6.3). 5, 6-epoxycholesterol did not show a dose dependent increase (Figure 6.3).

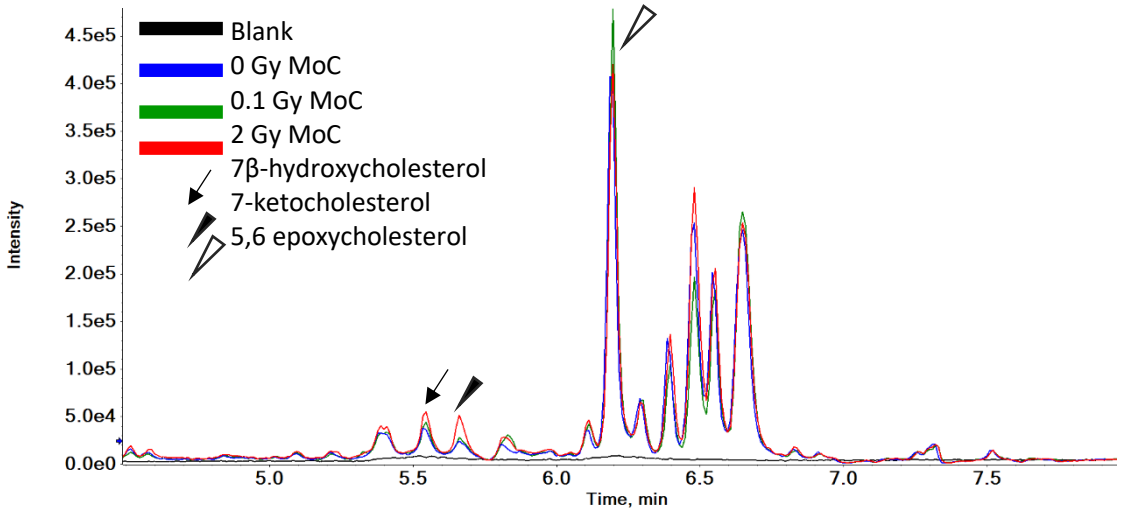

Figure 6.3: LC-MS Chromatograms of 0, 0.1 and 2 Gy irradiated mice 2 hours post IR exposure (eight eye lenses were pooled per sample). MoC: Mouse Cortex.

6.3.2. IR-induced oxysterol formation was transient in mice

To verify whether the IR-induced damage is maintained over time, groups of four mice were irradiated with 2 Gy and sacrificed 2 h, 24 h and 7 days post IR-exposure. The eye lenses of the four mice were pooled and the lipid membranes were extracted. Following lipid purification, quantitative LC-MS analysis of the cholesterol and oxysterols in these samples was performed. Oxysterol levels between different samples were normalised using the cholesterol analyte peak area as IR was shown to not induce significant changes in the cholesterol levels for IR doses of up to 50 Gy (as demonstrated in previous chapter).

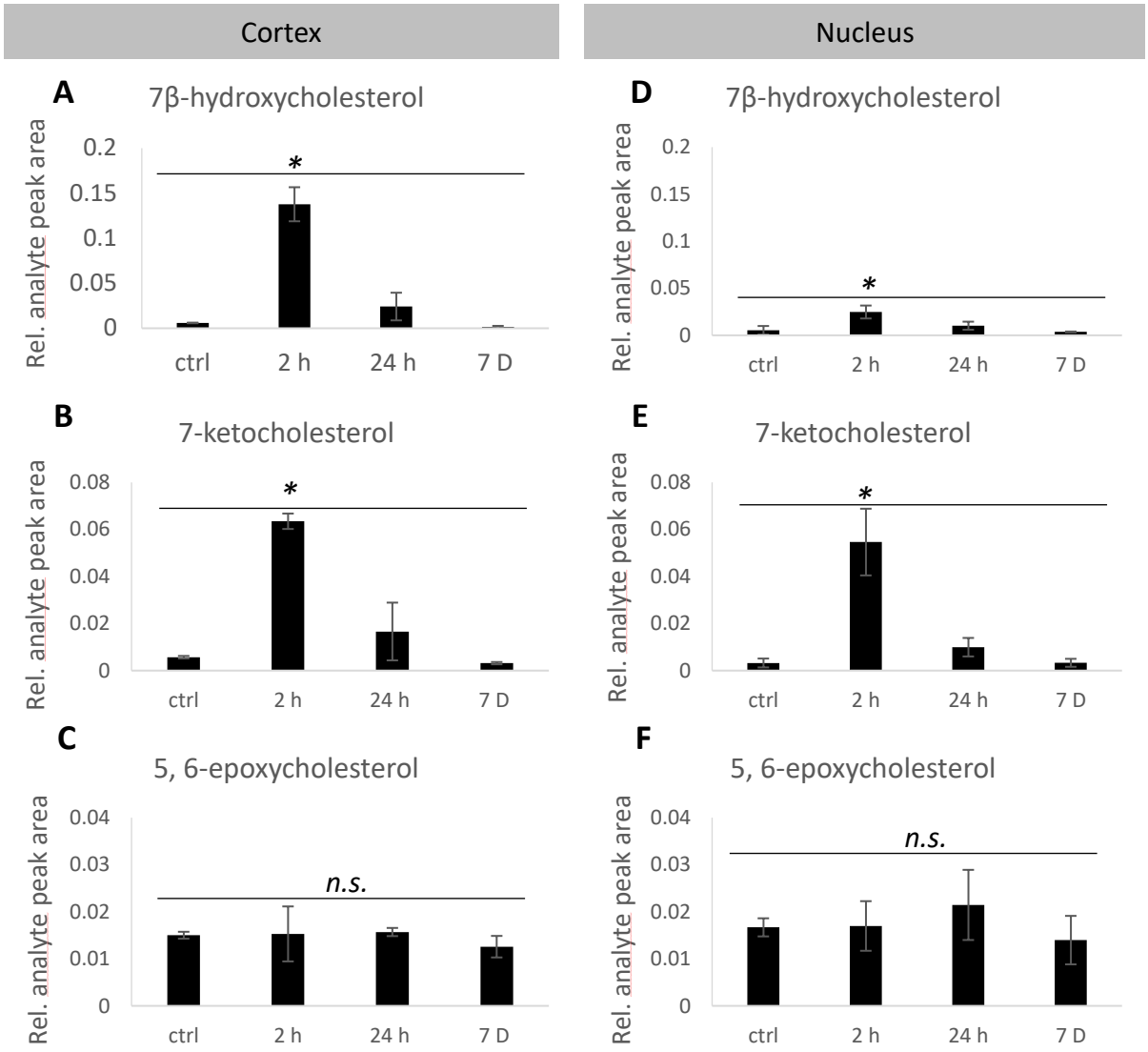

Figure 6.4: LC-MS quantification of in vivo *formed oxysterols in mice irradiated with 2 Gy and sacrificed at 2 hours, 24 hours and 7 days post-IR exposure. A) 7 β hydroxycholesterol, B) 7-ketocholesterol, and C) 5, 6-epoxycholesterol in mice lens cortex, D) 7 β hydroxycholesterol, E) 7-ketocholesterol and F) 5, 6-epoxycholesterol in mice lens nucleus, General Linear Model Analysis of Variance using time and location as independent factors and rel. analyte peak area as dependent factor was applied, *p< 0.05 n= 2 x 8 pooled eye lenses, n.s.: not significant, rel: relative.*

As shown in Figure 6.3 and Figure 6.4, exposing mice to IR lead to a significant rapid increase of 7β-hydroxycholesterol (p= 0.000) and 7-ketocholesterol (p= 0.000) *in vivo* in the cortex (Figure 6.4A and B) and the nucleus (Figure 6.4C and D) of the eye lens. After 24 h the levels of 7-ketocholesterol dropped back to concentrations similar to those prior to IR-exposure (Figure 6.4B and D; Figure 6.5). Although 7β-hydroxycholesterol was reduced to a level similar to the control within 24 h in the cortex (Figure 6.4A and Figure 6.5), Figure 6.4D and Figure 6.5 demonstrate that in the nucleus the significant increase in 7β-hydroxycholesterol 2 h post IR-exposure (p= 0.044) declined more gradual. In contrast to 7β-hydroxycholesterol and 7-ketocholesterol, 5, 6-epoxycholesterol did not show significant IR-induced changes over the 7 days (p= 0.451) (Figure 6.4A, B, D and E versus C and F; Figure 6.5). A comparison of the cortex and nucleus showed that the changes in oxysterol levels are more pronounced in the cortex than in the nucleus (Figure 6.4A and B versus C and D).

Cortex **Nucleus**

7β hydroxycholesterol

Tukey Pairwise Comparisons: Time (h)

Grouping Information Using the Tukey Method and 95% Confidence

Time (h)	N	Mean	Grouping
2	2	0.137713	A
24	2	0.024109	B
0	2	0.005890	B
168	2	0.001319	B

Tukey Pairwise Comparisons: Time (h)

Grouping Information Using the Tukey Method and 95% Confidence

Time (h)	N	Mean	Grouping
2	2	0.0248203	A
24	2	0.0102259	A B
0	2	0.0053552	B
168	2	0.0036613	B

7-keto cholesterol

Tukey Pairwise Comparisons: Time (h)

Grouping Information Using the Tukey Method and 95% Confidence

Time (h)	N	Mean	Grouping
2	2	0.0634829	A
24	2	0.0166162	B
0	2	0.0057035	B
168	2	0.0031645	B

Tukey Pairwise Comparisons: Time (h)

Grouping Information Using the Tukey Method and 95% Confidence

Time (h)	N	Mean	Grouping
2	2	0.0546419	A
24	2	0.0099516	B
168	2	0.0033090	B
0	2	0.0032372	B

5,6 epoxycholesterol

Tukey Pairwise Comparisons: Time (h)

Grouping Information Using the Tukey Method and 95% Confidence

Time (h)	N	Mean	Grouping
24	2	0.0156955	A
2	2	0.0152897	A
0	2	0.0150103	A
168	2	0.0125766	A

Tukey Pairwise Comparisons: Time (h)

Grouping Information Using the Tukey Method and 95% Confidence

Time (h)	N	Mean	Grouping
24	2	0.0214527	A
2	2	0.0169790	A
0	2	0.0166884	A
168	2	0.0139703	A

Figure 6.5: The post hoc test Tukey Pairwise comparison was performed after General Linear Model Analysis (Figure 6.4) using Minitab using time as independent factors and rel. analyte peak area as dependent factor. Means are grouped in A or B, means sharing a letter are not significantly different while those that do not share a letter are significantly different.

6.3.3. No IR exposure-dependent changes in the protein pattern detected via SDS-PAGE over time

Parallel with the 2 Gy IR-induced oxysterol formation time course experiment (Figure 6.4), SDS-PAGE was performed to investigate whether changes in the protein pattern occur. In the cortex and nucleus, the protein pattern in the lipid membrane extracts appears unchanged after 2 hours exposure and remains unaltered 7 days post IR-exposure (Figure 6.6).

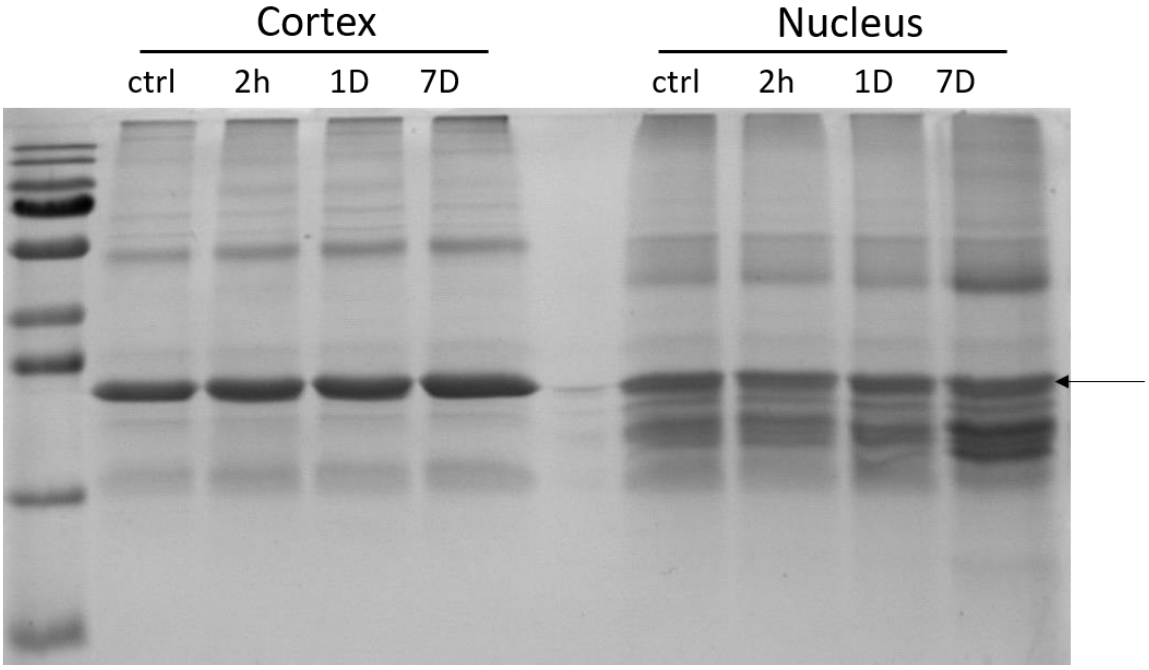

Figure 6.6: 10 µL of lipid membranes isolated from the lens cortex and lens nucleus of mouse exposed to2 Gy X-rays 2 hours, 24 hours and 7 days post exposure. The most prominent band visible is AQP0 (arrow). Protein identity suggestion was based on proteomics data in the appendix (appendix table 1 and 2). Non-irradiated mice of the same age were used as the control. Lipid membranes were solubilised with 1% (w/v) SDS buffer, run on a SDS-PAGE gel (15% (w/v) acrylamide) and stained with Coomassie Blue. The molecular weight markers in the first lane of each gel mark respectively 250, 130, 95, 72, 55, 36, 28, 17 and 10 kDa from top to bottom.

6.3.4. Retrospective power analysis

Table 6.1: Retrospective power analysis to determine the advised sample size for the in vivo IR-induced oxysterol formation experiment using Minitab.

	Sample size	Difference in mean value	Mean stdev	Actual power	Advised sample size for target power 0.8
Cortex control vs. 2h					
7β-hydroxycholesterol	2	0.132	0.035	0.525	3
7-ketocholesterol	2	0.058	0.002	1.000	2
5,6-epoxycholesterol	2	0.000	0.003	0.050	2176
Cortex control vs. 24h					
7β-hydroxycholesterol	2	0.018	0.008	0.271	5
7-ketocholesterol	2	0.011	0.006	0.175	7
5,6-epoxycholesterol	2	0.001	0.001	0.084	23
Nucleus control vs. 2h					
7β-hydroxycholesterol	2	0.019	0.006	0.417	3
7-ketocholesterol	2	0.051	0.008	0.869	2
5,6-epoxycholesterol	2	0.000	0.004	0.050	2408
Nucleus control vs. 24h					
7β-hydroxycholesterol	2	0.005	0.004	0.112	14
7-ketocholesterol	2	0.007	0.003	0.271	5
5,6-epoxycholesterol	2	0.005	0.005	0.095	17

Stdev: standard deviation

As stated in the previous chapter, to the best of our knowledge, only one attempt has been made to quantify cholesterol oxidation products (Girao et al., 1998). Therefore, a power analysis prior to embarking on this project was not feasible. Alternatively, a retrospective power analysis was executed determining the sample size for future experiments using differences in mean and average standard deviation generated during the *in vivo* IR-induced oxysterol formation experiment (Figure 6.4). The advised sample sizes were comparable with the actual sample sizes that was used during the *in vivo* IR-induced oxysterol formation for 7β-hydroxycholesterol and 7-ketocholesterol 2 h post IR-exposure in the lens cortex and nucleus compared to unexposed mice (Table 6.1). Calculations of the actual power showed values >0.8 for 7-ketocholesterol levels during the comparison of control and 2 h post-IR in the lens cortex and nucleus membrane extracts, while for 7β-hydroxycholesterol the power was slightly <0.8. However, comparison of control and 24 h post-IR exposure demonstrated power values <0.4 and

a larger sample size than the one used was advised in both fractions. The advised sample size for 5, 6-epoxycholesterol for comparisons between controls and 2 hours or 24 hours post-IR in the cortex and nucleus was >17, hence power analysis demonstrated values <0.1.

6.3.5. Uncertainty budget

Table 6.2: Uncertainty budget of the in vivo IR-induced oxysterol formation experiment.

Uncertainty contributor	qualitative uncertainty	Parameter Unit	Type of Evaluation	Distribution
Age of animals	minor	months	A	Gaussian
Sex	unknown	counts	B	Rectangular
Phenotypic variability	minor	counts	A	Gaussian
Genetic variability	minor	counts	A	Gaussian
Animal house conditions	minor	counts	A	Gaussian
Dose exposure within runs	minor	Gy	B	Rectangular
Dose exposure between runs	minor	Gy	A	Gaussian
Membrane extraction efficiency	minor	mg	B	Rectangular
Variabilities between efficiency of different membrane extractions	significant	counts	A	Gaussian
Purity of the samples	minor	counts	A	Gaussian
Pipetting	minor	mL	B	Rectangular
Lipid purification efficiency	minor	counts	B	Rectangular
Evaporation of solvent	minor	counts	B	Rectangular
Analyte peak area	minor	counts	A	Gaussian
Repeatability	significant	relative value	A	Gaussian

To assess the fitness of our measurements, a qualitative uncertainty budget analysis was performed (Table 6.2). A total of 15 contributors to uncertainty, one (sex) for which the contribution is still under investigation were recognized. Age of animals, phenotypic and genetic variability, animal house conditions, dose exposure between runs, purity of the samples, analyte peak area and repeatability, which show a Gaussian distribution, had a minor contribution to uncertainty. Dose exposure within runs, membrane extraction efficiency, pipetting, lipid purification efficiency and evaporation of solvent also had a minor contribution uncertainty, but show a rectangular distribution. Both “variability between efficiency of different membrane extractions” and repeatability had a significant contribution to uncertainty.

6.4. Discussion and conclusions

6.4.1. Dose dependence and oxysterol profiles in irradiated lens samples

Whole body irradiation of mice showed an oxysterol dose-dependent increase in the eye lenses. The observation that 0.1 Gy is able to induce the formation of oxysterols is vital given that occupational workers are exposed to these levels (Little et al., 2018). Higher levels of 7β-hydroxycholesterol and 7-ketocholesterol were detected in exposed eye lenses compared to those of unexposed mice, but not 5, 6-epoxycholesterol (Figure 6.3 Figure 6.4). In contrast to extracted membranes in which chiefly non-enzymatic processes are active, both non-enzymatic and enzymatic processes occur *in vivo*. Cholesterol epoxide hydrolase can hydrolyse 5, 6-epoxycholesterol to cholestane-3β,5α,6β-triol (Griffiths et al., 2016) and provides an explanation for the observation of 5, 6-epoxycholesterol in extracted membranes (see previous chapter), and the lack of elevation of this oxysterol in *in vivo* mouse samples (Figure 6.3). The possibility that the observed differences between our *in vitro* bovine lens data and *in vivo* mouse data might be species specific cannot be excluded. To preclude one of the aforementioned possibilities, the presence of cholesterol epoxide hydrolase in the eye lens of various species should be investigated to address this issue.

An experiment with a power >0.8 is generally accepted as reliable. Based on this assumption, the advised sample size was calculated (Table 6.1). This confirmed that the applied sample size is suitable to detect significant differences for 7-ketocholesterol 2 h post-IR exposure in the lens nucleus and cortex; however, for 7β-hydroxycholesterol, a slightly bigger sample size might be required to detect statistically significant changes 2 h post-IR exposure in both fractions (Table 6.1). The power to detect difference between control and 24 h post-IR was <0.4 for all measured oxysterols in both fractions, furthermore the sample size suggested to detect significant differences is easily achievable in practice. More repeats with more time points in between the 7 days should be performed to identify when the oxysterol levels return back to baseline levels. The major discrepancy between sample size utilised during the *in vivo* IR-induced oxysterol formation and the advised sample size for 5, 6-epoxycholesterol indicate that presumptively there are no statistically significant change in 5, 6-epoxycholesterol during 7 days post 2 Gy IR-exposure.

Previous literature support the view that oxidised sterols can bind to and restore the chaperone capacity of the lens chaperones HSPB1 and HSPB5 (Makley et al., 2015). Cholesterol is however an important signalling molecule in the sonic hedgehog (Shh) pathway (Kinnebrew et al., 2019) by regulating Shh binding to its receptor, Ptch1, which protects the lens against spontaneous and IR induced cataract (De Stefano et al., 2015). The transient increase in oxysterols could be modulated by the membrane associated lens chaperones that are embedded in the lipid bilayer (De Maio et al., 2019). There are other protein candidates to bind cholesterol and its derivatives such as the Niemann-Pick type C protein 1 and sterol transport protein Gramd1b that regulate cholesterol egress from cells via the autophagy pathway

(Hoglinger et al., 2019) and that are expressed in the 12 week old mouse lens (https://research.bioinformatics.udel.edu/iSyTE/ppi/index.php). The mechanism by which oxysterols derived from cholesterol could be reduced in or removed from the living lens after IR exposure needs further investigation given that lens lipids are very stable within their constituent membranes as shown by modern carbon measurements (Borchman et al., 2017, Hughes et al., 2015). Nevertheless, the range of inherited diseases that alter cholesterol and its derivatives (Barnes and Quinlan, 2017, Raza et al., 2017) or its precursors (Cenedella, 2009) and that are linked to cataractogenesis evidence the critical role played by these lipids in eye lens transparency and optical function.

Chronic exposure to lower doses is associated with long latency period for the development of cataracts (Hamada et al., 2019). Acute exposure of mice to 0.1 and 2 Gy induced cholesterol oxidation (Figure 6.3), however the time course experiment showed that the increase in oxysterol levels in the eye lens was transient. Further investigation should include chronic and fractionated exposures, more dose points and longer latency period to gain more insight into the involvement of cholesterol oxidation in radiation cataracts. C57BL/6J is considered as a radio-resistant strain (Nowosielska et al., 2012, Kataoka et al., 2006), further work should also include radio-sensitive strains such as CD1 (De Stefano et al., 2015).

6.4.2. Cholesterol in LFCs membranes helps protect against whole body IR-induced damage

High concentrations of cholesterol in the eye lens lipid membrane constrains the migration of molecules through LFCs (Widomska et al., 2007, Borchman and Yappert, 2010). Cholesterol oxidation products change the permeability of membranes and they themselves migrate better than cholesterol through cell membranes (Dias et al., 2019, Björkhem, 2002). The initial increase of oxysterol levels with a subsequent decrease could be due to chemical cascade reactions in which hydrophobic cholesterol molecules are oxidised to less hydrophobic oxysterols. These oxysterols will change the permeability of membranes (Theunissen et al., 1986, Vestergaard et al., 2011), potentially allowing the redistribution of anti-oxidants and oxysterol metabolising enzymes. The exchange of molecules between the aqueous humour and the lens (Davson, 1954) provides another procedure by which the lens could be clearing the IR-induced oxysterols. Dietary anti-oxidants, such as α-tocopherol, ascorbic acid and vitamin A, as well as the endogenous lenticular glutathione (Sweeney and Truscott, 1998, Varma and Richards, 1988, Krepler and Schmid, 2005, Yeum et al., 1995) are all potential chemical antioxidants. The increased sensitivity of the lens cortex to IR compared with the nucleus (Figure 6.4) could be due to the higher concentrations of cholesterol in the nucleus compared with the cortex, and the associated differences in membrane permeability (Mainali et al., 2015). This observation is in line with epidemiological data revealing that IR-induced cataractogenesis mainly presents as posterior subcapsular cataracts (Miller et al., 1967, Wilde and Sjostrand, 1997).

The levels of cholesterol in eye lens plasma membrane increase with age (Mainali et al., 2017), while the amount of anti-oxidants decreases with age (Pescosolido et al., 2016). To examine the protective

role of cholesterol and tocopherol towards preventing the build-up of oxysterols after IR exposure, tocopherol concentrations should be measured simultaneously with the levels of cholesterol and oxysterols after exposure of mice to IR at different ages.

6.4.3. Uncertainty budget: more parameters playing a role in the observed IR-induced effects

While 15 contributors to uncertainty have been identified, their level of contribution of most is negligible (Table 6.2). The animals selected for this experiments were born within two weeks difference and the experiment was performed when they all were in young adulthood (Shoji et al., 2016, Fox et al., 2007) which advocates that the contribution to uncertainty for age of the animals is minimal. Animal house conditions, genetic and phenotypic variability were minimised by performing the experiment with an inbred mouse strain and housing the mice in the same facility. The irradiator used to expose the mice to X-rays was calibrated before use and therewith the possible variations between and within dose exposures were minimised. Although in this experiment X-rays were chosen to represent IR, different types of IR and dose rates can act differently towards inducing damage to the lens plasma membrane (Barnard et al., 2019, Hall and Giaccia, 1973, Brown et al., 2013). Therefore, further work should include comparison of IR-induced damage from different IR sources and at diverse dose rates.

The membrane extraction efficiency, purity of the samples, pipetting and lipid purification efficiency are uncertainty contribution factors that mainly depend on the individual performing the experiment and the material used. The membrane extraction and lipid purification were performed by one individual and the same pipettes were used throughout the experiment. The purity of the samples was optimised by using ultrapure, high performance liquid chromatography grade solvents. Given that the samples prepared for mass spectrometry were dissolved in a limited amount of solvent, evaporation occured rapidly and could influence the comparison of various samples. Therefore evaporation was minimised by immediately closing the tubes with screw-top lids after addition of the solvent and storing the samples at -20 °C. The analyte peak area was calculated automatically using Analyst 1.6.2, however the program occasionally failed to detect the right peak which required the user to select the right peak manually.

The influence of sex on IR-induced cholesterol oxidation is unknown (Table 6.2). Solely female mice were utilised in the *in vivo* IR-induced oxysterol formation experiment. Therefore, excluding the possibility that male mice might generate different results is not possible. IR-induced cataracts are more prevalent in woman (Chodick et al., 2008, Azizova et al., 2018), but the biological mechanisms that mediates these processes are still under investigation with the main focus on oestrogen-mediated pathways (Zetterberg and Celojevic, 2015). Fist reports indicated that oestrogen is not the predominant mediator in sex-dependent sensitivity to IR (Henderson et al., 2009). Further investigations including female and male mice will elucidate the mechanism(s) and level to which sex contributes to *in vivo* IR-induced oxysterol formation. Repeatability and "variability between efficiency of different membrane

extractions" had a significant contribution to uncertainty. To minimise uncertainty of "variability between efficiency of different membrane extractions" the analyte peak are values were normalised to the internal cholesterol which are considered to be constant given that all the mice were averagely the same age and that in the previous chapter, irradiation of lens membrane extracts with much higher levels did not induce significant changes cholesterol levels (Mainali et al., 2017). Hence, the only remaining source of significant uncertainty was repeatability. This uncertainty was used for statistical comparisons and the error bars applied to the figures were based on the repeated measures (Figure 6.4).

Chapter 7: Age-related changes in oxysterol levels in the eye lens and hippocampus

7.1. Introduction

Although the plasma membrane of lens fibre cells (LFCs) is one of the cholesterol-richest cell membranes (Borchman and Yappert, 2010), the brain is the organ with the highest cholesterol concentration, containing approximately 25% of the total cholesterol in the human body (Dietschy, 2009). With age, an increase in oxidative stress is noted in both organs (Cobley et al., 2018, Nelson and Alkon, 2005, Pescosolido et al., 2016).

7.1.1. Cholesterol and cholesterol oxidation adducts in the brain

Cholesterol biosynthesis in the brain occurs at a high rate during the prenatal and adolescence developmental stages compared with the adult stage in which synthesis occurs at a very low level (Saher et al., 2005, Jurevics and Morell, 1995, Zhang and Liu, 2015). This is associated with the observation that most of cholesterol in the brain has an extremely long half-life, approximately 5 years (Bjorkhem et al., 1998), compared with the half-life of cholesterol in plasma which is proximately 2 days (Dietschy and Turley, 2004). The turnover of cholesterol in the brain is maintained largely by 24-hydroxylase that converts the excessive cholesterol into 24(S)-hydroxycholesterol, and to a lesser extent by cholesterol 27-hydroxylase and oxysterol 7α-hydroxylase that catalyse respectively the conversion of cholesterol into 27- hydroxycholesterol and 7α-hydroxy-3-oxo-4-cholestenoic acid (Meaney et al., 2007, Bjorkhem et al., 1998). In contrast to cholesterol, 24(S)-hydroxycholesterol and 7α-hydroxy-3-oxo-4-cholestenoic acid are able to pass the blood brain barrier (Meaney et al., 2007).

Cholesterol has multiple functions in the brain including reducing permeability to ions in myelin steath (Snipes and Suter, 1997), acting as a signalling molecule during embryonic brain development (Herz and Farese, 1999) and mediating synaptic transmission in neuronal cells (Petrov et al., 2016). Disruption of cholesterol homeostasis in the brain leads to pathogenesis; for example, mutations in 7-dehydrocholesterol-7-reductase, an enzyme in the cholesterol biosynthesis pathway, correlate with learning disabilities in Smith-Lemli-Opitz syndrome patients (Porter, 2008). Cholesterol oxidation products have been linked with a number of neurodegenerative diseases among which Alzheimer's disease (AD) is the most common (Kosari et al., 2012, Gamba et al., 2015). AD is a chronic neurodegenerative disease, and its pathogenesis is hallmarked by the deposition of amyloid β peptides (Aβ) (Hardy and Higgins, 1992). These Aβ-peptides interact with various receptors inducing disruptive changes in signalling pathways and leading to synaptic dysfunction, mainly in the cortex and hippocampus (Ferreira et al., 2015, Terry et al., 1991, Dickson et al., 1995). Oxysterols that are generated via non-enzymatic and enzymatic pathways, such as 7α-hydroxycholesterol, 4β-hydroxycholestrerol, and 7-ketocholesterol and exclusively autoxidative produced oxysterols, such as 7β-hydroxycholesterol and 5α/ β, 6α/β-epoxycholesterol, which can migrate through the blood brain barrier, have been found to be enriched in the brain of AD patients compared with a cohort without cognitive impairment (Figure 7.1) (Hascalovici et al., 2009, Testa et al., 2016). Although extensive *in*

vitro and *in vivo* studies have identified mechanisms through which oxysterols can contribute to AD pathogenesis (Jeitner et al., 2011, Phan et al., 2018, Testa et al., 2016, Liu et al., 2016, Nelson and Alkon, 2005, Luque-Contreras et al., 2014, Gamba et al., 2015), further investigation is required to determine whether increased cholesterol oxidation occurs upstream or downstream of the previously identified AD development mechanisms, as well as the overarching molecular system underlying the involvement of oxysterols in AD pathogenesis.

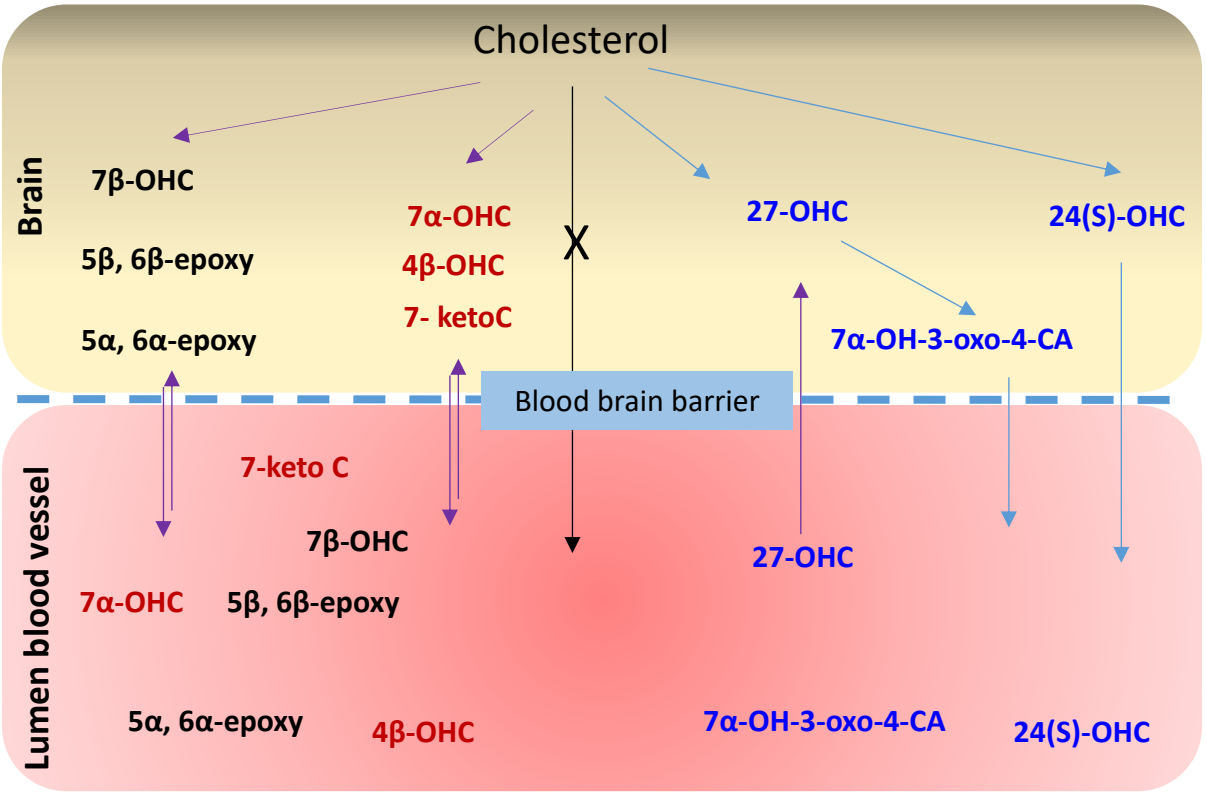

Figure 7.1: Schematic representation of cholesterol turnover in the brain. Black, oxysterols generated through autoxidation; Red; oxysterols that can be formed through enzymatic and non-enzymatic pathways; blue, oxysterols that are uniquely produced via enzymatic reactions. The blue arrows represent reactions that occur during cholesterol homeostasis, while the purple arrows indicate reactions upregulated in AD. 7α-OHC: 7α-hydroxycholesterol, 4β-OHC: 4β-hydroxycholestrerol, 7-keto C: 7-ketocholesterol, 7β-OHC: 7β-hydroxycholesterol, 5α, 6α-epoxy: 5α, 6α-epoxycholesterol, 5β, 6β epoxy: 5β, 6β- epoxycholesterol, 27-OHC: 27-hydroxycholesterol and 7α-OH-3-oxo-4-CA: 7α-hydroxy-3-oxo-4-cholestenoic acid.

7.1.2. Cholesterol: the common denominator of the brain and eye lens

Remarkably, the eye lens and the brain have a lot of common in terms of cholesterol homeostasis. The eye lens also produces most of its cholesterol during early development. Rat lens studies have shown that cholesterol biosynthesis occurs within the first few weeks after birth and subsequently, the anabolic pathway of cholesterol decreases significantly (Cenedella, 1983, Cenedella, 1982). However, post-mortem analysis of human eye lenses (>46 years of age) has shown that no significant modifications in cholesterol concentration occur although statins, inhibitors of 3-hydroxy-3-methylglutaryl coenzyme A reductase that is vital during cholesterol formation, were administered (Mitchell and Cenedella, 1999). Nevertheless, further analysis examining whether statins are able to enter the eye lenses would provide a deeper understanding of the cholesterol biosynthesis process in adult eye lenses. In contrast to the brain, the eye lens is capable of exchanging cholesterol with the surrounding tissues (Cenedella, 1983, Zelenka, 1984) and the exact developmental stage in which cholesterol synthesis in the eye lens is significantly reduced in the human body remains unknown.

Another peculiarity shared by the lens and brain is a suboptimal anti-oxidant system throughout life (Halliwell, 2006, Cobley et al., 2018). Although the brain uses on average 20% of the oxygen supply in the body, the levels of anti-oxidant agents such as glutathione and catalase are low compared with other tissues such as hepatocytes (Sinet et al., 1980, Baxter and Hardingham, 2016, Cobley et al., 2018). Lens transparency has to last a lifetime and therefore requires an efficient lifelong anti-oxidant system. However, the efficient collaboration between superoxide dismutase, catalase, glutathione peroxidase/ reductase, glutathione, vitamin E and C to protect the lens from oxidative stress is reduced due to a general decline in the levels of these enzymes with age (Uwineza et al., 2019, Giblin, 2000, Hamada et al., 2014). Furthermore, a gradual build-up of a glutathione barrier between lens cortex and nucleus, which occurs around the age of 40, prevents glutathione from reaching the nucleus (McGinty and Truscott, 2006, Giblin, 2000, Sweeney and Truscott, 1998).

Both, the brain and eye lens have low cholesterol turnover. In the eye lens, cell organelles are lost during maturation of LFCs to establish lens transparency (Bassnett, 2002, Bassnett and Beebe, 1992) and crystallins are compiled in the cytoplasm (Delaye and Tardieu, 1983). This, combined with the lens being a closed system in which cells are kept for life, allows for only a limited turnover in macromolecules including lipids (Hughes et al., 2015, Augusteyn, 2007, Lynnerup et al., 2008). Cholesterol turnover in the brain predominantly occurs via 24(S)- hydroxycholesterol, and calculations of the rate of secretion indicate that the turnover rate is approximately 0.4% of the total cholesterol in brain per day (Dietschy, 2009, Bjorkhem et al., 1998, Xie et al., 2003).

Metabolic dysfunction of cholesterol plays a vital role in the pathogenesis of age-related diseases such as cataracts and AD (reviewed by (Vejux et al., 2011, Zarrouk et al., 2014, Gamba et al., 2019)). Although oxysterol accumulation has been associated with both diseases (Girao et al., 1998, Hascalovici et al., 2009, Testa et al., 2016), the exact mechanism remains unclear.

7.2. Objectives and experimental design

Although there are parallels between cholesterol homeostasis in the brain and eye lens, the possibility of a common aetiology in age-related pathogenesis via deregulation of cholesterol homeostasis has not been investigated to date. Cholesterol and oxysterol adducts in hippocampi and LFCs were examined by LC-MS analysis of 6 and 30 months wild type (wt) C57BL/6J mice to verify whether age-related changes in cholesterol homeostasis in both tissues were correlated (Figure 7.2). First, cholesterol concentrations and the chromatograms of the oxysterols in the individual tissues were compared, followed by identification of specific sterols using standards and finally, the analyte peak area of the identified oxysterols was calculated.

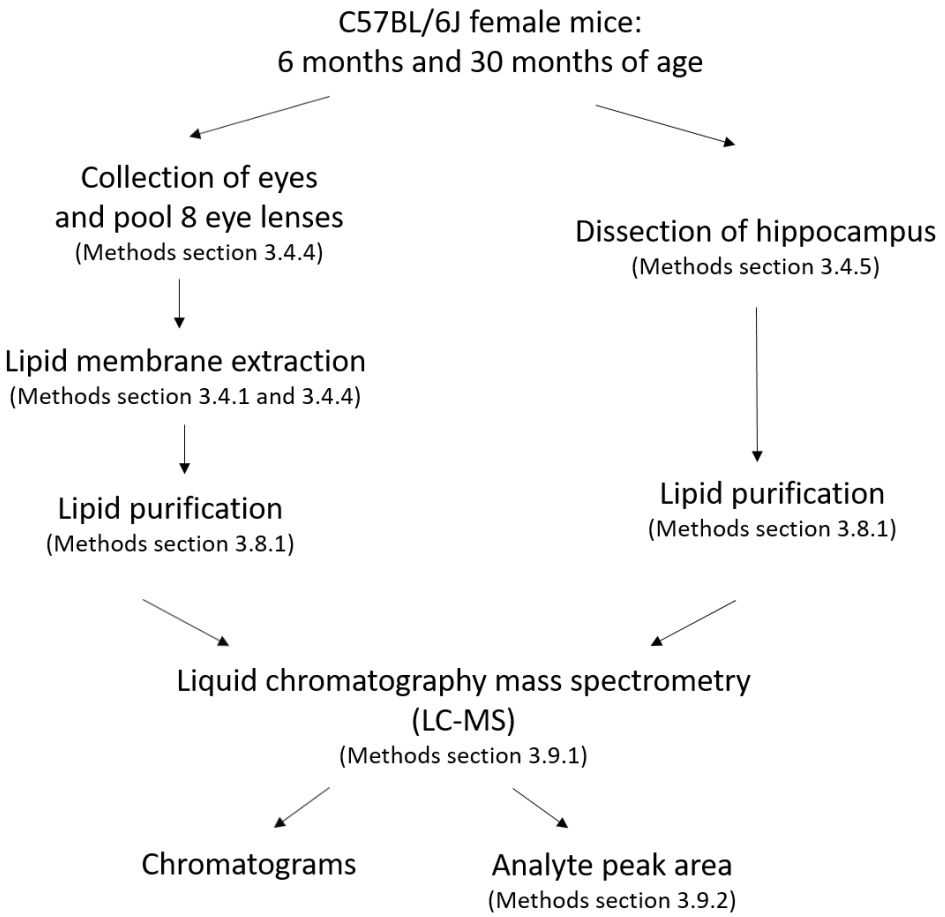

Figure 7.2: Schematic representation of experimental design of the age-related oxysterol levels modifications in the hippocampus and eye lenses experiment. Section numbers in the diagram refer to the material and methods chapter section in which the protocol is described.

7.3. Results

7.3.1. Age-dependent cholesterol changes occured in the eye lens, but not in the hippocampus

To compare age-related cholesterol modifications in eye lenses and hippocampi, the lipids from both tissues were extracted and the amount of cholesterol in the samples was determined by LC-MS (Figure 7.2). Although an age-dependent increase in cholesterol levels was observed in all examined tissues, the changes in the hippocampus ($p= 0.134$), cortical ($p= 0.992$) and the nuclear ($p= 1.000$) fractions were not significant (Figure 7.3A and B). The levels of cholesterol in the hippocampus were significantly higher than in the eye lens fractions ($p= 0.000$; Figure 7.3C vs. A and B). Comparison of the fold change between 6 and 30 months showed that the greatest increase in cholesterol levels occurred in the nuclear fraction of the eye lens (Figure 7.3A, B and C).

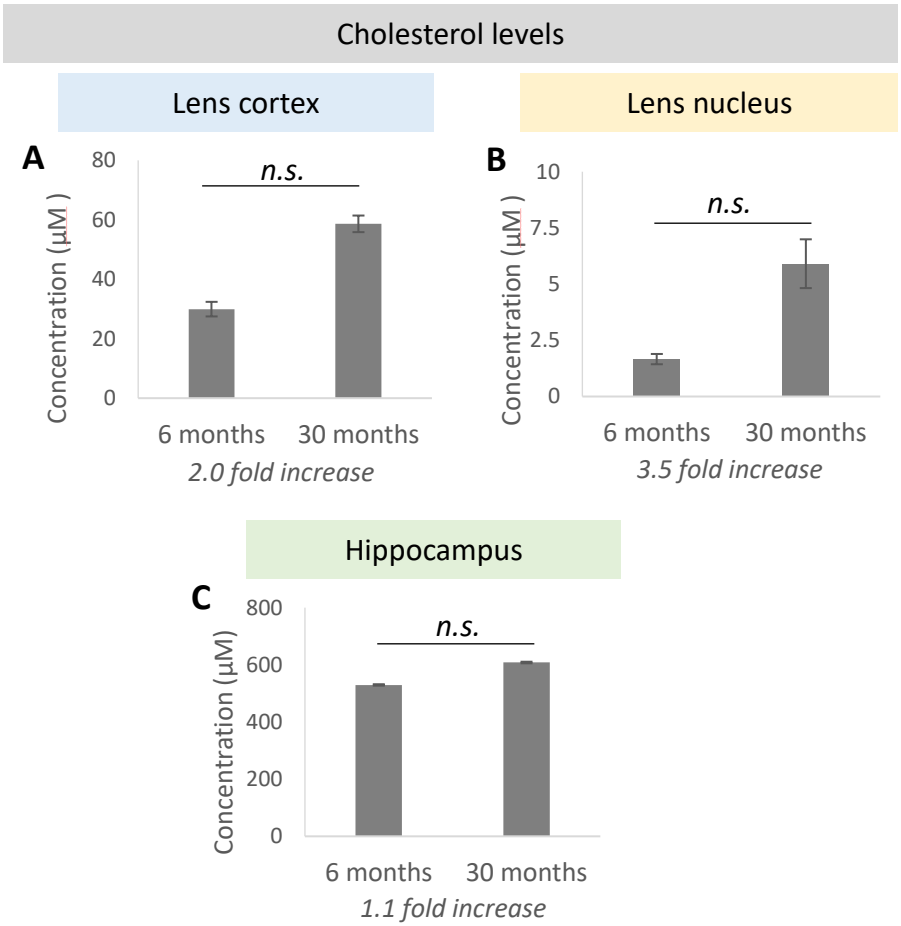

*Figure 7.3: LC-MS quantification of cholesterol concentration in the eye lenses and hippocampi of 6 and 30 month-old mice. 20 µM of cholesterol-d6 was added as the internal standard and was subsequently used to calculate the concentration (µM) of cholesterol in the samples. A) Cortical fraction of the eye lens, B) nuclear fraction of the eye lens and C) hippocampus. General Linear Model Analysis of Variance followed by Tukey pairwise comparison post hoc test using time and location as independent factors and concentration as dependent factor was applied for statistical analysis, *p< 0.05 n= 3 for hippocampus and n= 2 x 8 pooled eye lenses, n.s.: not significant.*

7.3.2. Oxysterol profiles in the hippocampus and eye lens were different

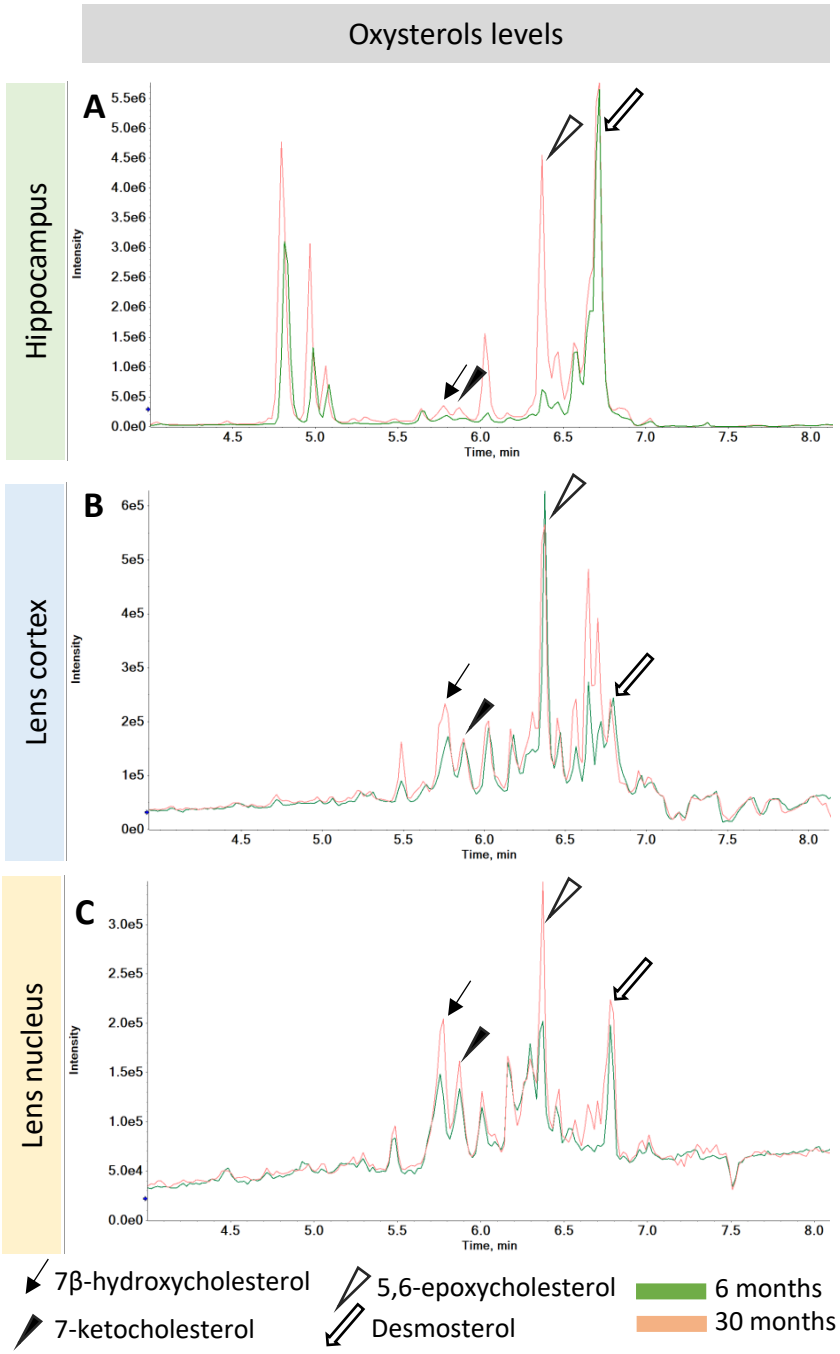

Figure 7.4: Chromatogram of LC-MS of A) the hippocampus, B) the cortex and C) the nucleus of the eye lens (8 pooled eye lenses per chromatogram) at 6 months (green) and 30 months (beige) after birth. The identified oxysterols are indicated with arrows.

The oxysterol profile of the hippocampus (Figure 7.4A) was different from the profiles observed in the lens cortex and the lens nucleus (Figure 7.4B and C). Cholesterol autoxidation products 7β-hydroxycholesterol, 7-ketocholesterol and 5,6-epoxycholesterol were detected in all examined tissues (Figure 7.4). Furthermore, desmosterol, the immediate precursor of cholesterol in cholesterol biosynthesis, was identified in the hippocampus as well as in the cortical and nuclear fraction of the eye lens (Figure 7.4A, B and C). A comparison of the chromatograms of the 6 month and 30 month-old mice suggested that the overall levels of oxysterols in the hippocampus (Figure 7.4A), the lens cortex (Figure 7.4B) and lens nucleus (Figure 7.4C) increased with age.

7.3.3. Contrasting age-related changes in desmosterol in the eye lens fractions

Despite the lack of statistical significance, a clear trend of an age-related increase in cholesterol was observed in the cortical and nuclear fractions of the lens (Figure 7.3A and B). In contrast to the IR-exposure experiments in the previous chapter, the internal cholesterol levels were not used as internal standards during the analysis of age-related alterations. However, cholesterol-d6 was added as technical control. The absolute values of the oxysterols in the 6 and 30 month-old mice were compared, and the oxysterol to cholesterol ratios were also plotted to determine the changes relative to the internal cholesterol concentrations.

An assessment of the desmosterol levels showed that no significant age-related changes occurred in the hippocampus ($p= 0.983$; Figure 7.5A). In contrast to the hippocampus, a significant decline in desmosterol was observed in the cortical lens fraction ($p= 0.048$; Figure 7.5B), while a significant increase was measured in the lens nucleus ($p= 0.038$; Figure 7.5C).

Interestingly, relative to cholesterol, desmosterol decreased with age in all measured tissues (Figure 7.5 D, E and F). While this decrease was not significant in the hippocampus ($p= 1.000$; Figure 7.5D) and in the lens cortex ($p= 0.460$; Figure 7.5E), the changes in the desmosterol:cholesterol ratio in the nuclear fraction of the lens were significant ($p= 0.000$; Figure 7.5F). Furthermore, the desmosterol:cholesterol ratio was significantly higher in the lens nucleus compared with the hippocampus ($p= 0.000$) and the lens cortex ($p= 0.000$; Figure 7.5F vs. D and E).

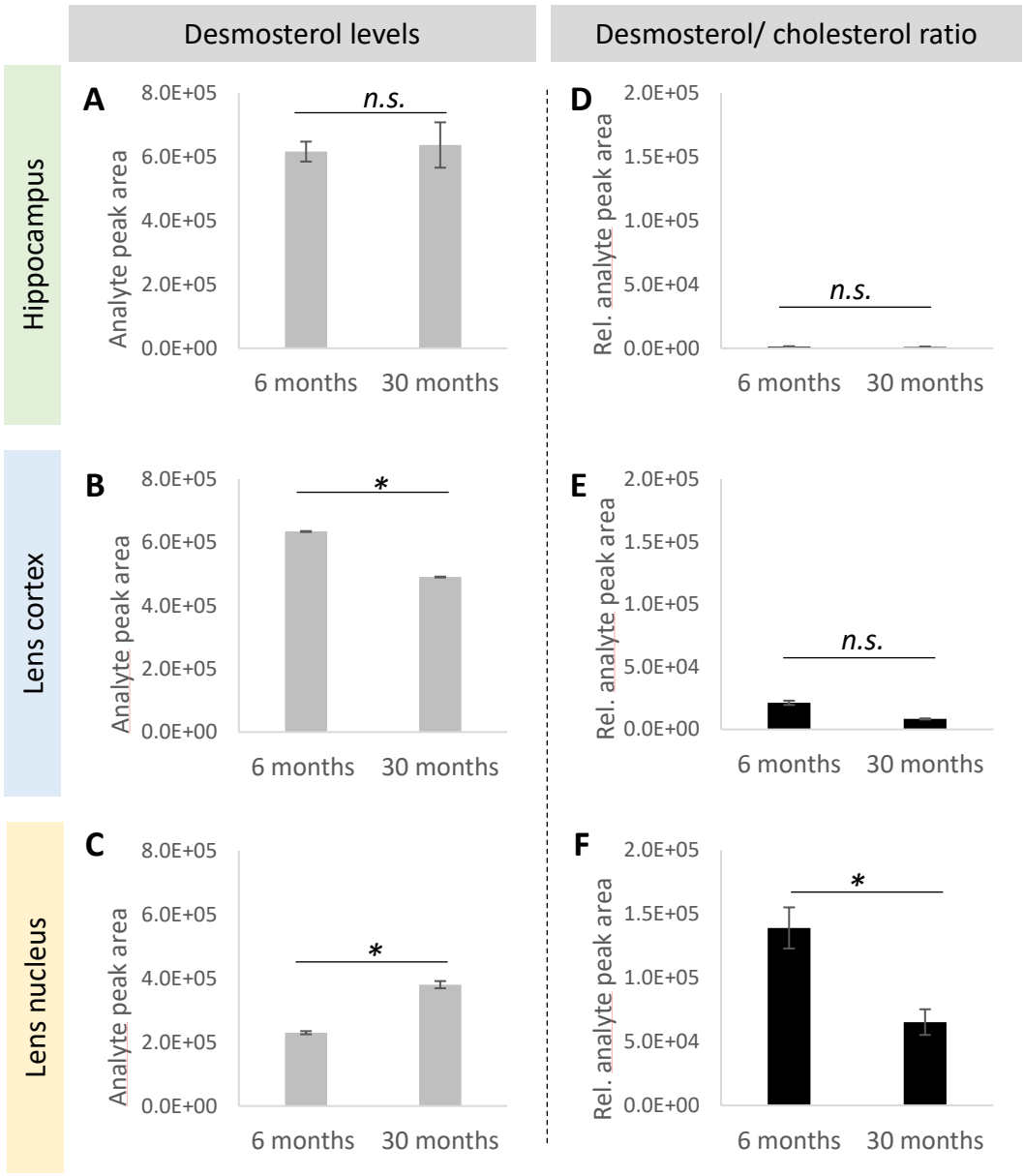

*Figure 7.5: LC-MS quantification of desmosterol in the hippocampus, the lens cortex and the lens nucleus of 6 and 30 month-old mice. The absolute values of the integrated analyte peak area of desmosterol are plotted for A) the hippocampus, B) the lens cortex and C) the lens nucleus. D), E) and F) respectively represent the absolute peak area relative to the internal cholesterol concentration for the hippocampus, the lens cortex and the lens nucleus. General Linear Model Analysis of Variance followed by Tukey pairwise comparison post hoc test using time and location as independent factors and (rel.) analyte peak area as dependent factor was applied for statistical analysis, *p< 0.05 n= 3 for hippocampus and n= 2 x 8 pooled eye lenses, n.s.: not significant, rel.: relative.*

7.3.4. An age-related increase of 7β-hydroxycholesterol occured solely in the hippocampus

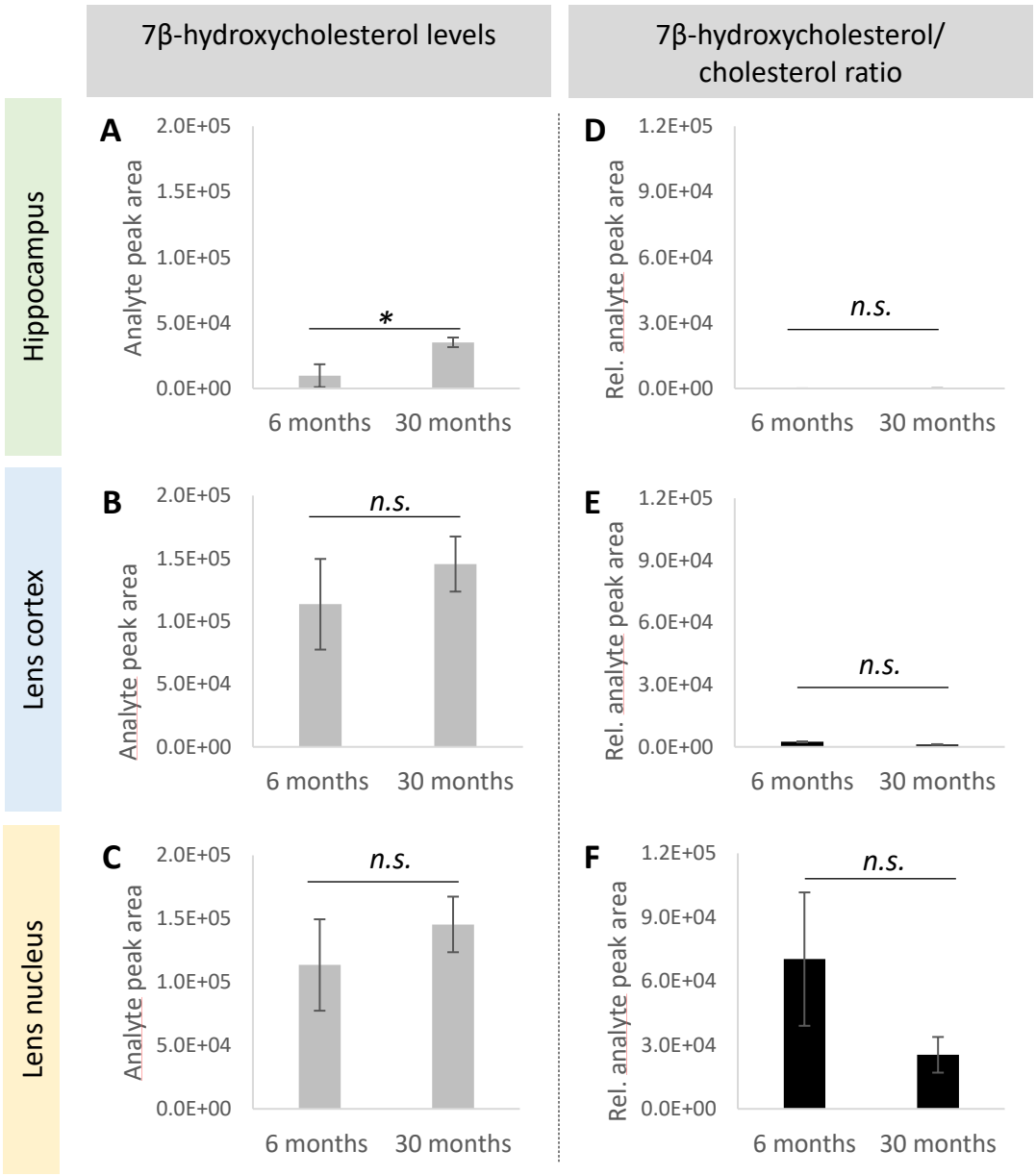

*Figure 7.6: LC-MS quantification of 7β-hydroxycholesterol in the hippocampus, the lens cortex and the lens nucleus of 6 and 30 month-old mice. The absolute values of the integrated analyte peak area of 7β-hydroxycholesterol are plotted for A) the hippocampus, B) the lens cortex and C) the lens nucleus. D), E) and F) respectively represent the absolute peak area relative to the internal cholesterol concentration for the hippocampus, the lens cortex and the lens nucleus. General Linear Model Analysis of Variance followed by Tukey pairwise comparison post hoc test using time and location as independent factors and (rel.) analyte peak area as dependent factor was applied for statistical analysis, *p< 0.05 n= 3 for hippocampus and n= 2 x 8 pooled eye lenses, n.s.: not significant, rel.: relative.*

Comparison of the amount of 7β-hydroxycholesterol in the 6 and 30 month-old mice showed that 7β-hydroxycholesterol tends to increase with age in the hippocampus and in the lens fractions (Figure 7.6A, B and C). However, while this increase was significant in the hippocampus (p= 0.020; Figure 7.6A), this trend was not significant in the cortical (p= 0.995; Figure 7.6B) and the nuclear (p= 0.995; Figure 7.6C) fractions.

Analysis of 7β-hydroxycholesterol relative to the internal cholesterol concentration showed that the 7β-hydroxycholesterol:cholesterol ratio was significantly higher in the lens nucleus compared with the lens cortex (p= 0.003) and the hippocampus (p= 0.002; Figure 7.6F vs. D and E). In the hippocampus, the 7β-hydroxycholesterol:cholesterol ratio increased with age, although not significantly (p= 1.000; Figure 7.6D). In contrast to the trend in the hippocampus, 7β-hydroxycholesterol showed a non-significant age-related decrease in the cortical (p= 1.000; Figure 7.6E) and nuclear (p= 0.058; Figure 7.6F) lens fractions relative to the internal cholesterol concentrations.

7.3.5. An age-associated increase of 7-ketocholesterol occured solely in the hippocampus

Based on the chromatograms, 7-ketocholesterol was one of the cholesterol autoxidation products that appeared to increase in an age-related manner in the hippocampus and the lens (Figure 7.4). Quantification of 7-ketocholesterol in these fractions demonstrated a significant increase in 7-ketocholesterol over time in the hippocampus (p= 0.002; Figure 7.7A) and a non-significant increase in the lens cortex (p= 0.998; Figure 7.7B) and the lens nucleus (p= 0.916; Figure 7.7C).

Relative to internal cholesterol concentration, 7-ketocholesterol showed a non-significant age-related increase in the hippocampus (p= 1.000; Figure 7.7D). In contrast, the 7-ketocholesterol:cholesterol ratio decreased with age in the lens (Figure 7.7E and F). Although this increase was significant in the lens nucleus (p= 0.006; Figure 7.7F), the changes in 7-ketocholesterol:cholesterol ratio were not significant in the lens cortex (p= 0.999; Figure 7.7C). Similar to the 7β-hydroxycholesterol:cholesterol ratio (Figure 7.6F vs. D and E), the 7-ketocholesterol:cholesterol ratio was significantly higher in the nuclear lens fraction than in the hippocampus (p= 0.000) and the cortical lens fraction (p= 0.000; Figure 7.7F vs. D and E).

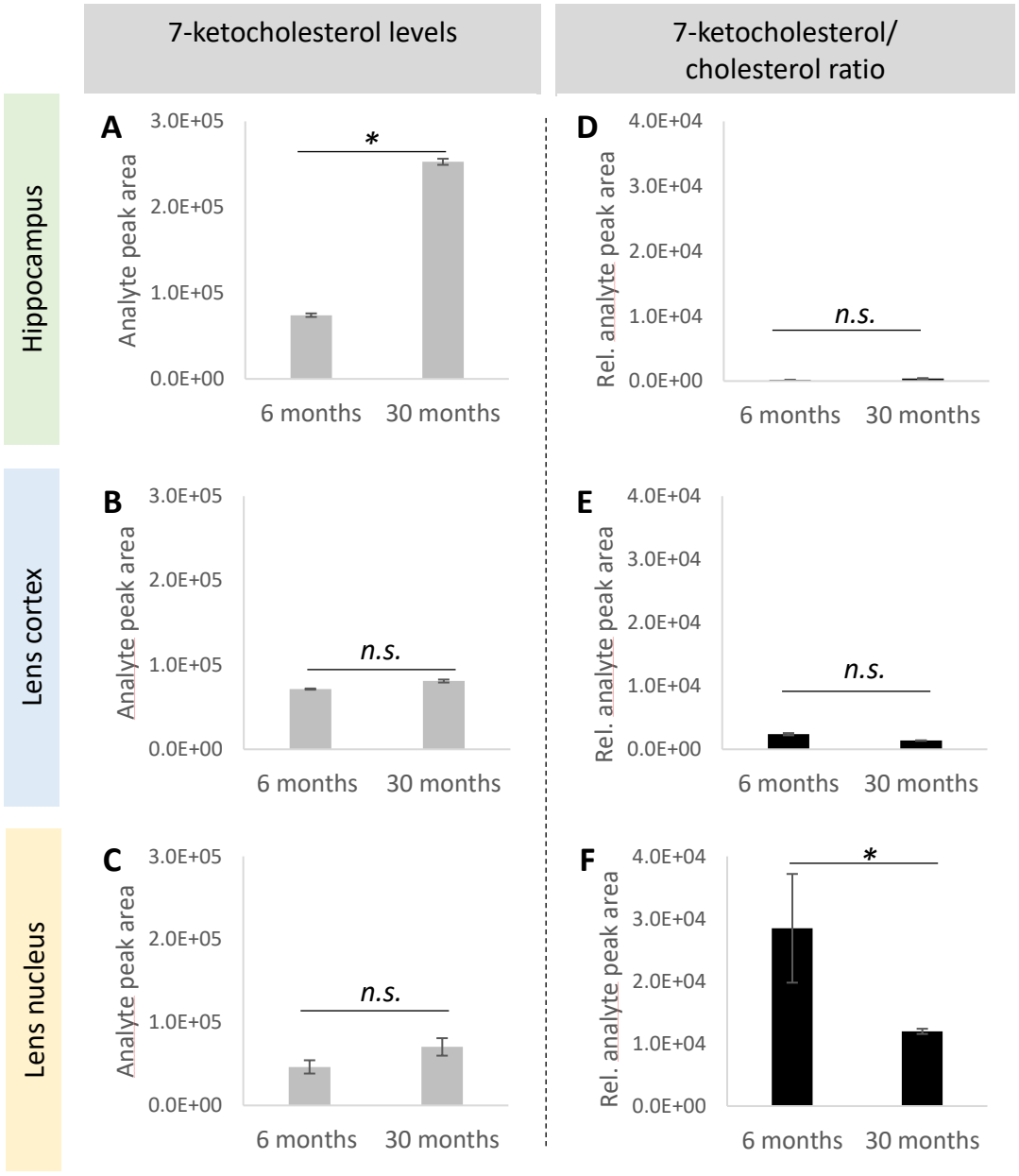

*Figure 7.7: LC-MS quantification of 7-ketocholesterol in the hippocampus, the lens cortex and the lens nucleus of 6 and 30 month-old mice. The absolute values of the integrated analyte peak area of 7-ketocholesterol are plotted for A) the hippocampus, B) the lens cortex and C) the lens nucleus. D), E) and F) respectively represent the absolute peak area relative to the internal cholesterol concentration for the hippocampus, the lens cortex and the lens nucleus. General Linear Model Analysis of Variance followed by Tukey pairwise comparison post hoc test using time and location as independent factors and (rel.) analyte peak area as dependent factor was applied for statistical analysis, *p< 0.05 n= 3 for the hippocampus and n= 2 x 8 pooled eye lenses, n.s.: not significant, rel.: relative.*

7.3.6. No significant age-related changes were observed for 5, 6-epoxycholesterol

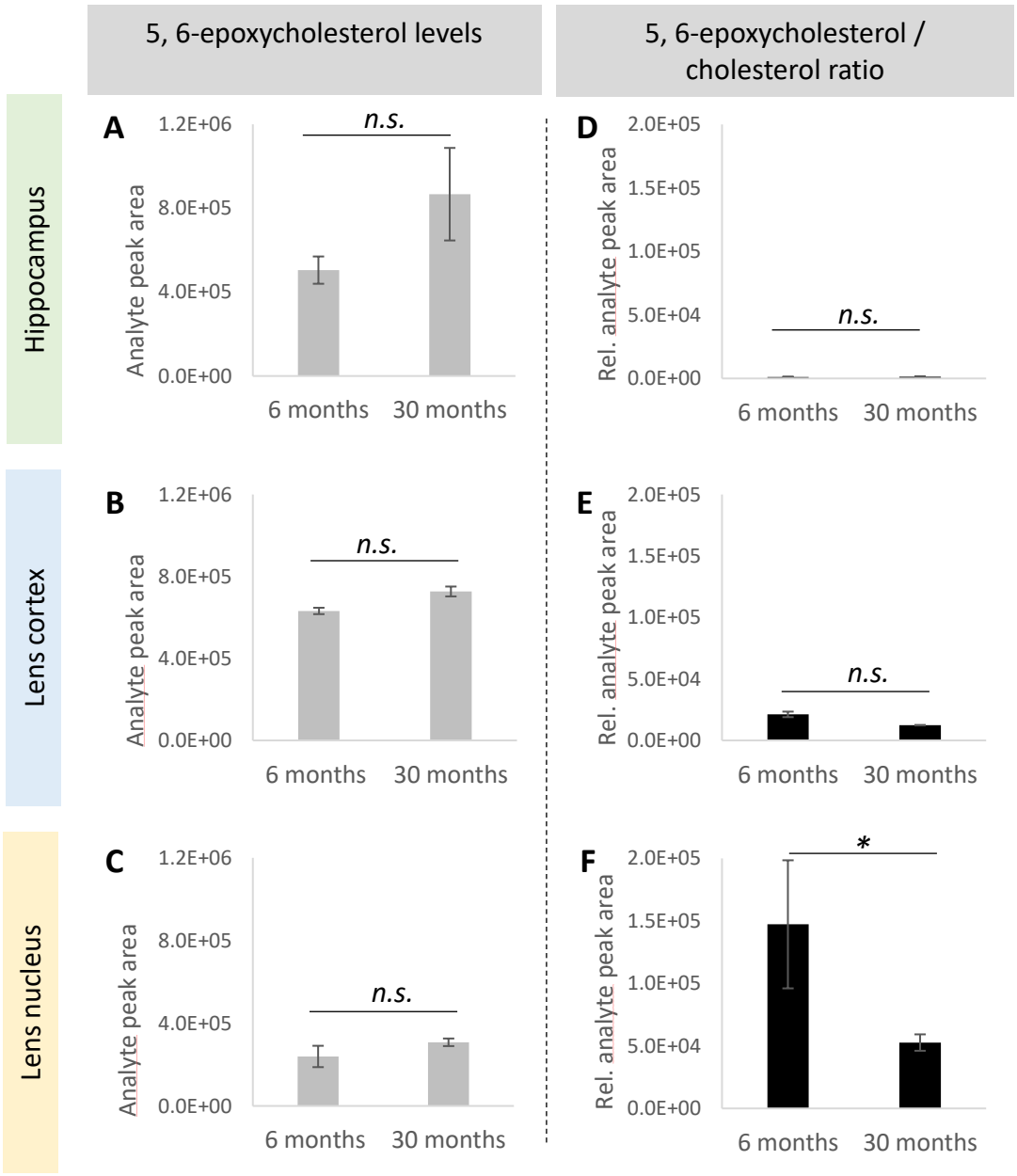

*Figure 7.8: LC-MS quantification of 5,6-epoxycholesterol in the hippocampus, the lens cortex and the lens nucleus of 6 and 30 month-old mice. The absolute values of the integrated analyte peak area of 5,6-epoxycholesterol are plotted for A) the hippocampus, B) the lens cortex and C) the lens nucleus. D), E) and F) respectively represent the absolute peak area relative to the internal cholesterol concentration for the hippocampus, the lens cortex and the lens nucleus. General Linear Model Analysis of Variance followed by Tukey pairwise comparison post hoc test using time and location as independent factors and (rel.) analyte peak area as dependent factor was applied for statistical analysis, *p< 0.05 n= 3 for hippocampus and n= 2 x 8 pooled eye lenses, n.s.: not significant, rel.: relative.*

Quantitative analysis of 5, 6-epoxycholesterol revealed that the age-related increase observed in the chromatograms (Figure 7.4) was not significant in the hippocampus (p= 0.066; Figure 7.8A), the lens cortex (p= 0.910; Figure 7.8B) and the lens nucleus (p= 0.974; Figure 7.8C).

Moreover, a non-significant age-related increase in the 5, 6-epoxycholesterol:cholesterol ratio was measured in the hippocampus (p= 1.000; Figure 7.8D), in contrast to a decrease in the 5, 6-epoxycholesterol:cholesterol ratio over time in the eye lens (Figure 7.8E and F). However, the observed decrease was not significant in the lens cortex (p= 0.998; Figure 7.8E), but was in the lens nucleus (p= 0.030; Figure 7.8F). The 5, 6-epoxycholesterol:cholesterol ratio was significantly higher in the nuclear lens fraction than in the hippocampus (p= 0.001) and the cortical lens fraction (p= 0.003; Figure 7.8F vs. D and E).

7.3.7. Retrospective power analysis

Studies measuring cholesterol and oxysterols in the hippocampus have generally used a sample size raging from n= 3 to n= 9 (Sodero et al., 2012, Ong et al., 2010, Brooks et al., 2017). This study used a sample size of n= 3; based on this sample size, the differences in mean values and the mean standard deviation, the actual power was calculated. Subsequently, the advised sample size to generate a target power of 0.8 in future experiments was estimated. The actual power for cholesterol and desmosterol in the hippocampus was much lower than 0.8 and thus a sample size greater than 3 was advised to detect age-associated differences for these adducts. On the other hand, the actual power for the cholesterol autoxidation products was approximately 0.8 and therewith the advised sample size was around the same as the sample size used during the investigation of age-related changes in the hippocampus (Table 7.1).

Table 7.1: Retrospective power analysis to determine the advised sample size for identifying age-related changes in sterol in mice using Minitab.

Absolute values	Sample size	Difference in mean value	Mean stdv	Actual power	Advised sample size for target power 0.8
Hippocampus 6 versus 30 months					
Cholesterol	3	78.445	58.138	0.248	10
Desmosterol	3	20666.667	51141.727	0.068	98
7β-hydroxycholesterol	3	25450.000	6187.184	0.957	3
7-ketocholesterol	3	178650.000	2793.072	1.000	2
5, 6-epoxycholesterol	3	362000.000	142835.570	0.647	4
Lens cortex 6 versus 30 months					
Cholesterol	2	28.698	2.621	0.997	2
Desmosterol	2	-144000.000	1414.214	1.000	2
7β-hydroxycholesterol	2	-2500.000	3889.087	0.069	39
7-ketocholesterol	2	9550.000	1237.437	0.948	2
5, 6-epoxycholesterol	2	95000.000	19798.990	0.691	3
Lens nucleus 6 versus 30 months					
Cholesterol	2	4.244	0.657	0.875	2
Desmosterol	2	150500.000	8131.728	1.000	2
7β-hydroxycholesterol	2	32000.000	28991.378	0.105	14
7-ketocholesterol	2	24100.000	9263.099	0.317	4
5, 6-epoxycholesterol	2	68500.000	35001.786	0.212	6

(Stdev: standard deviation)

In contrast to the hippocampus, the actual power for cholesterol and desmosterol in the lens cortex and nucleus was >0.8 (Table 7.1). Furthermore, the advised sample size for both sterols was equal to the sample size used to collect the data. 7β-hydroxycholesterol, with an actual power <0.2 in both lens fractions, exhibited a much greater advised sample size compared with the used sample size. In the lens cortex, the observed actual power for 5, 6-epoxycholesterol and 7-ketocholesterol was relatively close to 0.8 and the advised sample size nearly equalled the exercised sample size (Table 7.1). The actual power for these components in the lens nucleus was much lower than 0.8 and therefore the advised sample size was slightly greater than the applied sample size.

Table 7.2: Retrospective power analysis to determine the advised sample size for identifying age-related changes in sterols relative to the internal cholesterol concentration in mice using Minitab.

Relative values	Sample size	Difference in mean value	Mean stdv	Actual power	Advised sample size for target power 0.8
Hippocampus 6 versus 30 months					
Desmosterol	3	-269.340	195.208	0.257	10
7β-hydroxycholesterol	3	49.474	13.785	0.899	3
7-ketocholesterol	3	234.049	50.045	0.985	3
5, 6-epoxycholesterol	3	253.851	296.965	0.129	23
Lens cortex 6 versus 30 months					
Desmosterol	2	-12877.694	1057.289	0.999	2
7β-hydroxycholesterol	2	-1233.684	52.094	1.000	2
7-ketocholesterol	2	-1009.399	103.794	0.991	2
5, 6-epoxycholesterol	2	-8791.905	1217.066	0.925	2
Lens nucleus 6 versus 30 months					
Desmosterol	2	-73820.311	13094.379	0.798	3
7β-hydroxycholesterol	2	-44936.612	19844.888	0.260	5
7-ketocholesterol	2	-16505.321	4561.842	0.498	3
5, 6-epoxycholesterol	2	-94570.532	28893.220	0.436	3

(Stdev: standard deviation)

When investigating the changes in oxysterol levels relative to the internal cholesterol in the hippocampus, the cortical and nuclear fraction of the eye lens; the recommended sample size and actual power differed from that required to study absolute sterol levels (Table 7.1 vs. Table 7.2). In the hippocampus a sample size of 3 offered enough power (> 0.8) to detect age-related changes in sterols relative to the internal cholesterol concentration, thus, the advised sample size for 7β-hydroxycholesterol and 7-ketocholesterol was similar to the sample size applied during the experiment (Table 7.2). However, a greater sample size was recommended for 5, 6-epoxycholesterol and desmosterol in the hippocampus compared with the actual sample size.

In the lens cortex, the advised sample size equalled the exercised sample size, and the actual power for all examined sterol adducts was >0.8. However, the advised sample size in the lens nucleus was slightly greater than the exercised sample size and the associated power calculations all illustrate an actual power <0.8 (Table 7.2).

7.3.8. Uncertainty budget

A qualitative analysis of the uncertainty budget identified 16 factors that contribute to uncertainty during the investigation of age-related changes in sterol levels in the murine hippocampus and eye lenses (Table 7.3). Variability in age within a group of mice in the context of cholesterol and desmosterol, phenotypic and genetic variability, animal house conditions, dissection of the hippocampus, purity of the samples and analyte peak area are all factors with a Gaussian distribution that showed a minor contribution to uncertainty. Moreover, membrane extraction efficiency, pipetting, lipid purification efficiency and evaporation of solvent also had a minor contribution to uncertainty, but displayed a rectangular distribution. The uncertainty contribution of "variability in age within a group of mice in the context of autoxidation products", sex and time of sacrifice to the levels of sterols was unknown, and "variabilities between efficiency of different membrane extractions" and the repeatability, both showed a Gaussian distribution, and had a significant contribution to uncertainty.

Table 7.3: Uncertainty budget for age-related changes in sterols in the murine hippocampus and eye lenses.

Uncertainty contributor	Qualitative uncertainty	Parameter Unit	Type of Evaluation	Distribution
Variability in age within a group of mice in the context of cholesterol and desmosterol	minor	months	A	Gaussian
Variability in age within a group of mice in the context of autoxidation products	unknown	counts	A	Gaussian
Sex	unknown	counts	B	Rectangular
Phenotypic variability	minor	counts	A	Gaussian
Genetic variability	minor	counts	A	Gaussian
Animal house conditions	minor	counts	A	Gaussian
Time of sacrifice	unknown	counts	A	Gaussian
Dissection of the hippocampus	minor	mg	B	Gaussian
Membrane extraction efficiency	minor	mg	B	Rectangular
Variabilities between efficiency of different membrane extractions	significant	counts	A	Gaussian
Purity of the samples	minor	counts	A	Gaussian
Pipetting	minor	mL	B	Rectangular
Lipid purification efficiency	minor	counts	B	Rectangular
Evaporation of solvent	minor	counts	B	Rectangular
Analyte peak area	minor	counts	A	Gaussian
Repeatability	significant	Analyte peak area Relative value	A	Gaussian

7.4. Discussion and conclusions

7.4.1. Cholesterol accumulates in the eye lens, but not in the brain

Analysis of cholesterol levels in the eye lenses and the hippocampus of 6 and 30 month-old mice indicated that while the concentration of cholesterol remained widely constant in the hippocampus (Figure 7.3C), a trend of age-related cholesterol increase is observed in the lens cortex and nucleus (Figure 7.3A and B). These results are in line with previous studies: at 6 months, mice are considered to have reached maturity (Dutta and Sengupta, 2016). Measurements of cholesterol in the murine central nervous system during development showed that in adulthood, defined as >13 weeks after birth, cholesterol biosynthesis occurs at a constant rate and the pool of sterols remains steady (Quan et al., 2003). In addition, their data illustrated that these features are maintained in the cerebrum. LC-MS analysis of sterols in the hippocampus, providing a more in-depth analysis, showed that the hippocampus cholesterol concentrations remained constant throughout adulthood (Figure 7.3C). Measurements of desmosterol levels, a biomarker for active cholesterol biosynthesis (Dayspring et al., 2015), confirmed cholesterol biosynthesis in the hippocampus remained constant throughout ageing of adult mice (Figure 7.5A). Desmosterol:cholesterol ratios did not show any significant age-related changes, indicating that cholesterol biosynthesis is concurrent with cholesterol removal from the hippocampus (Figure 7.5D). As shown hitherto, to prevent a build-up of cholesterol in the brain and simultaneously also constantly replenish the brain with novel cholesterol, excessive cholesterol is removed by converting cholesterol into 24(S)-hydroxycholesterol and to a lesser extent into 7α-hydroxy-3-oxo-4-cholestenoic acid that can pass the blood brain barrier (Meaney et al., 2007, Bjorkhem et al., 1998). Power analysis of the absolute and relative data (Figure 7.3C, Figure 7.5A and D, Table 7.1 and Table 7.2) suggested that a lack of statistical power to attain valid conclusions. Given that the generated data are consistent with previous studies, the lack of statistical power was discredited and it was concluded that cholesterol and desmosterol levels in the hippocampus remain constant with age.

Using human LFCs, cholesterol levels were shown to increase in an age-dependent manner in the eye lens (de Vries et al., 1991, Mainali et al., 2017). This increase was more pronounced in the lens nucleus than in the lens cortex (Mainali et al., 2017). The same trend was recognised in aging mice (Figure 7.3A and B); cholesterol concentrations increased in the eye lens as the mice got older and this trend was stronger in the nuclear fraction which showed a 3.5-fold increase in the 30 month-old mice in comparison with the cortical fraction in which a 2.0-fold change was observed. A significant decrease in desmosterol was noted in the cortical fraction of the lens (Figure 7.5B), while relative to cholesterol levels, a non-significant decrease was demonstrated (Figure 7.5E). The decreasing trend of the desmosterol:cholesterol ratio in the cortical fraction of the lens observed in the 30 month-old mice compared with the 6 month-old mice implied an accumulation of cholesterol in the lens cortex. Desmosterol also showed an age-correlated increase in the lens nucleus (Figure 7.3B andFigure 7.5C),

although desmosterol:cholesterol ratio decreased with time (Figure 7.5F). These results suggested that cholesterol build-up also occurs in the lens nucleus. Given that the cholesterol accumulation observed in the lens cortex was much smaller than in the lens nucleus (Figure 7.5E vs. F) and limited turnover of macromolecules in the eye lens has been recognised (Lynnerup et al., 2008, Hughes et al., 2012), it is possible that some cholesterol is transported from the lens cortex into the lens nucleus. Surprisingly, a significant drop in desmosterol was observed in 30 month-old mice suggesting an age-related decrease in cholesterol biosynthesis in the cortical fraction of the eye lens (Figure 7.5B). Conceivably, in addition to the transport of cholesterol, desmosterol could also be transported to the lens nucleus. Desmosterol has been shown to be more likely to be transported compared with newly synthesized cholesterol (Johnson et al., 1995) and several studies have shown that desmosterol is among the cholesterol biosynthesis intermediate sterols that are transported from the endoplasmic reticulum to the plasma membrane before being converted into cholesterol (Yamauchi et al., 2007, Lusa et al., 2003, Echevarria et al., 1990). The transport of cholesterol and/ or desmosterol could happen through the circulation system executed by the membrane protein channel network that has been proposed to transfer ions and nutrients into the deeper layers of the lens (Donaldson et al., 2001, Mathias et al., 2007). Experiments involving radio-labelling of desmosterol and cholesterol could help elucidate the latter. Power analysis of cholesterol and desmosterol in the eye lens fractions showed that the actual power of the performed comparisons was ≥0.8 (Table 7.1 and Table 7.2), which suggested there is enough statistical power to detect significant differences. Though the latter was not observed when an ANOVA analysis for the cholesterol data was implemented (Figure 7.3A and B). This could be due to the high levels of cholesterol in the hippocampus, which prevented achieving significance.

A comparison of cholesterol and desmosterol levels in the eye lens and the hippocampus suggest that although cholesterol biosynthesis occurs in both organs, in the hippocampus synthesis occurs at a constant rate during adulthood while the rate changes with age in the eye lens (Figure 7.5A vs. B and C). Furthermore, while the levels in the hippocampus remained constant, cholesterol accumulated with age in the lens cortex and nucleus (Figure 7.5D vs. E and F). These results suggest that although both organs have high amounts of cholesterol, the mechanisms underpinning cholesterol homeostasis are different. This might be correlated to the distinct functions of cholesterol observed in both organs. In the lens, high levels of cholesterol have been mainly associated with anti-oxidant activity (Mainali et al., 2015, Girao et al., 1999), while in the brain cholesterol has multiple functions including a structural component for myelin, a precursor of steroid hormones and bile acid biosynthesis, as well as having an essential function in neuronal physiology (reviewed in (Zhang and Liu, 2015)).

7.4.2. The hippocampus has greater oxysterol variety than the eye lens

Compared with cholesterol, oxysterols are reactive molecules that can easily be converted into one another (Sottero et al., 2009, Zerbinati and Iuliano, 2017). The oxysterol profile of the hippocampus differed from that exhibited by the eye lens, though the lens cortex and nucleus showed the same

oxysterol profiles (Figure 7.4). The cells in the hippocampus preserve their cell organelles and therefore have high levels of the enzymes located in the endoplasmic reticulum and mitochondria required for enzymatic conversion of sterols compared to the eye lens (Mutemberezi et al., 2016). Although never fully investigated, LFCs probably have a very limited amount of the enzymes involved in sterol conversion; during the differentiation of LECs into young LFCs and the maturation process of these young LFCs into mature LFCs, the cell organelles are broken down (Bassnett, 2002). Concurrent with this, most of the enzymes enabling the enzymatic conversion of sterols are lost leading to decreased variety in oxysterols in the eye lens compared with the hippocampus.

7.4.3. Age-related changes in oxysterol levels are observed in the eye lens and hippocampus

The eye lens and the hippocampus have a great variety of oxysterols (Figure 7.4). The three oxysterols associated with age-related cataracts and AD, 7-ketocholesterol, 7β-hydroxycholesterol and 5, 6-epoxycholesterol (Hascalovici et al., 2009, Testa et al., 2016), were identified and quantified in the eye lens and the hippocampus of both 6 and 30 month-old mice (Figure 7.4,Figure 7.6, Figure 7.7 and Figure 7.8). Although the absolute quantification of these oxysterols showed a large variation (with statistical significance only in the brain), a trend of age-related increase was indisputable in both organs (Figure 7.6A, B and C; Figure 7.7A, B and C; Figure 7.8A, B and C). The observed large variation might have been partly due to the variation in age in both groups: 6 months (5 – 8 months) and 30 months (28 – 32 months) (Table 7.3). The power analysis indicated that a larger sample size could have the potential to increase the probability to detect significant changes in the cortical and nuclear fraction of the lens (Table 7.1). Further studies examining oxysterol levels in eye lenses and hippocampi of cataractogenic mice compared to their age-matched controls, and analysis of the same tissues in AD and wt mice will elucidate whether the age-related increase in oxysterol in cataracts and AD occurs concurrently. A few studies have identified etiological similarities in both diseases (Jun et al., 2012, Liu and Zhu, 2017, Reddy et al., 2017).

Relative to cholesterol, the hippocampus had the lowest amount of oxysterols, followed by the lens cortex and the lens nucleus respectively (Figure 7.6D, E and F; Figure 7.7D, E and F; Figure 7.8D, E and F). This could be attributed to the hippocampus being a vascular tissue and therefore providing these oxysterols a means of leaving the cells in the hippocampus; 7-ketocholesterol and 7β-hydroxycholesterol are among the oxysterols shown to be more mobile than cholesterol as they transfer more rapidly into lipoproteins and vesicles (Theunissen et al., 1986, Meaney et al., 2002). In addition, with the cell organelles intact, the peroxisomes provide enzymatic and non-enzymatic anti-oxidant defence mechanisms. On the other hand, the avascularity of the eye lens and the gradual degradation of cell organelles, which are essential to its function (Bassnett et al., 2011), probably lead to a weaker anti-oxidant defence mechanism compared with the hippocampus.

In contrast to the lens cortex, significant changes in the oxysterol:cholesterol ratio were observed in the lens nucleus (Figure 7.7E and F, Figure 7.8E and F). Two phenomena might be contributing to this: young LFCs situated in the lens cortex still having cell organelles (Bassnett, 2002) and the development of a glutathione barrier between the lens cortex and lens nucleus with age (Sweeney and Truscott, 1998). Interestingly, the main type of cataract associated with age-related cataracts is the nuclear cataract (Kanthan et al., 2008, Klein et al., 2008). This provides further evidence of the mechanism through which the previously reported accumulation of oxysterol adducts and the glutathione barrier contribute to the development of age-related cataracts (Sweeney and Truscott, 1998, Girao et al., 1998).

Cholesterol is a vital lipid in the hippocampus and in the eye lens. AD and cataracts are both iconic age-related diseases (Little, 2013, Association, 2015). Quantitative LC-MS analysis of 6 and 30 month-old mice demonstrated significant changes in the absolute amount of oxysterols in the hippocampus (Figure 7.6A and Figure 7.7A), in contrast to the eye lens where significant changes were observed only relative to cholesterol concentrations in the lens nucleus (Figure 7.7F and Figure 7.8F). Intriguingly, the latter raises the questions of whether AD pathogenesis is correlated with the absolute amount of oxysterols while cataracts are associated with relative amount of oxysterols.

7.4.4. Uncertainty budget: enhancement of the age-related changes in oxysterols in the eye lens and hippocampus

Although the data presented above generally allowed the identification of age-related trends, more could be done to gain a deeper understanding of the age-related changes occurring in the eye lens and in the hippocampus. The variability in age within a group of mice could have been reduced, which would have decreased the observed variability in the autoxidation generated oxysterol data and thus increased the probability of detecting significant differences. However, in the context of cholesterol and desmosterol, the contribution of "variability in age within a group of mice" is minor. Previous studies have shown minimal changes in cholesterol biosynthesis in the adult mammalian brain (Quan et al., 2003). Significant age-related changes in cholesterol and desmosterol levels still occur in the eye lenses of adult mammals (Mainali et al., 2017); however power analysis showed that the experiment had enough power to illuminate significant modifications (Table 7.3).

The correlation between oxysterol levels and sex has yet to be investigated. During these experiments solely female mice were used because they are deemed to be more sensitive to cataractogenesis and AD (Nirmalan et al., 2004, Zetterberg, 2016, Vina and Lloret, 2010, Podcasy and Epperson, 2016). Further investigation including male mice would provide a better representation of which age-related changes in oxysterol occur in the general population.

All the animals were bred and housed in the same research facility which minimised these factors' contribution to uncertainty; though the general human population does not live in the same environment, and the genetic and phenotypic variability is larger. Therefore, performing the same experiment with

various strains of mice housed in different conditions would give better insight into the age-related changes in oxysterols and how they contribute to pathogenesis in the hippocampus and eye lens.

Mice, like humans, are diurnal species (Refinetti, 2004). Melatonin, regulated by the circadian rhythm has been shown to mediate processes in the rat lens epithelium including the anti-oxidant system (Abe et al., 2000) and mitosis (von Sallmann and Grimes, 1966). Several studies have shown that the functionality of the hippocampus is closely interlinked with melatonin levels (Gorfine and Zisapel, 2007, Ramirez-Rodriguez et al., 2009, Yang et al., 2018). Furthermore, research using liver and gastrointestinal tissue revealed the involvement of the circadian rhythm in the regulation of cholesterol biosynthesis and oxysterol signalling (Kovac et al., 2019, Zhang et al., 2017). Taken together, though the contribution of the time of sacrifice to variability is estimated to be minor, it would still be interesting to measure the levels of sterols at different times of the day.

Dissection of the hippocampus, the membrane extraction efficiency, purity of the samples, pipetting and lipid purification efficiency are uncertainty contributors that mainly depend on the technical abilities of the researcher preparing the samples. Dissection of the hippocampus was mainly performed by a single individual and the remaining laboratory work was performed by one other investigator. As mentioned in the previous chapter, the purity of the samples was optimised by using ultrapure, high performance liquid chromatography grade solvents. Given that the samples prepared for mass spectrometry were dissolved in a limited amount of solvent, evaporation occurs rapidly and could influence the comparison of various samples. Evaporation was minimised by immediately closing the tubes with screw-top lids after addition of the solvent and storing them at -20 °C. The analyte peak area was calculated automatically using Analyst 1.6.2; however, the program occasionally failed to detect the right peak which required the user to select the right peak manually.

The contribution factors with significant levels of uncertainty were “variability between efficiency of different membrane extractions” and repeatability. Within each cohort the same amount of eye lenses were used and the entire left side hippocampus was used to reduce the contribution of “variability between efficiency of different membrane extractions”. Therefore, repeatability was used as a factor to assess the uncertainty in the measurements of age-related changes in oxysterol levels in the eye lens and hippocampus, i.e. error bars and statistical analysis (Figure 7.3, Figure 7.5, Figure 7.6, Figure 7.7 and Figure 7.8). Although the ratios between oxysterol and cholesterol enabled the comparison between tissues, studies aimed at identifying an oxysterol that remains constant in the lens and the hippocampus with age would enable normalisation using an internal standard instead of the technical standard, 25-hydroxycholesterol-d6, added only in the lipid purification step.

Chapter 8: The effect of anti-oxidants on IR-induced oxysterol formation

8.1. Introduction

As the eye lens is regularly exposed to light and therefore radiation, protection from oxidative stress generated by these sources is provided by the anti-oxidant system present in the eye. Although the physical barrier formed by lipid rafts limits the amount of oxidative agents in the eye lens, enzymatic and non-enzymatic anti-oxidants establish the main defence mechanism against oxidative stress in the lens (Girao et al., 1999, Varma, 1991).

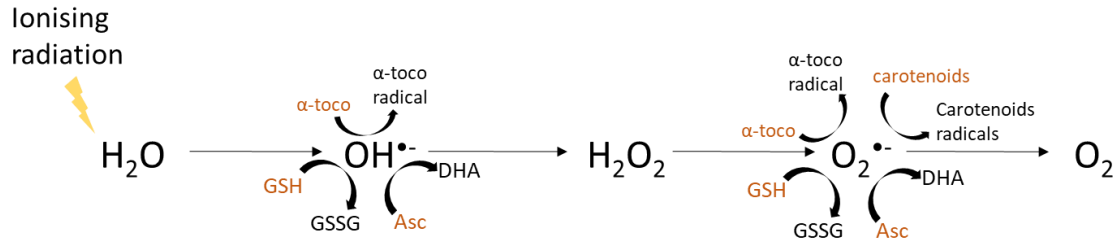

Figure 8.1: Scheme of free radicals generated by ionising radiation and the non-enzymatic anti-oxidants that can neutralise them. GSH, α-toco and Asc convert $OH^{\bullet-}$ into H_2O_2 while being oxidised to GSSG, α-toco radical and DHA respectively. GSH, α-toco, Asc and carotenoids convert $O_2^{\bullet-}$ into O_2 while being oxidised to respectively GSSG, α-toco radical, DHA and carotenoids radicals. α-toco: α-tocopherol, α-toco radical: α-tocopheryl radical, GSH: glutathione, GSSG: glutathione disulphide, Asc: ascorbic acid and DHA: dehydroascorbate anion

Non-enzymatic anti-oxidants neutralise free radicals by donating an electron (Yu, 1994). Ascorbic acid and GSH are the most highly concentrated non-enzymatic anti-oxidants in the lens (Consul and Nagpal, 1968, Pescosolido et al., 2016). Non-enzymatic degradation of H_2O_2 into H_2O and O_2 occurs through GSH, while ascorbic acid reduces hydroxyl radical ($OH^{\bullet-}$) and superoxide anion ($O_2^{\bullet-}$) (Yoshimura et al., 1999) (Figure 8.1). Although in much lower levels than ascorbic acid and GSH, α-tocopherol and carotenoids are also present in the lens (Yeum et al., 1995). α-Tocopherol reduces $O_2^{\bullet-}$ and $OH^{\bullet-}$, and carotenoids mediate the conversion of $O_2^{\bullet-}$ into less reactive molecules (Figure 8.1) (Li et al., 2014b). Furthermore, these anti-oxidants participate in each other's regeneration such as ascorbic acid converts α-tocopheryl radical into α-tocopherol (Packer et al., 1979), and GSH, together with dehydroascorbate reductase, reduces dehydroascorbate anion radicals back to ascorbic acid (Kisic et al., 2012).

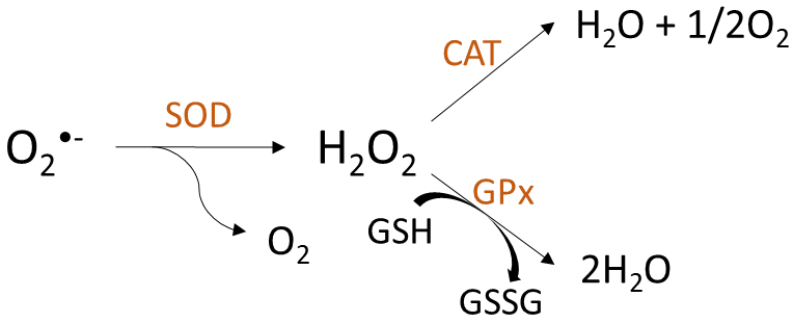

Figure 8.2: Diagram of the activity of enzymatic anti-oxidants activity in the lens. SOD catalyses the conversion of $O_2^{\bullet-}$ into H_2O_2. Subsequently H_2O_2 can be neutralised by conversion into H_2O, this is catalysed by CAT or GPx. SOD: superoxide dismutase, CAT: catalase, GPx: glutathione peroxidase, GSH: glutathione, GSSG: glutathione disulphide

Superoxide dismutase (SOD), catalase and glutathione (GSH) redox cycle enzymes are the main enzymatic anti-oxidants, and catalyse the transfer of electrons from specific substrates to free radicals (Chelikani et al., 2004, Marklund, 1984, Cabrera and Chihuailaf, 2011). The conversion of the free radicals superoxide radical anion ($O_2^{\bullet-}$) to hydrogen peroxide (H_2O_2) and oxygen (O_2) is catalysed by SOD (Figure 8.2). Subsequently, H_2O_2 is converted into H_2O by glutathione peroxidase with GSH as substrate. However, catalase can also stabilise H_2O_2 through conversion into H_2O and O_2.

Besides removing free radicals, anti-oxidants can also act on oxidised lipids and proteins. The liposoluble anti-oxidants α-tocopherol and carotenoids neutralise lipid peroxyl radicals and hereby stop lipid oxidation chain reactions (Sies et al., 1992, Packer et al., 1979). Although GSH and ascorbic acid also have a small role in reducing oxidised lipids (Sies et al., 1992), their contribution in repairing oxidised proteins is indispensable. These water soluble non-enzymatic anti-oxidants collaborate with thioltransferase, methionine sulfoxide reductases, NADPH-dependent thioredoxin/ thioredoxin reductase system and GSH disulphide reductase to repair oxidised methionines, cysteines and protein-protein disulphide bonds in the lens (reviewed by (Berthoud and Beyer, 2009)).

The presence of anti-oxidants in the eye lens is not uniformly divided. LECs and the outer layers of the cortex contain the highest levels of the above mentioned anti-oxidants, whereas the inner layers of the

cortex and the nucleus populated by LFCs without cell organelles hold lower anti-oxidant concentration (Bando and Obazawa, 1991, Bhuyan and Bhuyan, 1978, Spector et al., 1996, Sweeney and Truscott, 1998).

IR-induced oxidative stress is central to the pathogenesis of radiation cataracts (Ainsbury et al., 2016, Uwineza et al., 2019). Cataract incidence in mice provided with a dietary supplementation of anti-oxidants (including, selenomethionine, N-acetyl cysteine, ascorbic acid, α-lipoic acid and tocopherol) before and after exposure to 0.5 - 3 Gy was lower than in their exposed counterparts that were not given anti-oxidants (Davis et al., 2010). Exposure of LECs to UVA (± 3 J/ cm^2) caused degradation of cytoskeletal actin, inhibited catalase activity and reduced colony formation ability (Zigman et al., 1995). However, adding 2.5 - 10 mg/ mL α-tocopherol to these cells before exposure provided protection from UVA cytotoxicity. Human epidemiological studies investigating whether anti-oxidants can reduce the prevalence of cataracts have shown positive and negative results (Eggersdorfer and Wyss, 2018, Braakhuis et al., 2019, McCusker et al., 2016, Mares-Perlman et al., 2000, Kuzniarz et al., 2001).

8.2. Objectives and experimental design

Given that ionising radiation (IR) leads to the formation of free radicals followed by cholesterol oxidation, the potential of anti-oxidants to prevent or neutralise cholesterol oxidation adducts was examined. In the human lens, immediately after death, concentrations of 4 mM GSH were measured (Holm et al., 2013), while levels close to 3 mM ascorbic acid (Varma and Richards, 1988, Varma et al., 1979) were detected in the outer layers of the eye lens. Furthermore, α-tocopherol concentrations in the range of mM were shown to prevent lysophosphatidylcholine-induced lens membrane damage (Libondi et al., 1985). Therefore, 4 mM GSH, 3 mM ascorbic acid and 1 mM α-tocopherol were added pre- and post-IR exposure of bovine lens membrane extracts. Exposing the lens membranes to 50 Gy and harvesting these 18 days later were arbitrary chosen for proof of concept. Chromatograms of the oxysterol profile were generated via LC-MS (Figure 8.3). Furthermore, to study the mechanism through which α-tocopherol performs its function, deuterated lipids-lens membrane extracts binding experiment was performed (Figure 8.4).

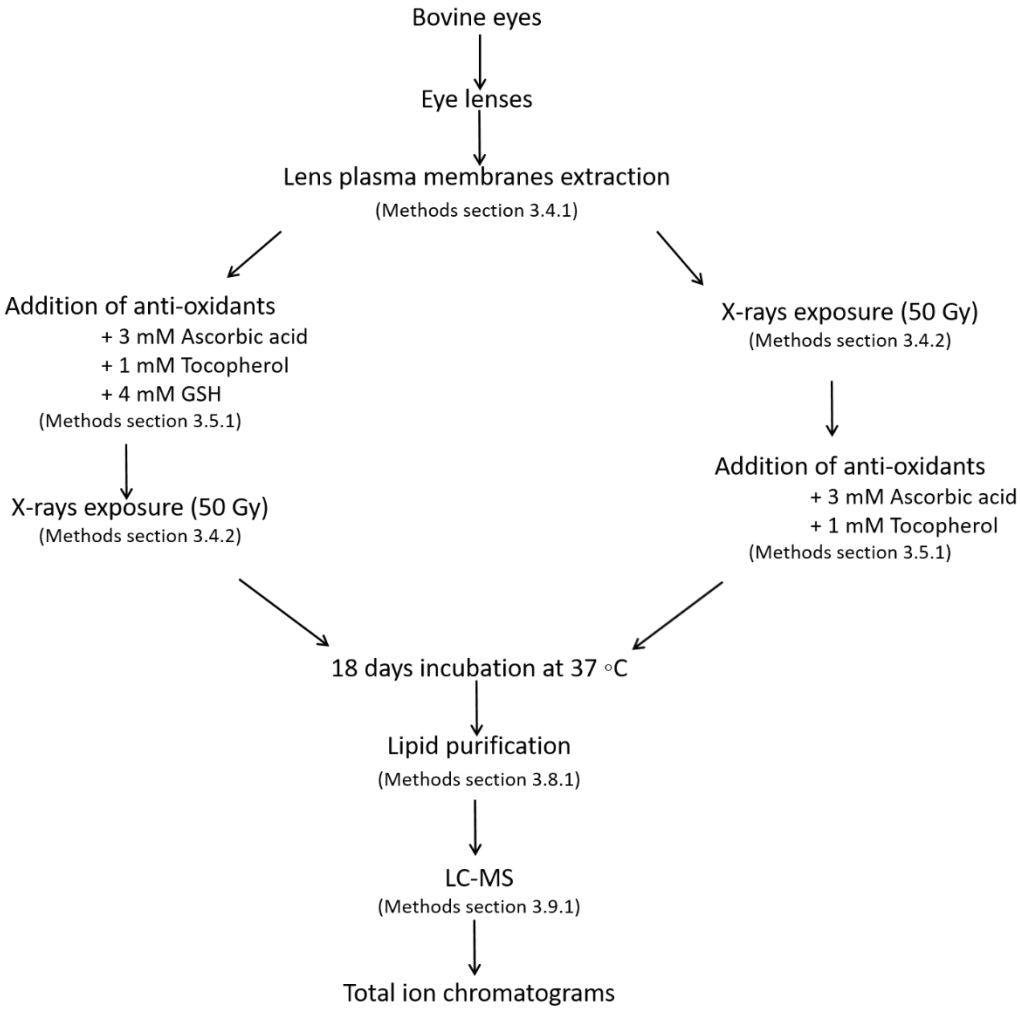

Figure 8.3: Schematic representation of experimental design used during the anti-oxidants protection of bovine lens membrane extracts from IR induced oxidative stress study. Section numbers refer to the material and methods chapter section in which the protocol was described. GSH: glutathione, LC-MS: liquid chromatography-mass spectrometry.

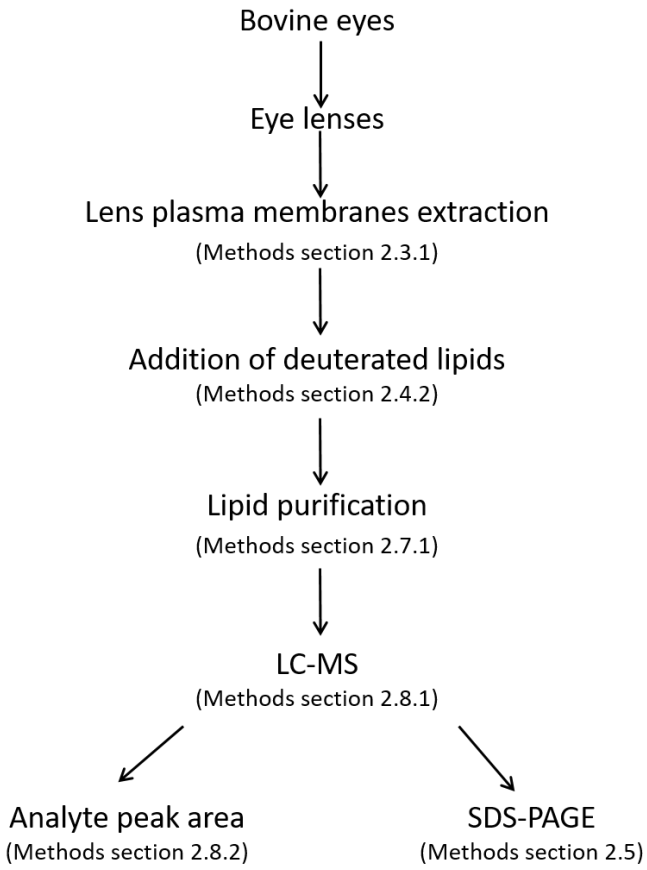

Figure 8.4: Scheme of experimental design of deuterated lipids membrane extract binding experiment. Section numbers refer to the material and methods chapter section in which the protocol was described. LC-MS: liquid chromatography-mass spectrometry.

8.3. Results

8.3.1. α-Tocopherol protected cortical bovine membrane extracts from IR-induced cholesterol oxidation

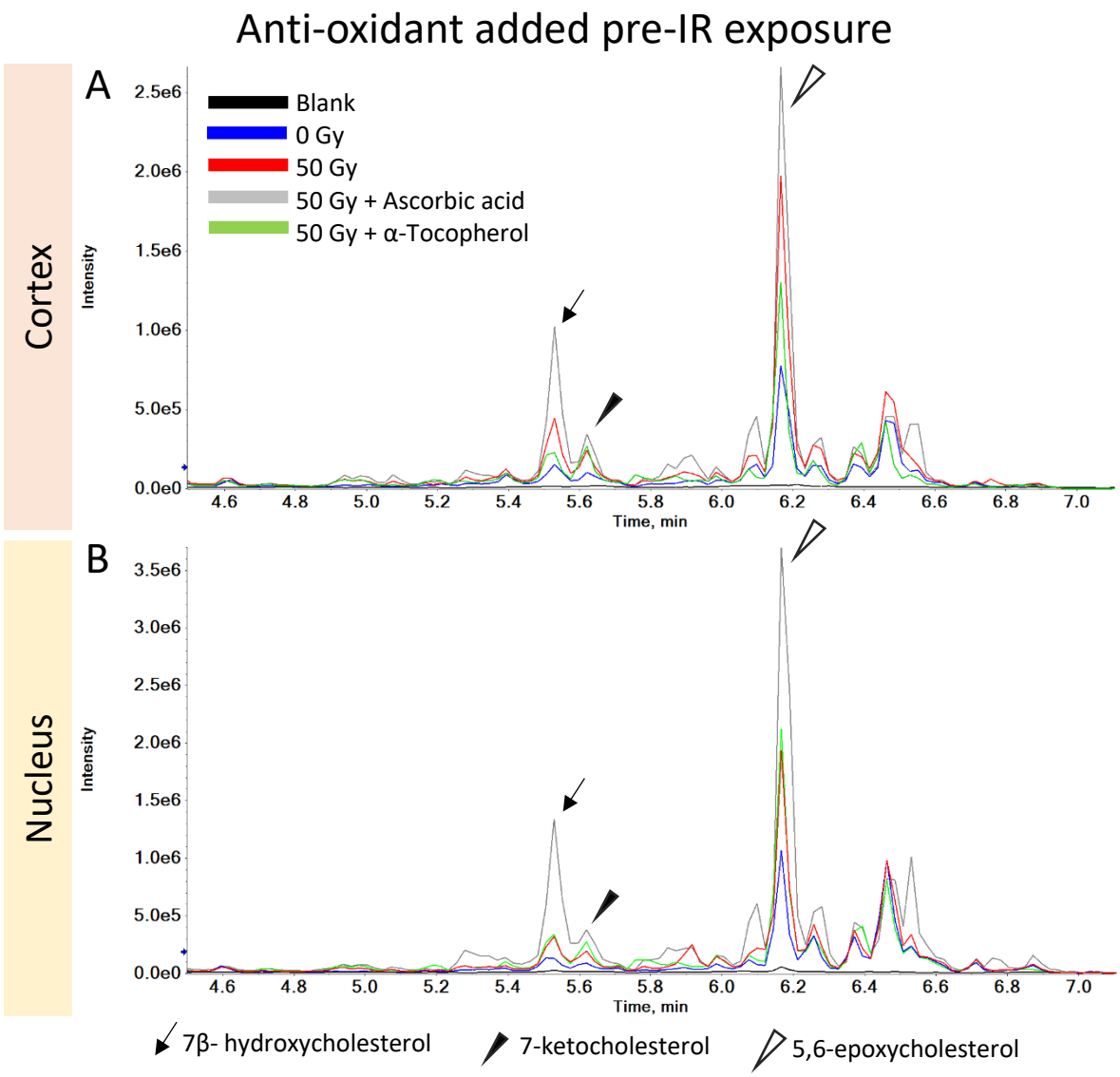

Figure 8.5: LC-MS chromatogram of A) the cortical and B) nuclear fraction of bovine lens membrane extracts to which anti-oxidants were added pre-IR exposure and were left to incubate at 37 °C for18 days after exposure to 50 Gy. Arrows point to the identified oxysterols using deuterated standards.

To investigate whether anti-oxidants could prevent IR-induced oxysterol formation, ascorbic acid or α-tocopherol were added to bovine lens membrane extracts and subsequently, these membranes were irradiated with 50 Gy (Figure 8.3). In line with previous chapters, analysis was performed with attention for 7β-hydroxycholesterol, 7-ketocholesterol and 5,6-epoxycholesterol. However, the main focus was on overall oxysterol levels. The addition of ascorbic acid to bovine lens membrane extracts followed by 50 Gy IR-exposure caused an increase in oxysterol levels, higher than the oxysterol augmentation observed in 50 Gy exposed membranes to which no anti-oxidants was added. This was observed in the cortex as well as in the nucleus (Figure 8.5A and B). In contrast to ascorbic acid, α-tocopherol reduced the increase in oxysterol levels observed in 50 Gy exposed lens cortex membrane extracts (Figure 8.5A). In the nuclear fraction, this protective effect of α-tocopherol was not observed (Figure 8.5B).

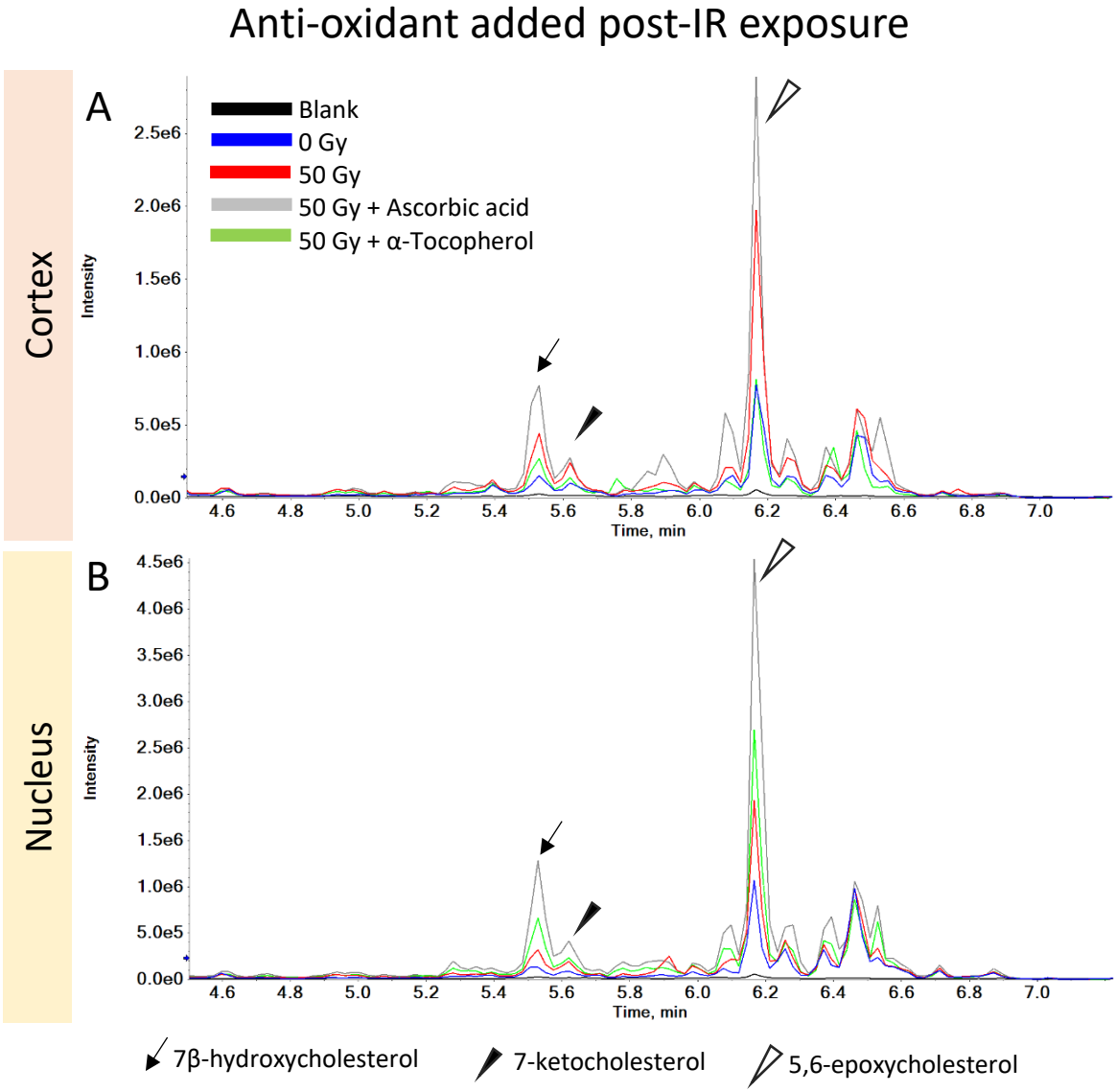

Figure 8.6: LC-MS chromatogram of A) the cortical and B) nuclear fraction of bovine lens membrane extracts to which anti-oxidants were added post-IR exposure and were left to incubate at 37 °C for18 days after exposure to 50 Gy. Arrows point to the identified oxysterols using deuterated standards.

As follow-up study, anti-oxidants were added 2 h after 50 Gy IR exposure to verify whether these anti-oxidant would act analogous to when added pre-IR exposure (Figure 8.3). Similar to the addition of ascorbic acid before IR exposure (Figure 8.5A and B), introducing ascorbic acid into IR-exposed bovine lens membrane extracts generated higher oxysterol levels than in the irradiated membranes to which no anti-oxidants were added (Figure 8.6A and B). In the cortical fraction, α-tocopherol was still able to reduce the levels of oxysterols present in membrane extracts after 50 Gy irradiation compared to membranes without added anti-oxidants (Figure 8.5A and Figure 8.6A). Furthermore, adding α-tocopherol after IR exposure in the lens nucleus membrane extracts lead to more oxysterol formation than introducing α-tocopherol before irradiation (Figure 8.6B vs. Figure 8.5B).

8.3.2. Adding GSH, α-tocopherol and ascorbic acid together to bovine lens membrane extracts did not reduce overall oxysterol levels in the nucleus

Various combinations of GSH, α-tocopherol and ascorbic acid were added to the nuclear fraction of bovine lens membrane extracts pre-IR exposure to examine whether a combination of anti-oxidants could adopt a protective role in the lens nucleus (Figure 8.3). Comparable to adding ascorbic acid, glutathione generated increased IR-induced oxysterol levels compared to 50 Gy irradiated membranes with no added anti-oxidants (Figure 8.7A). Intriguingly, although during this experiment α-tocopherol reduced the levels of 5,6-epoxycholesterol (Figure 8.7A), the levels of 7β-hydroxycholesterol and 7-ketocholesterol observed in the 50 Gy irradiated lens membrane extracts without anti-oxidants were the similar or higher than in the membrane extracts to which α-tocopherol was added.

Adding the combination of GSH and ascorbic acid caused an augmentation in the amount of oxysterol formed as a consequence of 50 Gy IR exposure in the lens nucleus membrane extracts (Figure 8.7B). Collectively, GSH, ascorbic acid and α-tocopherol were able to reduce 5,6-epoxycholesterol levels compared to the quantity in non-irradiated lens nucleus membrane extracts. Higher levels of 7β-hydroxycholesterol and 7-ketocholesterol were noted in the irradiated membranes to which the three anti-oxidants were added than in those to which no anti-oxidants were added (Figure 8.7B). Introducing ascorbic acid and α-tocopherol or GSH and α-tocopherol both caused an increase of 7β-hydroxycholesterol and 7-ketocholesterol formation in IR-exposed membranes, though not of 5,6-epoxycholesterol (Figure 8.7C). In general, all anti-oxidants, combined or individually, aggravated the effect of IR-induced oxysterol formation (Figure 8.5,Figure 8.6 and Figure 8.7).

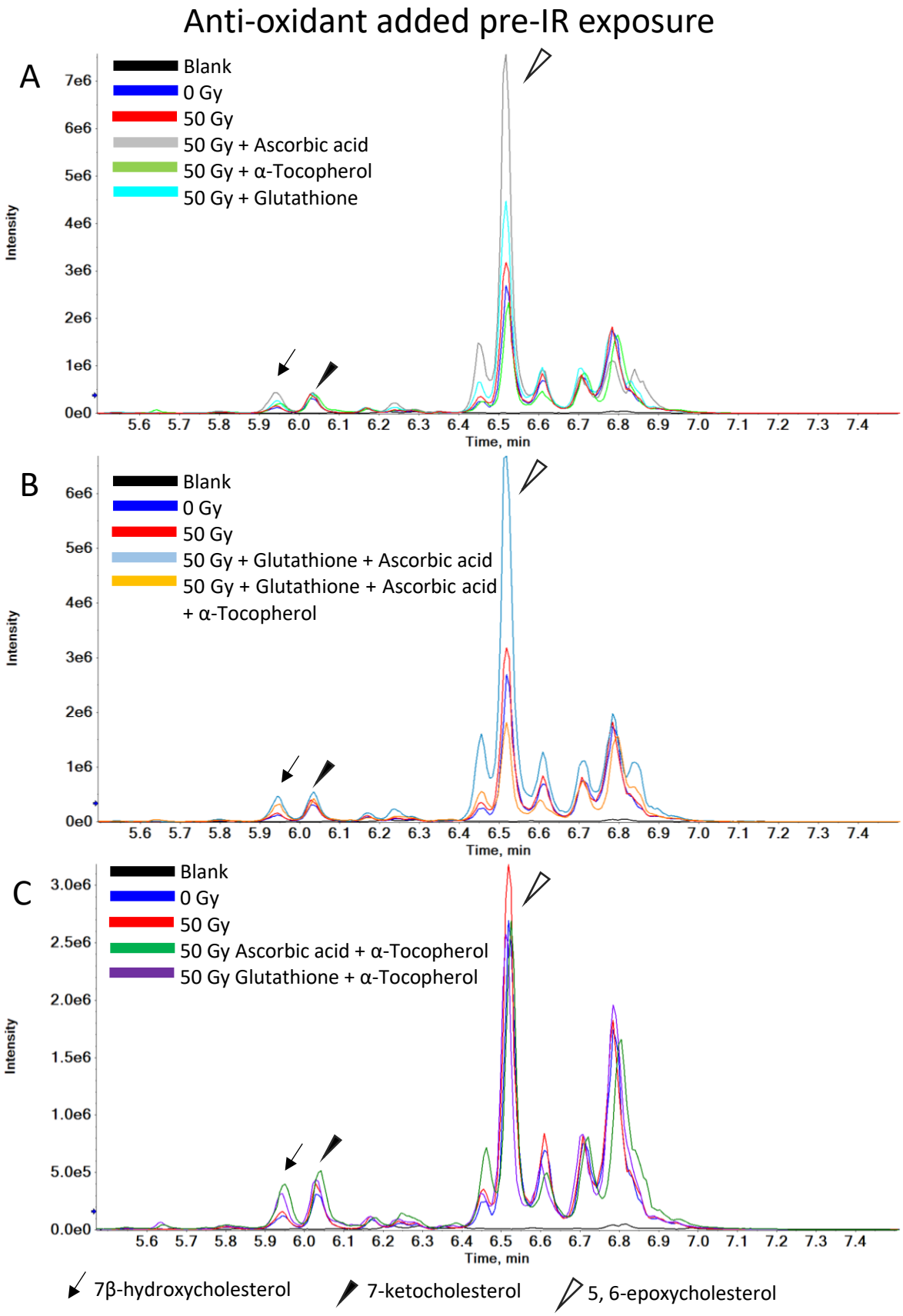

Figure 8.7: LC-MS chromatogram of lens nucleus membrane extracts to which A) tocopherol, glutathione or ascorbic acid, B) the combination of glutathione and ascorbic acid or glutathione, ascorbic acid and tocopherol, and C) ascorbic acid and tocopherol, or glutathione and tocopherol were added, and were left to incubate at 37 °C for18 days after exposure to 50 Gy. Arrows point to the identified oxysterols using deuterated standards.

8.3.3. Tocopherol-d6 binding to the bovine lens membrane extracts was transient

The mechanism through which α-tocopherol protects cholesterol in the lens plasma membrane from oxidative stress was investigated by measuring the membrane binding properties of α-tocopherol-d6, and cholesterol-d6 for comparison, to bovine lens membrane extracts over a time course of 7 days (Figure 8.4). LC-MS quantification of α-tocopherol-d6 levels bound to the membranes extracts showed that in the cortical and nuclear fraction of lens membrane extracts α-tocopherol-d6 progressively bound to the membranes and subsequently, after reaching peak levels, the amount of membrane bound α-tocopherol-d6 gradually decreased (Figure 8.8A and D). In the lens nucleus membrane extracts peak levels were measured after 1 day of incubation at 37 °C, though the changes observed over time in the nuclear fraction were not significant ($p > 0.05$; Figure 8.8A). However, significant changes were detected in lens cortex membrane extracts and maximum levels of α-tocopherol-d6 binding were achieved after 8 h incubation at 37 °C ($p < 0.001$; Figure 8.8D). Comparison of bound α-tocopherol-d6 peak levels in the cortical fraction with those in the nuclear fraction illustrated that the cortex can bind more α-tocopherol-d6 than the lens nucleus membrane extracts (Figure 8.8A vs. D). The association of α-tocopherol-d6 to the membranes did not affect internal cholesterol or tocopherol levels ($p > 0.05$; Figure 8.8B, C, E and F).

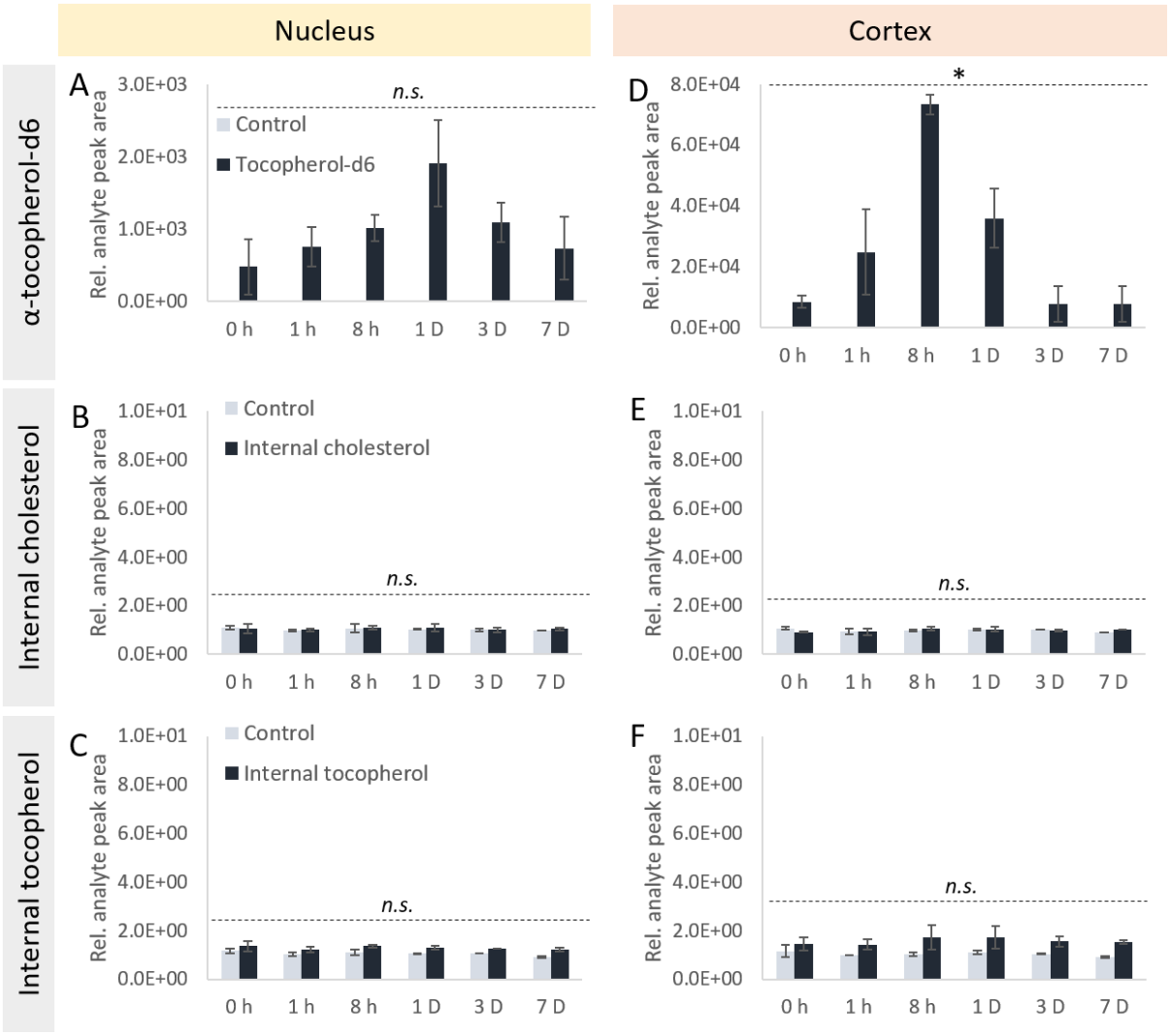

*Figure 8.8: LC-MS quantification of the levels of A) α-tocopherol-d6, B) internal cholesterol and C) internal tocopherol in bovine lens nucleus membrane extracts, and D) α-tocopherol-d6, E) internal cholesterol and F) internal tocopherol in bovine lens cortex membrane extracts relative to the levels in bovine lens membrane extracts to which no lipids or solvent was added. Control represents membrane extracts to which DCM:MeOH was added. Error bars represent standard deviation. General Linear Model Analysis of Variance followed by Tukey pairwise comparison post hoc test using time, component-of-interest and location as independent factors and rel. analyte peak area as dependent factor was applied for statistical analysis, *p< 0.05 n= 2, n.s.: not significant, rel.: relative.*

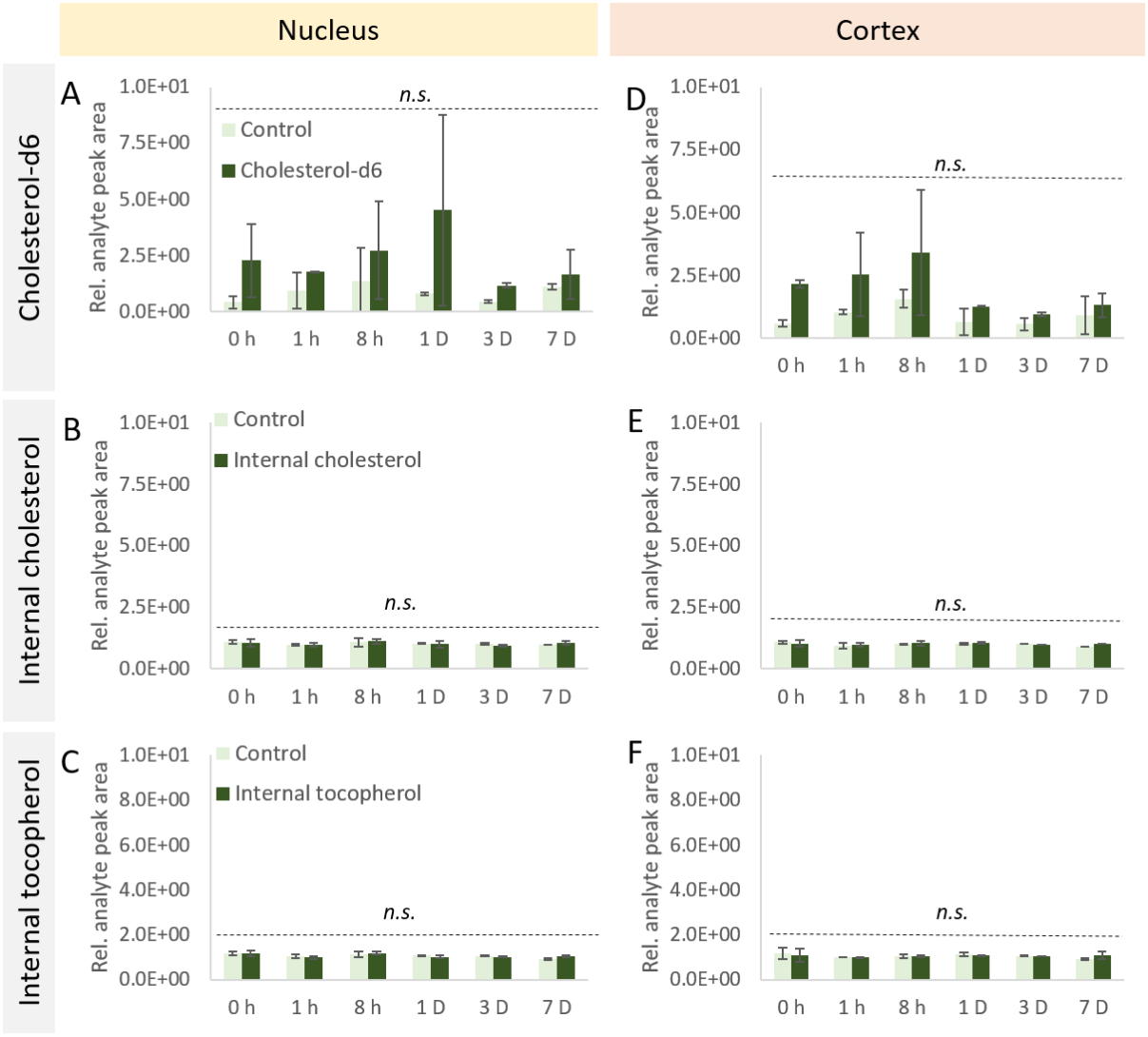

*Figure 8.9: LC-MS quantification of the levels of A) cholesterol-d6, B) internal cholesterol and C) internal tocopherol in bovine lens nucleus membrane extracts, and D) cholesterol-d6, E) internal cholesterol and F) internal tocopherol in bovine lens cortex membrane extracts relative to the levels in bovine lens membrane extracts to which no lipids or solvent was added. Control represents membrane extracts containing DCM:MeOH. Error bars represent standard deviation. General Linear Model Analysis of Variance followed by Tukey pairwise comparison post hoc test using time, component-of-interest and location as independent factors was applied for statistical analysis, *p< 0.05 n= 2, n.s.: not significant, rel.: relative.*

Although the same concentration of α-tocopherol-d6 and cholesterol-d6 was added to the membranes, the levels of cholesterol-d6 measured in the nuclear and cortical fraction were minimal in comparison to α-tocopherol-d6 (Figure 8.8A vs. Figure 8.9A, and Figure 8.8D vs. Figure 8.9D). Furthermore, the observed cholesterol-d6 membrane binding over time was not significant in the lens nucleus, neither in the lens cortex membrane extracts ($p > 0.05$; Figure 8.9A and D). The addition of cholesterol-d6 to these membrane extracts did not induce any significant modifications in the internal cholesterol and tocopherol levels (Figure 8.9B, C, E and F).

8.3.4. Adding α-tocopherol-d6 or cholesterol-d6 to lens membrane extracts appeared to not affect the protein pattern

To verify whether α-tocopherol-d6 or cholesterol-d6 modified the pattern of lens membrane proteins, an aliquot was collected during the above described α-tocopherol-d6 and cholesterol-d6 membrane binding experiment and these aliquots were ran on SDS-PAGE gels (Figure 8.4). The addition of α-tocopherol-d6, cholesterol-d6 or their solvent DCM:MeOH to cortical or nuclear lens membrane extracts appeared to not alter the protein pattern (Figure 8.10).

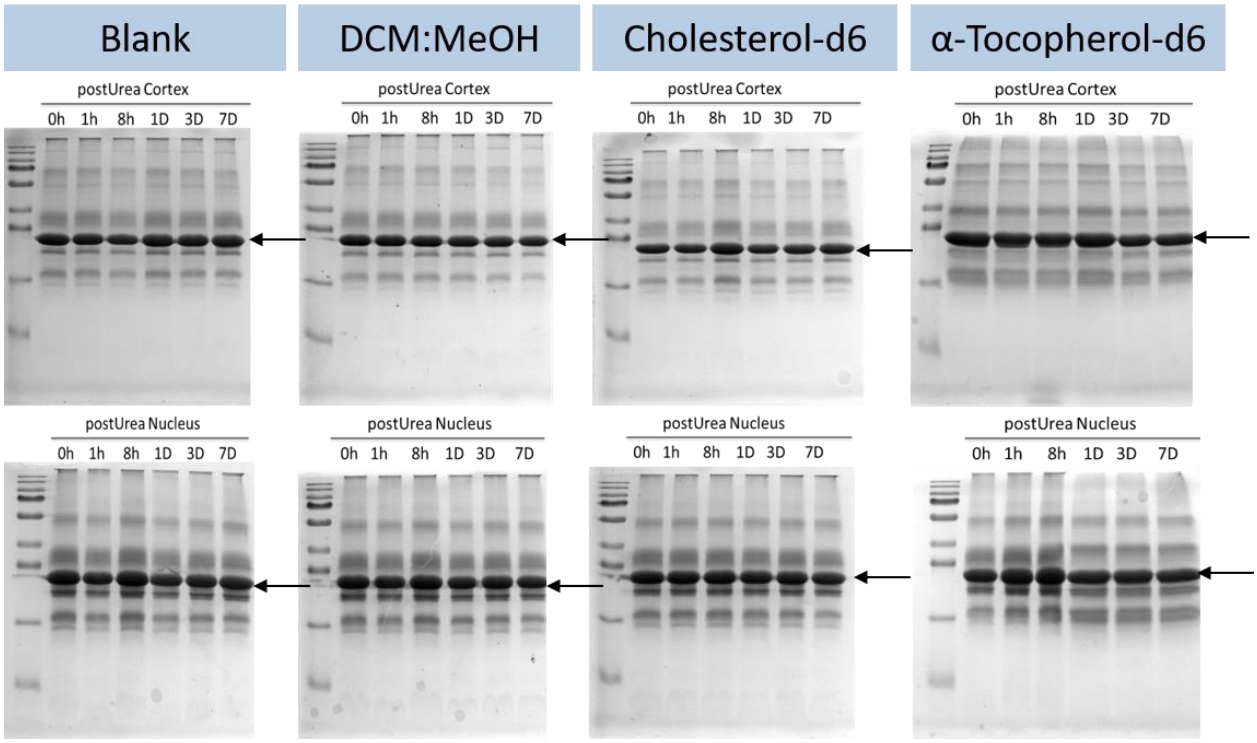

Figure 8.10: The images display the protein pattern of lens membrane proteins during the binding of α-tocopherol-d6 or cholesterol-d6 to bovine lens membrane extracts. The most prominent band visible is AQP0 (arrow). Protein identity suggestion was based on proteomics data in the appendix (appendix table 1 and 2). 15 µg protein of 1% (w/v) SDS solubilised lens membrane proteins were run on SDS-PAGE gels (15% (w/v) acrylamide) and stained with Coomassie Blue. The molecular weight markers in the first lane of each gel mark respectively 250, 130, 95, 72, 55, 36, 28, 17 and 10 kDa from top to bottom. First row illustrates the cortical fraction and the second row the nuclear fraction. H: hour(s), D: day(s).

8.3.5. Retrospective power analysis

The binding of lipids in bovine lens membrane extracts has not been investigated before. Therefore, a retrospective power analysis was performed. The actual power for measuring significant differences in the α-tocopherol-d6 binding experiment between 0 h and 1 day in the nucleus was < 0.8 for α-tocopherol-d6, internal cholesterol and tocopherol (Table 8.1). Accordingly, the advised sample size was 4 for α-Tocopherol-d6 and much larger for internal cholesterol and tocopherol. The actual power for measuring the differences between 0 and 8 h in bovine cortex membrane extracts after introducing α-tocopherol-d6 was 1 for α-tocopherol-d6, and <0.8 for the other components (Table 8.1). To detect significant alterations in α-tocopherol-d6 in lens cortex membrane extracts, the advised sample size was equal to the sample size used during the gathering of the data. Interestingly, a sample size of 4 was advised to observe significant changes in the internal cholesterol levels between 0 and 8 h, while for internal tocopherol the advised sample size is 35.

Table 8.1: Retrospective power analysis to determine the power and the advised sample size for the binding of α-tocopherol-d6 to bovine lens membrane extracts experiment using Minitab.

α-Tocopherol-d6	Sample size	Difference in mean value	Mean stdev	Actual power	Advised sample size for target power 0.8
Lens nucleus 0 hours versus 1 day					
α-Tocopherol-d6	2	1432.558	492.939	0.371	4
Internal cholesterol	2	0.021	0.182	0.051	1181
Internal tocopherol	2	-0.065	0.141	0.06	75
Lens cortex 0 versus 8 hours					
α-Tocopherol-d6	2	64868.542	2683.094	1	2
Internal cholesterol	2	0.155	0.039	0.56	4
Internal tocopherol	2	0.258	0.379	0.072	35

Stdev: standard deviation

Table 8.2: Retrospective power analysis to determine the power and the advised sample size for the binding of cholesterol-d6 to bovine lens membrane extracts experiment using Minitab.

Cholesterol-d6	Sample size	Difference in mean value	Mean stdev	Actual power	Advised sample size for target power 0.8
Lens nucleus 0 hours versus 1 day					
Cholesterol-d6	2	2.246	2.949	0.0765	29
Internal cholesterol	2	-0.062	0.137	0.059	78
Internal tocopherol	2	-0.146	0.109	0.13	10
Lens cortex 0 versus 8 hours					
Cholesterol-d6	2	1.273	1.320	0.092	18
Internal cholesterol	2	0.012	0.104	0.051	1181
Internal tocopherol	2	-0.031	0.175	0.051	502

Stdev: standard deviation

The actual power for detecting significant differences in cholesterol-d6, internal cholesterol and tocopherol in the lens nucleus membrane extracts between 0 h and 1 day after adding cholesterol-d6 was <0.8 (Table 8.2). Furthermore, the advised sample size for detecting significant modifications was ≥10 for all the measured adducts in the lens nucleus membrane extracts. Similar observations were made for the binding of cholesterol-d6 to bovine lens cortex membrane extracts (Table 8.2).

8.3.6. Uncertainty budget

Generating an uncertainty budget identified nine uncertainty contributors (Table 8.3). The Gaussian distributed factors "variability in age within a group of cows in the context of plasma membrane lipids and proteins composition"**,** membrane extraction efficiency, purity of samples, temperature of incubation room and analyte peak area offered a minor contribution to uncertainty in contrast to repeatability that showed a significant contribution to uncertainty. Membrane extraction efficiency, pipetting, lipid purification efficiency and evaporation of solvent showed a rectangular distribution and had a minor contribution to uncertainty.

Table 8.3: Uncertainty budget for the binding of α-tocopherol-d6 or cholesterol-d6 to the bovine lens membrane extracts experiment.

Uncertainty contributor	Qualitative uncertainty	Parameter Unit	Type of Evaluation	Distribution
Variability in age within a group of cows in the context of plasma membrane lipid and proteins composition	minor	months	A	Gaussian
Membrane extraction efficiency	minor	mg	B	Rectangular
Purity of samples	minor	counts	A	Gaussian
Temperature of incubation room	minor	°C	A	Gaussian
Pipetting	minor	mL	B	Rectangular
Lipid purification efficiency	minor	counts	B	Rectangular
Evaporation of solvent	minor	counts	B	Rectangular
Analyte peak area	minor	counts	A	Gaussian
Repeatability	significant	Relative analyte peak area	A	Gaussian

8.4. Discussion

8.4.1. Ascorbic acid and GSH act as pro-oxidants in IR-exposed membranes

The addition of ascorbic acid before and after exposure to IR caused an increase in cholesterol oxidation occurring in the lens nucleus and cortex membrane extracts compared to the level of oxysterol formation observed in IR-exposed membranes without the addition of anti-oxidants (Figure 8.5A and B, Figure 8.6A and B, Figure 8.7A). On the one hand, the lack of anti-oxidant activity could be explained by ascorbic acid being a hydrophilic anti-oxidant and therefore unable to remove free radicals in the lipophilic environment in which cholesterol resides (Pavlovic et al., 2005). On the other hand, in the presence of transition metals such as copper and iron which through metal-catalysed Haber-Weiss and Fenton reaction stimulate the formation of free radicals, ascorbic acid can act as a pro-oxidant by reducing these redox-active metals (Buettner and Jurkiewicz, 1996). The concentration of ascorbic acid can also determine whether ascorbic acid will act as an anti-oxidant or pro-oxidant. *In vitro* experiments suggest that in high concentration ascorbic acid will act as an anti-oxidant (Buettner and Jurkiewicz, 1996). In the presented data, a concentration of 3 mM ascorbic acid was used. Even though this is considered as a high concentration of ascorbic acid in humans (Varma and Richards, 1988), probably it is overrun by the high levels of IR (50 Gy). Further work including lower doses would shed light on this.

Similar to ascorbic acid, GSH acted as a pro-oxidant in the IR exposed lens membrane extracts (Figure 8.7A). In the presence of free radicals GSH can be converted to thiyl radicals, which can acts as lipid oxidising agents, and furthermore, GSH can enhance Fenton reactions (Sagrista et al., 2002, Schoneich et al., 1992). GSH has the chemical capacity of reducing oxidised ascorbic acid (Winkler et al., 1994, Rakete and Nagaraj, 2017), yet adding ascorbic acid and GSH together still enhanced cholesterol oxidation in lens nucleus membrane extracts (Figure 8.7B) which suggest that the concentrations of the added anti-oxidants were too low to act as anti-oxidants against the oxidative stress induced by 50 Gy, hence they acted as pro-oxidants.

8.4.2. Anti-oxidant activity of α-tocopherol occurs through binding into the membranes

α-Tocopherol is a fat soluble anti-oxidant that functions through removing free radicals and neutralising lipid peroxyl radicals (Maguire et al., 1989, Li et al., 2014b). In the cortical fraction of lens membrane, tocopherol acted as an anti-oxidant by preventing cholesterol oxidation (Figure 8.5A) or removing cholesterol oxidation adducts (Figure 8.6A). However, when α-tocopherol was added to lens nucleus membrane extracts, it was unable to protect cholesterol from oxidation (Figure 8.5B) and even operated as a pro-oxidant when added post-IR (Figure 8.6B). The mechanism through which this occurs is currently unknown and the first steps to unravel the process was taken by investigating the binding of tocopherol (in)to the membranes. The binding experiment revealed that α-tocopherol-d6 is able to insert itself in the cortical membranes showing significant differences between 0 and 8 h (Figure 8.8D), in

contrast to the nuclear membrane extracts in which no significant changes in α-tocopherol-d6 binding were observed over a time period of 7 days (Figure 8.8A). Lens nuclear membranes are known to be more rigid and therefore less accessible to molecules than cortical membrane extracts (Li et al., 1985, Widomska et al., 2017). Taken together, this suggests that the anti-oxidant activity of α-tocopherol partly depends on α-tocopherol being able to efficiently insert itself into the lipophilic environment. Unable to efficiently bind or insert itself into the lipophilic environment of the lens nucleus membrane extracts, α-tocopherol was prevented from performing its anti-oxidant function. This is supported by research showing tocopherol performs its anti-oxidative function mainly at the membrane's hydrophobic-hydrophilic interface (Marquardt et al., 2013).

In combination with other anti-oxidants α-tocopherol was still unable to act as an anti-oxidant in lens nucleus membrane extracts (Figure 8.7B and C), yet the pro-oxidant action of ascorbic acid and GSH was reduced in the presence of α-tocopherol (Figure 8.7C). GSH and ascorbic acid can reduce oxidised tocopherol (Motoyama et al., 1989, Pavlovic et al., 2005), and tocopherol can reduce transition metals (Kitts, 1997, Yamamoto and Niki, 1988). Presumably, GSH and ascorbic acid had a higher affinity for oxidised tocopherol than for transition metals and hence, collectively these chemical reactions were able to reduce the pro-oxidant function of glutathione and ascorbic acid. Notably, adding α-tocopherol post-IR generated higher levels than adding tocopherol pre-IR. This suggest that introducing α-tocopherol into an environment with high levels of oxidative stress compels it to act as a pro-oxidant.

Two hours after irradiation, oxysterol levels were significantly higher than in non-oxidised bovine membrane extracts (see chapter 5). Remarkably, α-tocopherol was able to remove these oxidised cholesterol adducts in bovine lens cortex membrane extracts (Figure 8.6A). Although tocopherol has been shown to inactivate radicals formed at C7 and C25 of cholesterol (Medina-Meza and Barnaba, 2013), a mechanism through which tocopherol can convert oxysterols back to cholesterol or another component has not been identified yet.

8.4.3. The amphipathic character of tocopherol enables binding into membranes

Cholesterol and tocopherol are both hydrophobic components, though cholesterol-d6 was unable to bind lens membranes contrary to α-tocopherol-d6 that inserted itself into membranes (Figure 8.8A and D vs. Figure 8.9A and D). Although α-tocopherol is lipophilic, it can behave as an amphipathic molecule due to its hydroxyl group (Wang and Quinn, 2000). This allowed tocopherol to efficiently migrate through a hydrophilic environment and insert itself into membranes (Figure 8.8A and D). Introducing cholesterol into a hydrophilic environment most probably lead to its aggregation and thereby cholesterol was unable to migrate into the membranes. The binding of α-tocopherol-d6 into membranes appeared to have no effect on internal cholesterol or tocopherol levels (Figure 8.8 B, C, E, and F; Figure 8.9 B, C, E and F), and also not on the protein pattern (Figure 8.10). However, power calculations suggested that repeating the experiment four times might allow the detection of significant changes in internal

cholesterol levels between 0 and 8 h (Table 8.1). This emphasises the need for more experimental repeats to understand the mechanism through which tocopherol is acting as an anti-oxidant. Furthermore, the observed time-dependent increase in α-tocopherol-d6 binding was transient. As a first step, the supernatant of these samples could be analysed to verify whether α-tocopherol-d6 dissociated as α-tocopherol-d6 and subsequently, NMR analysis of the membranes our using imaging the membranes with a cryogenic electron microscope could provide more insight in the possible structural changes α-tocopherol-d6 undergoes in the membranes.

Tocopherol mainly resides in lipid rafts and polyunsaturated phospholipid-rich domains (Royer et al., 2009, Lemaire-Ewing et al., 2010, Atkinson et al., 2010), therefore modifications in the protein pattern are improbable (Figure 8.10).

8.4.4. Qualitative uncertainty contribution of "variability in age within a group of cows in the context of plasma membrane lipid and proteins composition" needs to be re-evaluated

Most uncertainty contributors were estimated to have a minor contribution to uncertainty. However, "variability in age within a group of cows in the context of plasma membrane lipid and proteins composition" is one worth reconsidering (Table 8.3). α-Tocopherol was able to prevent and revert 5,6-epoxycholesterol formation (Figure 8.7A and B), and also stimulated the formation of 5,6-epoxycholesterol (Figure 8.5B and Figure 8.6B). Given that all the other uncertainty contributors generated systematic errors, the only variable between experimental repeats was membrane extracts and their cholesterol concentration which is dependent on age (Widomska et al., 2017). The age of the cows from which the lens membrane extracts were collected is around 6 months. During future experiments, the age of each individual animal should be noted and the variation should be minimised in order to better estimate the contribution of this variable to uncertainty. Given that the collected data was qualitative with more focus on the overall oxysterol profile, the experiments provided an answer to our research question despite this variability. However, further work through the generation of quantitative data and statistical analysis would reinforce the presented data.

Chapter 9: In vitro IR exposure induced advanced glycation end products formation

9.2. Introduction

9.2.1. Lenticular protein modifications leading to cataractogenesis

The most prevalent proteins in the eye lens are α-, β- and γ-crystallins comprising approximately 90% of the total dry mass of the lens (Horwitz et al., 1999, Taylor and Davies, 1987). The highly ordered structure established by these proteins in the lens fibre cells (LFCs) is vital for the refractive properties of the lens (Delaye and Tardieu, 1983). Mutations in the genes coding for these water soluble proteins have been associated with cataractogenesis (Huang et al., 2009, Graw, 2009, Litt et al., 1998). Besides these water soluble crystallins, the malfunctioning of water insoluble proteins has been associated with cataract formation including mutations in the membrane protein AQP0 (Geyer et al., 2006, Gu et al., 2007) and the cytoskeletal protein BFSP1 (Wang et al., 2013, Ramachandran et al., 2007).

Congenital cataracts involving mutations in genes coding for proteins such as crystallins and AQP0 are uncommon (Graw, 2004), however nearly half of the world blindness is caused by age-related cataracts (ARC) (Resnikoff et al., 2004, West, 2007). These develop partly through post-translation modifications (PTMs) in proteins contributing to the cataractogenic load (Uwineza et al., 2019). Although lens proteins are long-lived, with time spontaneous non-enzymatic racemisation, deamidation, truncations, glycations and isomerisation are observed (reviewed by (Schey et al., 2019)). These PTMs subsequently trigger the degradation and aggregation of proteins, render water soluble proteins insoluble and cause malfunctioning of proteins (Fujii et al., 2018, Srivastava et al., 2017, Korlimbinis et al., 2009). Another major source of protein damage in the eye lens is caused by the gradual increase of oxidative stress (Siew et al., 1981, Truscott, 2005). Measurements of protein oxidation levels in the eye lens showed that the lens nucleus of patients with senile age-related nuclear cataracts had increased levels of oxidised methionine and cysteine residues correlated with a decline of protein sulfhydryl groups compared to transparent lenses and the associated lens cortex (Truscott and Augusteyn, 1977, Garner and Spector, 1980). Furthermore, also diabetic, and myopic cataracts have been shown to contain increased protein oxidation levels through protein carbonylation assays (Boscia et al., 2000).

Although occurring to a much lower extent compared to the PTMs mentioned above, the Maillard reaction, i.e. glycation of proteins leading to the formation of advanced glycation end products (AGEs), is observed at increased levels in cataractogenic eye lenses compared to their age-matched controls (Franke et al., 2003, Tessier et al., 1999, Truscott and Friedrich, 2016, Smuda et al., 2015). Using LC-MS, Smuda and colleagues quantified 19 AGEs in human eye lenses and demonstrated that despite N^6-Carboxymethyl lysine (CML), N^6-carboxyethyl lysine (CEL), N^7-carboxyethyl arginine (CEA), methylglyoxal hydroimidazolone 1 (MG-H1), and N^6-lactoyl lysine being the most prevalent AGEs, only glyoxal lysine amide (GOLA) was highly correlated with age and cataract (Smuda et al., 2015). Furthermore, they noted that all the detected AGEs can be synthesized from the following precursors: methylglyoxal, glyoxal, the Amadori product of glucose and lysine, and vitamin C (Figure 9.1) (Smuda

et al., 2015). Investigation of the distribution of AGEs in the eye lens showed that these are mainly located in high molecular weight protein aggregates implying that these type of protein modifications also contribute to insolubilisation and aggregation of proteins (Zarina et al., 2000). Further work confirmed protein aggregation induced by AGEs (Linetsky et al., 2008). Moreover, age-related pigmentation of the lens has been linked to the accumulation of the AGEs pentosidine (Nagaraj et al., 1991).

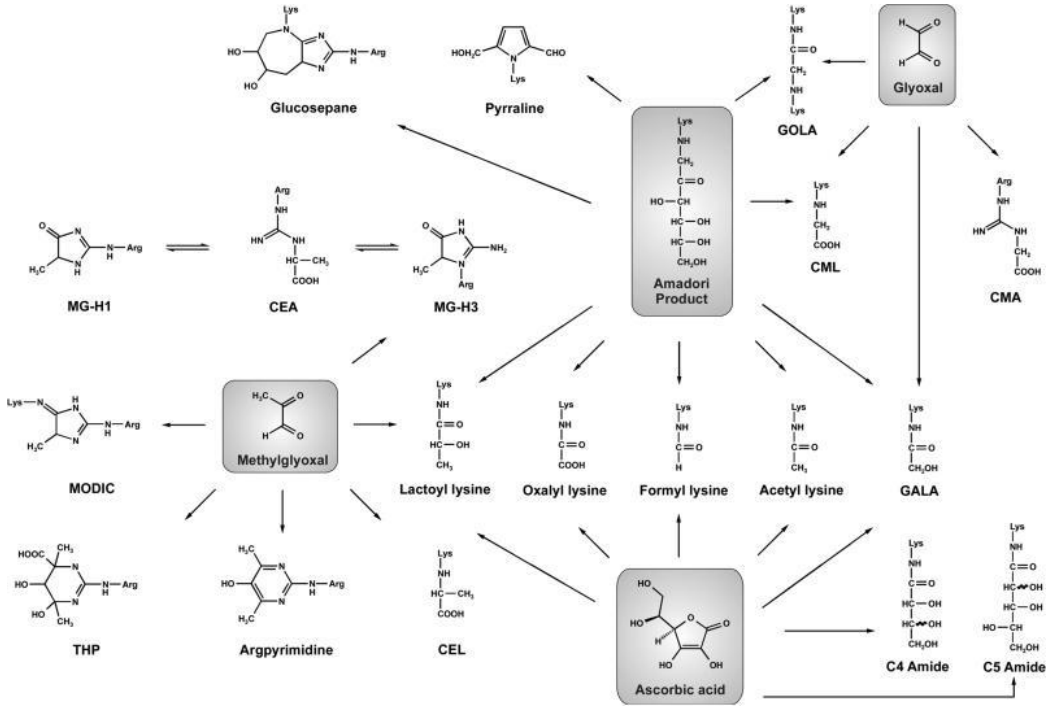

Figure 9.1: Schematic representation of 19 AGEs identified in human lenses and their precursors. With age, oxidative stress levels in the eye lens increase and stimulate the formation of advanced glycation end products from ascorbic acid, glyoxal, methlyglyoxal and Amadori products. GOLA: glyoxal lysine amide, MG-H1: methylglyoxal hydroimidazolone 1, CEA: N^7-carboxyethyl arginine, MG-H3: methylglyoxal hydroimidazolone 3, CML: N^6-Carboxymethyl lysine, CMA: N^6-carboxymethyl arginine, MODIC: methylglyoxal imidazolimine, THP: tetrahydropyrimidine, CEL: N^6-carboxyethyl lysine, GALA: glycolic acid lysine amide (source: Smuda et al., Biochemistry, 2015, image used with permission of the journal).

9.2.2. The effects of radiation on lens proteins

Increased oxidative stress induced by exposure to ionising radiation (IR) and non-IR has been shown to induce clouding of the lens through PTMs of crystallin including oxidation, truncation, isomeration, racemisation deamidation, misfolding and aggregation (Moreau and King, 2012, Fujii et al., 2004, Fujii et al., 2001, Simpanya et al., 2008, Giblin et al., 2002, Kim et al., 2016). Interestingly, ultra violet A (UVA)- light induced oxidation of tryptophan and ascorbic acid was found to enhance the formation of AGEs (Ortwerth et al., 2009). The oxidation of tryptophan lead to the formation of 3-hydroxykynurenine, which promotes the oxidation of ascorbic acid (Linetsky et al., 2014) and pentosidine synthesis (Nagaraj et al., 2010). Furthermore, kynurenine and direct UVA-light induced ascorbic acid oxides react with lens protein and generate AGEs (Prabhakaram and Ortwerth, 1992). Although non-IR has been shown to cause an increase in AGEs levels in the lens, the influence of IR on AGEs formation in the eye lens has not been investigated yet. Moreover, due to the lack of the suitable technology, the proteins bound by these AGEs have been difficult to identify.

9.3. Objectives and experimental design

To examine the effect of IR on integral membrane and membrane bound protein with emphasis on advanced glycation end products, plasma membrane extracts of 6 month-old bovine eye lenses were exposed to 5 and 50 Gy and examined via SDS-PAGE and LC-MS after acid hydrolysis (Figure 9.2). Furthermore, to compare age-related with IR-induced modifications, 6 and 30 month-old plasma membranes were exposed to 50 Gy and analysed with SDS-PAGE, OxyBlots, Western blots and LC-MS after VC1 pull down (Figure 9.3).

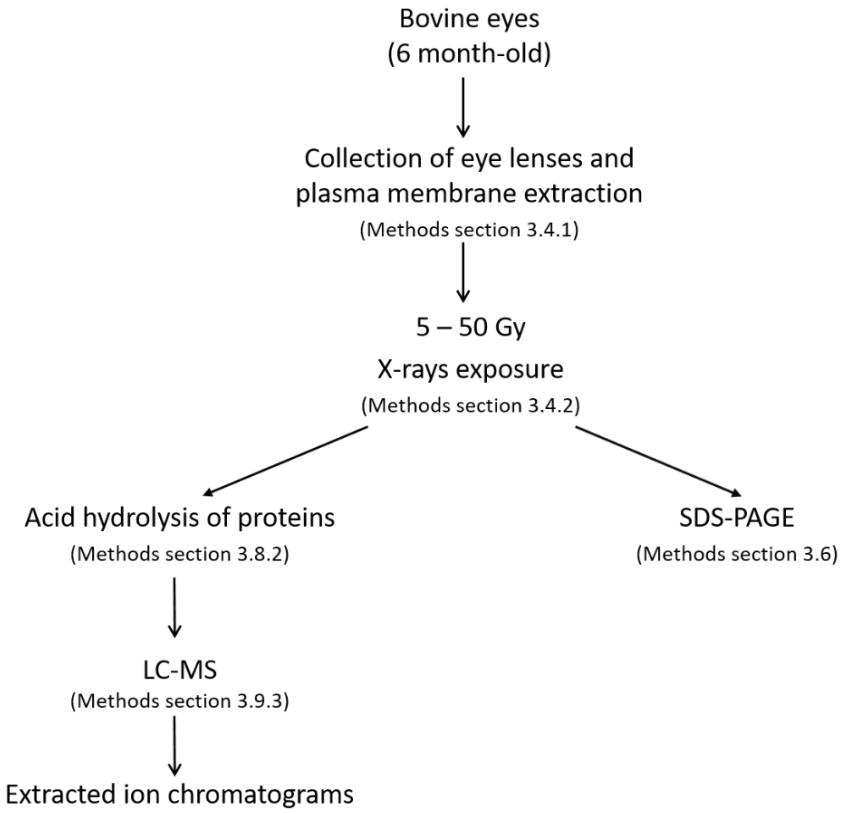

Figure 9.2: Diagram of experimental set up of in vitro IR exposure induced advanced glycation end products formation in 6 month-old bovine lens plasma membrane extracts. Section numbers refer to the material and methods chapter section in which the protocol was described. SDS-PAGE: sodium dodecyl sulphate polyacrylamide gel electrophoresis, LC-MS: liquid chromatography mass spectrometry.

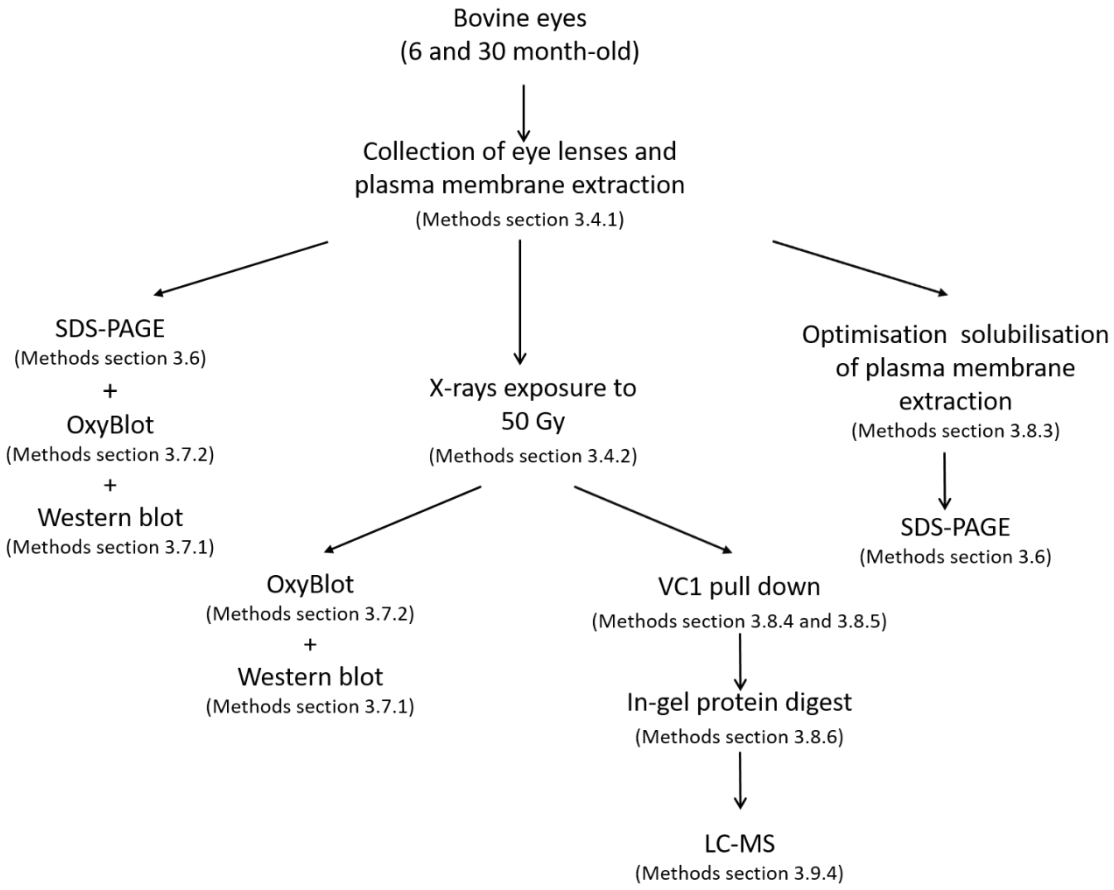

Figure 9.3: Schematic representation of experimental set up of in vitro IR exposure induced post-translational modifications in 6 month-old compared with 30 month-old bovine lens lipid membrane extracts. Section numbers refer to the material and methods chapter section in which the protocol was described. SDS-PAGE: sodium dodecyl sulphate polyacrylamide gel electrophoresis, LC-MS: liquid chromatography mass spectrometry.

9.4. Results

9.4.1. SDS PAGE analysis did not detect IR-dependent changes in the protein pattern of bovine lens membrane extracts

Preliminary analysis of bovine lens membrane extracts exposed to 0, 5 and 50 Gy X-rays by SDS-PAGE showed that the protein pattern appeared not to be altered in 5 or 50 Gy IR-exposed membranes compared to the unexposed membrane extracts (Figure 9.4). Notably, the nucleus contained less high molecular weight proteins than the cortex, which was conserved after exposure to 5 and 50 Gy (Figure 9.4).

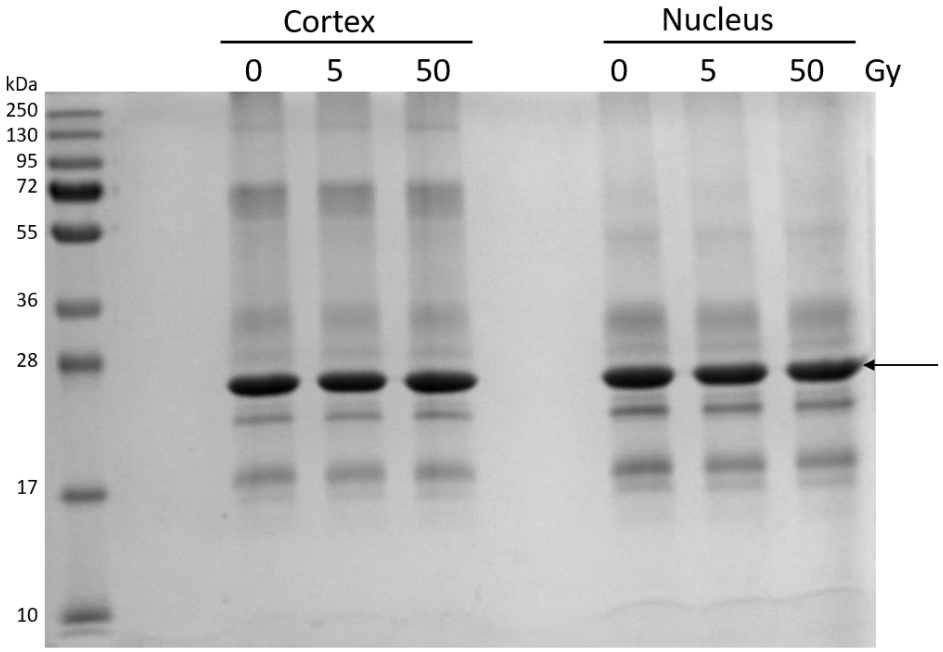

Figure 9.4: Lens membrane extracts from the cortex and the nucleus of bovine eye lenses were exposed to 0, 5 and 50 Gy of X-rays. Subsequently, 10 µg protein of 1% (w/v) SDS solubilised lens membrane proteins were run on a SDS-PAGE gel (15% (w/v) acrylamide) and stained with Coomassie Blue. The most prominent band visible is AQP0 (26 kDa, arrow). Protein identity suggestion made above was based on proteomics data in the appendix (appendix table 1 and 2).

9.4.2. IR exposure induced the formation of AGEs in lens membrane extracts

The effect of IR on AGEs has not been investigated yet. To verify their presence in bovine lens membrane extracts and whether they are formed as a result of exposure to IR, the nuclear and cortical fractions of bovine lens membrane extracts were exposed to 0, 5 and 50 Gy and after acid protein hydrolysis AGEs were analysed with LC-MS (Figure 9.2). Extracted ion chromatograms showed that the presence of the AGEs N^6-carboxymethyl arginine, formyl lysine, lactoyl lysine and glyoxal lysine amide in the cortical and the nuclear fractions of unexposed bovine lens membrane extracts (Figure 9.5 and Figure 9.6). Before exposure to X-rays, the levels of these AGEs were higher in the nucleus than in the cortex (Figure 9.5 vs. Figure 9.6). IR exposure lead to the increase of these AGEs adducts in both fractions, however, the increase was more pronounced in the cortex than in the nucleus (Figure 9.5 vs. Figure 9.6). Overlay of the 5 with the 50 Gy chromatogram revealed that the augmentation in AGEs was not proportionate to the applied IR dose in the lens cortex and nucleus membrane fractions (Figure 9.5 and Figure 9.6).

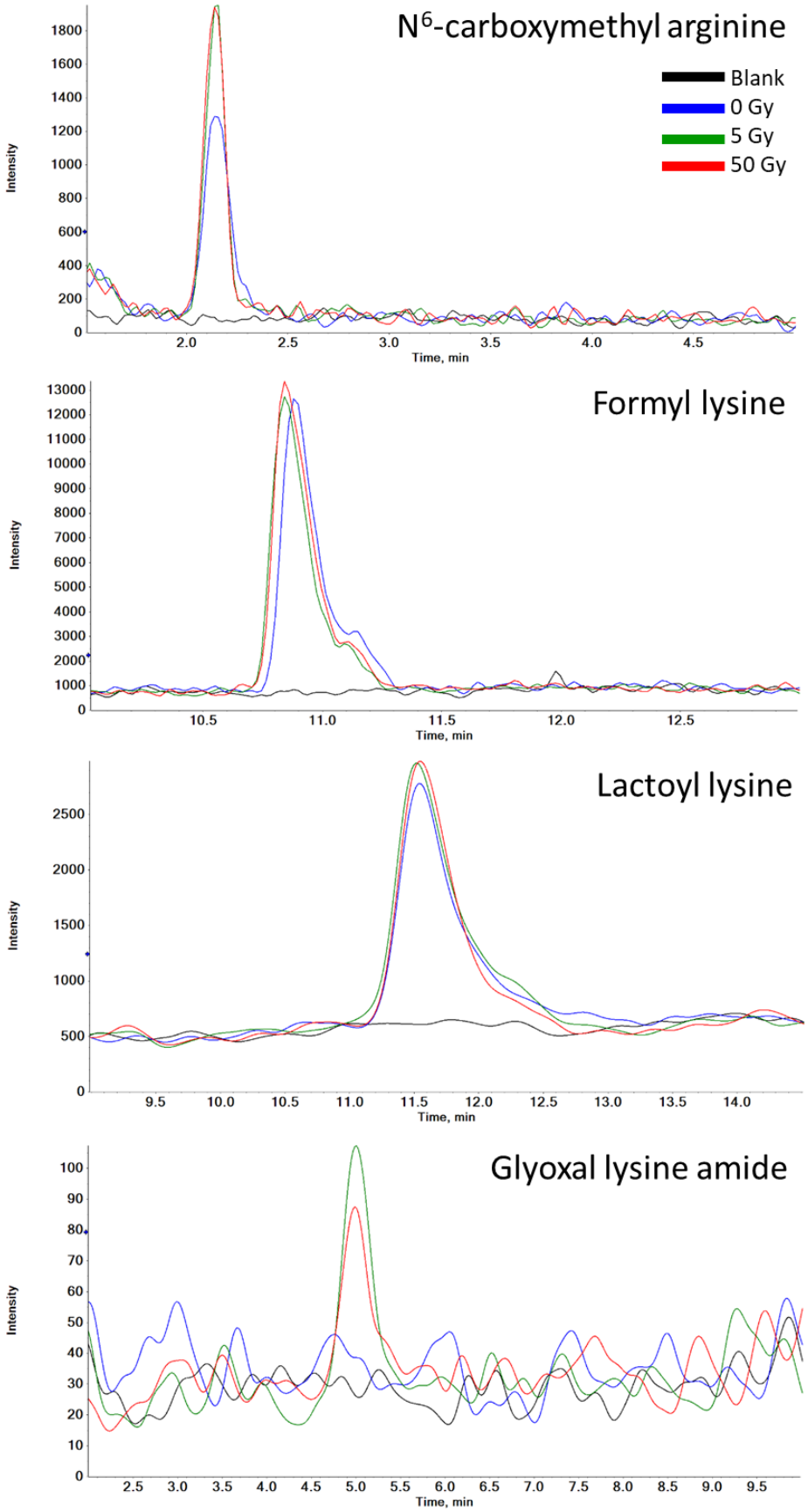

Figure 9.5: LC-MS extracted ion chromatograms of advanced glycation end products 2 hours after exposure of bovine lens nucleus membrane extracts to 5 and 50 Gy X-rays.

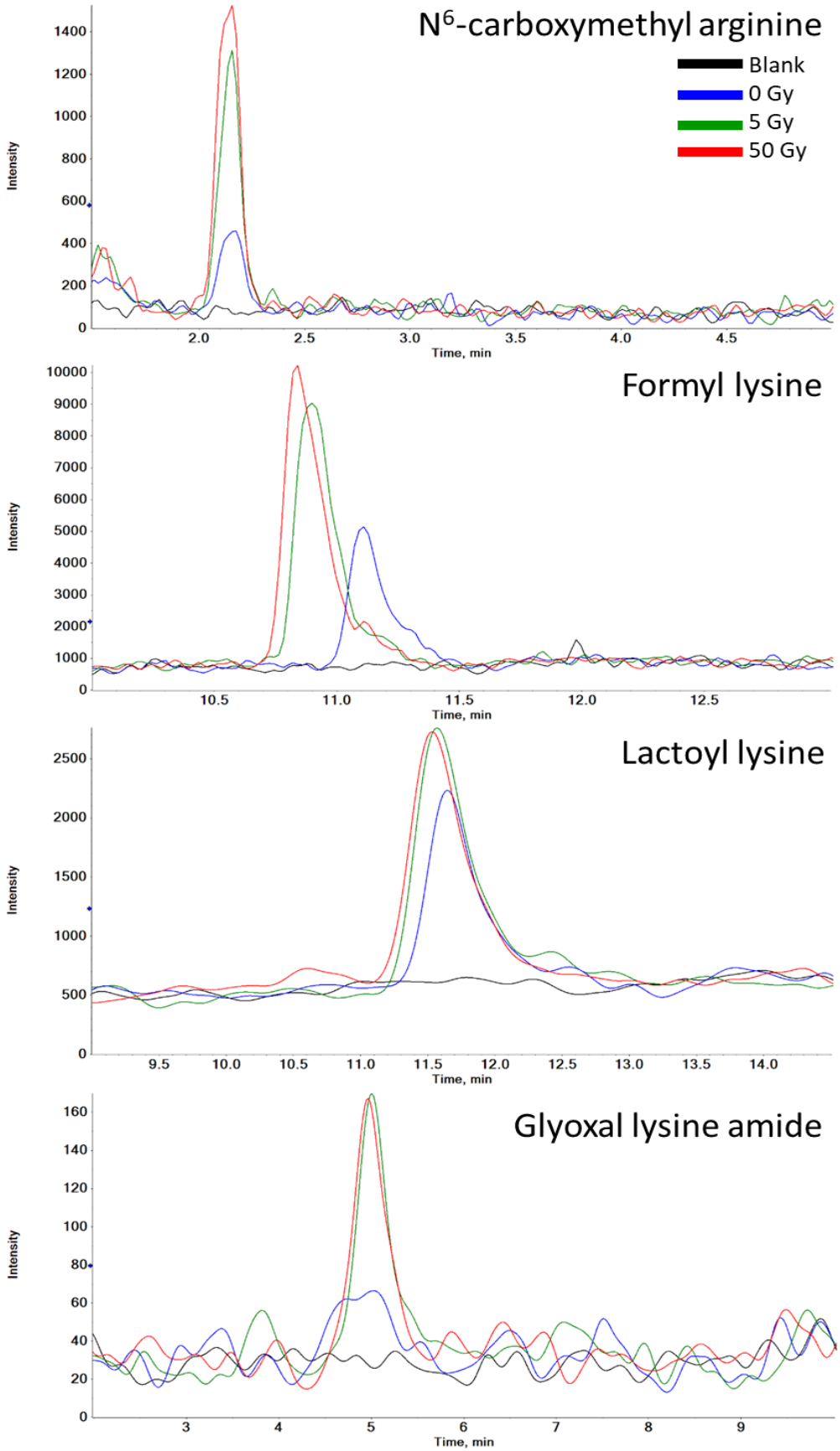

Figure 9.6: LC-MS extracted ion chromatograms of advanced glycation end products 2 hours after exposure of bovine lens cortex membrane extracts to 5 and 50 Gy X-rays.

9.4.3. Immediate IR-induced PTMs were different from age-related PTMs

Using bovine membrane proteins, analysis of age-related and IR induced modifications was performed via SDS-PAGE gel separations, Western blots and OxyBlots of 6 and 30 month-old bovine lens membrane extracts and their irradiated counterparts (Figure 9.3).

9.4.3.1. Protein oxidation decreased with age in membrane extracts

Comparison of the protein pattern between the membrane extracts from 6 and 30 month-old bovine eye lenses suggest that PTMs and dimerisation increased with age in all lens membrane fractions (Figure 9.7A and B). In both age groups, proteolysis was more prominent in the lens nucleus than in the lens cortex (Figure 9.7). Age-dependent PTMs has been shown in previous research (Tapodi et al., 2019).

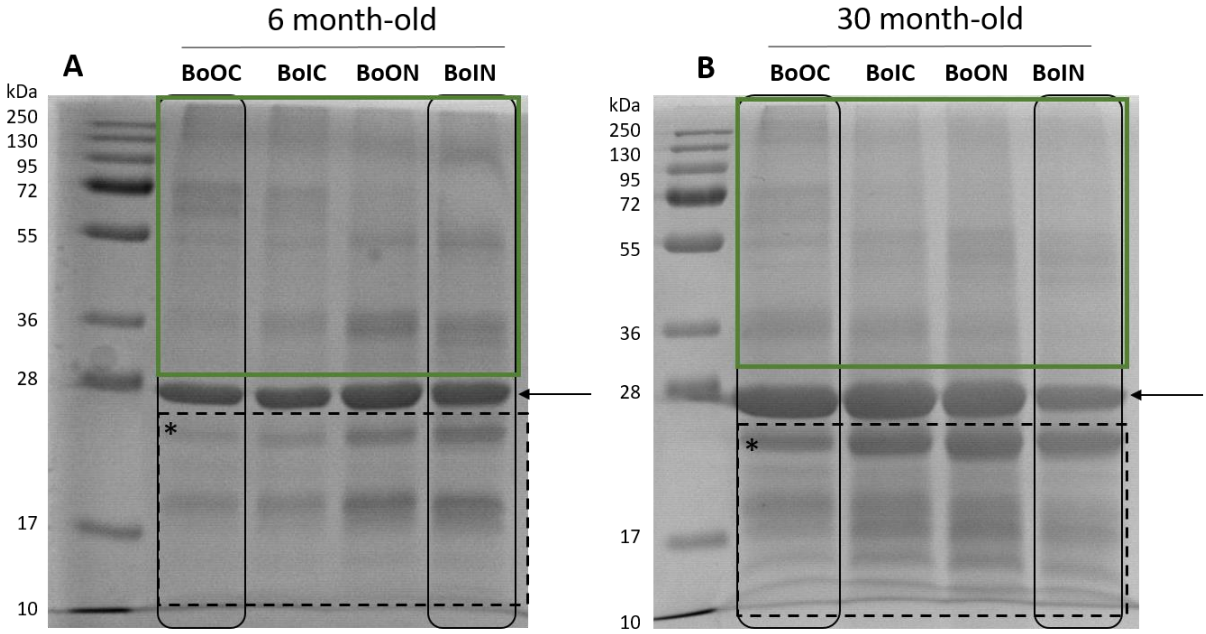

Figure 9.7: Membrane extracts were isolated from lenses of A) 6 month-old and B) 30 month-old bovine eye lenses. The most prominent band visible is AQP0 (26 kDa, arrow). The bands below 26 kDa include crystallins (20 kDa) and breakdown products of AQP0 (dashed box). A major product is indicated (*). The bands above 26 kDa contain vimentin, BFSP1 and AQP0 dimers and tetramers (green box). (Protein identity suggestions made above was based on proteomics data in the appendix (appendix table 1 and 2).). 15 µg protein of 1% (w/v) SDS solubilised lens membrane proteins were run on SDS-PAGE gels (15% (w/v) acrylamide) and stained with Coomassie Blue. The black box encircled fractions were used for immunoblot analysis. BoOC: bovine outer cortex, BoIC: bovine inner cortex, BoON: bovine outer nucleus, BoIN: bovine inner nucleus.

Protein carbonylation analysis is generally accepted as a measure of protein oxidation (Stadtman, 1992), therefore OxyBlots were performed with bovine outer cortex and inner nucleus fractions to detect age-related protein oxidation changes in lens membrane extracts (Figure 9.7, encircled). Intriguingly, comparison of the 6 with 30 month-old membrane extracts indicated that protein oxidation of integral membrane and membrane bound proteins decreased with age in the cortex and in the nucleus (Figure 9.8A). Moreover, the cortical fractions contained more oxidised proteins than the nuclear fraction (Figure 9.8A). AQP0, the most abundant protein in the lens plasma membrane (Bassnett et al., 2009), unlikely co-localised with the oxidised proteins (Figure 9.8B).

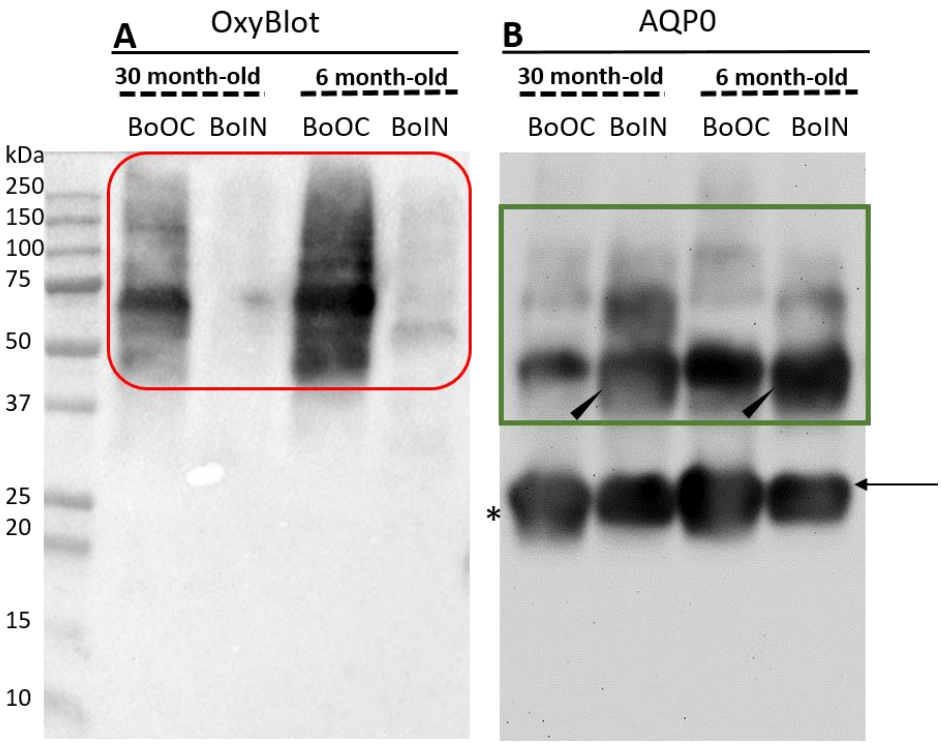

Figure 9.8: Immunoblots of 6 and 30 month-old bovine eye lens membrane extracts. 15 µg protein of 1% (w/v) SDS solubilised lens membrane proteins were run on a SDS-PAGE gel (15% (w/v) acrylamide). A) Oxyblot showing carbonylated proteins and B) same membrane immunoblotted with AQP0 antibody (1/2000 dilution). Full length AQP0 has a molecular weight of 26 kDa (arrow), with age AQP0 protein undergoes complex PTMs involving truncations, and formation of dimers and tetramers (green box). The inner nucleus, which contains older lens fibre cells than the outer cortex, has more of these dimers (arrow head). Dashed box in figure 9.7 suggests that besides full length AQP0, there are breakdown products of AQP0. A major product is indicated (*). The signals for full length AQP0 (arrow) and this major break down product (*) overlap at this exposure. BoOC: bovine outer cortex, BoIN: bovine inner nucleus.

9.4.3.2. IR appeared not to modify the protein oxidation levels in lens membrane extracts

As SDS-PAGE suggested that IR did not induce modifications in the protein pattern (Figure 9.4), OxyBlots (used to detected carbonylated proteins) and Western blots were used to investigate whether IR increased the levels of oxidised proteins in the bovine eye lens membrane extracts (Figure 9.3). Exposure to 50 Gy did not alter the amount of oxidised proteins in the membrane extracts (Figure 9.9A). Furthermore, immunoblotting with AQP0 illustrated that at 30 months AQP0 had endured more PTMs and this pattern remained unmodified after IR exposure (Figure 9.9B). Comparison of the cortical with the nuclear fraction demonstrated that the lens cortex contained more oxidised membrane proteins and less PTMs than in the nucleus (Figure 9.9A and B). In the 6 month-old nucleus membrane extracts one AQP0 band is more prominent in the irradiated sample, while in the cortex the same band is not detected after IR (Figure 9.9, black box).

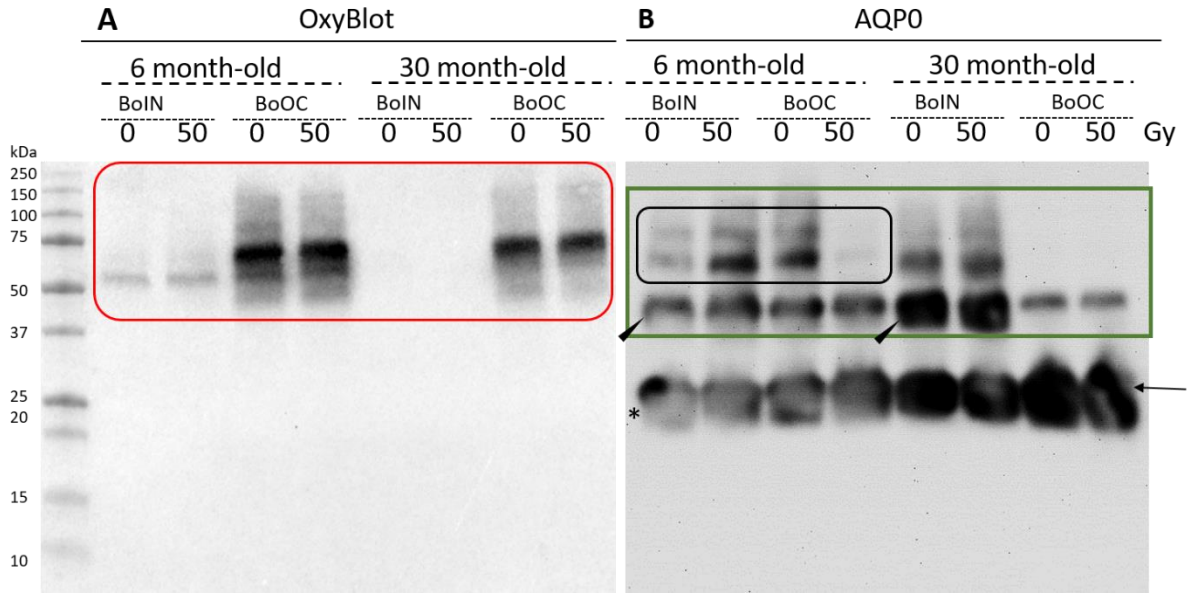

Figure 9.9: Immunoblots of 6 and 30 month-old bovine eye lens membrane extracts exposed to 50 Gy X-rays. 15 µg protein of 1% (w/v) SDS solubilised lens membrane proteins were run on SDS-PAGE gels (15% (w/v) acrylamide). A) Oxyblot showing carbonylated proteins and B) same membrane immunoblotted with AQP0 antibody (1/2000 dilution). Full length AQP0 has a molecular weight of 26 kDa (arrow), with age AQP0 protein undergoes complex PTMs involving truncation, and formation of dimers and tetramers (green box). The inner nucleus, which contains older lens fibre cells than the outer cortex, has more of these dimers (arrow head). Dashed box in figure 9.7 suggests that besides full length AQP0, there are breakdown products of AQP0. A major product is indicated (*). The signals for full length AQP0 (arrow) and this major break down product (*) overlap at this exposure. Comparison of the oxyblot and the AQP0 signals make the unequivocal identification of AQP0 as a carbonylated proteins impossible and therefore, the identity of these proteins remains to be determined (red box vs. green box). BoOC: bovine outer cortex, BoIN: bovine inner nucleus.

9.4.4. VC1 pull down identifies AGE bound proteins

To identify the proteins subjected to glycation with age and IR exposure (Figure 9.5 and Figure 9.6), the recent developed VC1 pull down technique was applied (Degani et al., 2017). This technique involves using the VC1 domain of the receptor for the advanced glycation end products to bind AGEs. Subsequently, these are pulled down, the isolated proteins are digested and analysed via LC-MS.

9.4.4.1. 1 % SDS for membrane proteins solubilisation

The VC1 pull down protocol was developed using water soluble proteins (Degani et al., 2017). Given that the lens membrane proteins are water insoluble and solubilising agents such as SDS interfere with VC1 pull down and trypsin digest, and obstructs LC-MS analysis, the minimal concentration required to solubilise lens membrane proteins was determined. Membrane extracts from 6 month-old bovine eye lenses were solubilised with 0, 0.1, 0.5, 1, 2 and 4 % SDS and analysed by SDS-PAGE (Figure 9.3). With increasing SDS concentration, more proteins were detected in the soluble fractions (Figure 9.10B). The use of 1% SDS generated the least insolubilised membrane proteins in the cortex and nucleus compared to lower percentage SDS (Figure 9.10C). However, comparison of the protein pattern pre-solubilisation and after solubilisation in the cortex showed that complete solubilisation was achieved only after addition of 4% SDS while in the nucleus optimal solubilisation occurred at 1% SDS (Figure 9.10B vs. A). 1% SDS was selected as the optimal trade-off (Figure 9.10, encircled).

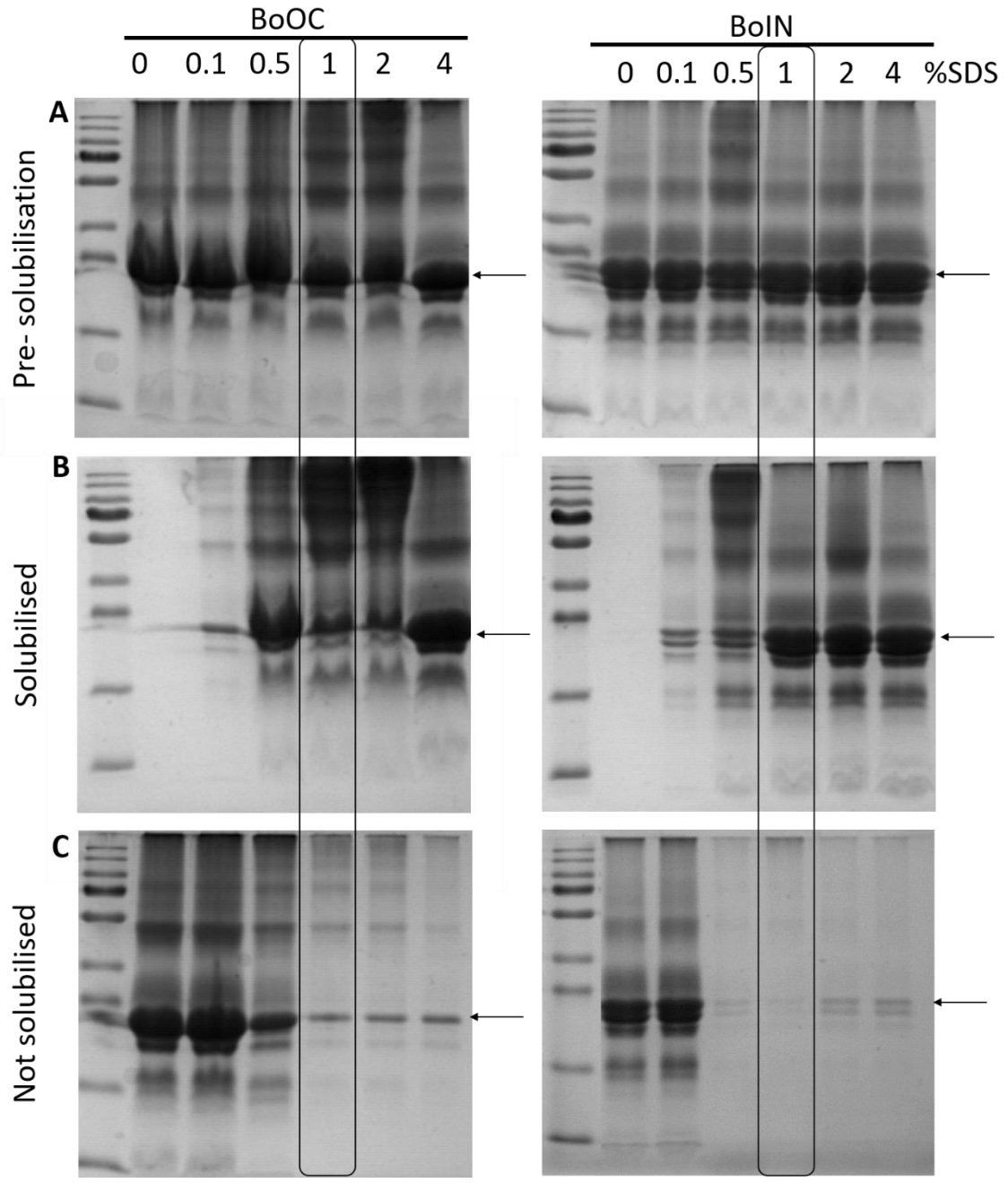

Figure 9.10: 20 µg protein of SDS solubilised lens membranes were run on SDS-PAGE gels (15% (w/v) acrylamide) stained with Coomassie Brilliant Blue. The image shows 6 month-old bovine cortical and nuclear membrane extracts solubilised with 0, 0.1, 0.5, 1, 2, 4 % SDS. A) Membrane proteins before solubilisation process, B) supernatant containing the solubilised proteins and C) pellet containing not solubilised proteins. 1% SDS was selected as the optimal solubilisation percentage (encircled). The molecular weight markers in the first lane of each gel mark respectively 250, 130, 95, 72, 55, 36, 28, 17 and 10 kDa from top to bottom. The most prominent band visible is AQP0 (arrow). Protein identity suggestion made above was based on proteomics data in the appendix (appendix table 1 and 2). BoOC: bovine outer cortex, BoIN: bovine inner nucleus.

9.4.4.2. VC1 resin pull down lens membrane proteins bound by AGEs adducts

A modified version of the VC1 pull down protocol established by Degani and colleagues enabled the application of this technique for water insoluble proteins (Degani et al., 2017). Comparison of the pull down eluate obtained from the control samples (no VC1 resin added) with the eluate from VC1 resin containing samples showed that AGEs bound proteins were pulled down by VC1 in the unexposed and 50 Gy exposed bovine outer cortex samples of 6 and 30 month-old lens membrane extracts. (Figure 9.11A and B encircled).

Although the same proteins were pulled down in both age groups, the amount of protein pulled down was higher in the 6 month-old membrane extracts (Figure 9.11A vs. B encircled). Therefore, only the bands in the 6 month-old extracts were selected for further with LC-MS.

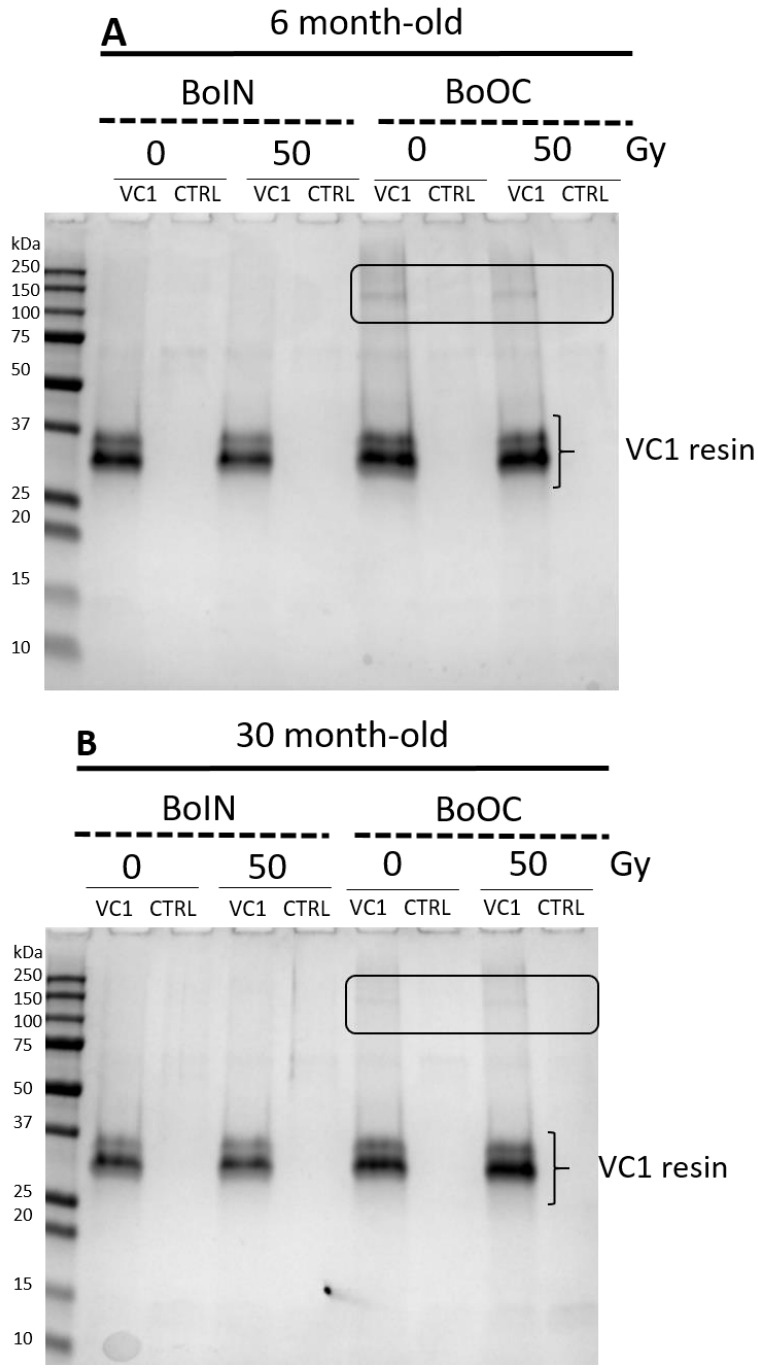

Figure 9.11: SDS-PAGE gels (15% (w/v) acrylamide) stained with Coomassie Brilliant Blue of VC1 pull down eluates of A) 6 and B) 30 month-old bovine cortical and nuclear membrane extracts exposed to 50 Gy X-rays. Protein bands pulled down by the VC1 resin are encircled. BoIN: bovine inner nucleus, BoOC: bovine outer cortex.

9.4.4.3. AGEs bound proteins are involved in similar biological processes

The 6 month-old bovine lens outer cortex membrane extracts contain more than 150 proteins (Appendix table 1). However, only eight proteins were identified in the 0 and 50 Gy irradiated VC1 pull down eluate: cadherin-2 (CDH2), β-catenin (CTNNB1), α-actin 2 (ACTA2), glucose transporter member 1 (SLC2A1), flotillin-2 (FLOT2), β-crystallin A4 (CRYBA4), α-crystallin A (CRYAA) and aquaporin 0 (AQP0, MIP) (Figure 9.12). Function of each protein is defined in Table 9.1.

Based on the generated proteomics data a protein-protein interaction network was computationally built, which revealed that two sets of proteins undergo physical interaction (p= 0.00012). In physiological environment, MIP, CRYBA4 and CRYAA can bind together, while CDH2 can physically interact with CTNNB1 or ACTA2. Physical interaction is not equal to functional interaction, therefore gene ontology enrichment analysis was performed to verify whether these proteins are involved in similar biological processes. This revealed that CDH2, ACTA2, CTNNB1, AQP0 and CRYAA have a common role in development (p= 0.00049). However, CTNNB1, AQP0 and CRYAA were shown to functionally interact during lens development (p= 0.0000463). CTNNB1 and CRYAA were annotated to share a role in establishing and maintaining the cellular structure of lenticular cells (p= 0.00049).

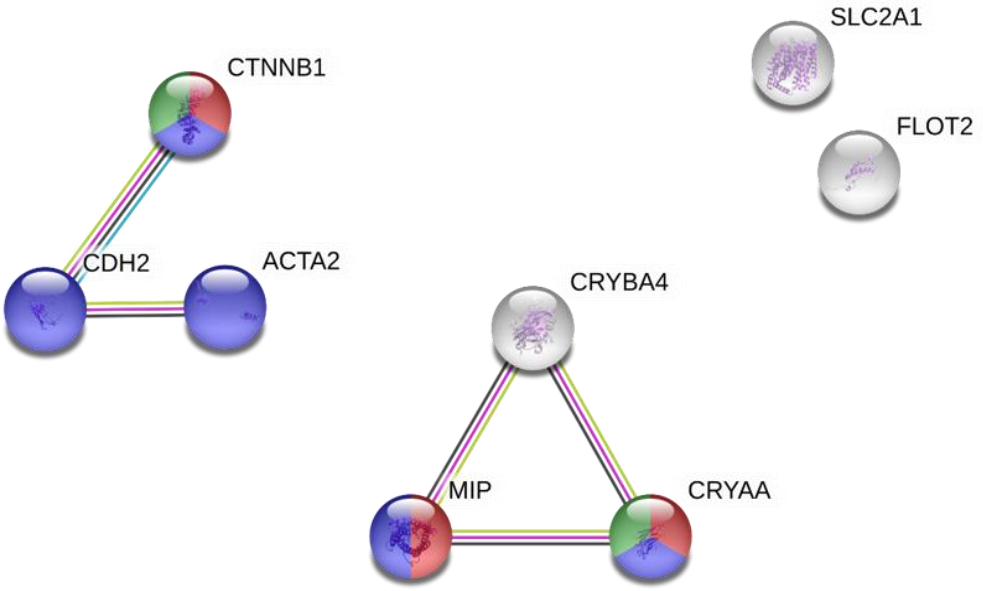

Network Stats	
Number of nodes	8
Number of edges	5
Average Node Degrees	1.25
Avg. Local clustering coefficient	0.625
Expected number of edges	0
PPI enrichment p-value	1.20E-04

BIOLOGICAL PROCESS (GO)				
GO-term	**Description**	**Count in gene set**	**False Discovery Rate**	
GO:0002088	lens development in camera-type eye	3 of 18	4.63E-05	
GO:0048731	system development	5 of 795	0.00049	
GO:0002089	lens morphogenesis in camera-type eye	2 of 7	0.00049	

Figure 9.12: Protein-protein interaction network and gene ontology analysis of the eight proteins identified in the 0 and 50 Gy IR exposed 6 month-old bovine lens outer cortex membrane extracts VC1 pull down eluate generated using LC-MS and the computer program STRING. Proteins connected through a line physically interact in vivo, while those that share a similar colour show a functional interaction. PPI: protein-protein interaction, GO: gene ontology, avg.: average.

9.5. Discussion and conclusion

9.5.1. Cholesterol could be protecting membrane proteins from major oxidation

The lens membrane extracts contains integral membrane proteins, in particular AQP0, and it has been reported that membrane associated proteins were more susceptible than soluble equivalents to oxidative damage (Kim et al., 2014). Using SDS PAGE and OxyBlot, no changes in either the protein pattern (Figure 9.4) or protein carbonylation (Figure 9.9A) 2 h post-IR exposure were detected. The lipids surrounding the integral membrane proteins might be protecting the integral membrane proteins from immediate damaging effects of IR-induced oxidative stress. Although proteins were found to be the primary target of free radicals in comparison to lipids in U937 cells (Du and Gebicki, 2004), lens membranes contain high levels of cholesterol which could offer the proteins protection against oxidative stress (Girao et al., 1999, Widomska et al., 2017, Sevanian and McLeod, 1987). Most probably, given that high levels of IR were applied (50 Gy), the protective cholesterol layer was damaged. The IR-induced cholesterol oxides caused a loss in membrane integrity, this permitted free radicals to migrate in the lens membrane and oxidise protein. IR-induced protein oxidation occurred at low levels and was not detected by OxyBlot. Further work should involve more sensitive techniques, i.e. LC-MS, able to accurately measure small modifications in protein oxidation.

Table 9.1: AGE bound proteins and their function (source: genecards.org)

Protein	Full name of protein	Function in the eye lens
CTNNB1	β-Catenin	- Essential component of adherens junctions required for creation and maintenance of epithelial cell layers - Downstream component of the canonical Wnt signalling pathway
CDH2	Cadherin-2, Calcium-dependent cell adhesion protein	Mediates homotypic cell-cell adhesion by dimerization with a CDH2 chain from another cell
ACTA2	α-Actin 2	Involved in cell motility
CRYBA4	β-Crystallin A4	Structural components of the vertebrate eye lens
MIP	Aquaporin 0	Water channel with a role in cell-to-cell adhesion and facilitates gap junction coupling
CRYAA	α-Crystallin A	- Contributes to the transparency and refractive index of the lens - Has chaperone-like activity, preventing aggregation of various proteins under a wide range of stress condition
SLC2A1	Glucose transporter member 1	Transports glucose through the membrane
FLOT2	Flotillin-2	Acts as a scaffolding protein within membranes containing caveolin

The biological mechanisms leading IR-induced cataractogenesis are poorly understood. The presented data revealed that IR stimulates the formation of AGEs, including glyoxal lysine that is highly associated with ARCs (Figure 9.5 and Figure 9.6), possibly identifying a novel mechanism through which IR-induced cataractogenesis occurs. Similar to IR-induced cholesterol oxidation (see chapter 5), IR-induced AGEs formation was not proportionate to dose and the cortex was more sensitive than the nucleus (Figure 9.5 vs. Figure 9.6). This further strengthens the theory that cholesterol acts as an anti-oxidant in lens membranes and that the level of protection offered is cholesterol-ratio dependent (Sevanian and McLeod, 1987, Girao et al., 1999).

Using the VC1 pull down technique, glycated proteins with divergent functions (Table 9.1) were shown to be involved in lens development, LFCs differentiation and lens growth (Figure 9.12). Dysregulation of both processes has been associated with IR-induced cataractogenesis (von Sallmann, 1950, Markiewicz et al., 2015). Combined quantification of AGEs and their associated proteins after IR exposure will advance our understanding of the involvement of AGEs in IR-induced cataract development.

9.5.2. Age-related decrease in oxidised membrane proteins

Age-related PTMs studies in lens water soluble and membrane proteins revealed that many observed age-related modifications in the lens are also induced by exposure to IR and non-IR (Ringens et al., 1982, Kopylova et al., 2011, Lund et al., 1996, Fujii et al., 2001, Kim et al., 2016, Uwineza et al., 2019). SDS-PAGE of 6 and 30 month-old bovine lens membrane confirmed age-related degradation of membrane proteins (Figure 9.7), but OxyBlot suggested age-related decrease in protein oxidation (Figure 9.8A) in contrast to the age-associated increase in protein oxidation that has been observed in previous research (reviewed by (Boscia et al., 2000)). The reduced level of protein oxidation in the lens nucleus compared to the lens cortex membrane extracts, and in 30 month-old relative to the 6 month-old membranes (Figure 9.8A) is most likely due to proteolytic processing occurring in the eye lens with time (Han and Schey, 2004, Korlimbinis et al., 2009, Liu et al., 2015, Grey and Schey, 2009).

The radiosensitivity of lenses is mediated by age at exposure (Merriam and Szechter, 1975). Assessment of age-dependent sensitivity of lens membranes to IR-induced protein oxidation suggested that 30 month-old membranes are not less sensitive to IR (Figure 9.9A), hence age-dependent radiosensitivity of the lens is not regulated through protein oxidation of integral membrane and membrane bound proteins. Although the oxyblots implied that the most prevalent protein in the lens membrane AQP0 does not undergo protein oxidation after IR-exposure of lens membranes (Figure 9.9B), VC1 pull down followed by LC-MS showed that AQP0 was bound by AGEs. However, quantitative studies are required to determine whether AGEs-bound AQP0 levels increase after exposure to IR.

In conclusion, IR-induced protein oxidation was not detected with SDS-PAGE, Oxyblots or Western blots. More sensitive techniques allowed the detection of IR-induced AGEs increase and with the VC1

pull down technique proteins bound by AGEs were identified. Further optimisation of the VC1 pull down protocol for plasma membrane proteins would allow the identification of the proteins to which the IR-induced AGEs bind.

Chapter 10: General discussion and conclusions

10.1. Main findings

The overarching objective of this project was to gain more insight into the mechanisms underlying ionising radiation (IR) induced cataracts. To achieve this, three different approaches were undertaken: the influence of IR on the lens epithelium cell density was examined (chapter 4), IR-induced alterations in the chemical structure of cholesterol were studied in bovine and mice lens membrane extracts (chapter 5 and 6), and protein modification as a consequence of IR-exposure was analysed in bovine lens membrane extracts (chapter 9).

To increase our understanding between the parallels of the age-related and IR-induced changes occurring in the lens, cholesterol and oxysterols concentrations were measured 6 and 30 month- old mice lens membrane extracts (chapter 7). Furthermore, the levels of cholesterol and oxysterols in the brain were also determined for comparison with the eye lens (chapter 7).

Given that the X- and γ-rays primarily induce damage by increasing oxidative stress, the possibility of anti-oxidants counteracting the damage caused by IR was investigated in bovine lens membrane extracts (chapter 8).

10.1.1. IR-induced changes in the lens epithelium are sex-, strain-, mutation-, dose-, dose rate- and latency time-dependent

Adult CD1 and C57BL/6J mice were exposed to 0.5, 1 and 2 Gy at a dose rate of 0.063 and 0.3 Gy/ min at an age of 10 weeks and their eye lenses were collected for lens epithelium cell density analysis 4 months post-IR (Figure 4.2). The CD1 strain showed low relative cell density in the central zone (CZ) compared to the peripheral zone (PZ) and the meridional rows (MR) (Figure 4.6). Male and female CD1 mice showed a lot of variation in relative cell density around the PZ and MR, this variation decreased after exposure to IR (Figure 4.7). C57BL/6J mice demonstrated low relative cell density in the CZ, which gradually increased and peaked in the PZ followed by a steady decrease in the MR (Figure 4.10). Doses of 0.5 and 1 Gy caused a decline in the PZ relative cell density of C57BL/6J in comparison to unexposed mice, in contrast to 2 Gy that induced a rise in PZ relative cell density relative to their unexposed counterparts (Figure 4.11). These dose-dependent changes were statistically significant in both strains. On the other hand, the sex- and *Ptch1*$^{+/-}$ mutation-dependent variations in cell density were not significant in unexposed and IR-exposed CD1 and C57BL/6J mice (Figure 4.6 - Figure 4.13). The dose rate significantly increased IR-sensitivity of LECs relative cell density in the CD1 mice (Figure 4.7), while no statistically significant changes were associated with dose rate in the C57BL/6J mice (Figure 4.11). In either strain, no cataracts were observed at 4 months post-IR of 0.5, 1 and 2 Gy. Analysis of the B6C3F1 mice exposed to 0.5, 1 and 2 Gy at a dose rate of 0.3 Gy/ min at 4 and 12 months post-IR demonstrated that also in this strain significant dose-dependent changes occurred (Figure 4.14 Figure 4.16). However, in contrast to the CD1 and C57BL/6J mice (Figure 4.6Figure 4.7,Figure 4.10 andFigure 4.11), females were significantly more sensitive to IR than males their male

counterparts in the B6C3F1 strain (Figure 4.14Figure 4.17). Moreover, introducing a heterozygous mutation in the Ercc2 gene also significantly increased the sensitivity of B6C3F1 mice lens epithelium cell density to IR (Figure 4.14Figure 4.15Figure 4.16Figure 4.17). No significant differences were noted between 4 and 12 months post-IR (Figure 4.14Figure 4.17). Furthermore, comparison of eye lens images showed that the cellular organisation of CD1 mice was different from B6C3F1 and C57BL/6J mice (Figure 4.5).

Collectively, these data confirm that dose rate, the Ptch1 and Ercc2 genes, sex, and time post-IR are all factors mediating IR-induced lens epithelium cell density changes. Whether the contribution of these factors elicits significant changes to radiation sensitivity depends on the genetic background and the applied dose.

10.1.2. The build-up of oxysterols in lens plasma membrane is triggered by IR exposure, and adding α-tocopherol in the lens cortex membranes prevents the this

Secondly, the impact of IR on lens membrane cholesterol was studied. For this, bovine lens membrane extracts were exposed to 5 and 50 Gy X-rays (Figure 5.2). Using liquid chromatography followed by mass spectrometry (LC-MS) the increase of 7β-hydroxycholesterol, 7-ketocholesterol and 5, 6-epoxycholesterol levels among other oxysterols was shown to be triggered by IR in a non-linear manner (Figure 5.6). *In vitro*, the observed IR-induced formed oxysterols persisted up to 18 days post-IR (Figure 5.7). Contrary to *in vitro* IR-induced oxysterol formation, the increase of 7β-hydroxycholesterol and 7-ketocholesterol *in vivo* after exposure to 2 Gy was transient and no significant changes were induced in 5, 6-epoxycholesterol levels by IR-exposure (Figure 6.4). Importantly, whole body X-rays exposure of doses as low as 0.1 Gy was shown to induce oxysterol formation (Figure 6.3). Both, the *in vitro* and *in vivo* assays indicated that the lens cortex is more sensitive than the lens nucleus (Table 5.2 and Figure 6.4). The addition of anti-oxidants to bovine lipid membranes pre- or post-IR generated divergent results depending of the anti-oxidant (chapter 8). Whilst α-tocopherol was able to reduce IR-induced oxysterol formation (Figure 8.5A) and stimulate the degradation (Figure 8.6A) of these oxysterols in bovine lens cortex membrane extracts, ascorbic acid acted as pro-oxidant and enhanced the amount of oxysterols formed after exposure to IR (Figure 8.5Figure 8.6A). In bovine lens nucleus membrane extracts, α-tocopherol, ascorbic acid and glutathione acted as pro-oxidants (Figure 8.5Figure 8.6B and Figure 8.7A). This can be attributed to ascorbic acid and glutathione being hydrophilic anti-oxidants and therefore, unable migrate in the lipophilic environment in which cholesterol resides and remove free radicals (Pavlovic et al., 2005). The presence of transition metals through which metal-catalysed Haber-Weiss and Fenton reaction stimulate the formation of free radicals also allow ascorbic acid and GSH to act as a pro-oxidant by reducing these redox-active metals (Buettner and Jurkiewicz, 1996, Schoneich et al., 1992, Sagrista et al., 2002). Combining α-tocopherol with ascorbic acid and glutathione reduced their pro-oxidant function (Figure 8.7C). Membrane binding experiments

showed that the amphiphilic structure of α-tocopherol enabled this molecule to bind into bovine lens cortex membrane extracts and perform its anti-oxidant function (Figure 8.8D). α-Tocopherol struggled to strongly bind into the bovine lens nucleus membrane extracts (Figure 8.8A). These findings suggest that although the higher concentration of cholesterol in the lens nucleus compared to the cortex allows cholesterol to perform its anti-oxidant role in the lens nucleus membrane more efficiently, it also attenuates the anti-oxidative role of α-tocopherol by constraining the binding of α-tocopherol into the membrane.

Furthermore, to compare age-related changes with IR-induced alterations in oxysterol levels in the eye lens and in the brain, 6 and 30 month- old murine lens membrane extracts and hippocampi lipids were analysed via LC-MS (Figure 7.2). Age-related increase in cholesterol and oxysterol levels was observed in the brain and in the eye lens (Figure 7.3), this trend of cholesterol increase in lens cortex and lens nucleus was much higher than in the hippocampus. While in the hippocampi significant increase in oxysterol levels was observed during absolute amount measurements, significant changes in oxysterols levels in the lens nucleus were observed relative to the internal cholesterol (Figure 7.6Figure 7.7Figure 7.8). In the lens cortex, no significant changes were observed in the absolute or relative data (Figure 7.6Figure 7.7Figure 7.8). Combined with the IR-induced oxysterol formation experiments, this provides an potential explanation for why age-related cataracts (ARC) are mainly associated with nuclear cataracts (Truscott, 2005) while radiation cataracts are primarily linked with posterior subcapsular cataracts (PSCs) ((Ainsbury et al., 2009, Hamada et al., 2019)). However, IR also damages the lens nucleus and can also trigger opacification in the lens nucleus (Azizova et al., 2018).

10.1.3. The formation of AGEs is stimulated by IR exposure

Lastly, IR-induced protein modifications were analysed in bovine lens membrane extracts (Figure 9.2Figure 9.3). SDS-PAGE analysis showed that 5 and 50 Gy did not induce changes in the protein pattern (Figure 9.4) and OxyBlots suggested that the levels of protein oxidation were not increased 2 hours post-IR (Figure 9.9). However, the use of a more sensitive technique, LC-MS, showed that the levels of AGEs increased after exposure of the membrane extracts to 5 and 50 Gy (Figure 9.5Figure 9.6). This increase was non-linear. Moreover, using the VC1 pull down method, CDH2, CTNNB1, ACTA2, SLC2A1, FLOT2, CRYBA4, CRYAA and AQP0 were identified as the AGEs bound proteins (Figure 9.11Figure 9.12). These proteins are involved in lens development processes including lens fibre cells (LFCs) differentiation, which is essential for the optical properties of the lens (von Sallmann, 1950, Markiewicz et al., 2015). Moreover, this provides an additional potential biomarker for IR-induced cataractogenesis.

Taken together, these three sets of studies identified multiple mechanisms (cell density changes, cholesterol oxidation and AGEs formation) through which IR increases the cataractogenic load. The initial IR-exposure immediately targets DNA replication leading to changes in cell density,

cholesterol resulting in less rigid membranes and glycation of lens membrane proteins simultaneously. However, these processes are also interconnected. Aberrant cell density is interlinked with irregular LFCs differentiation process including poor lining up of LFCs layers. Inadequate cell-to-cell organisation renders the lens membrane barrier more vulnerable given that IR has easier access to the lipids. The high concentrations of cholesterol in lens membrane provide a rigid barrier that offers protection from oxidative stress (Mainali et al., 2015, Plesnar et al., 2018). Oxidation of cholesterol decreases the rigidity of the lens membrane, which gives free radicals access to membrane proteins and deeper layers of the eye lens. Damaged lens membrane proteins lead to aberrant transport of nutrients and also tend to aggregate. The gradual build-up of all these destructive effects of IR exposure probably decrease the age at which an individual develops cataracts. Although a lot of parallels have been drawn between age-related changes and IR-induced modifications in the eye lens (Uwineza et al., 2019), comparison of the changes in oxysterol:cholesterol ratio in the lens cortex and in the nucleus showed differences in the aetiology of ARC and PSCs. Whereas ARC is associated with the build-up of oxysterol in the nucleus, increased levels of lens cortex oxysterols are correlated with PSCs.

10.2. Limitations and future work

These studies have identified new potential mechanisms through which IR-induced cataractogenesis occurs, though the presented data deserve further scrutiny.

10.2.1. Lens epithelium cell density analysis

During the cell density study (chapter 4), the eye lenses were examined at 4 and 12 months post-IR exposure (Figure 4.2). However, none of these mice developed obvious lens opacities, hence experiments including longer latency period are required to verify if the observed IR-induced changes in cell density translate into cataractogenesis. Furthermore, the molecular mechanisms underlying the IR-induced changes in cell density have not been fully elucidated. The Ercc2 gene, which codes for a TFIIH complex subunit, was shown to be implicated in regulating radiation sensitivity of B6C3F1 mice (Figure 4.14Figure 4.17). This gene mediates DNA repair and gene transcription (Fuss and Tainer, 2011) and therefore, mutations in this gene probably induced epigenetic changes. Additional research including chromatin immunoprecipitation is required to shed light on these potential epigenetic changes and their involvement in radiation sensitivity.

This study was the first to use an automated system to measure and then calculate relative cell density from the CZ till the MR for IR-induced alterations in the lens epithelium cell density (Figure 3.2). The lack of previous studies precluded a power analysis to determine the number of animals required for the detection of a statistically significant effect when there is a true effect to be found. The type of data generated from this technique is novel and although initial statistical analysis allowed the identification of significant changes, further exploration of the generated data with more advanced computer programs and statistical methods, which were beyond the scope of this thesis, could provide a more in-depth understanding of the differences between lens epithelium relative cell density in the distinct mice strains and the complexity of the IR-induced cell density modifications. Subsequently, retrospective power analysis will denote the actual power of the observed changes. As stated before, improvement to this tool is ongoing with the focus on changing the manual determination of distance from MR to CZ in the current program to reconstruct the position of each nuclei in 3D space, hence automatically establishing the distance from the MR to the CZ.

This data suggest that cell density has the potential of being a biomarker for IR-induced cataractogenesis. However, the issue around measurement of cell density in human is quite complex and further research is required.

10.2.2. Assessing cholesterol oxidation data

The hypothesis that IR stimulates the formation of free radicals, which subsequently lead to cholesterol oxidation has been confirmed (chapter 5 and 6). In line with epidemiological data showing that mainly PSCs are associated with radiation cataracts (Minamoto et al., 2004, Worgul

et al., 2007, Hall et al., 1999, Pastor-Valero, 2013), cortical membranes have been shown to be more sensitive to IR than the nucleus in bovine lens membrane extracts (Table 5.2) and in eye lenses of exposed mice (Figure 6.4). IR-induced oxysterol formation observed in the *in vivo* experiments was transient (Figure 6.4) which implies that the conversion of cholesterol to oxysterols, which modifies the permeability of the lens membrane (Vestergaard et al., 2011, Theunissen et al., 1986), allows anti-oxidants and oxysterol metabolising enzymes to prevent further oxidation and remove formed oxysterols. However, it is the accumulation of cholesterol oxides that was associated with cataracts (Girao et al., 1998). Further work including acute exposure to higher doses, and protracted or fractionated exposure to low doses will elucidate whether IR can induce the build-up of oxysterols *in vivo*. Another avenue worth considering is whether the changes in lens plasma membrane permeability (Vestergaard et al., 2011, Theunissen et al., 1986) induced by transient oxysterol formation have downstream effects that gradually lead to loss of lens transparency e.g. increasing the migration of Ca^{2+} in the lens that is known to promote PTMs (Giblin et al., 1984, Tang et al., 2003a).

This study is the first to suggest that IR-induced cholesterol oxidation is involved in the aetiology of radiation cataracts. Nevertheless, to confirm this, cholesterol oxides in the cortex and nucleus of eye lenses of ARC and radiation cataracts patients should be measured and compared to their age-matched controls using samples collected during large scale epidemiological studies e.g. the Mayak workers cohort (Azizova et al., 2018) and LFCs collected from patients who have undergone cataract surgery. If the radiation cataract patients show an accumulation of oxysterols mainly in the lens cortex, while ARC patients show cholesterol oxidation adducts build-up in their lens nucleus the mechanism proposed above will be confirmed *in vivo*. 7β-hydroxycholesterol, 7-ketocholesterol and 5, 6-epoxycholesterol were selected for further quantification studies (Figure 5.6). However, these were not the only oxysterols increased after IR exposure (Figure 5.4 and Table 5.1) and whether the selected oxysterols are the main oxysterols correlated with IR-induced cataracts has not been investigated. Measuring cholesterol oxides in the LFCs of human radiation cataracts patients followed by the identification of all oxysterols in the samples and statistical correlation analysis would confirm if the selected oxysterols are ideal biomarkers for radiation cataracts. Doses as low as 0.1 Gy have been shown to induce an increase in oxysterols (Figure 6.3). Whether this increase is significant still needs to be validated with quantification experiments.

Interestingly, magnetic resonance imaging is being used to monitor cholesterol levels in patients with high cholesterol levels and atherosclerosis (Lima et al., 2004, Zhao and Kerwin, 2012). Given that magnetic resonance imaging is a non-invasive technique that does not require radiation, this could possibly be optimised to detect IR-induced cholesterol oxidation in the eye lenses.

The age-related study showed significant changes in absolute oxysterol levels and oxysterol:cholesterol ratio with age (Figure 7.6Figure 7.7Figure 7.8). This raises the question whether it is the absolute or relative amount of oxysterols that is associated with cataractogenesis. Although the generated data points towards the relative amount, power analysis suggested that the applied sample size for the absolute values is overall too low to detect true effects (Table 7.2). Therefore, a bigger sample size and including more than two age points in the experiment is advised. Moreover, the lenses of mice showing lens opacities should be separated from their age-matched controls, which was not possible during this study due to the unavailability of required equipment.

Epidemiological studies indicate that females are more radio-sensitive than their male counterparts (Hamada et al., 2019, Azizova et al., 2018). Intriguingly, oestrogen and oxysterols are intertwined in similar biological processes (Norlin, 2008). They are both synthesised from cholesterol and regulate cholesterol metabolism. In liver and prostate cells, oestrogen has been found to suppress the expression of CYP27A1, a gene coding for the enzyme that catalyses the formation of 27-hydroxycholesterol (Tang et al., 2007). Moreover, oestrogen also activated the expression of CYP7B1, a gene encoding an enzyme involved in the metabolism of 27-hydroxycholesterol (Tang et al., 2006). In testicular cells, oestrogen was shown to reverse 25-hydroxycholesterol-induced apoptosis (Travert et al., 2006). These studies accentuate that oxysterols and oestrogen are involved in many similar physiological pathways and interact at several molecular levels in biological processes. These biological processes in which they interact could be contributing to the observed sex-dependent sensitivity to IR and merit further exploration in future research.

α-Tocopherol has been shown to be able to prevent IR-induced oxysterol formation and/ or remove oxysterols in bovine lens cortical membranes (Figure 8.5Figure 8.6A). Hypothetically, this means that α-tocopherol could be used to prevent radiation cataracts. Epidemiological data examining the association between anti-oxidants intake and cataracts is conflicting (Pastor-Valero, 2013, Christen et al., 2015). The lens membrane extracts binding experiments have shown that α-tocopherol partitioned to the lipid environment and bound into the lens cortex membrane after being added to bovine lens membranes dissolved in a hydrophilic buffer (Figure 8.8). Mechanistic studies examining whether α-tocopherol can migrate into the eye lens membranes after oral uptake or the use of eye drops should be performed before the use of α-tocopherol can be suggested to prevent IR-induced oxysterol formation *in vivo*. Furthermore, considering that the addition of α-tocopherol pre- and post-IR exposure reduced oxysterol levels, this anti-oxidants could potentially be used in aged patients exposed to radiation to prevent cataract formation. In the applied experimental settings, glutathione and ascorbic acid acted as pro-oxidants (Figure 8.5Figure 8.6 and Figure 8.7). Based on the obtained results, generating recommendations towards combining these various anti-oxidants at specific concentrations in order for them to prevent cholesterol oxidation in the human species is not possible. Still, as previous research has shown that their likelihood to act as pro-

oxidant or anti-oxidant depends on their concentration and the amount of oxidative stress in the environment (Buettner and Jurkiewicz, 1996, Sagrista et al., 2002, Schoneich et al., 1992), further work should continue to determine at what dose or anti-oxidant concentration the shift from anti-oxidant to pro-oxidant occurs. Subsequently, glutathione and ascorbic acid could also be considered as therapeutic agents.

10.2.3. Understanding the impact of IR-induced AGEs formation

This study is the first to show IR induces formation of AGEs in the eye lens, which are bound to proteins with a vital role in maintaining lens transparency (Figure 9.5Figure 9.6, Figure 9.11Figure 9.12; (Song et al., 2009, Markiewicz et al., 2015, von Sallmann, 1950)). The performed experiments generated qualitative results, further investigations including the generation of LC-MS quantitative data will reveal whether the observed IR-induced AGEs adducts increase is statistically significant. Furthermore, although the proteins to which these AGEs adducts bind have been identified (Figure 9.11Figure 9.12), the importance of these modifications is still unclear. Analogous to the IR-induced oxysterol formation study, the main AGEs adducts that are linked to radiation cataracts should be determined and together with the identification of the principal protein(s) to which these IR-induced AGEs bind, this can help elucidate the molecular pathway through which these AGEs contribute to lens clouding.

10.2.4. The applied dose levels

Although occupational workers are chronically exposed to doses much lower than 0.5 Gy (Little et al., 2018) and low dose rates are defined as <0.005 Gy/ min (ICRP, 2007), the mice and bovine lens membrane extracts used during this thesis work were exposed to acute doses with 0.5 Gy as the lowest applied dose and 0.063 Gy/ min as the minimum applied dose rate during the cell density studies (chapter 4). Furthermore, in the IR-induced cholesterol oxidation studies, exposure doses >5 Gy were used during the *in vitro* studies and 0.1 and 2 Gy were applied during the *in vivo* investigations. This project identified novel mechanisms that potentially contribute to low dose radiation cataractogenesis (chapter 4, 5, 6 and 9) and also a possible explanation for why radiation cataracts are mainly associated with PSCs (Table 5.2 and Figure 6.4; (Hamada et al., 2019)). Nonetheless, these mechanisms have not been connected with cataractous lenses yet. Future studies including lower doses, lower dose rates and longer incubation times will reveal whether these changes in lens epithelium cell density, and the accumulation of cholesterol oxidation and AGEs adducts are associated with IR-induced cataracts.

Occupational workers experience both chronic (all working hours) and fractioned (repeatedly every workday) exposure. Experiments reflecting these events are limited. The age at exposure has been shown to be a vital factor in IR-sensitivity of humans and mice (De Stefano et al., 2015), and future work studying the newly identified modifications triggered by IR should include multiple ages at exposure.

10.2.5. Bovine and murine lenses as model for human lenses

The use of model organisms is based on the notion that the biochemical reactions occurring in the model organism are similar to the ones taking place in human (Perlman, 2016). However, throughout evolution, the biological diversity between species has increased (Darwin, 1859). Preclinical studies have repeatedly struggled with reproducing and to translate data collected with model organisms (Justice and Dhillon, 2016) , this emphasises the importance of choosing one's model organism with rigor.

10.2.5.1. Using bovine lens membranes extracts as model

Bovine lens membrane extracts were used to study modifications in glycation of integral membrane proteins and cholesterol after exposure to IR (chapter 5, 8 and 9). Despite that the human eye lens membranes contain six times more cholesterol than bovine eye lens membranes (Deeley et al., 2008), bovine and human membranes still share biophysical properties that support the use of bovine lens membrane extracts to study IR-induced changes in lens membranes (Mainali et al., 2013). Comparison of human with bovine lens membrane showed that although their phospholipid composition differs, their order parameter profiles of phospholipid-cholesterol domain and oxygen transport parameter are similar (Mainali et al., 2013, Raguz et al., 2009, Mainali et al., 2011). Given that the efficiency of cholesterol oxidation and protein glycation depends on the free radicals migrating through the biophysical barrier and reacting with the cholesterol and proteins in the membranes (Reisz et al., 2014, Girao et al., 1999), bovine lens membranes are suitable to be used as model for IR-induced changes in human lens membranes. However, *in vitro* reactions are a simplified version of what occurs *in vivo* and therefore, the testing the generated data in *in vivo* is essential.

10.2.5.2. Using mice as model

Mice are invaluable models for studying human diseases *in vivo* (Perlman, 2016) and were used to investigate the influence of whole body IR-exposure on lens epithelium cell density and cholesterol (chapter 4 and 6). Additionally, mice were also used to study changes in cholesterol and oxysterols in an aging context (chapter 7). Cell density depends largely on the proliferative capacity of cells, which is commonly reflected in the gene expression pattern (Whitfield et al., 2006) and analysis of IR-induced alterations in gene expression in mice and human demonstrated that most of the triggered gene expression changes were similar (Ghandhi et al., 2019, Dressman et al., 2007, Paul and Amundson, 2008, Paul et al., 2015) and some were dissimilar (Ghandhi et al., 2019). Furthermore, comparison of the physiology of mice and human showed that the metabolic rate per gram of body weight of mice is seven times faster than in the human species (Schmidt-Nielsen, 1984), mice have higher rates of ROS production (Hulbert, 2008) and human eye lenses contain six times more cholesterol than mice eye lenses (Deeley et al., 2008). All these factors reflect sources of uncertainty during mouse-to-human translation and emphasise the importance of studies comparing specific biological mechanisms-of-interest. Future work should include establishing the

order parameter profiles of phospholipid-cholesterol domain and oxygen transport parameter of mice eye lenses in an IR and aging context, and compare these to human eye lenses. Previously, the cell density across the CZ and MR of the eye lens epithelium were shown to differ between human and C57BL/6 mice (as the mice showed a cell density peak in the PZ which was not observed in human lenses (Wu et al., 2015)). Interestingly, the changes in cell density across the lens epithelium Wu *et al.* observed in human are similar to the ones observed in the CD1 strain (Figure 4.6) (Wu et al., 2015) and suggest that for lens epithelium cell density studies this strain might be more suitable for comparison between the two species.

Lastly, although changes in cell density, oxysterol and AGEs levels have been shown to be valid mechanisms through which IR could be damaging the eye lens (chapter 4, 5, 6 and 9), it is not one factor that leads to the development of cataract, rather the collection of all changes induced by IR (Table 10.1) (Uwineza et al., 2019). Understanding how all these identified alterations and other factors affected by IR including DNA DSBs (Barnard et al., 2019), epigenetics, cytoplasmatic protein oxidation and aggregation (Kim et al., 2015) are interlinked is vital to comprehend their level of contribution to the cataractogenic load, hence to determine which factors to focus on for the development of therapeutics. Table 10.1 provides a list of biochemical and cell biological effects during aging and after IR exposure in the eye lens that have been identified in the past and the contribution of this thesis work has been marked in red. Nevertheless, more work for e.g. future PhD projects is unveiled given that the influence of IR on some biochemical and cell biological effects in Table 10.1 remain marked as not determined. The lens is a special tissue due to the fact that a significant portion of its cells does not have any cell organelles and all the lens cells are kept during a lifetime (Wride, 2011, Ainsbury et al., 2016). Moreover, understanding IR-induced changes is further complicated due to different biological processes being active in LECs vs. LFCs (Uwineza et al., 2019). The LDLensRad project was one of the first large integrative projects allowing to investigate many molecular processes at the same time and to combine these with the cataract phenotype. This project is still ongoing and publication of the generated results in a special issue in journal of radiation biology, combined with a meta-analysis, will advance our comprehension of the different effects that have been measured fit together.

Table 10.1: Overview of the biochemical and cell biological effects of aging and IR exposure on lens cells. The biological mechanisms underlying ionizing radiation (IR)-induced damage to the eye lens are not completely understood. A survey of the literature shows that aging and IR > 0.5 Gy can cause similar damage to the eye lens, while our knowledge of the effects of IR < 0.5 Gy is quite limited. This thesis work has contributed the sections marked in red. ND: not determined. Table adapted from Uwineza et al., 2019

	Ageing	IR > 0.5 Gy	IR ≤ 0.5 Gy
Gene expression	✓	✓	✓
DNA repair	✓	✓	✓
Cell density	✓	✓	✓
Proliferation	✓	✓	✓
Integrity of meridional rows	✓	✓	✓
Deamidation	✓	✓	ND
Racemisation	✓	✓	ND
Turncation	✓	✓	ND
Methionine oxidation	✓	✓	ND
Increase of disulfide bonds	✓	✓	ND
Increase of sphingomyelin and dihydrosphingomyelin	✓	ND	ND
Decrease of glycerolipids	✓	ND	ND
Advanced glycation end products	✓	✓	ND
Kynurenines	✓	ND	ND
Cholesterol oxidation	✓	✓	✓
Increase of cholesterol	✓	✓	✓
Cholesterol domain formation	✓	ND	ND

10.3. Clinical relevance and societal impact

Cataracts remain the main cause of blindness in the world (Roodhooft, 2002, WHO, 2020). Although cataract surgery provides a remedy, not everyone has easy access to this treatment. Epidemiological data showed correlation between IR and the development of cataracts (Hamada et al., 2019). The international commission on radiation protection reduced the occupational equivalent dose limits for the lens from 150 to 20 mSv per year averaged over a 5 years period, with no single year exceeding 50 mSv (Stewart et al., 2012). For radiation protection purposes, IR-induced cataracts were defined as tissue effects, i.e. detrimental biological activities that are tissue-specific and only appear above a certain dose threshold (ICRP, 1991), with a nominal threshold of 0.5 Gy independent of the dose rate as opposed to stochastic effects which are defined as biological events arising as a function of dose without threshold (Beck, 1982). The presented data show exposure to doses as low as 0.1 Gy affect important lens biomolecules (i.e. cholesterol; Figure 6.3), which alludes to that classification of stochastic and deterministic do not represent the full complexity of radiobiological response. Cataracts may, indeed, be both stochastic and deterministic.

Importantly, the differences in sensitivity of lens epithelium cell density to IR exposure between mice strains (chapter 4) suggest that genetic background mediates IR response. This data suggest it is not sufficient to set up radiation protection recommendations based on average population response regardless of sex, genetics and dose rate. Within the human species, differential radiation sensitivity has been observed (Rajaraman et al., 2018) and linking human cohorts with similar genetic background to specific mice strains based on their response to IR could allow a better understanding of the processes determining IR-sensitivity and thereby, more personalised recommended thresholds. In retrospective epidemiology acquiring the right dose estimate is rather challenging (Azizova et al., 2018, Azizova et al., 2008, Shore, 2016, Ainsbury et al., 2009), therefore including these parameters in prospective studies is more advisable. During prospective epidemiology, the dose rate should be taken into account given that the data presented in chapter 4 provides mechanistic evidence for its effect on IR-response sensitivity. Sex and time are parameters that have been included in most studies (Ainsbury et al., 2009, Hamada et al., 2019), more data with larger cohort and longer follow-up periods will contribute to the refinement of the existing findings. Although collecting genetic data during human epidemiology would help with understanding the influence of the genetic code on IR-sensitivity, major ethical debates should be conducted to discuss the morality.

The identification of the accumulation of oxysterols (chapter 5) and AGEs (chapter 9) as a consequence of IR exposure provides potential novel therapeutic targets. In addition, the anti-oxidant experiments have shown that α-tocopherol protects the lens cortex membranes from cholesterol oxidation (Figure 8.5Figure 8.6A) and thereby provides a mechanism that could be used

to mitigate IR-induced damage to the eye lens. It is tempting to suggest that α-tocopherol intake from early life on could contribute to improve quality of life of IR-exposed individuals. However, given that studies investigating whether increased anti-oxidants intake including α-tocopherol in human have generated contradictory results (Pescosolido et al., 2016, Braakhuis et al., 2019), more mechanistic studies are required to understand the wider systemic effects of anti-oxidants.

Appendix

Appendix 1: Matlab code

Detection of Nuclei

```
%% Clear
clc; close all; clear all;
%% Path - Libs
addpath('./lib/');
addpath('./lib/BOBlobDetector3D');
%% Load image
dirname = 'C:/Users/smgh17/OneDrive - Durham University/Alice/4 months HMGU/30431663/';
%dirname = 'C:\BACKUP\DURHAM\Projects\Durham_2016\Eye\';
%filename = 'AlexiaEyePin2';
filename = '30431663';
file_ext = '.tif';
%% Res
rx = 1.0; ry = rx; rz =1500/6200;
%% Load images
ims = BOReadImage3DC([dirname filename file_ext]);
%% Gray
ims = squeeze(max(ims,[],3));
ims = BONormalizeImageND(ims);
%% Filter
% disp('Filter');
% rx = 17; rz = 100; f = rz/rx;
% s = 12; s = [s s s/f];
% se = fspecial3('gaussian',s);
% imsf = imfilter(ims,se,'replicate');
%% Normalise images
%imsf = BONormalizeImageND(imsf);
%% Detect Centroids
ns = 2.3; t = 0.16; dirname
ns = [ns*rx ns*ry ns*rz];
np = BOBlobDetector3D(ims,[],ns,t);
%% Plot
figure; BOPlotMaxProjection2D(ims,np,1,1);
%% Save
x = np(:,1); y = np(:,2); z = np(:,3);
save(['./mat/' filename '_xyz.mat'],'x','y','z');
%dlmwrite([dirname filename '_cart.txt'],np(:,1:3),'delimiter','\t');
```

Annotate region of interest

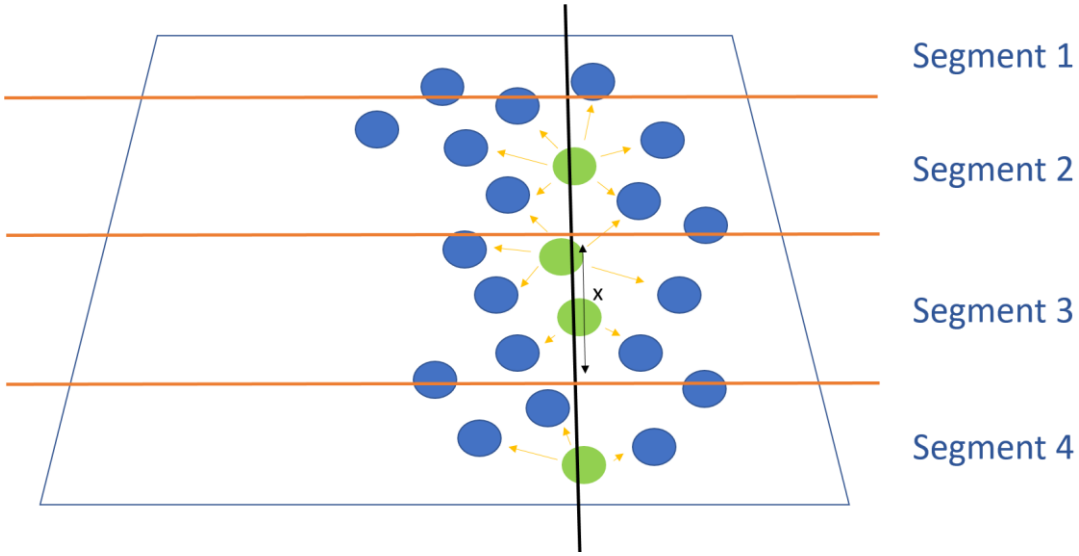

Appendix Figure 1: Schematic representation of annotation of region of interest (courtesy Alexia Kalligeraki, modified). The user-defined central line (black line) was used to determine which nuclei are in direct contact (green nuclei). Subsequently, these provided and anchor for a direct neighbour analysis. Nuclei were divided into an arbitrary number of segments (orange lines), with a constant segment length x (double-headed arrow). Within each segment, the absolute number of nuclei is normalised to number of nuclei per µm. A simplified way of explaining this calculation: "if I were to walk 1 µm in segment 1, how many nuclei would I encounter which are directly adjacent to the nuclei that are in contact with the line I'm walking on?". This process is then repeated for each user-defined segment and presented in a histogram where the x-axis is segment number and y-axis is the number of nuclei per µm of that segment. Given that each lens epithelium cell has one nucleus, the y-axis also displays the cell number/ µm of that segment (= relative cell density).

```
%% Clear
clc; close all; clear all;
%% Path - Libs
addpath('./lib/');
%% Settings
%dirname = 'C:\BACKUP\DURHAM\Projects\Durham_2016\Eye\';
dirname = 'C:/Users/smgh17/OneDrive - Durham University/Monika/4 months HMGU/30431663/';
filename = '30431663';
file_ext = '.tif';
```

```
file_ext2 = '.png';
%% Load images
ims = BOReadImage3DC([dirname filename file_ext]);
ims = squeeze(max(ims,[],3));
ims = BONormalizeImageND(ims);
%% Load XYZ
load(['./mat/' filename '_xyz.mat']);
%% Rectangle
figure; imagesc(squeeze(max(ims,[],3))); colormap jet; axis off; axis equal; axis tight;
zoom off; [xl,yl] = ginput(2);
hold on; plot(xl,yl,'r-','LineWidth',2);
%% Line
[xli,yli,ol] = drawLine([xl(1) yl(1)],[xl(2) yl(2)]);
figure; imagesc(max(ims,[],3)); colormap jet; axis off; axis equal; axis tight;
hold on; plot(xli,yli,'r-','LineWidth',2);
%% Generate rect mask image
rh = round(sqrt((xl(1)-xl(2))^2 + (yl(1)-yl(2))^2)); % rectangle height
rw = 100;  % rectangle width
imr = ones(rh,rw); % generate rectangle image of rh x rw size
imrd = zeros(rh,rw); % generate rectangle dist image of rh x rw size
imrd(1,:) = 1;
imrd = bwdist(imrd);
imro = imrotate(imr,rad2deg(ol)); % rotate rectangle image by ol angle
imrdo = imrotate(imrd,rad2deg(ol)); % rotate rectangle dist image by ol angle
[xro,yro] = ind2sub(size(imro),find(imro==1)); % pixels in rectangle
xroc = round(mean(xro)); % centre of rotated rectangle
yroc = round(mean(yro));
xrop = xro-xroc; % move origin of the rectangle pixels to (0,0)
yrop = yro-yroc;
xlc = round(mean(xli)); % centre of the line points
ylc = round(mean(yli));
xm = xlc + xrop; % mask points
ym = ylc + yrop;
immask = zeros(size(ims,1),size(ims,2)); % mask image containing the rotated rectangle
immask(sub2ind(size(immask),ym,xm)) = 1;
immaskd = zeros(size(ims,1),size(ims,2)); % mask dist image containing the rotated
rectangle
immaskd(sub2ind(size(immaskd),ym,xm)) = imrdo(sub2ind(size(imro),xro,yro));
ch = regionprops(immask,'ConvexHull');
ch = ch.ConvexHull;
%% Mask 3D
%immask3 = zeros(size(ims))==1;
%% Distance
zmin = min(z);
zmax = max(z);
zt = 0;
idx = z>zt;
xp = x(idx); yp = y(idx); zp = z(idx);
[in,on] = inpolygon(xp,yp,ch(:,2),ch(:,1));
xs = xp(in); ys = yp(in); zs = zp(in); % points in rectangle
%% Plot
```

```
imm = max(ims,[],3); % max projection of stack
imm(immask==1) = 1; % mask
figure; imagesc(imm); colormap jet; axis off; axis equal; axis tight;
hold on; plot(xli,yli,'r-','LineWidth',2);
hold on; plot(yp,xp,'y.');
hold on; plot(ys,xs,'go');
%% Save
save(['./mat/' filename '_xyz_r.mat'],'xs','ys','zs','xli','yli');
```

Calculation of cell density per area

```
%% Clear
clc; close all; clear all;
%% Settings
%dirname = 'C:\BACKUP\DURHAM\Projects\Durham_2016\Eye\';
dirname = 'C:/Users/smgh17/OneDrive - Durham University/Monika/4 months HMGU/30431663/';
filename = '30431663';
%filename = 'E1';
%filename = 'E4';
file_ext = '.tif';
file_ext2 = '.png';
%% Load XYZ in rect
load(['./mat/' filename '_xyz_r.mat']);
%% Res
rx = 1500; ry = rx; rz = 6200;
%% Fit
p = polyfitn([xs,ys],zs,3);
zg = polyvaln(p,[xs,ys]);
zgli = polyvaln(p,[yli',xli']);
%% Plot
% figure;
% plot3(ys,xs,zs,'g.');
% hold on;
% plot3(ys,xs,zg,'ro');
% plot3(xli,yli,zgli,'b-');
% box on; ax = gca; ax.BoxStyle = 'full';
%% Divide line into segments
ns = 100; % number of segments
%d = sqrt(diff(xli').^2 + diff(yli').^2 + diff(zgli).^2);
d = sqrt(diff(rx*xli').^2 + diff(ry*yli').^2 + diff(rz*zgli).^2);
ds = sum(d);
dsc = cumsum(d);
dn = ds/ns;
idx = zeros(ns+1,1);
idx(ns+1) = length(d);
for i=0:ns-1
   idx(i+1) = find(dsc>i*dn,1,'first');
end
%% Sort points into segments
sg = zeros(length(xs),1);
```

```
for i=1:ns
   p1 = [yli(idx(i)) xli(idx(i)) zgli(idx(i))];
   p2 = [yli(idx(i+1)) xli(idx(i+1)) zgli(idx(i+1))];
   %[p1; p2]
   for j=1:length(xs)
      p0 = [xs(j) ys(j) zs(j)];
      pi = BOLinePoint3D(p1,p2,p0);
      %hold on;
      % Is intersection point on the line segment?
      n1 = norm(pi-p1) + norm(pi-p2);
      n2 = norm(p1-p2);
      if abs(n1-n2)<1
         sg(j) = i;
         %plot3(pi(2),pi(1),pi(3), 'r.');
      end
   end
end
%% Plot
cmap = jet(ns+1);
figure;
%plot3(ys,xs,zs,'g.');
hold on;
%plot3(ys,xs,zg,'ro');
plot3(xli,yli,zgli,'b-');
for i=1:ns+1
   plot3(xli(idx(i)),yli(idx(i)),zgli(idx(i)),'bo');
end
for i=0:ns
   plot3(ys(sg==i),xs(sg==i),zs(sg==i),'.','MarkerSize',10,'MarkerFaceColor',cmap(i+1,:));
end
view(3); box on; ax = gca; ax.BoxStyle = 'full';
print('-dpng','-r300',['./plot/' filename '_stripes.png']);
%% Hist
for i=1:ns
   h(i) = sum(sg==i);
end
%figure; plot(1:ns,h,'r.-');
figure; plot(1:ns,h/ds,'r.-');
print('-dpng','-r300',['./plot/' filename '_density.png']);
%return
%% Plot
%% Load imagesH = [(1:ns)' h'];
ims = BOReadImage3DC([dirname filename file_ext]);
ims = squeeze(max(ims,[],3));
ims = BONormalizeImageND(ims);
imm = max(ims,[],3); % max projection of stack
%
figure; imagesc(imm); colormap gray; axis off; axis equal; axis tight;
hold on; plot(xli,yli,'r-','LineWidth',2);
%hold on; plot(ys,xs,'g.');
for i=1:ns
```

```
    plot(ys(sg==i),xs(sg==i),'o','MarkerSize',2,'MarkerFaceColor',cmap(i,:));
end
print('-dpng','-r300',['./plot/' filename '_stripes_im.png']);
%% Save
D = [xs ys zs sg];
H = [(1:ns)' (h/ds)'];
dlmwrite(['./mat/' filename '_xyz_class.txt'],D,'delimiter','\t');
dlmwrite(['./mat/' filename '_hist_class.txt'],H,'delimiter','\t');
```

Create histograms

```
%% Clear
clc; close all; clear all;
%%
filename = '30409527';
W = dlmread(['./mat/' filename '_hist_class.txt']);
filename = '30409809';
X = dlmread(['./mat/' filename '_hist_class.txt']);
filename = '30409530';
Y = dlmread(['./mat/' filename '_hist_class.txt']);
filename = '30409533';
Z = dlmread(['./mat/' filename '_hist_class.txt']);
filename = '30409520';
A = dlmread(['./mat/' filename '_hist_class.txt']);
filename = '30409524';
B = dlmread(['./mat/' filename '_hist_class.txt']);


%% Figure
figure;
plot(W(:,1),W(:,2),'r.-'); hold on;
plot(X(:,1),X(:,2),'r.-');
plot(Y(:,1),Y(:,2),'r.-');
plot(Y(:,1),Y(:,2),'r.-');
plot(A(:,1),A(:,2),'--black');
plot(B(:,1),B(:,2),'--black');


ylim([0 3*10^-5])
```

Appendix 2: Proteomic analysis of bovine lipid membrane extracts

Appendix table 1: 10 µg proteins of 1% SDS solubilised 6 month-old bovine cortex lipid membrane extracts were trypsin digested and analysed via LCMS. The list of proteins was generated through ProteinPilot™ 2.5.1. Software and Bovine data subtracted from Uniprot, and presents all the proteins present in bovine lipid membranes. The number of distinct peptides having at least 95% confidence are listed in the third column.

Name	Species	Peptides (95%)
Lens fiber major intrinsic protein (AQP0)	BOVINE	60
Gap junction alpha-3 protein	BOVINE	41
Spectrin beta chain	BOVINE	31
Periaxin	BOVINE	31
Lactase like	BOVINE	30
Filensin (BFSP1)	BOVINE	24
Ezrin	BOVINE	21
Phakinin	BOVINE	21
Neuronal cell adhesion molecule	BOVINE	18
Cadherin-2	BOVINE	17
Vimentin	BOVINE	16
Catenin beta-1	BOVINE	16
Beta-crystallin B2	BOVINE	15
Alpha-crystallin B chain	BOVINE	15
Radixin	BOVINE	15
Flotillin-2	BOVINE	14
Beta-crystallin B1	BOVINE	14
Actin, cytoplasmic 2	BOVINE	14
Actin, cytoplasmic 1	BOVINE	14
Alpha-crystallin A chain	BOVINE	14
Neural cell adhesion molecule 1	BOVINE	13
Flotillin-1	BOVINE	13
Brain acid soluble protein 1	BOVINE	12
Ras-related C3 botulinum toxin substrate 1	BOVINE	10
Beta-crystallin B3	BOVINE	10
Beta-crystallin A3	BOVINE	10

Spectrin alpha, non-erythrocytic 1	BOVINE	9
EPH receptor A2	BOVINE	9
Lens fiber membrane intrinsic protein	BOVINE	9
Integrin alpha-2	BOVINE	8
Integrin alpha-2 (Fragment)	BOVINE	8
Coxsackievirus and adenovirus receptor homolog	BOVINE	8
Ankyrin 3	BOVINE	8
RAB1A, member RAS oncogene family	BOVINE	7
Aquaporin 5	BOVINE	7
Transmembrane protein 47	BOVINE	7
Keratin, type I cytoskeletal 14	BOVINE	7
Sidekick cell adhesion molecule 2	BOVINE	6
Vesicle-associated membrane protein 3	BOVINE	6
Vesicle-associated membrane protein 2	BOVINE	6
Keratin, type I cytoskeletal 19	BOVINE	6
RAB2A, member RAS oncogene family	BOVINE	5
Integrin beta-1	BOVINE	5
Carbonic anhydrase 3	BOVINE	5
Ras-related protein Rab-11A	BOVINE	5
Ras-related protein Rab-11B	BOVINE	5
Paralemmin	BOVINE	5
Erythrocyte membrane protein band 4.1 like 2	BOVINE	5
SLC3A2 protein	BOVINE	5
Protein 4.1	BOVINE	5
Galectin	BOVINE	5
Tetraspanin	BOVINE	5
CD9 antigen	BOVINE	5
RAB10 protein	BOVINE	5
Keratin, type I cytoskeletal 17	BOVINE	5
Annexin A2	BOVINE	4

Ras-related protein Rab-5C	BOVINE	4
Histone H4	BOVINE	4
Solute carrier family 2, facilitated glucose transporter member 1	BOVINE	4
Beta A4 crystallin	BOVINE	4
Beta-crystallin A4	BOVINE	4
Cell adhesion molecule 1	BOVINE	4
RAB35, member RAS oncogene family	BOVINE	4
Cell division control protein 42 homolog	BOVINE	4
Ras-related protein Rab-5A	BOVINE	4
Ras-related protein Rab-1B	BOVINE	4
Syntaxin-7	BOVINE	3
Cell adhesion molecule 2	BOVINE	3
Ubiquitin-60S ribosomal protein L40	BOVINE	3
Ubiquitin-40S ribosomal protein S27a	BOVINE	3
Polyubiquitin-C	BOVINE	3
Polyubiquitin-B	BOVINE	3
RAS like proto-oncogene A	BOVINE	3
NADH-cytochrome b5 reductase	BOVINE	3
NADH-cytochrome b5 reductase 3	BOVINE	3
Phospholipid hydroperoxide glutathione peroxidase, mitochondrial	BOVINE	3
Charged multivesicular body protein 6	BOVINE	3
Beta-crystallin S	BOVINE	3
Gamma-crystallin A	BOVINE	3
Gamma-crystallin B	BOVINE	3
Gap junction alpha-1 protein	BOVINE	3
Beta-crystallin A2	BOVINE	3
CD47 molecule	BOVINE	3
Leukocyte surface antigen CD47	BOVINE	3
AP-2 complex subunit mu	BOVINE	3

Junctional adhesion molecule A	BOVINE	3
Caveolin-1	BOVINE	3
Receptor-type tyrosine-protein phosphatase	BOVINE	3
Keratin 12	BOVINE	3
Keratin 18	BOVINE	3
Ras-related protein Rab-7a	BOVINE	3
Zeta-crystallin	BOVINE	2
Syntaxin-4	BOVINE	2
N-acetylated alpha-linked acidic dipeptidase 2	BOVINE	2
MYO1B protein	BOVINE	2
Guanine nucleotide-binding protein G(s) subunit alpha isoforms short	BOVINE	2
PP1201 protein	BOVINE	2
Basigin	BOVINE	2
G protein-coupled receptor class C group 5 member B	BOVINE	2
RAB9A, member RAS oncogene family	BOVINE	2
RAB9B, member RAS oncogene family	BOVINE	2
Lens epithelial protein	BOVINE	2
Catenin alpha-1	BOVINE	2
Fatty acid-binding protein, epidermal	BOVINE	2
Blood-brain barrier large neutral amino acid transporter	BOVINE	2
JAM2 protein	BOVINE	2
Carbonic anhydrase 14	BOVINE	2
Syntaxin 2	BOVINE	2
JAM3 protein	BOVINE	2
Piezo-type mechanosensitive ion channel component	BOVINE	2
Glutathione S-transferase Mu 1	BOVINE	2
Annexin	BOVINE	2
Annexin A1	BOVINE	2
Paralemmin 2	BOVINE	2
RAB14 protein	BOVINE	2

G protein subunit alpha i2	BOVINE	2
Solute carrier family 16 member 3	BOVINE	2
CTNNA2 protein	BOVINE	2
Histone H3	BOVINE	1
Histone H3.3	BOVINE	1
Histone H3.2	BOVINE	1
Histone H3.1	BOVINE	1
Histone H3.3C	BOVINE	1
Elongation factor 1-alpha	BOVINE	1
Elongation factor 1-alpha 2	BOVINE	1
Elongation factor 1-alpha 1	BOVINE	1
STX12 protein	BOVINE	1
Phospholipid-transporting ATPase	BOVINE	1
Phospholipid-transporting ATPase IB	BOVINE	1
Heat shock protein beta-1	BOVINE	1
Glyceraldehyde-3-phosphate dehydrogenase	BOVINE	1
CKLF-like MARVEL transmembrane domain containing 7	BOVINE	1
Metalloproteinase inhibitor 3	BOVINE	1
Retinal dehydrogenase 1	BOVINE	1
Histone H2A	BOVINE	1
Histone H2A.J	BOVINE	1
Histone H2A.V	BOVINE	1
Histone H2A type 1	BOVINE	1
Histone H2A.Z	BOVINE	1
Histone H2A type 2-C	BOVINE	1
CD99 molecule (Xg blood group)	BOVINE	1
SYPL1 protein	BOVINE	1
Pyruvate kinase	BOVINE	1
Proteolipid protein 2	BOVINE	1
Secretory carrier-associated membrane protein 4	BOVINE	1
Ras-related protein Rap-1A	BOVINE	1

Ras-related protein Rap-1b	BOVINE	1
Hemoglobin subunit alpha	BOVINE	1
Claudin	BOVINE	1
CD151 antigen	BOVINE	1
Synaptosomal-associated protein	BOVINE	1
60S ribosomal protein L13a	BOVINE	1
Aldehyde dehydrogenase family 3 member B1	BOVINE	1
NPC intracellular cholesterol transporter 1	BOVINE	1
Synaptobrevin homolog YKT6	BOVINE	1
Secretory carrier-associated membrane protein	BOVINE	1
Sidekick cell adhesion molecule 1	BOVINE	1
Solute carrier family 24 member 2	BOVINE	1
Major prion protein	BOVINE	1
Alpha-enolase	BOVINE	1
Guanine nucleotide-binding protein G(I)/G(S)/G(O) subunit gamma-12	BOVINE	1
Solute carrier family 2 (Facilitated glucose transporter), member 3	BOVINE	1
Solute carrier family 2, facilitated glucose transporter member 3	BOVINE	1
Zinc finger protein 292	BOVINE	1

Appendix table 2: 10 µg proteins of 1% SDS solubilised 6 month-old bovine nucleus lipid membrane extracts were trypsin digested and analysed via LCMS. The list of proteins was generated through ProteinPilot™ 2.5.1. Software and Bovine data subtracted from Uniprot, and presents all the proteins present in bovine nucleus lipid membranes. The number of distinct peptides having at least 95% confidence are listed in the third column.

Name	Species	Peptides (95%)
Lens fiber major intrinsic protein (AQP0)	BOVINE	66
Gap junction alpha-3 protein	BOVINE	54
Alpha-crystallin A chain	BOVINE	46
Spectrin beta chain	BOVINE	39
Beta-crystallin B3	BOVINE	39
Alpha-crystallin B chain	BOVINE	37
Phakinin	BOVINE	33
Beta-crystallin B1	BOVINE	31
Filensin (BFSP1)	BOVINE	28
Glycogen phosphorylase, liver form	BOVINE	24
Cytosol aminopeptidase	BOVINE	24
NADH dehydrogenase [ubiquinone] 1 alpha subcomplex subunit 13	BOVINE	24
Beta-crystallin B2	BOVINE	23
Lactase like	BOVINE	22
Actin, cytoplasmic 2	BOVINE	18
Actin, cytoplasmic 1	BOVINE	18
Beta-crystallin A3	BOVINE	17
Lens fiber membrane intrinsic protein	BOVINE	17
Alpha-enolase	BOVINE	16
Gamma-crystallin B	BOVINE	16
Gamma-crystallin D	BOVINE	16
Solute carrier family 2, facilitated glucose transporter member 1	BOVINE	14
Ras-related C3 botulinum toxin substrate 1	BOVINE	14
Solute carrier family 2 (Facilitated glucose transporter), member 3	BOVINE	14
Solute carrier family 2, facilitated glucose transporter member 3	BOVINE	14

Gamma-crystallin F	BOVINE	14
Vimentin	BOVINE	13
Actin, gamma-enteric smooth muscle	BOVINE	13
Actin, aortic smooth muscle	BOVINE	13
Radixin	BOVINE	12
Elongation factor 2	BOVINE	12
Glyceraldehyde-3-phosphate dehydrogenase	BOVINE	12
Ezrin	BOVINE	12
Catenin beta-1	BOVINE	11
Histone H4	BOVINE	10
Annexin A2	BOVINE	10
PGM5 protein	BOVINE	10
Carbonic anhydrase 3	BOVINE	10
Spectrin alpha, non-erythrocytic 1	BOVINE	9
Zeta-crystallin	BOVINE	9
Flotillin-1	BOVINE	9
L-lactate dehydrogenase A chain	BOVINE	9
Cadherin-2	BOVINE	9
Cadherin-2 (Fragment)	BOVINE	9
RAB1A, member RAS oncogene family	BOVINE	9
Beta A4 crystallin	BOVINE	9
Beta-crystallin A4	BOVINE	9
Gamma-crystallin C	BOVINE	9
RAB14 protein	BOVINE	8
Vesicle amine transport 1	BOVINE	8
Galectin	BOVINE	8
Flotillin-2	BOVINE	7
Ras-related protein Rab-7a	BOVINE	7
Nudix (Nucleoside diphosphate linked moiety X)-type motif 16-like 1	BOVINE	7
Protein MGARP	BOVINE	7
NADH dehydrogenase [ubiquinone] iron-sulfur protein 7, mitochondrial	BOVINE	7
ATP synthase F(0) complex subunit B1, mitochondrial	BOVINE	7
Transmembrane protein 47	BOVINE	7
Vesicle-associated membrane protein 3	BOVINE	7

Vesicle-associated membrane protein 2	BOVINE	7
Trafficking protein particle complex subunit 1	BOVINE	6
Phosphoglycerate kinase 1	BOVINE	6
GTP-binding nuclear protein Ran	BOVINE	6
Rab GDP dissociation inhibitor beta	BOVINE	6
Protein 4.1	BOVINE	6
AP-2 complex subunit mu	BOVINE	6
L-lactate dehydrogenase B chain	BOVINE	6
Ras-related protein Rab-1B	BOVINE	6
Ras-related protein Rab-11B	BOVINE	5
Ras-related protein Rab-11A	BOVINE	5
Armadillo repeat gene deleted in velocardiofacial syndrome	BOVINE	5
ATP-dependent 6-phosphofructokinase, liver type	BOVINE	5
Ras-related protein Rab-5C	BOVINE	5
Neuronal cell adhesion molecule	BOVINE	5
Tubulin alpha chain	BOVINE	5
Tubulin alpha-1C chain	BOVINE	5
Tubulin alpha-1D chain	BOVINE	5
Tubulin alpha-1B chain	BOVINE	5
Annexin	BOVINE	5
Annexin A1	BOVINE	5
Crystallin gamma N	BOVINE	5
ADP-ribosylation factor 3	BOVINE	5
ADP-ribosylation factor 1	BOVINE	5
ADP-ribosylation factor 2	BOVINE	5
Phospholipid hydroperoxide glutathione peroxidase, mitochondrial	BOVINE	5
Importin 5	BOVINE	5
Phosphoglycerate mutase 1	BOVINE	5
Phospholipid-transporting ATPase IB	BOVINE	5
Cell adhesion molecule 1	BOVINE	5
Dynein light chain 1, cytoplasmic	BOVINE	5

Cell division control protein 42 homolog	BOVINE	5
Ras-related protein Rab-5A	BOVINE	5
Tubulin alpha-3 chain	BOVINE	4
Tubulin alpha-4A chain	BOVINE	4
V-type proton ATPase subunit D	BOVINE	4
NADH dehydrogenase [ubiquinone] 1 alpha subcomplex subunit 9, mitochondrial	BOVINE	4
Elongation factor 1-alpha	BOVINE	4
Elongation factor 1-alpha 1	BOVINE	4
Elongation factor 1-alpha 2	BOVINE	4
Beta-crystallin A2	BOVINE	4
Carbonic anhydrase 2	BOVINE	4
Heat shock protein HSP 90-alpha	BOVINE	4
Phospholipid-transporting ATPase	BOVINE	4
5'-nucleotidase domain containing 2	BOVINE	4
PRELI domain-containing protein 1, mitochondrial	BOVINE	4
NADH dehydrogenase [ubiquinone] 1 subunit C2	BOVINE	4
T-complex protein 1 subunit delta	BOVINE	4
Peroxiredoxin-6	BOVINE	4
Charged multivesicular body protein 6	BOVINE	4
Synaptobrevin homolog YKT6	BOVINE	4
Cytochrome c oxidase subunit 6C	BOVINE	4
Beta-crystallin S	BOVINE	4
Polyubiquitin-C	BOVINE	4
Polyubiquitin-B	BOVINE	4
Mitochondrial pyruvate carrier	BOVINE	4
GTP-binding protein SAR1b	BOVINE	4
GTP-binding protein SAR1a	BOVINE	4
Glycogen phosphorylase, brain form	BOVINE	4
RAB10 protein	BOVINE	4

Mitochondrial import inner membrane translocase subunit TIM17	BOVINE	3
Mitochondrial import inner membrane translocase subunit Tim17-B	BOVINE	3
NADH dehydrogenase [ubiquinone] 1 beta subcomplex subunit 5, mitochondrial	BOVINE	3
Periaxin	BOVINE	3
Aquaporin 5	BOVINE	3
NADH dehydrogenase [ubiquinone] 1 alpha subcomplex subunit 11	BOVINE	3
NADH dehydrogenase [ubiquinone] 1 beta subcomplex subunit 4	BOVINE	3
Protein FAM49B	BOVINE	3
G protein subunit alpha i2	BOVINE	3
Elongation factor 1-gamma	BOVINE	3
Pyruvate kinase	BOVINE	3
RAS like proto-oncogene A	BOVINE	3
ADP/ATP translocase 2	BOVINE	3
ADP/ATP translocase 3	BOVINE	3
Actin-related protein 2/3 complex subunit 4	BOVINE	3
Coxsackievirus and adenovirus receptor homolog	BOVINE	3
Ubiquitin-conjugating enzyme E2 N	BOVINE	3
Plectin	BOVINE	3
Mitochondrial 2-oxoglutarate/malate carrier protein	BOVINE	3
Cytochrome c oxidase subunit 7C, mitochondrial	BOVINE	3
Glucose-6-phosphate isomerase	BOVINE	3
Family with sequence similarity 173 member A	BOVINE	3
Vesicle amine transport 1 like	BOVINE	3
CD47 molecule	BOVINE	3
Leukocyte surface antigen CD47	BOVINE	3

SLC3A2 protein	BOVINE	3
Macrophage migration inhibitory factor	BOVINE	3
Transmembrane protein 126A	BOVINE	3
Neural cell adhesion molecule 1	BOVINE	3
Blood-brain barrier large neutral amino acid transporter	BOVINE	3
Alpha-1,4 glucan phosphorylase	BOVINE	3
Glycogen phosphorylase, muscle form	BOVINE	3
RAB2A, member RAS oncogene family	BOVINE	3
Dynein light chain 2, cytoplasmic	BOVINE	3
ADP-ribosylation factor 4	BOVINE	3
Glutathione S-transferase A4	BOVINE	3
Guanine nucleotide-binding protein G(s) subunit alpha isoforms short	BOVINE	3
Ras-related protein Rab-8B	BOVINE	3
Ras-related protein Rab-8A	BOVINE	3
G protein subunit alpha i3	BOVINE	2
Guanine nucleotide-binding protein G(i) subunit alpha-1	BOVINE	2
RALB protein	BOVINE	2
ADP/ATP translocase 1	BOVINE	2
Prohibitin-2	BOVINE	2
Erythrocyte membrane protein band 4.1 like 1	BOVINE	2
KRAS proto-oncogene, GTPase	BOVINE	2
Basigin	BOVINE	2
Profilin	BOVINE	2
Profilin-1	BOVINE	2
Heat shock protein beta-1	BOVINE	2
SYPL1 protein	BOVINE	2
26S proteasome non-ATPase regulatory subunit 2	BOVINE	2
Histone H2A	BOVINE	2
Histone H2A.J	BOVINE	2
Histone H2A type 1	BOVINE	2
Histone H2A type 2-C	BOVINE	2

Nucleosome assembly protein 1-like 4	BOVINE	2
Eukaryotic translation initiation factor 2 subunit 2	BOVINE	2
Single-pass membrane protein with coiled-coil domains 3	BOVINE	2
Gap junction alpha-1 protein	BOVINE	2
Gamma-glutamyl hydrolase	BOVINE	2
Ras-related protein Rab-13	BOVINE	2
Ras-related protein Rab-3C	BOVINE	2
RAB2B, member RAS oncogene family	BOVINE	2
T-complex protein 1 subunit gamma	BOVINE	2
Vesicle-associated membrane protein 5	BOVINE	2
Cytochrome c1, heme protein, mitochondrial	BOVINE	2
Destrin	BOVINE	2
Protein-L-isoaspartate(D-aspartate) O-methyltransferase	BOVINE	2
Ras-related protein Rab-4A	BOVINE	2
T-complex protein 1 subunit eta	BOVINE	2
CTNNA2 protein	BOVINE	2
Caveolin-1	BOVINE	2
Ras homolog family member G	BOVINE	2
Nucleoside diphosphate kinase	BOVINE	2
RAB3D, member RAS oncogene family	BOVINE	2
Ras-related protein Rab-3A	BOVINE	2
Transforming protein RhoA	BOVINE	2
RAB35, member RAS oncogene family	BOVINE	2
Histone H3	BOVINE	1
Histone H3.3	BOVINE	1
Histone H3.2	BOVINE	1
Histone H3.1	BOVINE	1
Histone H3.3C	BOVINE	1
Eukaryotic translation initiation factor 2 subunit 3	BOVINE	1

NADH dehydrogenase [ubiquinone] 1 beta subcomplex subunit 11, mitochondrial	BOVINE	1
Annexin A8	BOVINE	1
IST1 homolog	BOVINE	1
Histone H2B	BOVINE	1
Histone H2B type 1	BOVINE	1
26S proteasome non-ATPase regulatory subunit 3	BOVINE	1
Cytochrome b-c1 complex subunit 8	BOVINE	1
G protein-coupled receptor class C group 5 member B	BOVINE	1
MAGE family member D2	BOVINE	1
MOB kinase activator 1A	BOVINE	1
MOB kinase activator 1B	BOVINE	1
Lens epithelial protein	BOVINE	1
Tubulin beta chain	BOVINE	1
Tubulin beta-2B chain	BOVINE	1
Tubulin beta-4A chain	BOVINE	1
Tubulin beta-4B chain	BOVINE	1
Tubulin beta-3 chain	BOVINE	1
Tubulin beta-5 chain	BOVINE	1
Tubulin beta-6 chain	BOVINE	1
Abhydrolase domain containing 15	BOVINE	1
Uridine phosphorylase	BOVINE	1
Solute carrier family 25 member 36	BOVINE	1
Solute carrier family 25 member 33	BOVINE	1
Transmembrane protein 30B	BOVINE	1
Cell cycle control protein 50A	BOVINE	1
Translation initiation factor eIF-2B subunit delta	BOVINE	1
Steroid 5 alpha-reductase 2	BOVINE	1
Kelch repeat and BTB domain containing 11	BOVINE	1
SMYD family member 5	BOVINE	1
Cytochrome c oxidase subunit 7A2, mitochondrial	BOVINE	1
Cytochrome c oxidase subunit 7A1, mitochondrial	BOVINE	1

Cytochrome c oxidase subunit 7B, mitochondrial	BOVINE	1
Proteolipid protein 2	BOVINE	1
Alcohol dehydrogenase class-3	BOVINE	1
2-iminobutanoate/2-iminopropanoate deaminase	BOVINE	1
Proteasome subunit beta type-5	BOVINE	1
ATP synthase subunit f, mitochondrial	BOVINE	1
Ras-related protein Rap-1A	BOVINE	1
Ras-related protein Rap-1b	BOVINE	1
Mitochondrial import inner membrane translocase subunit Tim23	BOVINE	1
Hemoglobin subunit alpha	BOVINE	1
NPC intracellular cholesterol transporter 1	BOVINE	1
Syntaxin-4	BOVINE	1
cAMP-dependent protein kinase catalytic subunit alpha	BOVINE	1
cAMP-dependent protein kinase catalytic subunit beta	BOVINE	1
Integrin beta-1	BOVINE	1
Nicastrin	BOVINE	1
AP-2 complex subunit sigma	BOVINE	1
Peroxiredoxin-4	BOVINE	1
Peroxiredoxin-1	BOVINE	1
Integrin alpha-2	BOVINE	1
Essential MCU regulator, mitochondrial	BOVINE	1
Erythrocyte membrane protein band 4.1 like 2	BOVINE	1
Secretory carrier-associated membrane protein 4	BOVINE	1
Ras-related protein Rab-21	BOVINE	1
Syntaxin 2	BOVINE	1
Trafficking protein particle complex subunit 6B	BOVINE	1
CD9 antigen	BOVINE	1
Fructosamine 3 kinase related protein	BOVINE	1
Regulator of microtubule dynamics protein 1	BOVINE	1

14-3-3 protein epsilon	BOVINE	1
Brain acid soluble protein 1	BOVINE	1
Inositol monophosphatase 1	BOVINE	1
Peptidyl-prolyl cis-trans isomerase A	BOVINE	1
Ubiquitin conjugating enzyme E2 O	BOVINE	1
Urea transporter 1	BOVINE	1
Beta-centractin	BOVINE	1
Ubiquitin-conjugating enzyme E2 variant 1	BOVINE	1
Ubiquitin-conjugating enzyme E2 variant 2	BOVINE	1
Heat shock cognate 71 kDa protein	BOVINE	1
Heat shock 70 kDa protein 1-like	BOVINE	1
Coactosin-like protein	BOVINE	1
Annexin A4	BOVINE	1
Multidrug resistance-associated protein 1	BOVINE	1
Cytochrome b-c1 complex subunit 9	BOVINE	1
Dynein assembly factor 1, axonemal	BOVINE	1
Major prion protein	BOVINE	1
Phosphoglucomutase-1	BOVINE	1
Mediator of RNA polymerase II transcription subunit 27	BOVINE	1
Prostaglandin-H2 D-isomerase	BOVINE	1
6-phosphogluconate dehydrogenase, decarboxylating	BOVINE	1
14-3-3 protein eta	BOVINE	1
14-3-3 protein beta/alpha	BOVINE	1
14-3-3 protein gamma	BOVINE	1
14-3-3 protein theta	BOVINE	1
14-3-3 protein sigma	BOVINE	1
TBC1 domain family member 1	BOVINE	1
DGCR14 protein	BOVINE	1

References

ABDELJALIL, J., HAMID, M., ABDEL-MOUTTALIB, O., STÉPHANE, R., RAYMOND, R., JOHAN, A., JOSÉ, S., PIERRE, C. & SERGE, P. 2005. The optomotor response: A robust first-line visual screening method for mice. *Vision Research,* 45**,** 1439-1446.

ABE, M., ITOH, M. T., MIYATA, M., SHIMIZU, K. & SUMI, Y. 2000. Circadian rhythm of serotonin N -acetyltransferase activity in rat lens. *Exp Eye Res,* 70**,** 805-8.

ABELSON, P. H. & KRUGER, P. G. 1949. Cyclotron-induced radiation cataracts. *Science,* 110**,** 655-7.

AHUJA, R. P., BORCHMAN, D., DEAN, W. L., PATERSON, C. A., ZENG, J., ZHANG, Z., FERGUSON-YANKEY, S. & YAPPERT, M. C. 1999. Effect of oxidation on Ca2+ -ATPase activity and membrane lipids in lens epithelial microsomes. *Free Radic Biol Med,* 27**,** 177-85.

AINSBURY, E. A., BARNARD, S., BRIGHT, S., DALKE, C., JARRIN, M., KUNZE, S., TANNER, R., DYNLACHT, J. R., QUINLAN, R. A., GRAW, J., KADHIM, M. & HAMADA, N. 2016. Ionizing radiation induced cataracts: Recent biological and mechanistic developments and perspectives for future research. *Mutat Res,* 770**,** 238-261.

AINSBURY, E. A., BOUFFLER, S. D., DORR, W., GRAW, J., MUIRHEAD, C. R., EDWARDS, A. A. & COOPER, J. 2009. Radiation cataractogenesis: a review of recent studies. *Radiat Res,* 172**,** 1-9.

ALBERT, R. E., OMRAN, A. R., BRAUER, E. W., COHEN, N. C., SCHMIDT, H., DOVE, D. C., BECKER, M., BAUMRING, R. & BAER, R. L. 1968. Follow-up study of patients treated by x-ray epilation for tinea capitis. II. Results of clinical and laboratory examinations. *Arch Environ Health,* 17**,** 919-34.

ALKOZI, H. A., FRANCO, R. & PINTOR, J. J. 2017. Epigenetics in the Eye: An Overview of the Most Relevant Ocular Diseases. *Front Genet,* 8**,** 144.

ALTER, A. J. & LEINFELDER, P. J. 1953. Roentgen-ray cataract; effects of shielding of the lens and ciliary body. *AMA Arch Ophthalmol,* 49**,** 257-60.

ARMAROLI, N. & BALZANI, V. 2007. The future of energy supply: Challenges and opportunities. *Angew Chem Int Ed Engl,* 46**,** 52-66.

ASSOCIATION, A. S. 2015. 2015 Alzheimer's disease facts and figures. *Alzheimers Dement,* 11**,** 332-84.

ATKINSON, J., HARROUN, T., WASSALL, S. R., STILLWELL, W. & KATSARAS, J. 2010. The location and behavior of alpha-tocopherol in membranes. *Mol Nutr Food Res,* 54**,** 641-51.

AUGUSTEYN, R. C. 2007. Growth of the human eye lens. *Mol Vis,* 13**,** 252-7.

AZIZOVA, T. V., BRAGIN, E. V., HAMADA, N. & BANNIKOVA, M. V. 2016. Risk of Cataract Incidence in a Cohort of Mayak PA Workers following Chronic Occupational Radiation Exposure. *PLoS One,* 11**,** e0164357.

AZIZOVA, T. V., DAY, R. D., WALD, N., MUIRHEAD, C. R., O'HAGAN, J. A., SUMINA, M. V., BELYAEVA, Z. D., DRUZHININA, M. B., TEPLYAKOV, II, SEMENIKHINA, N. G., STETSENKO, L. A., GRIGORYEVA, E. S., KRUPENINA, L. N. & VLASENKO, E. V. 2008. The "clinic" medical-dosimetric database of Mayak production association workers: structure, characteristics and prospects of utilization. *Health Phys,* 94**,** 449-58.

AZIZOVA, T. V., HAMADA, N., GRIGORYEVA, E. S. & BRAGIN, E. V. 2018. Risk of various types of cataracts in a cohort of Mayak workers following chronic occupational exposure to ionizing radiation. *Eur J Epidemiol,* 33**,** 1193-1204.

AZZAM, E. I., JAY-GERIN, J. P. & PAIN, D. 2012. Ionizing radiation-induced metabolic oxidative stress and prolonged cell injury. *Cancer Lett,* 327**,** 48-60.

BABIZHAYEV, M. A., DEYEV, A. I. & LINBERG, L. F. 1988. Lipid peroxidation as a possible cause of cataract. *Mech Ageing Dev,* 44**,** 69-89.
BANDO, M. & OBAZAWA, H. 1991. Regional and subcellular distribution of ascorbate free radical reductase activity in the human lens. *Tokai J Exp Clin Med,* 16**,** 217-22.
BARBIERI, S., BAIOCCO, G., BABINI, G., MORINI, J., FRIEDLAND, W., BUONANNO, M., GRILJ, V., BRENNER, D. J. & OTTOLENGHI, A. 2019. MODELLING gamma-H2AX FOCI INDUCTION TO MIMIC LIMITATIONS IN THE SCORING TECHNIQUE. *Radiat Prot Dosimetry,* 183**,** 121-125.
BARNARD, S. G. R., MCCARRON, R., MOQUET, J., QUINLAN, R. & AINSBURY, E. 2019. Inverse dose-rate effect of ionising radiation on residual 53BP1 foci in the eye lens. *Sci Rep,* 9**,** 10418.
BARNARD, S. G. R., MOQUET, J., LLOYD, S., ELLENDER, M., AINSBURY, E. A. & QUINLAN, R. A. 2018. Dotting the eyes: mouse strain dependency of the lens epithelium to low dose radiation-induced DNA damage. *Int J Radiat Biol,* 94**,** 1116-1124.
BARNES, S. & QUINLAN, R. A. 2017. Small molecules, both dietary and endogenous, influence the onset of lens cataracts. *Exp Eye Res,* 156**,** 87-94.
BASSNETT, S. 2002. Lens organelle degradation. *Exp Eye Res,* 74**,** 1-6.
BASSNETT, S. & BEEBE, D. C. 1992. Coincident loss of mitochondria and nuclei during lens fiber cell differentiation. *Dev Dyn,* 194**,** 85-93.
BASSNETT, S., SHI, Y. & VRENSEN, G. F. 2011. Biological glass: structural determinants of eye lens transparency. *Philos Trans R Soc Lond B Biol Sci,* 366**,** 1250-64.
BASSNETT, S., WILMARTH, P. A. & DAVID, L. L. 2009. The membrane proteome of the mouse lens fiber cell. *Mol Vis,* 15**,** 2448-63.
BAXTER, P. S. & HARDINGHAM, G. E. 2016. Adaptive regulation of the brain's antioxidant defences by neurons and astrocytes. *Free Radic Biol Med,* 100**,** 147-152.
BECK, H. R. 1982. [Comments on the recommendations of the International Commission on Radiological Protection (ICRP 26, 27) relating to the definition and comparability of risks of harm]. *Strahlenschutz Forsch Prax,* 23**,** 165-75.
BERRODIN, T. J., SHEN, Q., QUINET, E. M., YUDT, M. R., FREEDMAN, L. P. & NAGPAL, S. 2010. Identification of 5alpha, 6alpha-epoxycholesterol as a novel modulator of liver X receptor activity. *Mol Pharmacol,* 78**,** 1046-58.
BERTHOUD, V. M. & BEYER, E. C. 2009. Oxidative stress, lens gap junctions, and cataracts. *Antioxid Redox Signal,* 11**,** 339-53.
BHUYAN, K. C. & BHUYAN, D. K. 1978. Superoxide dismutase of the eye: relative functions of superoxide dismutase and catalase in protecting the ocular lens from oxidative damage. *Biochim Biophys Acta,* 542**,** 28-38.
BHUYAN, K. C. & BHUYAN, D. K. 1984. Molecular mechanism of cataractogenesis: III. Toxic metabolites of oxygen as initiators of lipid peroxidation and cataract. *Curr Eye Res,* 3**,** 67-81.
BHUYAN, K. C., BHUYAN, D. K. & PODOS, S. M. 1986a. Lipid peroxidation in cataract of the human. *Life Sci,* 38**,** 1463-71.
BHUYAN, K. C., MASTER, R. W., COLES, R. S. & BHUYAN, D. K. 1986b. Molecular mechanisms of cataractogenesis: IV. Evidence of phospholipid . malondialdehyde adduct in human senile cataract. *Mech Ageing Dev,* 34**,** 289-96.
BIRKELDH, U., DOMÍNGUEZ-VICENT, A., LAURELL, C. G., BRAUTASET, R. & NILSSON, M. 2015. Objective assessment of cataract: Comparison between the Lens Opacities Classification System III and a Scheimpflug camera. *Acta Ophthalmologica,* 93.
BJORKHEM, I. 2006. Crossing the barrier: oxysterols as cholesterol transporters and metabolic modulators in the brain. *J Intern Med,* 260**,** 493-508.
BJÖRKHEM, I. 2002. Do oxysterols control cholesterol homeostasis? *J Clin Invest,* 110**,** 725-30.
BJORKHEM, I., LUTJOHANN, D., DICZFALUSY, U., STAHLE, L., AHLBORG, G. & WAHREN, J. 1998. Cholesterol homeostasis in human brain: turnover of 24S-hydroxycholesterol and evidence for a cerebral origin of most of this oxysterol in the circulation. *J Lipid Res,* 39**,** 1594-600.

BLIGH, E. G. & DYER, W. J. 1959. A rapid method of total lipid extraction and purification. *Can J Biochem Physiol,* 37**,** 911-7.
BORCHMAN, D., STIMMELMAYR, R. & GEORGE, J. C. 2017. Whales, lifespan, phospholipids, and cataracts. *J Lipid Res,* 58**,** 2289-2298.
BORCHMAN, D. & TANG, D. 1996. Binding capacity of alpha-crystallin to bovine lens lipids. *Exp Eye Res,* 63**,** 407-10.
BORCHMAN, D. & YAPPERT, M. C. 1998. Age-related lipid oxidation in human lenses. *Invest Ophthalmol Vis Sci,* 39**,** 1053-8.
BORCHMAN, D. & YAPPERT, M. C. 2010. Lipids and the ocular lens. *J Lipid Res,* 51**,** 2473-88.
BORCHMAN, D., YAPPERT, M. C. & AFZAL, M. 2004. Lens lipids and maximum lifespan. *Exp Eye Res,* 79**,** 761-8.
BOSCIA, F., GRATTAGLIANO, I., VENDEMIALE, G., MICELLI-FERRARI, T. & ALTOMARE, E. 2000. Protein oxidation and lens opacity in humans. *Invest Ophthalmol Vis Sci,* 41**,** 2461-5.
BRAAKHUIS, A. J., DONALDSON, C. I., LIM, J. C. & DONALDSON, P. J. 2019. Nutritional Strategies to Prevent Lens Cataract: Current Status and Future Strategies. *Nutrients,* 11.
BRAMLET, R. 1978. Presence of americium-241 in many smoke detectors. *Clin Nucl Med,* 3**,** 416.
BRENNAN, L. A., MCGREAL, R. S. & KANTOROW, M. 2012. Oxidative stress defense and repair systems of the ocular lens. *Front Biosci (Elite Ed),* 4**,** 141-55.
BROOKS, S. W., DYKES, A. C. & SCHREURS, B. G. 2017. A High-Cholesterol Diet Increases 27-Hydroxycholesterol and Modifies Estrogen Receptor Expression and Neurodegeneration in Rabbit Hippocampus. *J Alzheimers Dis,* 56**,** 185-196.
BROWN, T. L., LEMAY JR., E. H., BURSTEN, B. E., MURPHY, C., WOODWARD, P., LANGFORD, S., SAGATYS, D. & GEORGE, A. 2013. Chemistry: The Central Science. *Pearson.*
BUETTNER, G. R. & JURKIEWICZ, B. A. 1996. Catalytic metals, ascorbate and free radicals: combinations to avoid. *Radiat Res,* 145**,** 532-41.
BUONANNO, M., DE TOLEDO, S. M., PAIN, D. & AZZAM, E. I. 2011. Long-term consequences of radiation-induced bystander effects depend on radiation quality and dose and correlate with oxidative stress. *Radiat Res,* 175**,** 405-15.
CABRERA, M. P. & CHIHUAILAF, R. H. 2011. Antioxidants and the integrity of ocular tissues. *Vet Med Int,* 2011**,** 905153.
CAHN, A. 1881. Zur physiologischen und pathologischen Chemie des Auges. *Zeitschrift für physiologische Chemie,* 5**,** 213-232.
CARNE, N. A., BELL, S., BROWN, A. P., MAATTA, A., FLAGLER, M. J. & BENHAM, A. M. 2019. Reductive Stress Selectively Disrupts Collagen Homeostasis and Modifies Growth Factor-independent Signaling Through the MAPK/Akt Pathway in Human Dermal Fibroblasts. *Mol Cell Proteomics,* 18**,** 1123-1137.
CENEDELLA, R. J. 1982. Sterol synthesis by the ocular lens of the rat during postnatal development. *J Lipid Res,* 23**,** 619-26.
CENEDELLA, R. J. 1983. Source of cholesterol for the ocular lens, studied with U18666A: a cataract-producing inhibitor of lipid metabolism. *Exp Eye Res,* 37**,** 33-43.
CENEDELLA, R. J. 2009. Cholesterol synthesis inhibitor U18666A and the role of sterol metabolism and trafficking in numerous pathophysiological processes. *Lipids,* 44**,** 477-87.
CHALUPECKY, H. 1897. Ueber die wirkung der Roentgenstrahlen. *Centralblatt fuer praktische Augenheilkunde,* 21**,** 386–401.
CHANG, P. Y., BJORNSTAD, K. A., ROSEN, C. J., LIN, S. & BLAKELY, E. A. 2007. Particle radiation alters expression of matrix metalloproteases resulting in ECM remodeling in human lens cells. *Radiation and Environmental Biophysics,* 46**,** 187-194.
CHARLES, M. 2001. UNSCEAR report 2000: sources and effects of ionizing radiation. United Nations Scientific Comittee on the Effects of Atomic Radiation. *J Radiol Prot,* 21**,** 83-6.
CHELIKANI, P., FITA, I. & LOEWEN, P. C. 2004. Diversity of structures and properties among catalases. *Cell Mol Life Sci,* 61**,** 192-208.

CHEN, W., CHEN, G., HEAD, D. L., MANGELSDORF, D. J. & RUSSELL, D. W. 2007. Enzymatic reduction of oxysterols impairs LXR signaling in cultured cells and the livers of mice. *Cell Metab,* 5**,** 73-9.

CHODICK, G., BEKIROGLU, N., HAUPTMANN, M., ALEXANDER, B. H., FREEDMAN, D. M., DOODY, M. M., CHEUNG, L. C., SIMON, S. L., WEINSTOCK, R. M., BOUVILLE, A. & SIGURDSON, A. J. 2008. Risk of cataract after exposure to low doses of ionizing radiation: a 20-year prospective cohort study among US radiologic technologists. *Am J Epidemiol,* 168**,** 620-31.

CHODICK, G., SIGURDSON, A. J., KLEINERMAN, R. A., SKLAR, C. A., LEISENRING, W., MERTENS, A. C., STOVALL, M., SMITH, S. A., WEATHERS, R. E., VEIGA, L. H., ROBISON, L. L. & INSKIP, P. D. 2016. The Risk of Cataract among Survivors of Childhood and Adolescent Cancer: A Report from the Childhood Cancer Survivor Study. *Radiat Res,* 185**,** 366-74.

CHOSHI, K., TAKAKU, I., MISHIMA, H., TAKASE, T., NERIISHI, S., FINCH, S. C. & OTAKE, M. 1983. Ophthalmologic changes related to radiation exposure and age in adult health study sample, Hiroshima and Nagasaki. *Radiat Res,* 96**,** 560-79.

CHRISTEN, W. G., GLYNN, R. J., GAZIANO, J. M., DARKE, A. K., CROWLEY, J. J., GOODMAN, P. J., LIPPMAN, S. M., LAD, T. E., BEARDEN, J. D., GOODMAN, G. E., MINASIAN, L. M., THOMPSON, I. M., JR., BLANKE, C. D. & KLEIN, E. A. 2015. Age-related cataract in men in the selenium and vitamin e cancer prevention trial eye endpoints study: a randomized clinical trial. *JAMA Ophthalmol,* 133**,** 17-24.

CHUMAK, V. V., WORGUL, B. V., KUNDIYEV, Y. I., SERGIYENKO, N. M., VITTE, P. M., MEDVEDOVSKY, C., BAKHANOVA, E. V., JUNK, A. K., KYRYCHENKO, O. Y., MUSIJACHENKO, N. V., SHOLOM, S. V., SHYLO, S. A., VITTE, O. P., XU, S., XUE, X. & SHORE, R. E. 2007. Dosimetry for a study of low-dose radiation cataracts among Chernobyl clean-up workers. *Radiat Res,* 167**,** 606-14.

CHYLACK, L. T., JR., PETERSON, L. E., FEIVESON, A. H., WEAR, M. L., MANUEL, F. K., TUNG, W. H., HARDY, D. S., MARAK, L. J. & CUCINOTTA, F. A. 2009. NASA study of cataract in astronauts (NASCA). Report 1: Cross-sectional study of the relationship of exposure to space radiation and risk of lens opacity. *Radiat Res,* 172**,** 10-20.

CLARK, J. I., MATSUSHIMA, H., DAVID, L. L. & CLARK, J. M. 1999. Lens cytoskeleton and transparency: a model. *Eye (Lond),* 13 (Pt 3b)**,** 417-24.

CLEMENT, S., VELASCO, P. T., MURTHY, S. N., WILSON, J. H., LUKAS, T. J., GOLDMAN, R. D. & LORAND, L. 1998. The intermediate filament protein, vimentin, in the lens is a target for cross-linking by transglutaminase. *J Biol Chem,* 273**,** 7604-9.

CLUTTON, S. M., TOWNSEND, K. M., WALKER, C., ANSELL, J. D. & WRIGHT, E. G. 1996. Radiation-induced genomic instability and persisting oxidative stress in primary bone marrow cultures. *Carcinogenesis,* 17**,** 1633-9.

COBLEY, J. N., FIORELLO, M. L. & BAILEY, D. M. 2018. 13 reasons why the brain is susceptible to oxidative stress. *Redox Biol,* 15**,** 490-503.

COGAN, D. G., DONALDSON, D. D. & REESE, A. B. 1952. Clinical and pathological characteristics of radiation cataract. *AMA Arch Ophthalmol,* 47**,** 55-70.

COGAN, D. G., MARTIN, S. F. & KIMURA, S. J. 1949. Atom bomb cataracts. *Science,* 110**,** 654.

CONSUL, B. N. & NAGPAL, P. N. 1968. Quantitative study of the variations in the levels of glutathione and ascorbic acid in human lenses with senile cataract. *Eye Ear Nose Throat Mon,* 47**,** 336-9.

COTLIER, E. & RICE, P. 1971. Cataracts in the Smith-Lemli-Opitz syndrome. *Am J Ophthalmol,* 72**,** 955-9.

COURNIL, A. & KIRKWOOD, T. B. 2001. If you would live long, choose your parents well. *Trends Genet,* 17**,** 233-5.

CSISZAR, A., PODLUTSKY, A., WOLIN, M. S., LOSONCZY, G., PACHER, P. & UNGVARI, Z. 2009. Oxidative stress and accelerated vascular aging: implications for cigarette smoking. *Front Biosci (Landmark Ed),* 14**,** 3128-44.

CUCINOTTA, F. A., MANUEL, F. K., JONES, J., ISZARD, G., MURREY, J., DJOJONEGRO, B. & WEAR, M. 2001. Space radiation and cataracts in astronauts. *Radiat Res,* 156**,** 460-6.

DALKE, C., NEFF, F., BAINS, S. K., BRIGHT, S., LORD, D., REITMEIR, P., RÖßLER, U., SAMAGA, D., UNGER, K., BRASELMANN, H., WAGNER, F., GREITER, M., GOMOLKA, M., HORNHARDT, S., KUNZE, S., KEMPF, S. J., GARRETT, L., HÖLTER, S. M., WURST, W., ROSEMANN, M., AZIMZADEH, O., TAPIO, S., AUBELE, M., THEIS, F., HOESCHEN, C., SLIJEPCEVIC, P., KADHIM, M., ATKINSON, M., ZITZELSBERGER, H., KULKA, U. & GRAW, J. 2018. Lifetime study in mice after acute low-dose ionizing radiation: a multifactorial study with special focus on cataract risk. *Radiat Environ Biophys,* 57**,** 99-113.

DARLEY-USMAR, V. M., HOGG, N., O'LEARY, V. J., WILSON, M. T. & MONCADA, S. 1992. The simultaneous generation of superoxide and nitric oxide can initiate lipid peroxidation in human low density lipoprotein. *Free Radic Res Commun,* 17**,** 9-20.

DARWIN, C. 1859. *On the Origin of Species by Means of Natural Selection,* London.

DAVIS, J. G., WAN, X. S., WARE, J. H. & KENNEDY, A. R. 2010. Dietary supplements reduce the cataractogenic potential of proton and HZE-particle radiation in mice. *Radiat Res,* 173**,** 353-61.

DAVSON, H. 1954. Nutrition of the lens by way of aqueous humour. *J Physiol,* 124**,** 42-3p.

DAWES, L. J., DUNCAN, G. & WORMSTONE, I. M. 2013. Age-related differences in signaling efficiency of human lens cells underpin differential wound healing response rates following cataract surgery. *Invest Ophthalmol Vis Sci,* 54**,** 333-42.

DAYSPRING, T. D., VARVEL, S. A., GHAEDI, L., THISELTON, D. L., BRUTON, J. & MCCONNELL, J. P. 2015. Biomarkers of cholesterol homeostasis in a clinical laboratory database sample comprising 667,718 patients. *J Clin Lipidol,* 9**,** 807-816.

DE MAIO, A., CAUVI, D. M., CAPONE, R., BELLO, I., EGBERTS, W. V., ARISPE, N. & BOELENS, W. 2019. The small heat shock proteins, HSPB1 and HSPB5, interact differently with lipid membranes. *Cell Stress Chaperones,* 24**,** 947-956.

DE STEFANO, I., TANNO, B., GIARDULLO, P., LEONARDI, S., PASQUALI, E., ANTONELLI, F., TANORI, M., CASCIATI, A., PAZZAGLIA, S., SARAN, A. & MANCUSO, M. 2015. The Patched 1 tumor-suppressor gene protects the mouse lens from spontaneous and radiation-induced cataract. *Am J Pathol,* 185**,** 85-95.

DE VRIES, A. C., VERMEER, M. A., HENDRIKS, A. L., BLOEMENDAL, H. & COHEN, L. H. 1991. Biosynthetic capacity of the human lens upon aging. *Exp Eye Res,* 53**,** 519-24.

DEELEY, J. M., MITCHELL, T. W., WEI, X., KORTH, J., NEALON, J. R., BLANKSBY, S. J. & TRUSCOTT, R. J. 2008. Human lens lipids differ markedly from those of commonly used experimental animals. *Biochim Biophys Acta,* 1781**,** 288-98.

DEGANI, G., ALTOMARE, A. A., COLZANI, M., MARTINO, C., MAZZOLARI, A., FRITZ, G., VISTOLI, G., POPOLO, L. & ALDINI, G. 2017. A capture method based on the VC1 domain reveals new binding properties of the human receptor for advanced glycation end products (RAGE). *Redox Biol,* 11**,** 275-285.

DELAYE, M. & TARDIEU, A. 1983. Short-range order of crystallin proteins accounts for eye lens transparency. *Nature,* 302**,** 415-7.

DENNIS, E. A. 2015. Introduction to Thematic Review Series: Phospholipases: Central Role in Lipid Signaling and Disease. *J Lipid Res,* 56**,** 1245-7.

DIAS, I. H., BORAH, K., AMIN, B., GRIFFITHS, H. R., SASSI, K., LIZARD, G., IRIONDO, A. & MARTINEZ-LAGE, P. 2019. Localisation of oxysterols at the sub-cellular level and in biological fluids. *J Steroid Biochem Mol Biol,* 193**,** 105426.

DICKSON, D. W., CRYSTAL, H. A., BEVONA, C., HONER, W., VINCENT, I. & DAVIES, P. 1995. Correlations of synaptic and pathological markers with cognition of the elderly. *Neurobiol Aging,* 16**,** 285-98; discussion 298-304.

DIETSCHY, J. M. 2009. Central nervous system: cholesterol turnover, brain development and neurodegeneration. *Biol Chem,* 390**,** 287-93.

DIETSCHY, J. M. & TURLEY, S. D. 2004. Thematic review series: brain Lipids. Cholesterol metabolism in the central nervous system during early development and in the mature animal. *J Lipid Res,* 45**,** 1375-97.

DO, K. H. 2016. General Principles of Radiation Protection in Fields of Diagnostic Medical Exposure. *J Korean Med Sci,* 31 Suppl 1**,** S6-9.

DONALDSON, P., KISTLER, J. & MATHIAS, R. T. 2001. Molecular solutions to mammalian lens transparency. *News Physiol Sci,* 16**,** 118-23.

DONALDSON, P. J., CHEE, K. S., LIM, J. C. & WEBB, K. F. 2009. Regulation of lens volume: implications for lens transparency. *Exp Eye Res,* 88**,** 144-50.

DONALDSON, P. J., GREY, A. C., MACEO HEILMAN, B., LIM, J. C. & VAGHEFI, E. 2017. The physiological optics of the lens. *Prog Retin Eye Res,* 56**,** e1-e24.

DOVRAT, A., SCHARF, J. & GERSHON, D. 1984. Glyceraldehyde 3-phosphate dehydrogenase activity in rat and human lenses and the fate of enzyme molecules in the aging lens. *Mech Ageing Dev,* 28**,** 187-91.

DRESSMAN, H. K., MURAMOTO, G. G., CHAO, N. J., MEADOWS, S., MARSHALL, D., GINSBURG, G. S., NEVINS, J. R. & CHUTE, J. P. 2007. Gene expression signatures that predict radiation exposure in mice and humans. *PLoS Med,* 4**,** e106.

DU, J. & GEBICKI, J. M. 2004. Proteins are major initial cell targets of hydroxyl free radicals. *Int J Biochem Cell Biol,* 36**,** 2334-43.

DUTTA, S. & SENGUPTA, P. 2016. Men and mice: Relating their ages. *Life Sci,* 152**,** 244-8.

ECHEVARRIA, F., NORTON, R. A., NES, W. D. & LANGE, Y. 1990. Zymosterol is located in the plasma membrane of cultured human fibroblasts. *J Biol Chem,* 265**,** 8484-9.

EDWARDS, A. A. & LLOYD, D. C. 1998. Risks from ionising radiation: deterministic effects. *J Radiol Prot,* 18**,** 175-83.

EGGERSDORFER, M. & WYSS, A. 2018. Carotenoids in human nutrition and health. *Arch Biochem Biophys,* 652**,** 18-26.

ELDRED, J. A., DAWES, L. J. & WORMSTONE, I. M. 2011. The lens as a model for fibrotic disease. *Philos Trans R Soc Lond B Biol Sci,* 366**,** 1301-19.

EVANS, D. G., LADUSANS, E. J., RIMMER, S., BURNELL, L. D., THAKKER, N. & FARNDON, P. A. 1993. Complications of the naevoid basal cell carcinoma syndrome: results of a population based study. *J Med Genet,* 30**,** 460-4.

FELDMAN, G. L. & FELDMAN, L. S. 1965. NEW CONCEPTS OF HUMAN LENTICULAR LIPIDS AND THEIR POSSIBLE ROLE IN CATARACTS. *Invest Ophthalmol,* 4**,** 162-6.

FERGUSON, S. R., BORCHMAN, D. & YAPPERT, M. C. 1996. Confirmation of the identity of the major phospholipid in human lens membranes. *Invest Ophthalmol Vis Sci,* 37**,** 1703-6.

FERREIRA, S. T., LOURENCO, M. V., OLIVEIRA, M. M. & DE FELICE, F. G. 2015. Soluble amyloid-beta oligomers as synaptotoxins leading to cognitive impairment in Alzheimer's disease. *Front Cell Neurosci,* 9**,** 191.

FOX, J. G., BARTHOLD, S. W., DAVISSON, M. T., NEWCOMER, C. E., QUIMBY, F. W. & SMITH, A. L. 2007. The Mouse in Biomedical Research. *Elsevier Inc.*

FRAGA, M. F., BALLESTAR, E., PAZ, M. F., ROPERO, S., SETIEN, F., BALLESTAR, M. L., HEINE-SUNER, D., CIGUDOSA, J. C., URIOSTE, M., BENITEZ, J., BOIX-CHORNET, M., SANCHEZ-AGUILERA, A., LING, C., CARLSSON, E., POULSEN, P., VAAG, A., STEPHAN, Z., SPECTOR, T. D., WU, Y. Z., PLASS, C. & ESTELLER, M. 2005. Epigenetic differences arise during the lifetime of monozygotic twins. *Proc Natl Acad Sci U S A,* 102**,** 10604-9.

FRANKE, S., DAWCZYNSKI, J., STROBEL, J., NIWA, T., STAHL, P. & STEIN, G. 2003. Increased levels of advanced glycation end products in human cataractous lenses. *J Cataract Refract Surg,* 29**,** 998-1004.

FUJII, N., HIROKI, K., MATSUMOTO, S., MASUDA, K., INOUE, M., TANAKA, Y., AWAKURA, M. & AKABOSHI, M. 2001. Correlation between the loss of the chaperone-like activity and the oxidation, isomerization and racemization of gamma-irradiated alpha-crystallin. *Photochem Photobiol,* 74**,** 477-82.

FUJII, N., SAKAUE, H., SASAKI, H. & FUJII, N. 2012. A rapid, comprehensive liquid chromatography-mass spectrometry (LC-MS)-based survey of the Asp isomers in crystallins from human cataract lenses. *J Biol Chem,* 287**,** 39992-40002.

FUJII, N., TAKATA, T., FUJII, N., AKI, K. & SAKAUE, H. 2018. D-Amino acids in protein: The mirror of life as a molecular index of aging. *Biochim Biophys Acta Proteins Proteom,* 1866**,** 840-847.

FUJII, N., UCHIDA, H. & SAITO, T. 2004. The damaging effect of UV-C irradiation on lens alpha-crystallin. *Mol Vis,* 10**,** 814-20.

FUKUTSU, K., KASE, S., ISHIJIMA, K., KINOSHITA, R. & ISHIDA, S. 2018. The clinical features of radiation cataract in patients with ocular adnexal mucosa-associated lymphoid tissue lymphoma. *Radiat Oncol,* 13**,** 95.

FUSS, J. O. & TAINER, J. A. 2011. XPB and XPD helicases in TFIIH orchestrate DNA duplex opening and damage verification to coordinate repair with transcription and cell cycle via CAK kinase. *DNA Repair (Amst),* 10**,** 697-713.

GAMBA, P., STAURENGHI, E., TESTA, G., GIANNELLI, S., SOTTERO, B. & LEONARDUZZI, G. 2019. A Crosstalk Between Brain Cholesterol Oxidation and Glucose Metabolism in Alzheimer's Disease. *Front Neurosci,* 13**,** 556.

GAMBA, P., TESTA, G., GARGIULO, S., STAURENGHI, E., POLI, G. & LEONARDUZZI, G. 2015. Oxidized cholesterol as the driving force behind the development of Alzheimer's disease. *Front Aging Neurosci,* 7**,** 119.

GARNER, M. H. & SPECTOR, A. 1980. Selective oxidation of cysteine and methionine in normal and senile cataractous lenses. *Proc Natl Acad Sci U S A,* 77**,** 1274-7.

GEYER, D. D., SPENCE, M. A., JOHANNES, M., FLODMAN, P., CLANCY, K. P., BERRY, R., SPARKES, R. S., JONSEN, M. D., ISENBERG, S. J. & BATEMAN, J. B. 2006. Novel single-base deletional mutation in major intrinsic protein (MIP) in autosomal dominant cataract. *Am J Ophthalmol,* 141**,** 761-3.

GHANDHI, S. A., SMILENOV, L., SHURYAK, I., PUJOL-CANADELL, M. & AMUNDSON, S. A. 2019. Discordant gene responses to radiation in humans and mice and the role of hematopoietically humanized mice in the search for radiation biomarkers. *Scientific Reports,* 9**,** 19434.

GIBLIN, F. J. 2000. Glutathione: a vital lens antioxidant. *J Ocul Pharmacol Ther,* 16**,** 121-35.

GIBLIN, F. J., HIGHTOWER, K. R., RAGATZKI, P. A. & REDDY, V. N. 1984. Calcium-induced high molecular weight proteins in the intact rabbit lens. *Exp Eye Res,* 39**,** 9-17.

GIBLIN, F. J., LEVERENZ, V. R., PADGAONKAR, V. A., UNAKAR, N. J., DANG, L., LIN, L. R., LOU, M. F., REDDY, V. N., BORCHMAN, D. & DILLON, J. P. 2002. UVA light in vivo reaches the nucleus of the guinea pig lens and produces deleterious, oxidative effects. *Exp Eye Res,* 75**,** 445-58.

GILBERT, E. S. 2009. The impact of dosimetry uncertainties on dose-response analyses. *Health Phys,* 97**,** 487-92.

GIRAO, H., MOTA, C. & PEREIRA, P. 1999. Cholesterol may act as an antioxidant in lens membranes. *Curr Eye Res,* 18**,** 448-54.

GIRAO, H., MOTA, M. C., RAMALHO, J. & PEREIRA, P. 1998. Cholesterol oxides accumulate in human cataracts. *Exp Eye Res,* 66**,** 645-52.

GIRAO, H., SHANG, F. & PEREIRA, P. 2003. 7-ketocholesterol stimulates differentiation of lens epithelial cells. *Mol Vis,* 9**,** 497-501.

GIROTTI, A. W. & KORYTOWSKI, W. 2000. Cholesterol as a singlet oxygen detector in biological systems. *Methods Enzymol,* 319**,** 85-100.

GLASSER, A. & CAMPBELL, M. C. 1998. Presbyopia and the optical changes in the human crystalline lens with age. *Vision Res,* 38**,** 209-29.

GOLD, M. G., REICHOW, S. L., O'NEILL, S. E., WEISBROD, C. R., LANGEBERG, L. K., BRUCE, J. E., GONEN, T. & SCOTT, J. D. 2012. AKAP2 anchors PKA with aquaporin-0 to support ocular lens transparency. *EMBO Mol Med,* 4**,** 15-26.

GOLDMANN, H. & LIECHTI, A. 1938. Experimentelle untersuchungen über die genese des röntgenstars. *Albrecht von Graefes Arch Ophthalmol* 138**,** 722–736.

GORALSKA, M., FERRELL, J., HARNED, J., LALL, M., NAGAR, S., FLEISHER, L. N. & MCGAHAN, M. C. 2009. Iron metabolism in the eye: a review. *Exp Eye Res,* 88**,** 204-15.
GORFINE, T. & ZISAPEL, N. 2007. Melatonin and the human hippocampus, a time dependent interplay. *J Pineal Res,* 43**,** 80-6.
GRAUPNER, A., EIDE, D. M., BREDE, D. A., ELLENDER, M., LINDBO HANSEN, E., OUGHTON, D. H., BOUFFLER, S. D., BRUNBORG, G. & OLSEN, A. K. 2017. Genotoxic effects of high dose rate X-ray and low dose rate gamma radiation in Apc(Min/+) mice. *Environ Mol Mutagen,* 58**,** 560-569.
GRAW, J. 2004. Congenital hereditary cataracts. *Int J Dev Biol,* 48**,** 1031-44.
GRAW, J. 2009. Genetics of crystallins: cataract and beyond. *Exp Eye Res,* 88**,** 173-89.
GREY, A. C. & SCHEY, K. L. 2009. Age-related changes in the spatial distribution of human lens alpha-crystallin products by MALDI imaging mass spectrometry. *Invest Ophthalmol Vis Sci,* 50**,** 4319-29.
GRIFFITHS, W. J., ABDEL-KHALIK, J., HEARN, T., YUTUC, E., MORGAN, A. H. & WANG, Y. 2016. Current trends in oxysterol research. *Biochem Soc Trans,* 44**,** 652-8.
GU, F., ZHAI, H., LI, D., ZHAO, L., LI, C., HUANG, S. & MA, X. 2007. A novel mutation in major intrinsic protein of the lens gene (MIP) underlies autosomal dominant cataract in a Chinese family. *Mol Vis,* 13**,** 1651-6.
GUGGENMOOS-HOLZMANN, I., ENGEL, B., HENKE, V. & NAUMANN, G. O. 1989. Cell density of human lens epithelium in women higher than in men. *Invest Ophthalmol Vis Sci,* 30**,** 330-2.
HAINES, D. D., JUHASZ, B. & TOSAKI, A. 2013. Management of multicellular senescence and oxidative stress. *Journal of Cellular and Molecular Medicine,* 17**,** 936-957.
HALL, E. J. & GIACCIA, A. J. 1973. Radiobiology for the Radiologist. *Lippincott Williams & Wilkins***,** 576.
HALL, P., GRANATH, F., LUNDELL, M., OLSSON, K. & HOLM, L. E. 1999. Lenticular opacities in individuals exposed to ionizing radiation in infancy. *Radiat Res,* 152**,** 190-5.
HALLIWELL, B. 2006. Oxidative stress and neurodegeneration: where are we now? *J Neurochem,* 97**,** 1634-58.
HALLIWELL, B. & GUTTERIDGE, J. M. 1986. Oxygen free radicals and iron in relation to biology and medicine: some problems and concepts. *Arch Biochem Biophys,* 246**,** 501-14.
HAMADA, N. 2017. Ionizing radiation response of primary normal human lens epithelial cells. *PLoS One,* 12**,** e0181530.
HAMADA, N., AZIZOVA, T. V. & LITTLE, M. P. 2019. An update on effects of ionizing radiation exposure on the eye. *Br J Radiol***,** 20190829.
HAMADA, N. & FUJIMICHI, Y. 2014. Classification of radiation effects for dose limitation purposes: history, current situation and future prospects. *J Radiat Res,* 55**,** 629-40.
HAMADA, N. & FUJIMICHI, Y. 2015. Role of carcinogenesis related mechanisms in cataractogenesis and its implications for ionizing radiation cataractogenesis. *Cancer Lett,* 368**,** 262-74.
HAMADA, N., FUJIMICHI, Y., IWASAKI, T., FUJII, N., FURUHASHI, M., KUBO, E., MINAMINO, T., NOMURA, T. & SATO, H. 2014. Emerging issues in radiogenic cataracts and cardiovascular disease. *J Radiat Res,* 55**,** 831-46.
HAMADA, N., MAEDA, M., OTSUKA, K. & TOMITA, M. 2011. Signaling pathways underpinning the manifestations of ionizing radiation-induced bystander effects. *Curr Mol Pharmacol,* 4**,** 79-95.
HAMILTON, W. J. 1949. Early stages of human development. *Ann R Coll Surg Engl,* 4**,** 281-94.
HAN, J. & SCHEY, K. L. 2004. Proteolysis and mass spectrometric analysis of an integral membrane: aquaporin 0. *J Proteome Res,* 3**,** 807-12.
HANNA, C. & O'BRIEN, J. E. 1963. Lens epithelial cell proliferation and migration in radiation cataracts. *Radiat Res,* 19**,** 1-11.
HARDY, J. A. & HIGGINS, G. A. 1992. Alzheimer's disease: the amyloid cascade hypothesis. *Science,* 256**,** 184-5.
HARRELL, C. R., DJONOV, V., FELLABAUM, C. & VOLAREVIC, V. 2018. Risks of Using Sterilization by Gamma Radiation: The Other Side of the Coin. *Int J Med Sci,* 15**,** 274-279.

HARRISON, J. D. & STATHER, J. W. 1996. The assessment of doses and effects from intakes of radioactive particles. *J Anat,* 189 (Pt 3)**,** 521-30.
HASCALOVICI, J. R., VAYA, J., KHATIB, S., HOLCROFT, C. A., ZUKOR, H., SONG, W., ARVANITAKIS, Z., BENNETT, D. A. & SCHIPPER, H. M. 2009. Brain sterol dysregulation in sporadic AD and MCI: relationship to heme oxygenase-1. *J Neurochem,* 110**,** 1241-53.
HAYDEN, J. H., ROTHSTEIN, H., WORGUL, B. V. & MERRIAM, G. R., JR. 1980. Hypophysectomy exerts a radioprotective effect on frog lens. *Experientia,* 36**,** 116-8.
HELBIG, H., HINZ, J. P., KELLNER, U. & FOERSTER, M. H. 1993. Oxygen in the anterior chamber of the human eye. *Ger J Ophthalmol,* 2**,** 161-4.
HENDERSON, M. A., VALLURI, S., DESROSIERS, C., LOPEZ, J. T., BATUELLO, C. N., CAPERELL-GRANT, A., MENDONCA, M. S., POWERS, E. M., BIGSBY, R. M. & DYNLACHT, J. R. 2009. Effect of gender on radiation-induced cataractogenesis. *Radiat Res,* 172**,** 129-33.
HERUYE, S. H., MAFFOFOU NKENYI, L. N., SINGH, N. U., YALZADEH, D., NGELE, K. K., NJIE-MBYE, Y. F., OHIA, S. E. & OPERE, C. A. 2020. Current Trends in the Pharmacotherapy of Cataracts. *Pharmaceuticals (Basel),* 13.
HERZ, J. & FARESE, R. V., JR. 1999. The LDL receptor gene family, apolipoprotein B and cholesterol in embryonic development. *J Nutr,* 129**,** 473s-475s.
HEYWORTH, P., THOMPSON, G. M., TABANDEH, H. & MCGUIGAN, S. 1993. The relationship between clinical classification of cataract and lens hardness. *Eye (Lond),* 7 (Pt 6)**,** 726-30.
HOEHENWARTER, W., KLOSE, J. & JUNGBLUT, P. R. 2006. Eye lens proteomics. *Amino Acids,* 30**,** 369-89.
HOGLINGER, D., BURGOYNE, T., SANCHEZ-HERAS, E., HARTWIG, P., COLACO, A., NEWTON, J., FUTTER, C. E., SPIEGEL, S., PLATT, F. M. & EDEN, E. R. 2019. NPC1 regulates ER contacts with endocytic organelles to mediate cholesterol egress. *Nat Commun,* 10**,** 4276.
HOLEKAMP, N. M., SHUI, Y. B. & BEEBE, D. C. 2005. Vitrectomy surgery increases oxygen exposure to the lens: a possible mechanism for nuclear cataract formation. *Am J Ophthalmol,* 139**,** 302-10.
HOLM, T., BRØGGER-JENSEN, M. R., JOHNSON, L. & KESSEL, L. 2013. Glutathione preservation during storage of rat lenses in optisol-GS and castor oil. *PLoS One,* 8**,** e79620.
HOOI, M. Y. & TRUSCOTT, R. J. 2011. Racemisation and human cataract. D-Ser, D-Asp/Asn and D-Thr are higher in the lifelong proteins of cataract lenses than in age-matched normal lenses. *Age (Dordr),* 33**,** 131-41.
HORWITZ, J. 1992. Alpha-crystallin can function as a molecular chaperone. *Proc Natl Acad Sci U S A,* 89**,** 10449-53.
HORWITZ, J., BOVA, M. P., DING, L. L., HALEY, D. A. & STEWART, P. L. 1999. Lens alpha-crystallin: function and structure. *Eye (Lond),* 13 (Pt 3b)**,** 403-8.
HUANG, L., GRAMI, V., MARRERO, Y., TANG, D., YAPPERT, M. C., RASI, V. & BORCHMAN, D. 2005. Human lens phospholipid changes with age and cataract. *Invest Ophthalmol Vis Sci,* 46**,** 1682-9.
HUANG, Q., DING, L., PHAN, K. B., CHENG, C., XIA, C. H., GONG, X. & HORWITZ, J. 2009. Mechanism of cataract formation in alphaA-crystallin Y118D mutation. *Invest Ophthalmol Vis Sci,* 50**,** 2919-26.
HUGHES, J. R., DEELEY, J. M., BLANKSBY, S. J., LEISCH, F., ELLIS, S. R., TRUSCOTT, R. J. & MITCHELL, T. W. 2012. Instability of the cellular lipidome with age. *Age (Dordr),* 34**,** 935-47.
HUGHES, J. R., LEVCHENKO, V. A., BLANKSBY, S. J., MITCHELL, T. W., WILLIAMS, A. & TRUSCOTT, R. J. 2015. No turnover in lens lipids for the entire human lifespan. *Elife,* 4.
HULBERT, A. J. 2008. The links between membrane composition, metabolic rate and lifespan. *Comp Biochem Physiol A Mol Integr Physiol,* 150**,** 196-203.

ICRP 1955. RECOMMENDATIONS of the International Commission on Radiological Protection; revised December 1, 1954. *Br J Radiol,* Suppl. 6**,** 1-92.
ICRP 1991. 1990 Recommendations of the International Commission on Radiological Protection. *Ann ICRP,* 21**,** 1-201.
ICRP 2007. The 2007 Recommendations of the International Commission on Radiological Protection. ICRP publication 103. *Ann ICRP,* 37**,** 1-332.
INSTITUTE-OF-MEDICINE 1996. *Radiation In Medicine: A Need For Regulatory Reform,* Washington, National Academy of Sciences.
IULIANO, L. 2011. Pathways of cholesterol oxidation via non-enzymatic mechanisms. *Chem Phys Lipids,* 164**,** 457-68.
JACOB, R. F., CENEDELLA, R. J. & MASON, R. P. 2001. Evidence for distinct cholesterol domains in fiber cell membranes from cataractous human lenses. *J Biol Chem,* 276**,** 13573-8.
JACOB, S., BOVEDA, S., BAR, O., BREZIN, A., MACCIA, C., LAURIER, D. & BERNIER, M. O. 2013. Interventional cardiologists and risk of radiation-induced cataract: results of a French multicenter observational study. *Int J Cardiol,* 167**,** 1843-7.
JACOBSEN, E. M., DAVIS, A. K. & ALPEN, E. L. 1958. Effect of fractionation of beta irradiation on rat skin. *Radiat Res,* 9**,** 358-68.
JANOWSKI, B. A., WILLY, P. J., DEVI, T. R., FALCK, J. R. & MANGELSDORF, D. J. 1996. An oxysterol signalling pathway mediated by the nuclear receptor LXR alpha. *Nature,* 383**,** 728-31.
JEITNER, T. M., VOLOSHYNA, I. & REISS, A. B. 2011. Oxysterol derivatives of cholesterol in neurodegenerative disorders. *Curr Med Chem,* 18**,** 1515-25.
JIANG, J. & HUI, C. C. 2008. Hedgehog signaling in development and cancer. *Dev Cell,* 15**,** 801-12.
JIN, H., RANDAZZO, J., ZHANG, P. & KADOR, P. F. 2010. Multifunctional antioxidants for the treatment of age-related diseases. *J Med Chem,* 53**,** 1117-27.
JOHNSON, W. J., FISCHER, R. T., PHILLIPS, M. C. & ROTHBLAT, G. H. 1995. Efflux of newly synthesized cholesterol and biosynthetic sterol intermediates from cells. Dependence on acceptor type and on enrichment of cells with cholesterol. *J Biol Chem,* 270**,** 25037-46.
JONES, J. A., MCCARTEN, M., MANUEL, K., DJOJONEGORO, B., MURRAY, J., FEIVERSEN, A. & WEAR, M. 2007. Cataract formation mechanisms and risk in aviation and space crews. *Aviat Space Environ Med,* 78**,** A56-66.
JOSEPH, S. B., MCKILLIGIN, E., PEI, L., WATSON, M. A., COLLINS, A. R., LAFFITTE, B. A., CHEN, M., NOH, G., GOODMAN, J., HAGGER, G. N., TRAN, J., TIPPIN, T. K., WANG, X., LUSIS, A. J., HSUEH, W. A., LAW, R. E., COLLINS, J. L., WILLSON, T. M. & TONTONOZ, P. 2002. Synthetic LXR ligand inhibits the development of atherosclerosis in mice. *Proc Natl Acad Sci U S A,* 99**,** 7604-9.
JUN, G., MONCASTER, J. A., KOUTRAS, C., SESHADRI, S., BUROS, J., MCKEE, A. C., LEVESQUE, G., WOLF, P. A., ST GEORGE-HYSLOP, P., GOLDSTEIN, L. E. & FARRER, L. A. 2012. delta-Catenin is genetically and biologically associated with cortical cataract and future Alzheimer-related structural and functional brain changes. *PLoS One,* 7**,** e43728.
JUREVICS, H. & MORELL, P. 1995. Cholesterol for synthesis of myelin is made locally, not imported into brain. *J Neurochem,* 64**,** 895-901.
JUSTICE, M. J. & DHILLON, P. 2016. Using the mouse to model human disease: increasing validity and reproducibility. *Dis Model Mech,* 9**,** 101-3.
KADHIM, M., SALOMAA, S., WRIGHT, E., HILDEBRANDT, G., BELYAKOV, O. V., PRISE, K. M. & LITTLE, M. P. 2013. Non-targeted effects of ionising radiation--implications for low dose risk. *Mutat Res,* 752**,** 84-98.
KAESTNER, L. & MINETTI, G. 2017. The potential of erythrocytes as cellular aging models. *Cell Death Differ,* 24**,** 1475-1477.
KANTHAN, G. L., WANG, J. J., ROCHTCHINA, E., TAN, A. G., LEE, A., CHIA, E. M. & MITCHELL, P. 2008. Ten-year incidence of age-related cataract and cataract surgery in an

older Australian population. The Blue Mountains Eye Study. *Ophthalmology,* 115**,** 808-814.e1.
KARIMI, N., MONFARED, A. S., HADDADI, G. H., SOLEYMANI, A., MOHAMMADI, E., HAJIAN-TILAKI, K. & BORZOUEISILEH, S. 2017. Radioprotective effect of hesperidin on reducing oxidative stress in the lens tissue of rats. *Int J Pharm Investig,* 7**,** 149-154.
KATAOKA, T., MIZUGUCHI, Y., NOTOHARA, K., TAGUCHI, T. & YAMAOKA, K. 2006. Histological changes in spleens of radio-sensitive and radio-resistant mice exposed to low-dose X-ray irradiation. *Physiol Chem Phys Med NMR,* 38**,** 21-9.
KHOKHRYAKOV, V. V., KHOKHRYAKOV, V. F., SUSLOVA, K. G., VOSTROTIN, V. V., VVEDENSKY, V. E., SOKOLOVA, A. B., KRAHENBUHL, M. P., BIRCHALL, A., MILLER, S. C., SCHADILOV, A. E. & EPHIMOV, A. V. 2013. Mayak Worker Dosimetry System 2008 (MWDS-2008): assessment of internal dose from measurement results of plutonium activity in urine. *Health Phys,* 104**,** 366-78.
KIM, I., SAITO, T., FUJII, N., KANAMOTO, T., CHATAKE, T. & FUJII, N. 2015. Site specific oxidation of amino acid residues in rat lens gamma-crystallin induced by low-dose gamma-irradiation. *Biochem Biophys Res Commun,* 466**,** 622-8.
KIM, I., SAITO, T., FUJII, N., KANAMOTO, T. & FUJII, N. 2016. One-shot LC-MS/MS analysis of post-translational modifications including oxidation and deamidation of rat lens alpha- and beta-crystallins induced by gamma-irradiation. *Amino Acids,* 48**,** 2855-2866.
KIM, J. H., JENROW, K. A. & BROWN, S. L. 2014. Mechanisms of radiation-induced normal tissue toxicity and implications for future clinical trials. *Radiat Oncol J,* 32**,** 103-15.
KINNEBREW, M., IVERSON, E. J., PATEL, B. B., PUSAPATI, G. V., KONG, J. H., JOHNSON, K. A., LUCHETTI, G., ECKERT, K. M., MCDONALD, J. G., COVEY, D. F., SIEBOLD, C., RADHAKRISHNAN, A. & ROHATGI, R. 2019. Cholesterol accessibility at the ciliary membrane controls hedgehog signaling. *Elife,* 8.
KINSELLA, T. J. 2009. Understanding DNA damage response and DNA repair pathways: applications to more targeted cancer therapeutics. *Semin Oncol,* 36**,** S42-51.
KISIC, B., MIRIC, D., ZORIC, L., ILIC, A. & DRAGOJEVIC, I. 2012. Antioxidant capacity of lenses with age-related cataract. *Oxid Med Cell Longev,* 2012**,** 467130.
KITTS, D. D. 1997. An evaluation of the multiple effects of the antioxidant vitamins. *Trends in Food Science & Technology,* 8**,** 198-203.
KLEIMAN, N. J., WANG, R. R. & SPECTOR, A. 1990. Hydrogen peroxide-induced DNA damage in bovine lens epithelial cells. *Mutat Res,* 240**,** 35-45.
KLEIN, B. E., KLEIN, R., LEE, K. E. & GANGNON, R. E. 2008. Incidence of age-related cataract over a 15-year interval the Beaver Dam Eye Study. *Ophthalmology,* 115**,** 477-82.
KOCH, C. J. & GIANDOMENICO, A. R. 1994. The alkaline elution technique for measuring DNA single strand breaks: increased reliability and sensitivity. *Anal Biochem,* 220**,** 58-65.
KOLB, H. 1995. Gross Anatomy of the Eye. *In:* KOLB, H., FERNANDEZ, E. & NELSON, R. (eds.) *Webvision: The Organization of the Retina and Visual System.* Salt Lake City (UT): University of Utah Health Sciences Center.
KOPYLOVA, L. V., CHEREPANOV, I. V., SNYTNIKOVA, O. A., RUMYANTSEVA, Y. V., KOLOSOVA, N. G., TSENTALOVICH, Y. P. & SAGDEEV, R. Z. 2011. Age-related changes in the water-soluble lens protein composition of Wistar and accelerated-senescence OXYS rats. *Mol Vis,* 17**,** 1457-67.
KORLIMBINIS, A., BERRY, Y., THIBAULT, D., SCHEY, K. L. & TRUSCOTT, R. J. 2009. Protein aging: truncation of aquaporin 0 in human lens regions is a continuous age-dependent process. *Exp Eye Res,* 88**,** 966-73.
KOSARI, S., BADOER, E., NGUYEN, J. C., KILLCROSS, A. S. & JENKINS, T. A. 2012. Effect of western and high fat diets on memory and cholinergic measures in the rat. *Behav Brain Res,* 235**,** 98-103.
KOVAC, U., SKUBIC, C., BOHINC, L., ROZMAN, D. & REZEN, T. 2019. Oxysterols and Gastrointestinal Cancers Around the Clock. *Front Endocrinol (Lausanne),* 10**,** 483.
KREPLER, K. & SCHMID, R. 2005. Alpha-tocopherol in plasma, red blood cells and lenses with and without cataract. *Am J Ophthalmol,* 139**,** 266-70.

KULIG, W., CWIKLIK, L., JURKIEWICZ, P., ROG, T. & VATTULAINEN, I. 2016. Cholesterol oxidation products and their biological importance. *Chem Phys Lipids,* 199**,** 144-160.

KUNZE, S., DALKE, C., FUCHS, H., KLAFTEN, M., ROSSLER, U., HORNHARDT, S., GOMOLKA, M., PUK, O., SABRAUTZKI, S., KULKA, U., HRABE DE ANGELIS, M. & GRAW, J. 2015. New mutation in the mouse Xpd/Ercc2 gene leads to recessive cataracts. *PLoS One,* 10**,** e0125304.

KUZNIARZ, M., MITCHELL, P., CUMMING, R. G. & FLOOD, V. M. 2001. Use of vitamin supplements and cataract: the Blue Mountains Eye Study. *Am J Ophthalmol,* 132**,** 19-26.

LAEMMLI, U. K. 1970. Cleavage of structural proteins during the assembly of the head of bacteriophage T4. *Nature,* 227**,** 680-5.

LALA, D. S. 2004. Liver X receptors and atherosclerosis. *IDrugs,* 7**,** 563-9.

LAMPI, K. J., WILMARTH, P. A., MURRAY, M. R. & DAVID, L. L. 2014. Lens beta-crystallins: the role of deamidation and related modifications in aging and cataract. *Prog Biophys Mol Biol,* 115**,** 21-31.

LEINFELDER, P. J. & RILEY, E. F. 1956. Further studies of effects of x-radiation on partially shielded lens of rabbit. *AMA Arch Ophthalmol,* 55**,** 84-6.

LEMAIRE-EWING, S., DESRUMAUX, C., NEEL, D. & LAGROST, L. 2010. Vitamin E transport, membrane incorporation and cell metabolism: Is alpha-tocopherol in lipid rafts an oar in the lifeboat? *Mol Nutr Food Res,* 54**,** 631-40.

LI, F., WANG, Y., ZHANG, G., ZHOU, J., YANG, L. & GUAN, H. 2014a. Expression and methylation of DNA repair genes in lens epithelium cells of age-related cataract. *Mutat Res,* 766-767**,** 31-6.

LI, L. K., SO, L. & SPECTOR, A. 1985. Membrane cholesterol and phospholipid in consecutive concentric sections of human lenses. *J Lipid Res,* 26**,** 600-9.

LI, S., CHEN, G., ZHANG, C., WU, M., WU, S. & LIU, Q. 2014b. Research progress of natural antioxidants in foods for the treatment of diseases. *Food Science and Human Wellness,* 3**,** 110-116.

LIAN, Y., XIAO, J., JI, X., GUAN, S., GE, H., LI, F., NING, L. & LIU, J. 2015. Protracted low-dose radiation exposure and cataract in a cohort of Chinese industry radiographers. *Occup Environ Med,* 72**,** 640-7.

LIBONDI, T., MENZIONE, M. & AURICCHIO, G. 1985. In vitro effect of alpha-tocopherol on lysophosphatidylcholine-induced lens damage. *Exp Eye Res,* 40**,** 661-6.

LIMA, J. A., DESAI, M. Y., STEEN, H., WARREN, W. P., GAUTAM, S. & LAI, S. 2004. Statin-induced cholesterol lowering and plaque regression after 6 months of magnetic resonance imaging-monitored therapy. *Circulation,* 110**,** 2336-41.

LIMOLI, C. L., KAPLAN, M. I., GIEDZINSKI, E. & MORGAN, W. F. 2001. Attenuation of radiation-induced genomic instability by free radical scavengers and cellular proliferation. *Free Radic Biol Med,* 31**,** 10-9.

LIN, C. M., YEH, P. T., DOYLE, P., TSAN, Y. T. & CHEN, P. C. 2016. Association Between 131I Treatment for Thyroid Cancer and Risk of Receiving Cataract Surgery: A Cohort Study from Taiwan. *J Nucl Med,* 57**,** 836-41.

LINETSKY, M., RAGHAVAN, C. T., JOHAR, K., FAN, X., MONNIER, V. M., VASAVADA, A. R. & NAGARAJ, R. H. 2014. UVA light-excited kynurenines oxidize ascorbate and modify lens proteins through the formation of advanced glycation end products: implications for human lens aging and cataract formation. *J Biol Chem,* 289**,** 17111-23.

LINETSKY, M., SHIPOVA, E., CHENG, R. & ORTWERTH, B. J. 2008. Glycation by ascorbic acid oxidation products leads to the aggregation of lens proteins. *Biochim Biophys Acta,* 1782**,** 22-34.

LITT, M., KRAMER, P., LAMORTICELLA, D. M., MURPHEY, W., LOVRIEN, E. W. & WELEBER, R. G. 1998. Autosomal dominant congenital cataract associated with a missense mutation in the human alpha crystallin gene CRYAA. *Hum Mol Genet,* 7**,** 471-4.

LITTLE, M. P. 2013. A review of non-cancer effects, especially circulatory and ocular diseases. *Radiat Environ Biophys,* 52**,** 435-49.

LITTLE, M. P., KITAHARA, C. M., CAHOON, E. K., BERNIER, M. O., VELAZQUEZ-KRONEN, R., DOODY, M. M., BORREGO, D., MILLER, J. S., ALEXANDER, B. H.,

SIMON, S. L., PRESTON, D. L., HAMADA, N., LINET, M. S. & MEYER, C. 2018. Occupational radiation exposure and risk of cataract incidence in a cohort of US radiologic technologists. *Eur J Epidemiol,* 33**,** 1179-1191.

LIU, K., LYU, L., CHIN, D., GAO, J., SUN, X., SHANG, F., CACERES, A., CHANG, M. L., ROWAN, S., PENG, J., MATHIAS, R., KASAHARA, H., JIANG, S. & TAYLOR, A. 2015. Altered ubiquitin causes perturbed calcium homeostasis, hyperactivation of calpain, dysregulated differentiation, and cataract. *Proc Natl Acad Sci U S A,* 112**,** 1071-6.

LIU, Q., AN, Y., YU, H., LU, Y., FENG, L., WANG, C. & XIAO, R. 2016. Relationship between oxysterols and mild cognitive impairment in the elderly: a case-control study. *Lipids Health Dis,* 15**,** 177.

LIU, S. S. & ZHU, S. Q. 2017. [Correlation between Alzheimer disease and cataract]. *Zhonghua Yan Ke Za Zhi,* 53**,** 314-316.

LOH, A., HADZIAHMETOVIC, M. & DUNAIEF, J. L. 2009. Iron homeostasis and eye disease. *Biochim Biophys Acta,* 1790**,** 637-49.

LOVICU, F. J. & MCAVOY, J. W. 1999. Spatial and temporal expression of p57(KIP2) during murine lens development. *Mech Dev,* 86**,** 165-9.

LUND, A. L., SMITH, J. B. & SMITH, D. L. 1996. Modifications of the water-insoluble human lens alpha-crystallins. *Exp Eye Res,* 63**,** 661-72.

LUNDELL, M. 1994. Estimates of absorbed dose in different organs in children treated with radium for skin hemangiomas. *Radiat Res,* 140**,** 327-33.

LUQUE-CONTRERAS, D., CARVAJAL, K., TORAL-RIOS, D., FRANCO-BOCANEGRA, D. & CAMPOS-PENA, V. 2014. Oxidative stress and metabolic syndrome: cause or consequence of Alzheimer's disease? *Oxid Med Cell Longev,* 2014**,** 497802.

LUSA, S., HEINO, S. & IKONEN, E. 2003. Differential mobilization of newly synthesized cholesterol and biosynthetic sterol precursors from cells. *J Biol Chem,* 278**,** 19844-51.

LYNNERUP, N., KJELDSEN, H., HEEGAARD, S., JACOBSEN, C. & HEINEMEIER, J. 2008. Radiocarbon dating of the human eye lens crystallines reveal proteins without carbon turnover throughout life. *PLoS One,* 3**,** e1529.

LYONS, B., JAMIE, J. F. & TRUSCOTT, R. J. 2014. Separate mechanisms for age-related truncation and racemisation of peptide-bound serine. *Amino Acids,* 46**,** 199-207.

MAGUIRE, J. J., WILSON, D. S. & PACKER, L. 1989. Mitochondrial electron transport-linked tocopheroxyl radical reduction. *J Biol Chem,* 264**,** 21462-5.

MAINALI, L., RAGUZ, M., CAMENISCH, T. G., HYDE, J. S. & SUBCZYNSKI, W. K. 2011. Spin-label saturation-recovery EPR at W-band: applications to eye lens lipid membranes. *J Magn Reson,* 212**,** 86-94.

MAINALI, L., RAGUZ, M., O'BRIEN, W. J. & SUBCZYNSKI, W. K. 2013. Properties of membranes derived from the total lipids extracted from the human lens cortex and nucleus. *Biochim Biophys Acta,* 1828**,** 1432-40.

MAINALI, L., RAGUZ, M., O'BRIEN, W. J. & SUBCZYNSKI, W. K. 2015. Properties of membranes derived from the total lipids extracted from clear and cataractous lenses of 61-70-year-old human donors. *Eur Biophys J,* 44**,** 91-102.

MAINALI, L., RAGUZ, M., O'BRIEN, W. J. & SUBCZYNSKI, W. K. 2017. Changes in the Properties and Organization of Human Lens Lipid Membranes Occurring with Age. *Curr Eye Res,* 42**,** 721-731.

MAIRS, W. D. 2016. Occupational dose constraints for the lens of the eye for interventional radiologists and interventional cardiologists in the UK. *Br J Radiol,* 89**,** 20150551.

MAKLEY, L. N., MCMENIMEN, K. A., DEVREE, B. T., GOLDMAN, J. W., MCGLASSON, B. N., RAJAGOPAL, P., DUNYAK, B. M., MCQUADE, T. J., THOMPSON, A. D., SUNAHARA, R., KLEVIT, R. E., ANDLEY, U. P. & GESTWICKI, J. E. 2015. Pharmacological chaperone for alpha-crystallin partially restores transparency in cataract models. *Science,* 350**,** 674-7.

MARES-PERLMAN, J. A., LYLE, B. J., KLEIN, R., FISHER, A. I., BRADY, W. E., VANDENLANGENBERG, G. M., TRABULSI, J. N. & PALTA, M. 2000. Vitamin supplement use and incident cataracts in a population-based study. *Arch Ophthalmol,* 118**,** 1556-63.

MARKIEWICZ, E., BARNARD, S., HAINES, J., COSTER, M., VAN GEEL, O., WU, W., RICHARDS, S., AINSBURY, E., ROTHKAMM, K., BOUFFLER, S. & QUINLAN, R. A. 2015. Nonlinear ionizing radiation-induced changes in eye lens cell proliferation, cyclin D1 expression and lens shape. 5**,** 150011.

MARKLUND, S. L. 1984. Extracellular superoxide dismutase and other superoxide dismutase isoenzymes in tissues from nine mammalian species. *Biochem J,* 222**,** 649-55.

MARQUARDT, D., WILLIAMS, J. A., KUCERKA, N., ATKINSON, J., WASSALL, S. R., KATSARAS, J. & HARROUN, T. A. 2013. Tocopherol activity correlates with its location in a membrane: a new perspective on the antioxidant vitamin E. *J Am Chem Soc,* 135**,** 7523-33.

MARTIN, K. O., REISS, A. B., LATHE, R. & JAVITT, N. B. 1997. 7 alpha-hydroxylation of 27-hydroxycholesterol: biologic role in the regulation of cholesterol synthesis. *J Lipid Res,* 38**,** 1053-8.

MASORO, E. J. & AUSTAD, S. N. 2011. Handbook of the Biology of Aging. *Elsevier Inc.***,** 520.

MATHIAS, R. T., KISTLER, J. & DONALDSON, P. 2007. The lens circulation. *J Membr Biol,* 216**,** 1-16.

MATHIAS, R. T., WHITE, T. W. & GONG, X. 2010. Lens gap junctions in growth, differentiation, and homeostasis. *Physiol Rev,* 90**,** 179-206.

MATHIESON, T., FRANKEN, H., KOSINSKI, J., KURZAWA, N., ZINN, N., SWEETMAN, G., POECKEL, D., RATNU, V. S., SCHRAMM, M., BECHER, I., STEIDEL, M., NOH, K. M., BERGAMINI, G., BECK, M., BANTSCHEFF, M. & SAVITSKI, M. M. 2018. Systematic analysis of protein turnover in primary cells. *Nat Commun,* 9**,** 689.

MATSUYAMA, M., TANAKA, H., INOKO, A., GOTO, H., YONEMURA, S., KOBORI, K., HAYASHI, Y., KONDO, E., ITOHARA, S., IZAWA, I. & INAGAKI, M. 2013. Defect of mitotic vimentin phosphorylation causes microophthalmia and cataract via aneuploidy and senescence in lens epithelial cells. *J Biol Chem,* 288**,** 35626-35.

MC LAUGHLIN, J. P. 2015. Some characteristics and effects of natural radiation. *Radiat Prot Dosimetry,* 167**,** 2-7.

MCAVOY, J. W., CHAMBERLAIN, C. G., DE IONGH, R. U., RICHARDSON, N. A. & LOVICU, F. J. 1991. The role of fibroblast growth factor in eye lens development. *Ann N Y Acad Sci,* 638**,** 256-74.

MCCUSKER, M. M., DURRANI, K., PAYETTE, M. J. & SUCHECKI, J. 2016. An eye on nutrition: The role of vitamins, essential fatty acids, and antioxidants in age-related macular degeneration, dry eye syndrome, and cataract. *Clin Dermatol,* 34**,** 276-85.

MCDONALD, J. G., SMITH, D. D., STILES, A. R. & RUSSELL, D. W. 2012. A comprehensive method for extraction and quantitative analysis of sterols and secosteroids from human plasma. *J Lipid Res,* 53**,** 1399-409.

MCGINTY, S. J. & TRUSCOTT, R. J. 2006. Presbyopia: the first stage of nuclear cataract? *Ophthalmic Res,* 38**,** 137-48.

MCNULTY, R., WANG, H., MATHIAS, R. T., ORTWERTH, B. J., TRUSCOTT, R. J. & BASSNETT, S. 2004. Regulation of tissue oxygen levels in the mammalian lens. *J Physiol,* 559**,** 883-98.

MEANEY, S., BODIN, K., DICZFALUSY, U. & BJORKHEM, I. 2002. On the rate of translocation in vitro and kinetics in vivo of the major oxysterols in human circulation: critical importance of the position of the oxygen function. *J Lipid Res,* 43**,** 2130-5.

MEANEY, S., HEVERIN, M., PANZENBOECK, U., EKSTROM, L., AXELSSON, M., ANDERSSON, U., DICZFALUSY, U., PIKULEVA, I., WAHREN, J., SATTLER, W. & BJORKHEM, I. 2007. Novel route for elimination of brain oxysterols across the blood-brain barrier: conversion into 7alpha-hydroxy-3-oxo-4-cholestenoic acid. *J Lipid Res,* 48**,** 944-51.

MEDINA-MEZA, I. G. & BARNABA, C. 2013. Kinetics of Cholesterol Oxidation in Model Systems and Foods: Current Status. *Food Engineering Reviews,* 5**,** 171-184.

MENKO, A. S., KLUKAS, K. A. & JOHNSON, R. G. 1984. Chicken embryo lens cultures mimic differentiation in the lens. *Dev Biol,* 103**,** 129-41.

MERRIAM, G. R., JR. & FOCHT, E. F. 1957. A clinical study of radiation cataracts and the relationship to dose. *Am J Roentgenol Radium Ther Nucl Med,* 77**,** 759-85.
MERRIAM, G. R., JR. & SZECHTER, A. 1975. The relative radiosensitivity of rat lenses as a function of age. *Radiat Res,* 62**,** 488-97.
MICELLI-FERRARI, T., VENDEMIALE, G., GRATTAGLIANO, I., BOSCIA, F., ARNESE, L., ALTOMARE, E. & CARDIA, L. 1996. Role of lipid peroxidation in the pathogenesis of myopic and senile cataract. *Br J Ophthalmol,* 80**,** 840-3.
MICHAEL, R. & BRON, A. J. 2011. The ageing lens and cataract: a model of normal and pathological ageing. *Philos Trans R Soc Lond B Biol Sci,* 366**,** 1278-92.
MICHEL, M., JACOB, S., ROGER, G., PELOSSE, B., LAURIER, D., LE POINTE, H. D. & BERNIER, M.-O. 2012. Eye lens radiation exposure and repeated head CT scans: A problem to keep in mind. *European Journal of Radiology,* 81**,** 1896-1900.
MILLER, R. J., FUJINO, T. & NEFZGER, M. D. 1967. Lens findings in Atomic bomb survivors. A review of major ophthalmic surveys at the atomic Bomb Casualty Commission (1949-1962). *Arch Ophthalmol,* 78**,** 697-704.
MINAMOTO, A., TANIGUCHI, H., YOSHITANI, N., MUKAI, S., YOKOYAMA, T., KUMAGAMI, T., TSUDA, Y., MISHIMA, H. K., AMEMIYA, T., NAKASHIMA, E., NERIISHI, K., HIDA, A., FUJIWARA, S., SUZUKI, G. & AKAHOSHI, M. 2004. Cataract in atomic bomb survivors. *International Journal of Radiation Biology,* 80**,** 339-345.
MITCHELL, J. & CENEDELLA, R. J. 1999. Human lens cholesterol concentrations in patients who used lovastatin or simvastatin. *Arch Ophthalmol,* 117**,** 653-7.
MOREAU, K. L. & KING, J. A. 2012. Protein misfolding and aggregation in cataract disease and prospects for prevention. *Trends Mol Med,* 18**,** 273-82.
MOTOYAMA, T., MIKI, M., MINO, M., TAKAHASHI, M. & NIKI, E. 1989. Synergistic inhibition of oxidation in dispersed phosphatidylcholine liposomes by a combination of vitamin E and cysteine. *Arch Biochem Biophys,* 270**,** 655-61.
MUTEMBEREZI, V., GUILLEMOT-LEGRIS, O. & MUCCIOLI, G. G. 2016. Oxysterols: From cholesterol metabolites to key mediators. *Prog Lipid Res,* 64**,** 152-169.
NAGARAJ, R. H., LINETSKY, M. & STITT, A. W. 2012. The pathogenic role of Maillard reaction in the aging eye. *Amino Acids,* 42**,** 1205-20.
NAGARAJ, R. H., PADMANABHA, S., MAILANKOT, M., STANISZEWSKA, M., MUN, L. J., GLOMB, M. A. & LINETSKY, M. D. 2010. Modulation of advanced glycation endproduct synthesis by kynurenines in human lens proteins. *Biochim Biophys Acta,* 1804**,** 829-38.
NAGARAJ, R. H., SELL, D. R., PRABHAKARAM, M., ORTWERTH, B. J. & MONNIER, V. M. 1991. High correlation between pentosidine protein crosslinks and pigmentation implicates ascorbate oxidation in human lens senescence and cataractogenesis. *Proc Natl Acad Sci U S A,* 88**,** 10257-61.
NAKASHIMA, E., NERIISHI, K. & MINAMOTO, A. 2006. A reanalysis of atomic-bomb cataract data, 2000-2002: a threshold analysis. *Health Phys,* 90**,** 154-60.
NARENDRAN, N., LUZHNA, L. & KOVALCHUK, O. 2019. Sex Difference of Radiation Response in Occupational and Accidental Exposure. *Front Genet,* 10**,** 260.
NELSON, T. J. & ALKON, D. L. 2005. Oxidation of cholesterol by amyloid precursor protein and beta-amyloid peptide. *J Biol Chem,* 280**,** 7377-87.
NÉMETH-CAHALAN, K. L., CLEMENS, D. M. & HALL, J. E. 2013. Regulation of AQP0 water permeability is enhanced by cooperativity. *J Gen Physiol,* 141**,** 287-95.
NERIISHI, K., NAKASHIMA, E., MINAMOTO, A., FUJIWARA, S., AKAHOSHI, M., MISHIMA, H. K., KITAOKA, T. & SHORE, R. E. 2007. Postoperative cataract cases among atomic bomb survivors: radiation dose response and threshold. *Radiat Res,* 168**,** 404-8.
NIRMALAN, P. K., ROBIN, A. L., KATZ, J., TIELSCH, J. M., THULASIRAJ, R. D., KRISHNADAS, R. & RAMAKRISHNAN, R. 2004. Risk factors for age related cataract in a rural population of southern India: the Aravind Comprehensive Eye Study. *Br J Ophthalmol,* 88**,** 989-94.

NOORDAM, P. C., KILLIAN, A., OUDE ELFERINK, R. F. & DE GIER, J. 1982. Comparative study on the properties of saturated phosphatidylethanolamine and phosphatidylcholine bilayers: barrier characteristics and susceptibility to phospholipase A2 degradation. *Chem Phys Lipids,* 31**,** 191-204.

NORLIN, M. 2008. Regulation of cellular steroid levels with special focus on oxysterol and estrogen metabolism. *Future Lipidology,* 3**,** 337-346.

NOWOSIELSKA, E. M., CHEDA, A., WREMBEL-WARGOCKA, J. & JANIAK, M. K. 2012. Effect of low doses of low-let radiation on the innate anti-tumor reactions in radioresistant and radiosensitive mice. *Dose Response,* 10**,** 500-15.

O'MALLEY, S., WEITMAN, D., OLDING, M. & SEKHAR, L. 1997. Multiple neoplasms following craniospinal irradiation for medulloblastoma in a patient with nevoid basal cell carcinoma syndrome. Case report. *J Neurosurg,* 86**,** 286-8.

OBORINA, E. M. & YAPPERT, M. C. 2003. Effect of sphingomyelin versus dipalmitoylphosphatidylcholine on the extent of lipid oxidation. *Chem Phys Lipids,* 123**,** 223-32.

OGUNI, M., SETOGAWA, T., OTANI, H., HATTA, T. & TANAKA, O. 1994. Development of the lens in human embryos: a histochemical and ultrastructural study. *Acta Anat (Basel),* 149**,** 31-8.

OLSON, B. J. S. C. & MARKWELL, J. 2007. Assays for Determination of Protein Concentration. *Current Protocols in Protein Science,* 48**,** 3.4.1-3.4.29.

ONG, W. Y., KIM, J. H., HE, X., CHEN, P., FAROOQUI, A. A. & JENNER, A. M. 2010. Changes in brain cholesterol metabolome after excitotoxicity. *Mol Neurobiol,* 41**,** 299-313.

ORTWERTH, B. J., BHATTACHARYYA, J. & SHIPOVA, E. 2009. Tryptophan metabolites from young human lenses and the photooxidation of ascorbic acid by UVA light. *Invest Ophthalmol Vis Sci,* 50**,** 3311-9.

OSNES-RINGEN, Ø., BERG, K. H., MOE, M. C., ZETTERSTRÖM, C., RØGER, M. & NICOLAISSEN, B. 2016. Cell death pattern in lens epithelium of cataract patients. *Acta Ophthalmologica,* 94**,** 514-520.

PACKER, J. E., SLATER, T. F. & WILLSON, R. L. 1979. Direct observation of a free radical interaction between vitamin E and vitamin C. *Nature,* 278**,** 737-8.

PAMPLONA, R. 2008. Membrane phospholipids, lipoxidative damage and molecular integrity: a causal role in aging and longevity. *Biochim Biophys Acta,* 1777**,** 1249-62.

PARASASSI, T., GIUSTI, A. M., RAIMONDI, M., RAVAGNAN, G., SAPORA, O. & GRATTON, E. 1995. Cholesterol protects the phospholipid bilayer from oxidative damage. *Free Radic Biol Med,* 19**,** 511-6.

PASTOR-VALERO, M. 2013. Fruit and vegetable intake and vitamins C and E are associated with a reduced prevalence of cataract in a Spanish Mediterranean population. *BMC Ophthalmol,* 13**,** 52.

PAUL, S. & AMUNDSON, S. A. 2008. Development of gene expression signatures for practical radiation biodosimetry. *Int J Radiat Oncol Biol Phys,* 71**,** 1236-1244.

PAUL, S., SMILENOV, L. B., ELLISTON, C. D. & AMUNDSON, S. A. 2015. Radiation Dose-Rate Effects on Gene Expression in a Mouse Biodosimetry Model. *Radiat Res,* 184**,** 24-32.

PAVLOVIC, V., CEKIC, S., RANKOVIC, G. & STOILJKOVIC, N. 2005. Antioxidant and Pro-oxidant Effect of Ascocbic Acid. *Acta Medica Medianae,* 44**,** 65-9.

PEARSON, A. A. 1980. The development of the eyelids. Part I. External features. *J Anat,* 130**,** 33-42.

PÉREZ, V. I., BOKOV, A., VAN REMMEN, H., MELE, J., RAN, Q., IKENO, Y. & RICHARDSON, A. 2009. Is the oxidative stress theory of aging dead? *Biochim Biophys Acta,* 1790**,** 1005-14.

PERLMAN, R. L. 2016. Mouse models of human disease: An evolutionary perspective. *Evol Med Public Health,* 2016**,** 170-6.

PESCOSOLIDO, N., BARBATO, A., GIANNOTTI, R., KOMAIHA, C. & LENARDUZZI, F. 2016. Age-related changes in the kinetics of human lenses: prevention of the cataract. *International Journal of Ophthalmology,* 9**,** 1506-1517.

PETROV, A. M., KASIMOV, M. R. & ZEFIROV, A. L. 2016. Brain Cholesterol Metabolism and Its Defects: Linkage to Neurodegenerative Diseases and Synaptic Dysfunction. *Acta Naturae,* 8**,** 58-73.

PHAN, H. T. T., SHIMOKAWA, N., SHARMA, N., TAKAGI, M. & VESTERGAARD, M. C. 2018. Strikingly different effects of cholesterol and 7-ketocholesterol on lipid bilayer-mediated aggregation of amyloid beta (1-42). *Biochem Biophys Rep,* 14**,** 98-103.

PIRIE, A. & DRANCE, S. M. 1959. Modification of x-ray damage to the lens by partial shielding. *Int J Radiat Biol Relat Stud Phys Chem Med,* 1**,** 293-304.

PLESNAR, E., SZCZELINA, R., SUBCZYNSKI, W. K. & PASENKIEWICZ-GIERULA, M. 2018. Is the cholesterol bilayer domain a barrier to oxygen transport into the eye lens? *Biochim Biophys Acta,* 1860**,** 434-441.

PODCASY, J. L. & EPPERSON, C. N. 2016. Considering sex and gender in Alzheimer disease and other dementias. *Dialogues Clin Neurosci,* 18**,** 437-446.

PORTER, F. D. 2008. Smith–Lemli–Opitz syndrome: pathogenesis, diagnosis and management. *European Journal of Human Genetics,* 16**,** 535-541.

PRABHAKARAM, M. & ORTWERTH, B. J. 1992. The glycation and cross-linking of isolated lens crystallins by ascorbic acid. *Exp Eye Res,* 55**,** 451-9.

QUAN, G., XIE, C., DIETSCHY, J. M. & TURLEY, S. D. 2003. Ontogenesis and regulation of cholesterol metabolism in the central nervous system of the mouse. *Brain Res Dev Brain Res,* 146**,** 87-98.

RAFFERTY, N. S. & RAFFERTY, K. A., JR. 1981. Cell population kinetics of the mouse lens epithelium. *J Cell Physiol,* 107**,** 309-15.

RAFNSSON, V., OLAFSDOTTIR, E., HRAFNKELSSON, J., SASAKI, H., ARNARSSON, A. & JONASSON, F. 2005. Cosmic radiation increases the risk of nuclear cataract in airline pilots: a population-based case-control study. *Arch Ophthalmol,* 123**,** 1102-5.

RAGUZ, M., WIDOMSKA, J., DILLON, J., GAILLARD, E. R. & SUBCZYNSKI, W. K. 2009. Physical properties of the lipid bilayer membrane made of cortical and nuclear bovine lens lipids: EPR spin-labeling studies. *Biochim Biophys Acta,* 1788**,** 2380-8.

RAJARAMAN, P., HAUPTMANN, M., BOUFFLER, S. & WOJCIK, A. 2018. Human individual radiation sensitivity and prospects for prediction. *Ann ICRP,* 47**,** 126-141.

RAKETE, S. & NAGARAJ, R. H. 2017. UVA Light-mediated Ascorbate Oxidation in Human Lenses. *Photochem Photobiol,* 93**,** 1091-1095.

RAMACHANDRAN, R. D., PERUMALSAMY, V. & HEJTMANCIK, J. F. 2007. Autosomal recessive juvenile onset cataract associated with mutation in BFSP1. *Hum Genet,* 121**,** 475-82.

RAMIREZ-RODRIGUEZ, G., KLEMPIN, F., BABU, H., BENITEZ-KING, G. & KEMPERMANN, G. 2009. Melatonin modulates cell survival of new neurons in the hippocampus of adult mice. *Neuropsychopharmacology,* 34**,** 2180-91.

RAVINDRAN, R. & JAISWAL, A. K. 2019. Wholesomeness and safety aspects of irradiated foods. *Food Chem,* 285**,** 363-368.

RAZA, S. T., ABBAS, S., CHANDRA, A., SINGH, L., RIZVI, S. & MAHDI, F. 2017. Association of angiotensin-converting enzyme, CYP46A1 genes polymorphism with senile cataract. *Oman J Ophthalmol,* 10**,** 21-25.

REDDY, G. B., REDDY, P. Y. & SUROLIA, A. 2017. Alzheimer's and Danish dementia peptides induce cataract and perturb retinal architecture in rats. *Biomol Concepts,* 8**,** 45-84.

REDFERN, W. S., STOREY, S., TSE, K., HUSSAIN, Q., MAUNG, K. P., VALENTIN, J.-P., AHMED, G., BIGLEY, A., HEATHCOTE, D. & MCKAY, J. S. 2011. Evaluation of a convenient method of assessing rodent visual function in safety pharmacology studies: Effects of sodium iodate on visual acuity and retinal morphology in albino and pigmented rats and mice. *Journal of Pharmacological and Toxicological Methods,* 63**,** 102-114.

REFINETTI, R. 2004. Daily activity patterns of a nocturnal and a diurnal rodent in a seminatural environment. *Physiol Behav,* 82**,** 285-94.

REISZ, J. A., BANSAL, N., QIAN, J., ZHAO, W. & FURDUI, C. M. 2014. Effects of ionizing radiation on biological molecules--mechanisms of damage and emerging methods of detection. *Antioxid Redox Signal,* 21**,** 260-92.

RENDIC, S. & GUENGERICH, F. P. 2012. Summary of information on the effects of ionizing and non-ionizing radiation on cytochrome P450 and other drug metabolizing enzymes and transporters. *Curr Drug Metab,* 13**,** 787-814.

RESNIKOFF, S., PASCOLINI, D., ETYA'ALE, D., KOCUR, I., PARARAJASEGARAM, R., POKHAREL, G. P. & MARIOTTI, S. P. 2004. Global data on visual impairment in the year 2002. *Bull World Health Organ,* 82**,** 844-51.

RINGENS, P. J., HOENDERS, H. J. & BLOEMENDAL, H. 1982. Effect of aging on the water-soluble and water-insoluble protein pattern in normal human lens. *Exp Eye Res,* 34**,** 201-7.

RODRIGUEZ, I. R., CLARK, M. E., LEE, J. W. & CURCIO, C. A. 2014. 7-ketocholesterol accumulates in ocular tissues as a consequence of aging and is present in high levels in drusen. *Exp Eye Res,* 128**,** 151-5.

ROODHOOFT, J. M. 2002. Leading causes of blindness worldwide. *Bull Soc Belge Ophtalmol***,** 19-25.

ROTHKAMM, K., BARNARD, S., MOQUET, J., ELLENDER, M., RANA, Z. & BURDAK-ROTHKAMM, S. 2015. DNA damage foci: Meaning and significance. *Environ Mol Mutagen,* 56**,** 491-504.

ROTHKAMM, K., KRUGER, I., THOMPSON, L. H. & LOBRICH, M. 2003. Pathways of DNA double-strand break repair during the mammalian cell cycle. *Mol Cell Biol,* 23**,** 5706-15.

ROTHSTEIN, H., WORGUL, B. V., MEDVEDOVSKY, C. & MERRIAM, G. R., JR. 1982. G0/G1 arrest of cell proliferation in the ocular lens prevents development of radiation cataract. *Ophthalmic Res,* 14**,** 215-20.

ROYER, M. C., LEMAIRE-EWING, S., DESRUMAUX, C., MONIER, S., PAIS DE BARROS, J. P., ATHIAS, A., NEEL, D. & LAGROST, L. 2009. 7-ketocholesterol incorporation into sphingolipid/cholesterol-enriched (lipid raft) domains is impaired by vitamin E: a specific role for alpha-tocopherol with consequences on cell death. *J Biol Chem,* 284**,** 15826-34.

RUJOI, M., JIN, J., BORCHMAN, D., TANG, D. & YAPPERT, M. C. 2003. Isolation and lipid characterization of cholesterol-enriched fractions in cortical and nuclear human lens fibers. *Invest Ophthalmol Vis Sci,* 44**,** 1634-42.

SAGRISTA, M. L., GARCIA, A. E., AFRICA DE MADARIAGA, M. & MORA, M. 2002. Antioxidant and pro-oxidant effect of the thiolic compounds N-acetyl-L-cysteine and glutathione against free radical-induced lipid peroxidation. *Free Radic Res,* 36**,** 329-40.

SAHER, G., BRUGGER, B., LAPPE-SIEFKE, C., MOBIUS, W., TOZAWA, R., WEHR, M. C., WIELAND, F., ISHIBASHI, S. & NAVE, K. A. 2005. High cholesterol level is essential for myelin membrane growth. *Nat Neurosci,* 8**,** 468-75.

SANDILANDS, A., PRESCOTT, A. R., WEGENER, A., ZOLTOSKI, R. K., HUTCHESON, A. M., MASAKI, S., KUSZAK, J. R. & QUINLAN, R. A. 2003. Knockout of the intermediate filament protein CP49 destabilises the lens fibre cell cytoskeleton and decreases lens optical quality, but does not induce cataract. *Exp Eye Res,* 76**,** 385-91.

SARAN, A. 2010. Basal cell carcinoma and the carcinogenic role of aberrant Hedgehog signaling. *Future Oncol,* 6**,** 1003-14.

SARGIS, R. M. & SUBBAIAH, P. V. 2006. Protection of membrane cholesterol by sphingomyelin against free radical-mediated oxidation. *Free Radic Biol Med,* 40**,** 2092-102.

SCHARF, J., DOVRAT, A. & GERSHON, D. 1987. Defective superoxide-dismutase molecules accumulate with age in human lenses. *Graefes Arch Clin Exp Ophthalmol,* 225**,** 133-6.

SCHEY, K. L., WANG, Z., FRIEDRICH, M. G., GARLAND, D. L. & TRUSCOTT, R. J. W. 2019. Spatiotemporal changes in the human lens proteome: Critical insights into long-lived proteins. *Prog Retin Eye Res***,** 100802.

SCHMIDT-NIELSEN, K. 1984. *Scaling: Why is Animal Size So Important?,* Cambridge, Cambridge University Press.

SCHONEICH, C., DILLINGER, U., VON BRUCHHAUSEN, F. & ASMUS, K. D. 1992. Oxidation of polyunsaturated fatty acids and lipids through thiyl and sulfonyl radicals: reaction kinetics, and influence of oxygen and structure of thiyl radicals. *Arch Biochem Biophys,* 292**,** 456-67.

SCHREURS, A., SABANOV, V. & BALSCHUN, D. 2017. Distinct Properties of Long-Term Potentiation in the Dentate Gyrus along the Dorsoventral Axis: Influence of Age and Inhibition. *Sci Rep,* 7**,** 5157.

SCHURMAN, S. H., DUNN, C. A., GREAVES, R., YU, B., FERRUCCI, L., CROTEAU, D. L., SEIDMAN, M. M. & BOHR, V. A. 2012. Age-related disease association of endogenous γ-H2AX foci in mononuclear cells derived from leukapheresis. *PLoS One,* 7**,** e45728.

SCOTT, B. R. 2007. Health risk evaluations for ingestion exposure of humans to polonium-210. *Dose Response,* 5**,** 94-122.

SEVANIAN, A. & MCLEOD, L. L. 1987. Cholesterol autoxidation in phospholipid membrane bilayers. *Lipids,* 22**,** 627-36.

SHAFIE, S. M., BARRIA VON-BISCHHOFFSHAUSEN, F. R. & BATEMAN, J. B. 2006. Autosomal dominant cataract: intrafamilial phenotypic variability, interocular asymmetry, and variable progression in four Chilean families. *Am J Ophthalmol,* 141**,** 750-2.

SHANG, F., NOWELL, T. R., JR. & TAYLOR, A. 2001. Removal of oxidatively damaged proteins from lens cells by the ubiquitin-proteasome pathway. *Exp Eye Res,* 73**,** 229-38.

SHARMA, K. K. & SANTHOSHKUMAR, P. 2009. Lens aging: effects of crystallins. *Biochim Biophys Acta,* 1790**,** 1095-108.

SHEN, Z. 2011. Genomic instability and cancer: an introduction. *Journal of Molecular Cell Biology,* 3**,** 1-3.

SHOJI, H., TAKAO, K., HATTORI, S. & MIYAKAWA, T. 2016. Age-related changes in behavior in C57BL/6J mice from young adulthood to middle age. *Mol Brain,* 9**,** 11.

SHORE, R. E. 2016. Radiation and cataract risk: Impact of recent epidemiologic studies on ICRP judgments. *Mutat Res,* 770**,** 231-237.

SHORE, R. E., NERIISHI, K. & NAKASHIMA, E. 2010. Epidemiological studies of cataract risk at low to moderate radiation doses: (not) seeing is believing. *Radiat Res,* 174**,** 889-94.

SIDJANIN, D., ZIGMAN, S. & REDDAN, J. 1993. DNA damage and repair in rabbit lens epithelial cells following UVA radiation. *Curr Eye Res,* 12**,** 773-81.

SIES, H., STAHL, W. & SUNDQUIST, A. R. 1992. Antioxidant functions of vitamins. Vitamins E and C, beta-carotene, and other carotenoids. *Ann N Y Acad Sci,* 669**,** 7-20.

SIEVERT, R. M. & FAILLA, G. 1959. Recommendations of the International Commission on Radiological Protection. *Health Physics*.

SIEW, E. L., OPALECKY, D. & BETTELHEIM, F. A. 1981. Light scattering of normal human lens. II. Age dependence of the light scattering parameters. *Exp Eye Res,* 33**,** 603-14.

SIMONELLI, F., NESTI, A., PENSA, M., ROMANO, L., SAVASTANO, S., RINALDI, E. & AURICCHIO, G. 1989. Lipid peroxidation and human cataractogenesis in diabetes and severe myopia. *Exp Eye Res,* 49**,** 181-7.

SIMPANYA, M. F., ANSARI, R. R., LEVERENZ, V. & GIBLIN, F. J. 2008. Measurement of lens protein aggregation in vivo using dynamic light scattering in a guinea pig/UVA model for nuclear cataract. *Photochem Photobiol,* 84**,** 1589-95.

SINET, P. M., HEIKKILA, R. E. & COHEN, G. 1980. Hydrogen peroxide production by rat brain in vivo. *J Neurochem,* 34**,** 1421-8.

SINGH, A. & SINGH, H. 1982. Time-scale and nature of radiation-biological damage: approaches to radiation protection and post-irradiation therapy. *Prog Biophys Mol Biol,* 39**,** 69-107.

SMITH, L. L. 1987. Cholesterol autoxidation 1981-1986. *Chem Phys Lipids,* 44**,** 87-125.

SMITH, L. L. 1991. Another cholesterol hypothesis: cholesterol as antioxidant. *Free Radic Biol Med,* 11**,** 47-61.

SMITH, L. L., KULIG, M. J. & TENG, J. I. 1977. Sterol metabolism. XL. On the failure of superoxide radical anion to react with cholesterol. *Chem Phys Lipids,* 20**,** 211-5.

SMITH, P. K., KROHN, R. I., HERMANSON, G. T., MALLIA, A. K., GARTNER, F. H., PROVENZANO, M. D., FUJIMOTO, E. K., GOEKE, N. M., OLSON, B. J. & KLENK, D. C. 1985. Measurement of protein using bicinchoninic acid. *Anal Biochem,* 150**,** 76-85.

SMUDA, M., HENNING, C., RAGHAVAN, C. T., JOHAR, K., VASAVADA, A. R., NAGARAJ, R. H. & GLOMB, M. A. 2015. Comprehensive analysis of maillard protein modifications in human lenses: effect of age and cataract. *Biochemistry,* 54**,** 2500-7.

SNIPES, G. J. & SUTER, U. 1997. Cholesterol and myelin. *Subcell Biochem,* 28**,** 173-204.

SODERO, A. O., VRIENS, J., GHOSH, D., STEGNER, D., BRACHET, A., PALLOTTO, M., SASSOE-POGNETTO, M., BROUWERS, J. F., HELMS, J. B., NIESWANDT, B., VOETS, T. & DOTTI, C. G. 2012. Cholesterol loss during glutamate-mediated excitotoxicity. *Embo j,* 31**,** 1764-73.

SONG, S. H., LANDSBURY, A., DAHM, R., LIU, Y. Z., ZHANG, Q. J. & QUINLAN, R. A. 2009. Functions of the intermediate filament cytoskeleton in the eye lens

Journal of Clinical Investigation, 119**,** 1837-1848.

SOTTERO, B., GAMBA, P., GARGIULO, S., LEONARDUZZI, G. & POLI, G. 2009. Cholesterol oxidation products and disease: an emerging topic of interest in medicinal chemistry. *Curr Med Chem,* 16**,** 685-705.

SPECTOR, A., YANG, Y., HO, Y. S., MAGNENAT, J. L., WANG, R. R., MA, W. & LI, W. C. 1996. Variation in cellular glutathione peroxidase activity in lens epithelial cells, transgenics and knockouts does not significantly change the response to H2O2 stress. *Exp Eye Res,* 62**,** 521-40.

SPITZ, D. R. & HAUER-JENSEN, M. 2014. Ionizing radiation-induced responses: where free radical chemistry meets redox biology and medicine. *Antioxid Redox Signal,* 20**,** 1407-9.

SRINIVASAN, B. D. & HARDING, C. V. 1965. CELLULAR PROLIFERATION IN THE LENS. *Invest Ophthalmol,* 4**,** 452-70.

SRIVASTAVA, O. P., SRIVASTAVA, K., CHAVES, J. M. & GILL, A. K. 2017. Post-translationally modified human lens crystallin fragments show aggregation in vitro. *Biochem Biophys Rep,* 10**,** 94-131.

STADTMAN, E. R. 1992. Protein oxidation and aging. *Science,* 257**,** 1220-4.

STATE COLLEGE, P. M., INC. 2017. Minitab 18 Statistical Software. *[Computer software]*.

STEWART, D. N., LANGO, J., NAMBIAR, K. P., FALSO, M. J., FITZGERALD, P. G., ROCKE, D. M., HAMMOCK, B. D. & BUCHHOLZ, B. A. 2013. Carbon turnover in the water-soluble protein of the adult human lens. *Mol Vis,* 19**,** 463-75.

STEWART, F. A., AKLEYEV, A. V., HAUER-JENSEN, M., HENDRY, J. H., KLEIMAN, N. J., MACVITTIE, T. J., ALEMAN, B. M., EDGAR, A. B., MABUCHI, K., MUIRHEAD, C. R., SHORE, R. E. & WALLACE, W. H. 2012. ICRP publication 118: ICRP statement on tissue reactions and early and late effects of radiation in normal tissues and organs--threshold doses for tissue reactions in a radiation protection context. *Ann ICRP,* 41**,** 1-322.

SUBCZYNSKI, W. K., RAGUZ, M., WIDOMSKA, J., MAINALI, L. & KONOVALOV, A. 2012. Functions of cholesterol and the cholesterol bilayer domain specific to the fiber-cell plasma membrane of the eye lens. *J Membr Biol,* 245**,** 51-68.

SUBCZYNSKI, W. K., WIDOMSKA, J. & MAINALI, L. 2017. Factors Determining the Oxygen Permeability of Biological Membranes: Oxygen Transport Across Eye Lens Fiber-Cell Plasma Membranes. *Adv Exp Med Biol,* 977**,** 27-34.

SWEENEY, M. H. & TRUSCOTT, R. J. 1998. An impediment to glutathione diffusion in older normal human lenses: a possible precondition for nuclear cataract. *Exp Eye Res,* 67**,** 587-95.

TALBOTT, C. M., VOROBYOV, I., BORCHMAN, D., TAYLOR, K. G., DUPRE, D. B. & YAPPERT, M. C. 2000. Conformational studies of sphingolipids by NMR spectroscopy. II. Sphingomyelin. *Biochim Biophys Acta,* 1467**,** 326-37.

TALENS, R. P., CHRISTENSEN, K., PUTTER, H., WILLEMSEN, G., CHRISTIANSEN, L., KREMER, D., SUCHIMAN, H. E., SLAGBOOM, P. E., BOOMSMA, D. I. & HEIJMANS, B. T. 2012. Epigenetic variation during the adult lifespan: cross-sectional and longitudinal data on monozygotic twin pairs. *Aging Cell,* 11**,** 694-703.

TANG, D., BORCHMAN, D., SCHWARZ, A. K., YAPPERT, M. C., VRENSEN, G. F., VAN MARLE, J. & DUPRE, D. B. 2003a. Light scattering of human lens vesicles in vitro. *Exp Eye Res,* 76**,** 605-12.

TANG, D., BORCHMAN, D., YAPPERT, M. C., VRENSEN, G. F. & RASI, V. 2003b. Influence of age, diabetes, and cataract on calcium, lipid-calcium, and protein-calcium relationships in human lenses. *Invest Ophthalmol Vis Sci,* 44**,** 2059-66.

TANG, W., EGGERTSEN, G., CHIANG, J. Y. & NORLIN, M. 2006. Estrogen-mediated regulation of CYP7B1: a possible role for controlling DHEA levels in human tissues. *J Steroid Biochem Mol Biol,* 100**,** 42-51.

TANG, W., NORLIN, M. & WIKVALL, K. 2007. Regulation of human CYP27A1 by estrogens and androgens in HepG2 and prostate cells. *Arch Biochem Biophys,* 462**,** 13-20.

TAPODI, A., CLEMENS, D. M., UWINEZA, A., GOLDBERG, M. W., THINON, E., HEAL, W. P., TATE, E. W., NEMETH-CAHALAN, K., VORONTSOVA, I., JARRIN, M., HALL, J. E. & QUINLAN, R. A. 2019. BFSP1 C-terminal domains released by post-translational processing events can alter significantly the calcium regulation of AQP0 water permeability. *Exp Eye Res*.

TAPPEL, A. L. 1973. Lipid peroxidation damage to cell components. *Fed Proc,* 32**,** 1870-4.

TAYLOR, A. & DAVIES, K. J. 1987. Protein oxidation and loss of protease activity may lead to cataract formation in the aged lens. *Free Radic Biol Med,* 3**,** 371-7.

TAYLOR, F. R., SAUCIER, S. E., SHOWN, E. P., PARISH, E. J. & KANDUTSCH, A. A. 1984. Correlation between oxysterol binding to a cytosolic binding protein and potency in the repression of hydroxymethylglutaryl coenzyme A reductase. *J Biol Chem,* 259**,** 12382-7.

TERRY, R. D., MASLIAH, E., SALMON, D. P., BUTTERS, N., DETERESA, R., HILL, R., HANSEN, L. A. & KATZMAN, R. 1991. Physical basis of cognitive alterations in Alzheimer's disease: synapse loss is the major correlate of cognitive impairment. *Ann Neurol,* 30**,** 572-80.

TESSIER, F., OBRENOVICH, M. & MONNIER, V. M. 1999. Structure and mechanism of formation of human lens fluorophore LM-1. Relationship to vesperlysine A and the advanced Maillard reaction in aging, diabetes, and cataractogenesis. *J Biol Chem,* 274**,** 20796-804.

TESTA, G., STAURENGHI, E., ZERBINATI, C., GARGIULO, S., IULIANO, L., GIACCONE, G., FANTÒ, F., POLI, G., LEONARDUZZI, G. & GAMBA, P. 2016. Changes in brain oxysterols at different stages of Alzheimer's disease: Their involvement in neuroinflammation. *Redox Biol,* 10**,** 24-33.

THEUNISSEN, J. J., JACKSON, R. L., KEMPEN, H. J. & DEMEL, R. A. 1986. Membrane properties of oxysterols. Interfacial orientation, influence on membrane permeability and redistribution between membranes. *Biochim Biophys Acta,* 860**,** 66-74.

THOME, C., CHAMBERS, D. B., HOOKER, A. M., THOMPSON, J. W. & BOREHAM, D. R. 2018. Deterministic Effects to the Lens of the Eye Following Ionizing Radiation Exposure: is There Evidence to Support a Reduction in Threshold Dose? *Health Phys,* 114**,** 328-343.

TIMMERS, P. R., MOUNIER, N., LALL, K., FISCHER, K., NING, Z., FENG, X., BRETHERICK, A. D., CLARK, D. W., AGBESSI, M., AHSAN, H., ALVES, I., ANDIAPPAN, A., AWADALLA, P., BATTLE, A., BONDER, M. J., BOOMSMA, D., CHRISTIANSEN, M., CLARINGBOULD, A., DEELEN, P., VAN DONGEN, J., ESKO, T., FAVE, M., FRANKE, L., FRAYLING, T., GHARIB, S. A., GIBSON, G., HEMANI, G., JANSEN, R., KALNAPENKIS, A., KASELA, S., KETTUNEN, J., KIM, Y., KIRSTEN, H., KOVACS, P., KROHN, K., KRONBERG-GUZMAN, J., KUKUSHKINA, V., KUTALIK, Z., KAHONEN, M., LEE, B., LEHTIMAKI, T., LOEFFLER, M., MARIGORTA, U., METSPALU, A., VAN MEURS, J., MILANI, L., MULLER-NURASYID, M., NAUCK, M., NIVARD, M., PENNINX, B., PEROLA, M., PERVJAKOVA, N., PIERCE, B., POWELL, J., PROKISCH, H., PSATY, B. M., RAITAKARI, O., RING, S., RIPATTI, S., ROTZSCHKE, O., RUEGER, S., SAHA, A., SCHOLZ, M., SCHRAMM, K., SEPPALA, I., STUMVOLL, M., SULLIVAN, P., TEUMER, A., THIERY, J., TONG, L., TONJES, A., VERLOUW, J., VISSCHER, P. M., VOSA, U., VOLKER, U., YAGHOOTKAR, H., YANG, J., ZENG, B., ZHANG, F., AGBESSI, M., AHSAN, H., ALVES, I., ANDIAPPAN, A., AWADALLA, P., BATTLE, A., BONDER, M. J., BOOMSMA, D., CHRISTIANSEN, M., CLARINGBOULD, A., DEELEN, P., VAN DONGEN, J., ESKO, T., FAVE, M., FRANKE, L., FRAYLING, T., GHARIB, S. A., GIBSON, G., HEMANI, G., JANSEN, R., KALNAPENKIS, A., et al. 2019. Genomics of 1 million parent lifespans implicates novel pathways and common diseases and distinguishes survival chances. *Elife,* 8.

TONG, J., CANTY, J. T., BRIGGS, M. M. & MCINTOSH, T. J. 2013. The water permeability of lens aquaporin-0 depends on its lipid bilayer environment. *Exp Eye Res,* 113**,** 32-40.
TRAVERT, C., CARREAU, S. & LE GOFF, D. 2006. Induction of apoptosis by 25-hydroxycholesterol in adult rat Leydig cells: protective effect of 17beta-estradiol. *Reprod Toxicol,* 22**,** 564-70.
TRUSCOTT, R. J. 2005. Age-related nuclear cataract-oxidation is the key. *Exp Eye Res,* 80**,** 709-25.
TRUSCOTT, R. J. & AUGUSTEYN, R. C. 1977. Oxidative changes in human lens proteins during senile nuclear cataract formation. *Biochim Biophys Acta,* 492**,** 43-52.
TRUSCOTT, R. J. & FRIEDRICH, M. G. 2016. The etiology of human age-related cataract. Proteins don't last forever. *Biochim Biophys Acta,* 1860**,** 192-8.
TURNER, H. C., SHURYAK, I., TAVERAS, M., BERTUCCI, A., PERRIER, J. R., CHEN, C., ELLISTON, C. D., JOHNSON, G. W., SMILENOV, L. B., AMUNDSON, S. A. & BRENNER, D. J. 2015. Effect of dose rate on residual gamma-H2AX levels and frequency of micronuclei in X-irradiated mouse lymphocytes. *Radiat Res,* 183**,** 315-24.
UPTON, A. C., CHRISTENBERRY, K. W., FURTH, J., HURST, G. S. & MELVILLE, G. S. 1956. The relative biological effectiveness of neutrons, x-rays, and gamma rays for the production of lens opacities: observations on mice, rats, guinea-pigs, and rabbits. *Radiology,* 67**,** 686-96.
UWINEZA, A., KALLIGERAKI, A. A., HAMADA, N., JARRIN, M. & QUINLAN, R. A. 2019. Cataractogenic load - A concept to study the contribution of ionizing radiation to accelerated aging in the eye lens. *Mutat Res,* 779**,** 68-81.
VAN DE VEN, M., ANDRESSOO, J. O., VAN DER HORST, G. T., HOEIJMAKERS, J. H. & MITCHELL, J. R. 2012. Effects of compound heterozygosity at the Xpd locus on cancer and ageing in mouse models. *DNA Repair (Amst),* 11**,** 874-83.
VARMA, S. D. 1991. Scientific basis for medical therapy of cataracts by antioxidants. *Am J Clin Nutr,* 53**,** 335s-345s.
VARMA, S. D., CHAND, D., SHARMA, Y. R., KUCK, J. F., JR. & RICHARDS, R. D. 1984. Oxidative stress on lens and cataract formation: role of light and oxygen. *Curr Eye Res,* 3**,** 35-57.
VARMA, S. D., KUMAR, S. & RICHARDS, R. D. 1979. Light-induced damage to ocular lens cation pump: prevention by vitamin C. *Proc Natl Acad Sci U S A,* 76**,** 3504-6.
VARMA, S. D. & RICHARDS, R. D. 1988. Ascorbic acid and the eye lens. *Ophthalmic Res,* 20**,** 164-73.
VEJUX, A., SAMADI, M. & LIZARD, G. 2011. Contribution of cholesterol and oxysterols in the physiopathology of cataract: implication for the development of pharmacological treatments. *J Ophthalmol,* 2011**,** 471947.
VESTERGAARD, M. C., YODA, T., HAMADA, T., AKAZAWA OGAWA, Y., YOSHIDA, Y. & TAKAGI, M. 2011. The effect of oxycholesterols on thermo-induced membrane dynamics. *Biochim Biophys Acta,* 1808**,** 2245-51.
VINA, J. & LLORET, A. 2010. Why women have more Alzheimer's disease than men: gender and mitochondrial toxicity of amyloid-beta peptide. *J Alzheimers Dis,* 20 Suppl 2**,** S527-33.
VOGEL, H. 2010. X-ray control of borders and of internal security. *Jbr-btr,* 93**,** 210-4.
VON SALLMANN, L. 1950. Experimental Studies on Early Lens Changes after X-Ray Irradiation. *Trans Am Ophthalmol Soc,* 48**,** 228-42.
VON SALLMANN, L. 1952. Experimental studies on early lens changes after roentgen irradiation. III. Effect of x-radiation on mitotic activity and nuclear fragmentation of lens epithelium in normal and cysteine-treated rabbits. *AMA Arch Ophthalmol,* 47**,** 305-20.
VON SALLMANN, L. & GRIMES, P. 1966. Effect of age on cell division, 3H-thymidine incorporation, and diurnal rhythm in the lens epithelium of rats. *Invest Ophthalmol,* 5**,** 560-7.
VON SALLMANN, L., MUNOZ, C. M. & DRUNGIS, A. 1953. Effects of beta irradiation on the rabbit lens. *AMA Arch Ophthalmol,* 50**,** 727-36.

VON SALLMANN, L., TOBIAS, C. A., ANGER, H. O., WELCH, C., KIMURA, S. F., MUNOZ, C. M. & DRUNGIS, A. 1955. Effects of high-energy particles, X-rays, and aging on lens epithelium. *AMA Arch Ophthalmol,* 54**,** 489-514.

WALKER, R. I., CERVENY, T. J. & ALT, L. A. 1989. *Medical consequences of nuclear warfare,* Maryland, Armed Forces Radiobiology Research Institute.

WANG, C. W., HUANG, C. C., CHOU, P. H., CHANG, Y. P., WEI, S., GUENGERICH, F. P., CHOU, Y. C., WANG, S. F., LAI, P. S., SOUČEK, P. & UENG, Y. F. 2017a. 7-ketocholesterol and 27-hydroxycholesterol decreased doxorubicin sensitivity in breast cancer cells: estrogenic activity and mTOR pathway. *Oncotarget,* 8**,** 66033-66050.

WANG, H., ZHANG, T., WU, D. & ZHANG, J. 2013. A novel beaded filament structural protein 1 (BFSP1) gene mutation associated with autosomal dominant congenital cataract in a Chinese family. *Mol Vis,* 19**,** 2590-5.

WANG, X. & QUINN, P. J. 2000. The location and function of vitamin E in membranes (review). *Mol Membr Biol,* 17**,** 143-56.

WANG, Y., AKIBA, S. & SUN, Q. 2016a. Survey of lens opacities of residents living in high radiation background area in Yangjiang, Guangdong province (in Chinese). *China J. Radiol. Med. Prot.*

WANG, Y., LI, F., ZHANG, G., KANG, L. & GUAN, H. 2016b. Ultraviolet-B induces ERCC6 repression in lens epithelium cells of age-related nuclear cataract through coordinated DNA hypermethylation and histone deacetylation. *Clin Epigenetics,* 8**,** 62.

WANG, Y., ZHANG, J., WU, J. & GUAN, H. 2017b. Expression of DNA repair genes in lens cortex of age-related cortical cataract. *Exp Mol Pathol,* 102**,** 219-223.

WEALE, R. A. 1962. PRESBYOPIA. *British Journal of Ophthalmology,* 46**,** 660-668.

WEST, S. 2007. Epidemiology of cataract: accomplishments over 25 years and future directions. *Ophthalmic Epidemiol,* 14**,** 173-8.

WHITFIELD, M. L., GEORGE, L. K., GRANT, G. D. & PEROU, C. M. 2006. Common markers of proliferation. *Nat Rev Cancer,* 6**,** 99-106.

WHO. 2020. *World report on vision* [Online]. Geneva: World Health Organisation. [Accessed 20 2020].

WIDOMSKA, J., RAGUZ, M. & SUBCZYNSKI, W. K. 2007. Oxygen permeability of the lipid bilayer membrane made of calf lens lipids. *Biochim Biophys Acta,* 1768**,** 2635-45.

WIDOMSKA, J., SUBCZYNSKI, W. K., MAINALI, L. & RAGUZ, M. 2017. Cholesterol Bilayer Domains in the Eye Lens Health: A Review. *Cell Biochemistry and Biophysics,* 75**,** 387-398.

WILDE, G. & SJOSTRAND, J. 1997. A clinical study of radiation cataract formation in adult life following gamma irradiation of the lens in early childhood. *Br J Ophthalmol,* 81**,** 261-6.

WILKER, S. C., DAGNELIE, G. & GOLDBERG, M. F. 2010. Retinitis pigmentosa and punctate cataracts in mevalonic aciduria. *Retin Cases Brief Rep,* 4**,** 34-6.

WINKLER, B. S., ORSELLI, S. M. & REX, T. S. 1994. The redox couple between glutathione and ascorbic acid: a chemical and physiological perspective. *Free Radic Biol Med,* 17**,** 333-49.

WORGUL, B. V., KUNDIYEV, Y. I., SERGIYENKO, N. M., CHUMAK, V. V., VITTE, P. M., MEDVEDOVSKY, C., BAKHANOVA, E. V., JUNK, A. K., KYRYCHENKO, O. Y., MUSIJACHENKO, N. V., SHYLO, S. A., VITTE, O. P., XU, S., XUE, X. & SHORE, R. E. 2007. Cataracts among Chernobyl clean-up workers: implications regarding permissible eye exposures. *Radiat Res,* 167**,** 233-43.

WORGUL, B. V., MERRIAM, G. R., JR. & MEDVEDOVSKY, C. 1989. Cortical cataract development--an expression of primary damage to the lens epithelium. *Lens Eye Toxic Res,* 6**,** 559-71.

WORMSTONE, I. M. & WRIDE, M. A. 2011. The ocular lens: a classic model for development, physiology and disease. *Philos Trans R Soc Lond B Biol Sci,* 366**,** 1190-2.

WRIDE, M. A. 2011. Lens fibre cell differentiation and organelle loss: many paths lead to clarity. *Philos Trans R Soc Lond B Biol Sci,* 366**,** 1219-33.

WU, J. J., WU, W., THOLOZAN, F. M., SAUNTER, C. D., GIRKIN, J. M. & QUINLAN, R. A. 2015. A dimensionless ordered pull-through model of the mammalian lens epithelium

evidences scaling across species and explains the age-dependent changes in cell density in the human lens. *J R Soc Interface,* 12**,** 20150391.
XIE, C., LUND, E. G., TURLEY, S. D., RUSSELL, D. W. & DIETSCHY, J. M. 2003. Quantitation of two pathways for cholesterol excretion from the brain in normal mice and mice with neurodegeneration. *J Lipid Res,* 44**,** 1780-9.
YAMADA, M., WONG, F. L., FUJIWARA, S., AKAHOSHI, M. & SUZUKI, G. 2004. Noncancer disease incidence in atomic bomb survivors, 1958-1998. *Radiat Res,* 161**,** 622-32.
YAMAMOTO, K. & NIKI, E. 1988. Interaction of alpha-tocopherol with iron: antioxidant and prooxidant effects of alpha-tocopherol in the oxidation of lipids in aqueous dispersions in the presence of iron. *Biochim Biophys Acta,* 958**,** 19-23.
YAMAUCHI, Y., REID, P. C., SPERRY, J. B., FURUKAWA, K., TAKEYA, M., CHANG, C. C. & CHANG, T. Y. 2007. Plasma membrane rafts complete cholesterol synthesis by participating in retrograde movement of precursor sterols. *J Biol Chem,* 282**,** 34994-5004.
YANG, L., WANG, J., DENG, Y., GONG, C., LI, Q., CHEN, Q., LI, H., JIANG, C., ZHOU, R., HAI, K., WU, W. & LI, T. 2018. Melatonin improves neurological outcomes and preserves hippocampal mitochondrial function in a rat model of cardiac arrest. *PLoS One,* 13**,** e0207098.
YANSHOLE, L. V., CHEREPANOV, I. V., SNYTNIKOVA, O. A., YANSHOLE, V. V., SAGDEEV, R. Z. & TSENTALOVICH, Y. P. 2013. Cataract-specific posttranslational modifications and changes in the composition of urea-soluble protein fraction from the rat lens. *Mol Vis,* 19**,** 2196-208.
YEUM, K. J., TAYLOR, A., TANG, G. & RUSSELL, R. M. 1995. Measurement of carotenoids, retinoids, and tocopherols in human lenses. *Invest Ophthalmol Vis Sci,* 36**,** 2756-61.
YIN, H., XU, L. & PORTER, N. A. 2011. Free radical lipid peroxidation: mechanisms and analysis. *Chem Rev,* 111**,** 5944-72.
YOSHIMURA, Y., INOMATA, T., NAKAZAWA, H., KUBO, H., YAMAGUCHI, F. & ARIGA, T. 1999. Evaluation of free radical scavenging activities of antioxidants with an H(2)O(2)/NaOH/DMSO system by electron spin resonance. *J Agric Food Chem,* 47**,** 4653-6.
YU, B. P. 1994. Cellular defenses against damage from reactive oxygen species. *Physiol Rev,* 74**,** 139-62.
YUAN, M. K., TSAI, D. C., CHANG, S. C., YUAN, M. C., CHANG, S. J., CHEN, H. W. & LEU, H. B. 2013. The risk of cataract associated with repeated head and neck CT studies: a nationwide population-based study. *AJR Am J Roentgenol,* 201**,** 626-30.
ZARINA, S., ZHAO, H. R. & ABRAHAM, E. C. 2000. Advanced glycation end products in human senile and diabetic cataractous lenses. *Mol Cell Biochem,* 210**,** 29-34.
ZARROUK, A., VEJUX, A., MACKRILL, J., O'CALLAGHAN, Y., HAMMAMI, M., O'BRIEN, N. & LIZARD, G. 2014. Involvement of oxysterols in age-related diseases and ageing processes. *Ageing Res Rev,* 18**,** 148-62.
ZELENKA, P. S. 1984. Lens lipids. *Curr Eye Res,* 3**,** 1337-59.
ZERBINATI, C. & IULIANO, L. 2017. Cholesterol and related sterols autoxidation. *Free Radic Biol Med,* 111**,** 151-155.
ZETTERBERG, M. 2016. Age-related eye disease and gender. *Maturitas,* 83**,** 19-26.
ZETTERBERG, M. & CELOJEVIC, D. 2015. Gender and Cataract – The Role of Estrogen. *Current Eye Research,* 40**,** 176-190.
ZHANG, J. & LIU, Q. 2015. Cholesterol metabolism and homeostasis in the brain. *Protein Cell,* 6**,** 254-64.
ZHANG, X., BAI, Q., XU, L., KAKIYAMA, G., PANDAK, W. M., JR., ZHANG, Z. & REN, S. 2012. Cytosolic sulfotransferase 2B1b promotes hepatocyte proliferation gene expression in vivo and in vitro. *Am J Physiol Gastrointest Liver Physiol,* 303**,** G344-55.
ZHANG, Y., PAPAZYAN, R., DAMLE, M., FANG, B., JAGER, J., FENG, D., PEED, L. C., GUAN, D., SUN, Z. & LAZAR, M. A. 2017. The hepatic circadian clock fine-tunes the lipogenic response to feeding through RORalpha/gamma. *Genes Dev,* 31**,** 1202-1211.

ZHANG, Z. F., ZHANG, J., HUI, Y. N., ZHENG, M. H., LIU, X. P., KADOR, P. F., WANG, Y. S., YAO, L. B. & ZHOU, J. 2011. Up-regulation of NDRG2 in senescent lens epithelial cells contributes to age-related cataract in human. *PLoS One,* 6**,** e26102.

ZHAO, X. Q. & KERWIN, W. S. 2012. Utilizing imaging tools in lipidology: examining the potential of MRI for monitoring cholesterol therapy. *Clin Lipidol,* 7**,** 329-343.

ZHU, X., KORLIMBINIS, A. & TRUSCOTT, R. J. 2010. Age-dependent denaturation of enzymes in the human lens: a paradigm for organismic aging? *Rejuvenation Res,* 13**,** 553-60.

ZHU, X. J., ZHANG, K. K., HE, W. W., DU, Y., HOOI, M. & LU, Y. 2018. Racemization at the Asp 58 residue in alphaA-crystallin from the lens of high myopic cataract patients. *J Cell Mol Med,* 22**,** 1118-1126.

ZIEDEN, B., KAMINSKAS, A., KRISTENSON, M., KUCINSKIENE, Z., VESSBY, B., OLSSON, A. G. & DICZFALUSY, U. 1999. Increased plasma 7 beta-hydroxycholesterol concentrations in a population with a high risk for cardiovascular disease. *Arterioscler Thromb Vasc Biol,* 19**,** 967-71.

ZIGLER, J. S., JR., JERNIGAN, H. M., JR., GARLAND, D. & REDDY, V. N. 1985. The effects of "oxygen radicals" generated in the medium on lenses in organ culture: inhibition of damage by chelated iron. *Arch Biochem Biophys,* 241**,** 163-72.

ZIGMAN, S., MCDANIEL, T., SCHULTZ, J. B., REDDAN, J. & MEYDANI, M. 1995. Damage to cultured lens epithelial cells of squirrels and rabbits by UV-A (99.9%) plus UV-B (0.1%) radiation and alpha tocopherol protection. *Mol Cell Biochem,* 143**,** 35-46.